University of London

NOVEL MOLECULAR IMPRINTED NANOGELS AS DRUG DELIVERY VEHICLES FOR TAMOXIFEN

A thesis presented in part fulfilment of the Degree of
Doctor of Philosophy at the University of London

By

JUDITH VICTORIA RAY, BSc in Chemistry, University of Liverpool

July 2014

School of Biological and Chemical Sciences

Queen Mary
University of London

Statement of originality

I, Judith Ray, confirm that the research included within this thesis is my own work or that where it has been carried out in collaboration with, or supported by others, that this is duly acknowledged below and my contribution indicated. Previously published material is also acknowledged below.

I attest that I have exercised reasonable care to ensure that the work is original, and does not to the best of my knowledge break any UK law, infringe any third party's copyright or other Intellectual Property Right, or contain any confidential material.

I accept that the College has the right to use plagiarism detection software to check the electronic version of the thesis.

I confirm that this thesis has not been previously submitted for the award of a degree by this or any other university.

Signature: 

Date: 09-07-2014

Details of collaboration and publications:

Abstract

The field of nanomedicine has witnessed an incredible expansion, from a total market value in 2003 of $500 million expected to rise to $160 billion by 2015 (Global Industry Analysts, Inc.). The nanomedicine industry is forecasted to grow and have a significant impact on the economy, with sectors such as biomaterials, diagnostics and drug delivery expected to play a major role. This thesis gives a detailed account of the synthesis and characterisation of molecularly imprinted nanogels for drug delivery. Their toxicity and potential use as a targeted carrier to cancerous cells is evaluated.

Initially an overview of nanomaterials and their uses in many areas such as agriculture, energy storage and technology are discussed. The impact of nanomaterials on the life sciences is examined; in particular their application in drug delivery is focussed upon. Chapters 2, 3 and 4 make up the results and discussion of this work. Chapter 2 focuses on developing the synthesis of the acrylamide based nanogels and, vitally, incorporating a suitable fluorescent tag in order to track the nanogels *in vitro* and *in vivo*. Fundamentally toxicity studies carried out on the nanogels, both *in vitro* and *in vivo* in *Danio rerio* (zebrafish) are reported in Chapter 3 to ensure the nanogels are biocompatible. Chapter 4 introduces an innovative approach, molecular imprinting, to incorporating a drug into the nanogels. The upload and release of Tamoxifen (a drug used to treat breast cancer) at reduced pH, was also analysed. Finally future development of the carrier is discussed and key issues that need to be addressed.

This thesis is dedicated to my grandfathers;

to Bumpy, who always wanted one of his children to do a PhD, hopefully a granddaughter will do!
Donald Lawrence EGGLETON (b. 1925)

and to Granddad, who I dearly wish could have been here to see this day.
Anthony Charles RAY (1931-2005)

Acknowledgements

Firstly I would like to sincerely thank my supervisor Prof. Marina Resmini for all the fantastic opportunities and experiences she has given me with all of her European networks; they are invaluable. I would also like to thank her for her continued advice and support throughout my PhD.

Many thanks go to Dr Caroline Brennan for all her help and patience with the zebrafish; this project would not have been possible without her skills, knowledge and expertise. I also thank Caroline and Dr Isaac Abrahams for their helpful advice and comments as members of my panel. Dr Huijun Zhu and Claudia Moia at Cranfield University, and Dr Diana Velluto at QMUL's School of Medicine are thanked for all their work and collaboration with the *in vitro* studies.

QMUL and EPSRC are thanked for funding this project and the European commission are thanked for funding the year abroad in industry as part of the IAPP IRMED project.

For all the help with orders and consumables I would like to thank Alan Bradshaw for the early years and Agha Shah for the latter. I am also very grateful to Jay, John and Janet in JP stores, Jalal, Ian, Harold, Greg and all the technicians in the fish facility for their help over the years. Special thanks to Sylvie for help with many things, including my French!

Paolo and Diana deserve special thanks for their incredible support and much needed help in the laboratory. Ania and Rita are thanked for their warm welcome to the laboratory and their help and support in the early days. I thank all those in my year group, (Nicky, KJ, Lee, Fabri) and in particular Tanya and Freda for their advice and support throughout the years. There are many others to thank in JP including Sofia, Giorgio, Gabriele, Huihui, Ben, Rob, Síobhan, Geoff, to name just a few, for their support and continued kindness and friendship. Special thanks go to Fosca for all her help in the last few months.

Je remercie POLYINTELL, de m'avoir accueillie comme une 'early stage researcher' en 2011. Je remercie en particulier le Dr Céline Pérollier pour sa supervision et Olivier, Delphine, Florent, Melissa et Benoit pour leur aide dans le laboratoire.

There are several people from my early education who I would like to thank, including Miss Grice, Miss Clough and Mr Hurdman for all their extra support; without them I would not have the outlook, nor have received the support I needed to be where I am today. Mr Poole is also due very special thanks for his enthusiasm for chemistry, which led me down this fascinating career path.

Before embarking on this PhD I worked for almost two years at IOTA NanoSolutions, where I had an exciting introduction to the chemical industry and I thank everyone at IOTA for making it such a vibrant place to work; it was having such an enjoyable experience there that cemented a career in science for me. Many thanks go to Dr Alison Foster for being a wholly supportive and positive manager and to Dr Jim Long who ultimately inspired me to do a PhD.

Lastly but by no means least, I would like to thank my parents for their continued support, endless reading of my thesis, motivation and financial support; I couldn't have completed this thesis without any of it. It may have taken me 28 years to appreciate you but I certainly do now! Thanks also go to my sister for her continued support and motivation. Special thanks go to Nicola for being the most supportive friend, keeping me motivated and visiting me everywhere I go. Enfin, je remercie Florent pour tout son amour, son soutien et sa patience pendant ma thèse et sa motivation pour continuer, malgré la séparation causée. Je ne peux pas suffisamment le remercier pour le soutien par tous les moyens possibles qu'il m'a donné lors de l'écriture de cette thèse.

Abbreviations

A = Acrylamide

AA = Acrylic acid

AIBN = Azobisisobutyronitrile

ACN = Acetonitrile

BBB= Blood brain barrier

C_M = Monomer concentration

dpf = Days post fertilisation

DCM = Dichloromethane

DMF = Dimethylformamide

DLS = Dynamic light scattering

DMSO = Dimethylsulfoxide

EBA = N, N' Ethylenebisacrylamide

FM = Functional monomer

HPLC = High Performance Liquid Chromatography

hpf = Hours post fertilisation

LDH = Lactate dehydrogenase

MBA = Methylenebisacrylamide

MIP = Molecularly Imprinted Polymer

MS222 = Tricaine methanesulfonate

MTT = 3-(4,5-dimethylthiazol-2-yl)-2,5-diphenyl tetrazoliumbromide

MWCN = multiwalled carbon nanotube

NG = Nanogel

NIP = Non-Imprinted Polymer

NMR = Nuclear magnetic resonance

NP = Nanoparticle

OECD = Organisation for economic coordination and development

PNs = Polymer nanopaticles

PTU = 1-phenyl-2-thiourea

PBS = Phosphate buffer solution

QDs = Quantum dots

SEM = Scanning electron microscopy

SWCN = Single walled carbon nanotube

SLN = Solid lipid nanoparticle

TCA = 7-[4-(trifluoromethyl)coumarin] acrylamide

TMAC = 7-amino-4-(trifluoromethyl) coumarin

TEM = Transmission electron microscopy

XL = Cross-linker

Contents

1

1 Introduction

1.1 Nanotechnology and its impact on developments and applications, especially in the life sciences

1.1.1 Nanotechnology

There has been a growing interest in a relatively new area of technology defined as nanotechnology. This interest has grown since it was discovered that materials, which are just nanometers in size, display unusual and interesting properties that macromolecules do not exhibit. Nanotechnology is difficult to define, however most scientists agree that it is "the study and control of manmade materials that are between 1 and 100 nm in length" and these nanoscale proportions give the materials special properties[1].

Nanotechnology has had and continues to have a significant impact on our lives, improving it in many ways. Computers, for example, in the last few years have developed from a standard desktop to one that can fit in the palm of the hand, with devises such as the iPhone.

1.1.2 A brief history of nanotechnology

1.1.2.1 Early manifestations

Some of the earliest nanotechnologists were ancient Romans (30 BC-640 AD) although they did not realise this at the time. The Lycurgus Cup, seen in figure 1, is a famous artefact that was found from this period which appears green when lit from outside the cup, however when a light is placed inside the cup it turns red: this effect is due to the glass containing gold and silver nanoparticles[2]. Other artefacts, which seem to be failed attempts at recreating this effect have also been found from this period (and no other successful examples have been discovered) so the cup is believed to have been created by accident. Stained glass windows were produced throughout the medieval period (500-1450 AD) and are formed by metal nanoparticles being trapped in a glass matrix. Gold nanoparticles formed the red glass and silver nanoparticles formed the yellow glass. It is because the metals are in nanoparticulate form that they exhibit these colours and later it became known as just one of many differences in properties of metals between their macromolecular states. However it was Michael

Faraday who realised, in the mid 1800's, that gold colloids, now known to be nanoparticles had special optical and electrical properties[3].

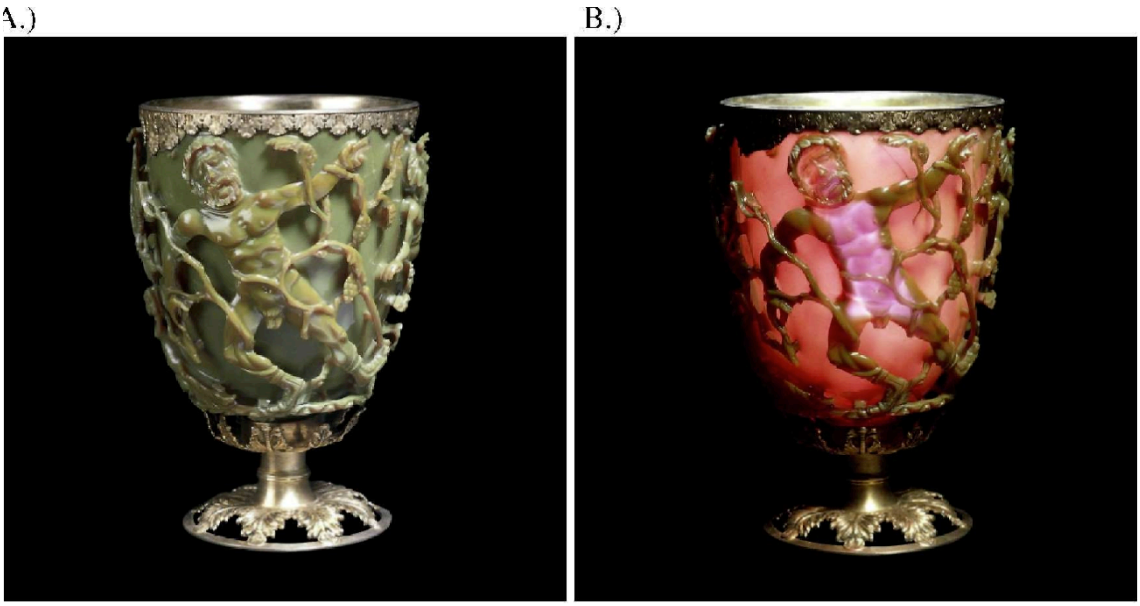

Figure 1 - The Lycurgus cup, A) is without a light inside and B) with a light inside, showing the special optical properties of the gold nanoparticles[3].

1.1.2.2 Nanotechnology consciously used

It was not until 1959 that the concept of nanotechnology was originally thought of and consciously used. Richard Feynman was an American physicist who, with Julian Schwinger and Sin-Itiro Tomonaga, won the Nobel Prize in 1965 for their work on quantum electrodynamics.[4] Feynman is famous for a lecture he gave entitled 'There's plenty of room at the bottom', in which Feynman described the possibility of writing out the entire Britannica encyclopaedia on the head of a pin.[5] He also described the possibility of miniaturising the computer (which at that time was as big as a room) using machines to control smaller machines to manipulate individual atoms and molecules. This idea only became a reality 30 years later, in 1990, when Don Eigler (who worked for IBM) discovered that he could use a scanning tunnelling microscope (STM) to move single atoms around to form the letters of his employer, an image of which can be seen in figure 2.[6]

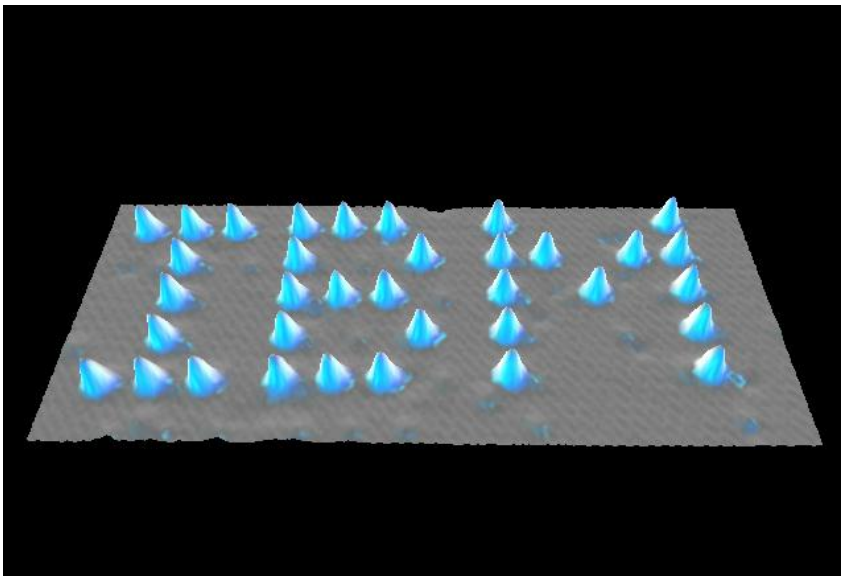

Figure 2 - Image captured by Don Eigler when he moved single atoms around, using a scanning tunnelling microscope, to form the letters of his employer, IBM.[7]

1.1.2.3 Nanotechnology formally defined

Nanotechnology was not given its name until 1974 when Norio Taniguchi, a Science University Professor in Tokyo, *defined* the term 'nanotechnology' in a paper, he wrote:

"*Nano-technology* mainly consists of the processing of, separation, consolidation, and deformation of materials by one atom or molecule."[8]

This is still used as a basic definition of nanotechnology today although it has evolved over time, for example, to include materials up to 100 nm.[8]

In November 1996 it was attempted to coordinate all work on the nanoscale as members of several agencies met regularly to discuss developments made. This group continued to meet informally until September 1998 when it was named officially as the Interagency Working Group on Nanotechnology (IWGN) under the National Science and Technology Council (NSTC). In August 1999 the group submitted the first draft of a plan of an initiative in nanotechnology to the President's Council of Advisors for Science and Technology (PCAST) which ended in the group gaining substantial funding in its 2001 submission to congress and the Clinton administration raised the level of nanoscale science and technology to federal initiative.[9] Since 2001 nanotechnology has developed vastly in many areas, including life sciences, pharmaceuticals and drug delivery.

1.2 Applications of nanotechnology in different areas

1.2.1 Nanotechnology in agriculture

Nano science has benefited many areas of research and human life. One area of science that has benefited from the developments in nanotechnology is agriculture. When analysing the amount of published/patented research in agriculture, the majority of research has been on plant protection products rather than fertilizers, which accounted for less than a quarter of the research focus. Nanotechnology has helped plant protection by assisting with the dispersion, protection and controlling the release of actives as well as aiding photocatalysis.[10] All these developments have had great effects on increasing output and maintaining the health of crops.[11] However, this is just one small area of research. Another area of research that is seeing huge change, due to research at the nano scale, is energy.

1.2.2 Nanotechnology and energy efficiency

Energy, its storage and conversion from one form to another, is currently a very lucrative and seductive area of research and has benefited tremendously from the developments in nano science. Nanotechnology has been exploited in the conversion of solar energy to electricity.[12, 13] This is because much of the solar energy, which hits a solar panel, is not absorbed. This can be due either to some photons having too little energy to allow absorbtion, or some with very high energy, being only partially absorbed meaning that some energy is therefore wasted. Nanomaterials are being developed to try to make the process more efficient and utilise as much of the energy as possible.[13]

The finite resource of fossil fuels available is rapidly running out and therefore finding new ways of converting natural sources of energy and storing it is fundamental to sustaining and improving quality of life. It is here that nanomaterials, due to their small size and special characteristics, are enabling new, ever improved batteries that can last longer and store more energy, significantly enough to power electric cars.[14] However batteries are merely one example of improvements in energy usage that have seen the benefit that nanomaterials can bring: technology in general has developed rapidly since developments in the nano world.

1.2.3 Nanotechnology and computer science

Information technology and computing have completely changed our lives in the last couple of decades, enabling computers to be reduced from the size of a room to remarkably powerful hand-held phones, tablets and laptops.

1.2.4 Moore's Prediction

It was Moore in 1965 who suggested that the size of features in devices would reduce by a factor of 0.7 every three years, which has turned out to be true with components decreasing in size in line with this prediction, as shown by the graph in figure 3, and companies use Moore's exponential decrease as targets to keep up with competitors.[15] This appears to be tailing off due to lithography limitations. Lithography in electronics is where silicon wafers (used to make chips) are coated in a light-sensitive layer. Light is shined through a stencil, or mask, burning the photoresist away in undesired areas, after which they are etched away. However in order to do this a UV-light with 193 nm wavelength is required. Therefore the limit is imposed by the wavelength of the light and the size of the mask. A Dutch company is currently working on a technique they believe will be ready by 2015 on using 10 nm masks and an EUV light with a wavelength of 13.5 nm which will enable the trend to continue for a few more years.[16]

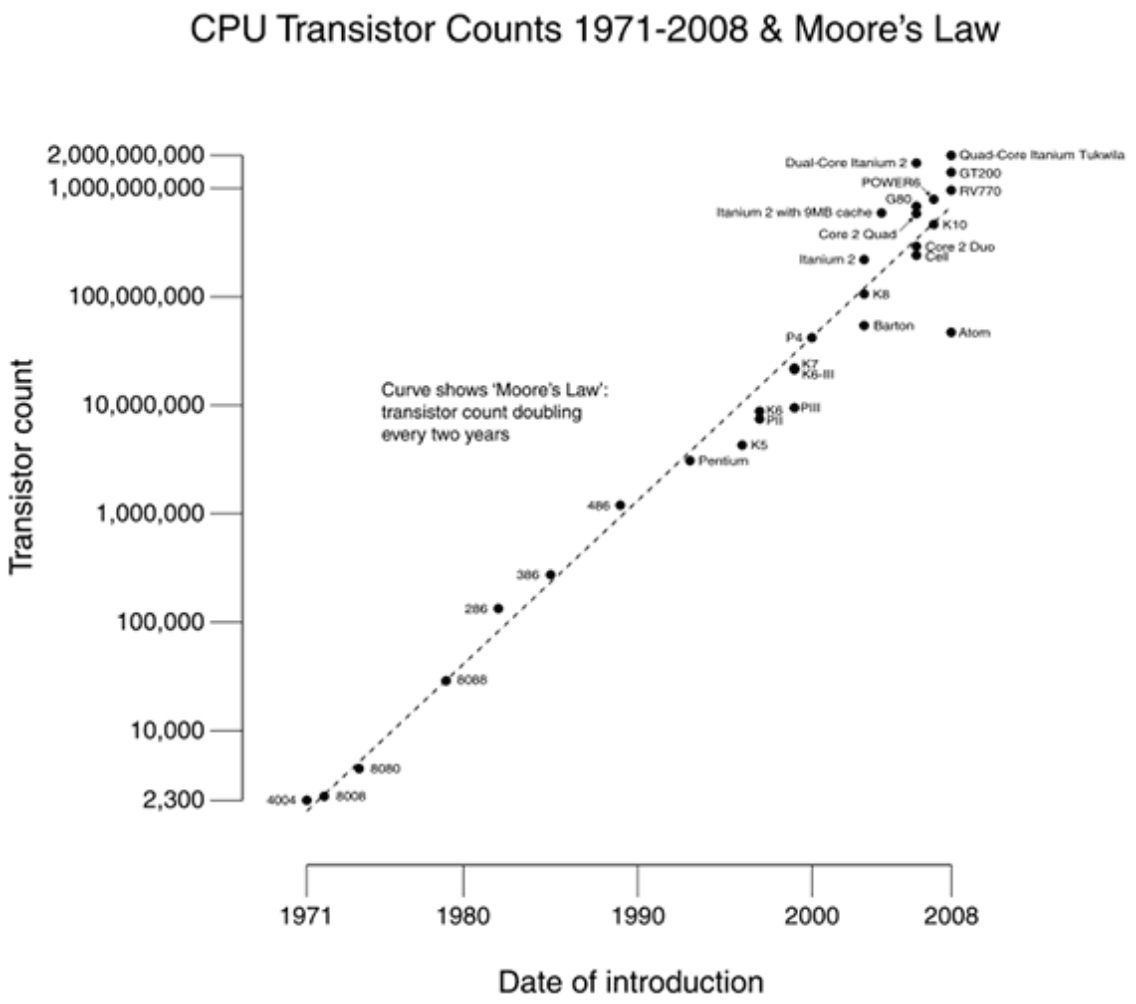

Figure 3 – A graph to show the trend in electronics conforming to Moore's prediction in 1965[17].

In turn, such advances in technology have indirectly benefited many other areas of our lives (including those of energy storage, agriculture). The trend towards smaller and smaller devices directly impact business practice and human life in the wider sense, as there are few jobs or activities that these days do not at one time or another require the use of information technology or a computer, even if it is just to communicate. Nanotechnology has demonstrably benefited human life in a variety of fields and one further very important area where its research and development has had a huge impact is that of health and the life sciences.

1.2.5 Nanotechnology and its use in the life sciences

The UK has one of the most successful Life Sciences industries viewed from the global perspective. Life Sciences includes everything from synthetic and industrial

biotechnology through pharmaceuticals to medical devices and diagnostics. The UK Life Sciences industry is growing faster than the UK economy in general, with an annual turnover of more than £50bn. In global terms, Life Sciences are having to change rapidly in direct response to lifestyle changes, extended life expectancy and contemporary rises in chronic conditions such as diabetes, obesity and dementia. To address these important issues, traditional methods are no longer suitable or sufficient.

Advances in computing and rapid developments in genomics are opening up new and exciting areas for research in medicine. However, because these materials are required to be ever more sophisticated the research is becoming ever more expensive and time consuming. Older methods and research for 'one drug fits all' is no longer appropriate. The possibility of, and consequent need for, more cleverly tailored drugs and medicines to target specific genes and genetic characteristics are slowly becoming a reality. Due to these significant changes in approach, and with the new perspective offered by nanotechnological thinking, we are obtaining increasing knowledge on how different medications affect different people in different ways. This makes it ever more difficult to jump through all the necessary rules and regulations to actually get the medication to market and guarantee its safety. It now takes on average 20 years and $1bn to develop a new drug.[18]

Nanotechnology and the special properties nanomaterials possess give great opportunities to accomplishing some of these tailored medicines. However introducing nanomaterials into the drug market raises several issues including the question of intellectual property rights. Traditionally pharmaceuticals would go through a 7 step model, presented in figure 4, and take approximately 9 years between identification of a drug and its large scale use in healthcare.

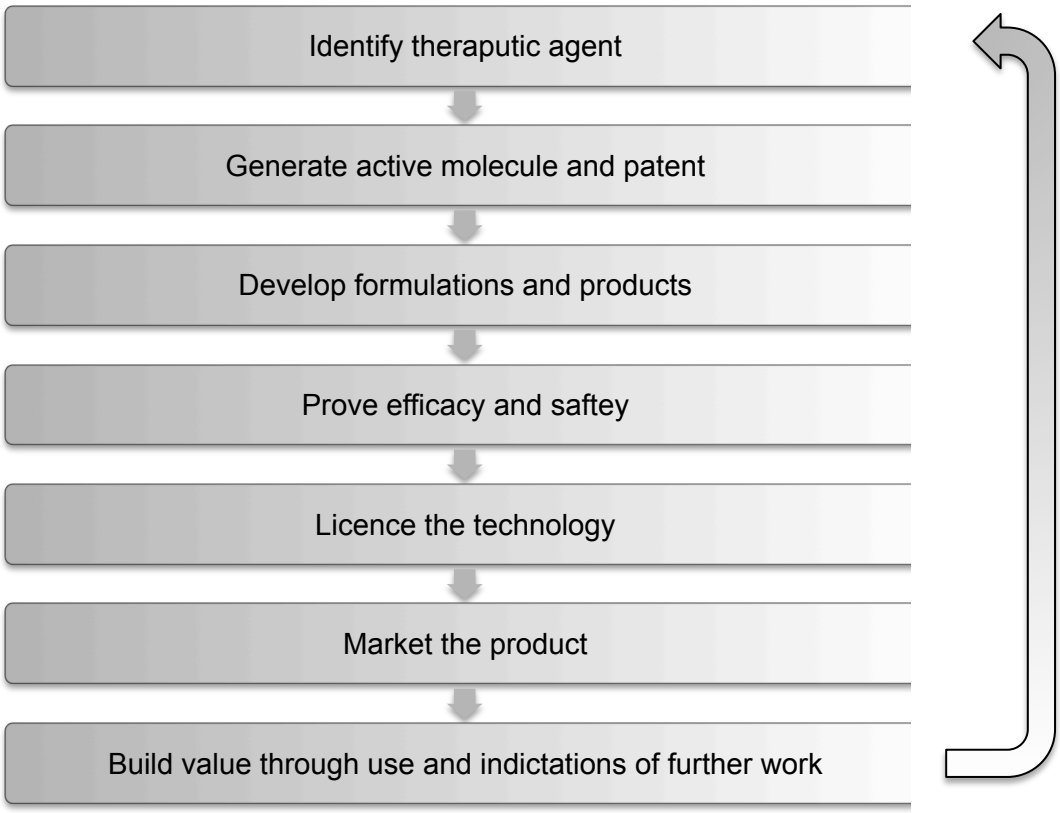

Figure 4 - 7 step diagram showing the development stages of a drug.[19]

When nanomaterials are added into this model, it significantly increases the timeframe of getting the drug to market and therefore there is often only a year or two before the drug patent expires. This therefore greatly limits the profits made by the pharmaceutical company. One way in which the market is bypassing this problem is the formation of many SME's dealing in nanotechnologies and them licensing their technology to larger pharmaceutical companies to get a drug to market, substantially reducing the time and cost incurred by the drug developer.[20] The UK government is also aware that SME's developing new diagnostics and treatments can be crippled by the cost of phase III clinical trials, meaning many, particularly personalised, therapies are never being put into use due to financial constraints. The government is working alongside the EU to support innovative materials and methods to treat, diagnose and prevent terminal or seriously debilitating diseases by fast-tracking these medicines through conditional authorisation or accelerated assessment of products where there are currently no effective therapies.[18]

Not only are the government fast-tracking very promising research in the life sciences but they are also keen to pump money into SME's in the early years when their main

focus is on research and development and therefore their income is limited. This period in a SME's lifetime is often referred to as the 'Valley of Death' and means that numerous potential new therapies are 'dead in the water' before commercialisation is even a possibility. The government's willingness to allocate millions of pounds to life sciences research shows just how important this research is, both for maintaining human life but also by stimulating the economy. Nanotechnology accounts for more and more of the life sciences sector. For example, in drug delivery alone Nanotechnology was forecasted in 2008 to account for 11% of the total market in 2012[20] and the sector is still growing rapidly.

Nanotechnology and its rapid development has had a huge effect on the life sciences and transitioning medicines from a 'one for all' mentality to personalised medicines. Nanotechnology has great potential for many applications in the life sciences, not just drug delivery, including cosmetics, imaging[21, 22], sensors[23], dentistry, and more. The development of nanotechnology over the last 30 years has seen huge benefit to the life sciences and human health and has been gathered together under a new term, nanomedicine.

1.3 Applications of nanotechnology in medicine

Nanomedicine is a relatively new term which covers the medical application of nanotechnology.[24] Nanomedicine covers a variety of materials and structures, many of which existed before the term. Although some nanomedicines have been researched for the last three decades or more, and nanomedicines have rapidly developed in the last decade, many applications still have not made it to regular clinical use[25] because there is a large concern surrounding the toxicity of nanomaterials both long term to the environment and also their effects in the body.

There are 5 main areas of development in nanomedicine that are enabling the development of personalised treatments, biomarkers, miniature biochips and the development of nanomaterials for drug delivery, diagnostics and regenerative medicine. Research into biomarkers has been incredibly important to pinpoint signs the body gives off that a problem exists and therefore detection and treatment is occurring faster and earlier than ever before.

Biomarkers are biological molecules that are found in blood, fluids or tissues in the body that indicate that a particular condition or disease is absent/present or even just signals that a normal or abnormal process is occurring in the body. Biomarkers can be related, but not limited, to DNA, RNA, epigenetic changes, protein and antibody expression. These biomarkers are used in many ways for medical purposes: one important development in using biomarkers is detecting colon cancer by using a biomarker in the blood,[26] as a new 'simple' blood test enhances the patient's compliance over what would previously have involved complex and uncomfortable internal investigations. Biomarkers have also been established both in the blood and in serum both to indicate increased risk of developing cardiovascular disease and also as indicators that a blood vessel leading to the heart is blocked, since identifiable biomarkers are released in the blood.[26] Blood markers for Alzheimer's is also currently being researched to try to diagnose and treat the condition earlier and more efficiently.[27] Research into biomarkers is facilitating faster and earlier diagnosis of many life threatening and life altering diseases helping to prolong life and to maintain a better quality of life for longer.[28, 29,30] One big area of research for biomarkers is that related to cancer. A breakdown of patents currently filed, according to a report by John bates in 2008 can be seen in figure 5.

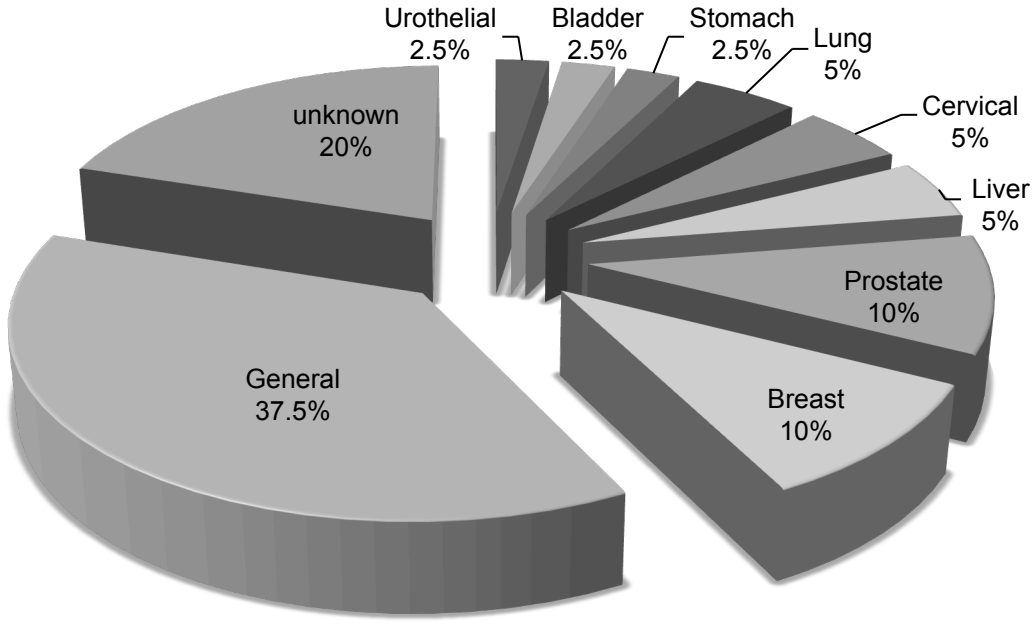

Figure 5 - Biomarker patent filings according to type of cancer.[31]

Much research has also gone into the design and application of biochips. Biochips are essentially a microchip that is, often but not only, designed to work in a biological environment for example inside living organisms. Some of the most well-known biochips are those used to identify animals however, more recently biochips have been developed in medicine, for use in biosensing.[32] One of the first biosensors was for glucose. In this case it was just the probe that was inserted into the body.[33] More recent medical research is an investigation of the incorporation of entire sensors onto a biochip, which would then need to be coated in a biocompatible material in order to protect both the sensor and the person in which the sensor is to be inserted from degradation and leakage.[32]

These developments in nanomedicine are highly significant in terms of the changes in approach, allowing treatments that, before the 'discovery' of nanotechnology, simply would not have been possible. The development of vast numbers of nanomaterials that has dramatically expanded research in nanomedicine, particularly in drug delivery, diagnostics and regenerative medicine.

1.3.1 Drug delivery

Nanotechnology potentially offers major benefits in drug delivery due to the unique properties of nanomaterials. However, due to the extensive testing and research needed to produce drugs, pharmaceutical companies are reluctant to then spend the same amount of time and money on a delivery device, in effect doubling the time and cost needed to produce the drug alone.[19] Drug delivery methods are therefore very much seen as a secondary and conservative area of research. However the delivery of a drug can be fundamental in whether the drug itself is useable and therefore could be the lifesaving ingredient in many cases. For example free drugs are often insoluble in water. This limitation can prevent a drug from being able to be administered altogether. Where the administration of some free drugs is possible the lack of bioavailability often hinders their ability to work to their full potential. Nanomaterials can help overcome both of these issues by making administration of otherwise resistant drugs possible, in addition to making target-specific drugs with controlled or directed delivery and hence improving their efficiency.

1.3.1.1 Traditional delivery methods

There are five major routes for drug delivery, parental injection, oral (absorption through the gastrointestinal tract), transdermal, transmucosal and pulmonary delivery.

Each has its advantages and disadvantages. Delivering drugs via injection, for example, is the most widely used administrative method. However, most of the time it needs to be done by a medical professional, it is not well liked by patients and can cause local damage to the skin and other tissues and runs a minor risk of infection at the administered site. Oral delivery is normally the preferred route for administration but preventing degradation of the drug in the gut/upper GI tract can be a problem when treating cancer of the colon. Oral administration is a preferred route of administration for patients over inserting a lower intestine suppository. Therefore if these degradation problems can be overcome and a delivery system can bypass these two sections without degradation and/or absorption of the drug and then, in addition to these two factors the drug is released directly and only in the colon itself, then there is great potential for application of the system.[19]

Transdermal delivery, through the skin, has been available for the past couple of decades and patient compliance is high as it is painless and user-friendly. This method of delivery is also advantageous as it gives a slow steady release of a drug keeping concentrations in the blood consistent[19]. Limitations relating to skin permeation are a constraint and drug incorporation can itself be poor in patches and creams. If a high concentration of drug is required and required quickly an alternative administrative route would need to be used. Transmucosal delivery can overcome the permeability problems of the skin as buccal mucosa, which lines the inside cheeks, is 40000 times more permeable. Oral, nasal, rectal, vaginal and ocular cavities are all used as routes to deliver drugs and huge amounts of research has been put into each. Saliva is also highly useful for dissolving medications as humans produce between 0.5 and 2 litres every day, which is essentially water based and can be used to hydrate drugs administered through oral mucosa. The last area for drug delivery is directly into the lungs, pulmonary delivery, which have a huge surface area allowing for good drug absorption and drugs can be self administered. The major challenge in this delivery route is to avoid phagocytosis and other systems protecting the body from foreign bodies. Nanomaterials can be used to help deliver drugs in all of these routes, overcoming the associated issues.

1.3.1.2 New, ‘nano’ delivery methods

Nanotechnology has completely revolutionised drug delivery. For example if a drug was desired to be administered orally (which has the best patient compliance) and the drug was not water-soluble or it could not pass through the lining of the digestive

system, a drug, which had proven efficacy, would have been unusable since getting the drug to the required site was impossible using this administration route. With so much research now carried out at the nano scale, more and more drugs have become available for treatments because nanocarriers can deliver the drug to the target site faster and with pinpoint accuracy[34]. Not only this, such drug delivery devices can help reduce side effects, increase bioavailability by comparison with the free drug and enable more sophisticated treatments than ever before. Examples of nanomaterials and their use in drug delivery are described in section 1.5 of this chapter.

1.3.2 Diagnostics

Drug delivery is not the only application in which nanomaterials are used in medicine. Many nanomaterials are also used for sensing. Early-stage detection and diagnosis of disease-related biomarkers is an important area of research to help to preserve life and the development and functionalisation of nanomaterials is making this a possibility.[35] Biosensing has seen significant changes over the last decade due to the development and integration of nanomaterials. A biosensor is a device that couples the recognition element (a biological receptor) with a chemical or physical transducer, see figure 6. These two elements work together to give a concentration of a target analyte by measuring a biological response.[36] As nanomaterials can be 'tailor-made' for size, shape, surface charge, physiochemical characteristics and even attach polymers or bioactive molecules such as antibodies, increasing their biocompatibility, they have become highly attractive for use in biosensing. Paper-based biosensors are of particular interest due to paper being so cheap and accessible. One of the first and most well-known paper based sensor is the pregnancy test, readily available to all and easy to use as a diagnostic tool, which detects human chorionic gonadotropin produced by a fertilised ovum.[37]

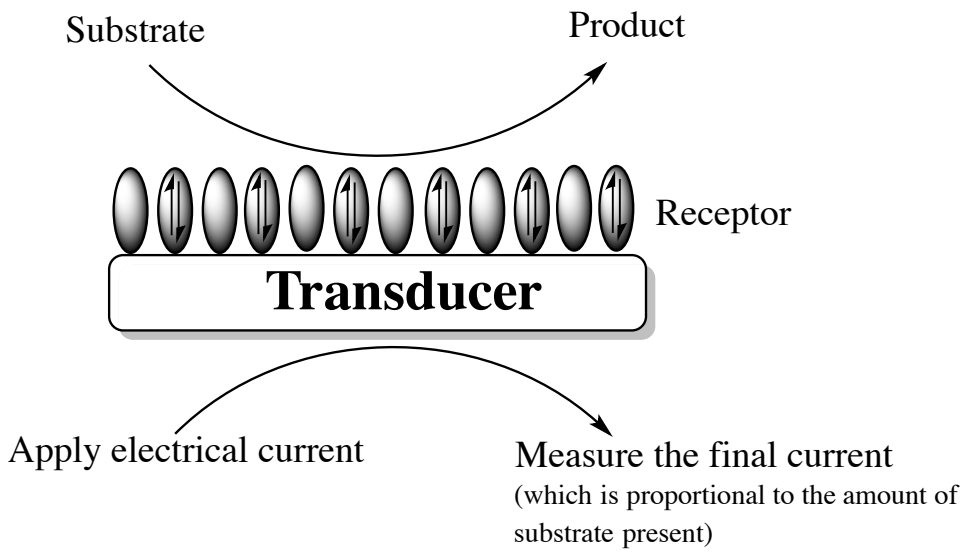

Figure 6 – A diagram to show the basic mechanism of common biosensors.

1.3.3 Tissue engineering and regenerative medicine

Tissue engineering is a relatively new area of research, which essentially follows on from medical treatments such as skin grafts and can now mean like-for-like tissue can be used,[38] speed up healing times[39] and also help prevent tissue rejection.[40] Tissue engineering was first given its name in the 1980's but at the turn of the century another term, 'regenerative medicine' also became widespread.[41, 42] Tissue engineering uses many different methods but the use of biomaterials as scaffolds to support and encourage tissue growth is commonly accepted as one of the most important of these.

There are two man approaches to tissue engineering. The first is where tissue is harvested from the body and the cells are loaded onto biomaterials *in vitro*, allowed to grow and expand on the scaffold, after which the tissue is then replaced in the body and helps to speed up the healing process. The alternative method is to place the scaffold in the body at the site of required regeneration of cells in order to encourage growth at the damaged site. In both cases the biocompatible scaffold decomposes in the body over time, at which point it purpose has been served. The biomaterials used in tissue engineering and regenerative medicine are vast in number and have different characteristics according to the tissue that is in need of repair.[43] In some instances differentiated cells are used that are identical to that of the target site, in others stem cells are used and manipulated to develop into the required tissue.[44]

One area of tissue engineering which is notoriously difficult to achieve, is that of bone regeneration. Saiz *et al* discuss developments in bone regeneration which has been

proven difficult to accomplish. In the paper they demonstrate the need for a biocompatible scaffold, which in turn needs some signals, to promote cell growth and prevent scaffold rejection (often delivered by nanomaterials) before cells are, normally, injected into the scaffold, shown in figure 7.[45]

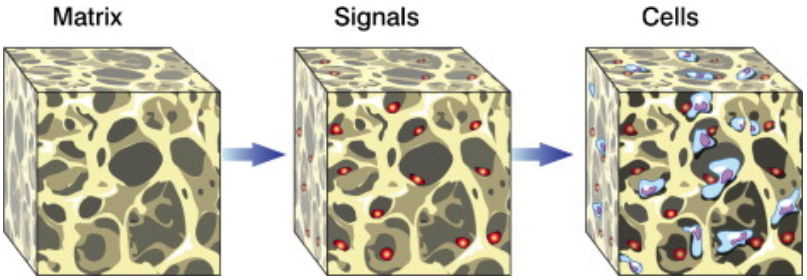

Figure 7- The components required for successful cell growth and bone regeneration.[45]

1.4 Advances in nanomaterials

Nanomaterials are at the forefront of research in nanotechnology and are indispensable in biological and medical applications[46] due to their size and properties. Nanomaterials are "materials (polymers, semiconductors, ceramics, oxides, metals, etc.) with particle sizes in the 1–100 nm range in at least one dimension". Functionalised nanomaterials are completely transforming many areas of science. Indicative of this boom in nanoscience is the fact that between 1990 (when there were zero) and March 2012, 161 Journals covering research in the 'nano' area were created.[47] There are many different nanomaterials that now exist, too many to cover all of them in the introduction of this thesis, however there are three main categories into which most nanomaterials fall, carbon-based, inorganic and polymeric-based nanomaterials. Many nanomaterials use combinations of these materials, and some fall outside of these categories. Here are just a few examples of some nanomaterials and their impact on life science.

1.4.1 Carbon based nanomaterials

Some of the first nanomaterials to be discovered were fullerenes. These were initially discovered by Prof. R.F. Curl, R.E. Smalley and Sir H. W. Kroto in 1985, for which they received the Nobel Prize in 1996.[48] Fullerenes can be in the form of a sphere, ellipsoid or tube that are made wholly of carbon and are hollow. The spherical fullerenes are also known as 'bucky balls', both were named after Richard Buckminster Fuller, who was an American architect,[49] due to their similarity to his geodesic domes. The C60 spherical fullerene is of particular interest in medicine due several potential exploitable

features. One of these is the C60's ability to fit inside the hydrophobic cavity of HIV proteases, which in turn blocks the catalytic enzyme site, inhibiting the substrate. Fullerenes also have the ability to carry genes/ drugs, used in diagnostics and are also able to cleave DNA due to their ability to produce singlet oxygen in the presence of light combined with direct electron transfer from the fullerene and DNA bases excited state. However their solubility is limited, methods such as encapsulation, suspension (using co-solvent methods) and chemical functionalisation have helped overcome this to a certain degree.[48]

Carbon nanotubes were developed not long after the discovery of fullerenes, in 1991.[50] There are two types of carbon nanotubes – single walled carbon nanotubes (SWCNT) and multiwalled carbon nanotubes (MWCNT).[51] SWCNTs are formed from a single graphite sheet rolled into a seamless cylinder and MWCNTs are made up of several graphite sheets each rolled into a cylinder inside one another with differing diameters up to 100nm. The length of the nanotubes can vary from a few nanometers to a few micrometers. Carbon nanotubes can be functionalised covalently and non-covalently to improve their solubility and also have the potential to be used in medical imaging.[52, 53] Carbon nanotubes also conduct electricity which gives them potential as conductive scaffolds, conducting electrical signals across tissue constructs enabling electrophysical functions in certain cells such as neurons and cardiac tissue.[53]

Another carbon based nanomaterial are nanodiamonds. Nanodiamonds are diamond powders that have been formed by detonating diamonds to between 5-100 nm, they vary in their purity depending on how they are isolated from impurities after detonation. Nanodiamonds can be ground through milling and then dispersed in water to form a colloidal solution. Water can then be removed to a greater or lesser extent to form a gel of the required density. Even if almost all water is removed (down to 2-3% the nanodiamonds will readily redisperse in water,[54] giving them ideal characteristics for medical applications, the process of formation is presented in figure 8. Nanodiamonds can also be oxidised and carboxylated in strong acid to make them hydrophilic. They can be further functionised either covalently or non-covalently to enable a drug to be adsorbed onto their surface.[55] Nanodiamonds have been explored for use in drug delivery both for the delivery of small molecules such as doxorubicin[56] for cancer therapies and also have shown protein release. Insulin is being investigated as a potential wound healing agent by way of promoting the formation of blood vessels. Insulin has been shown to be released from nanodiamonds at basic pH,[57] which is

often observed when a wound becomes infected by bacteria. Nanodiamonds have also been explored for imaging purposes.[58] Gd(III) is used as a contrast agent providing cells that are similar magnetically but have different histology in magnetic resonance imaging (MRI). When covalently bound to nanodiamonds Gd(III) has shown an almost 10-fold increase in sensitivity over free Gd(III).[59]

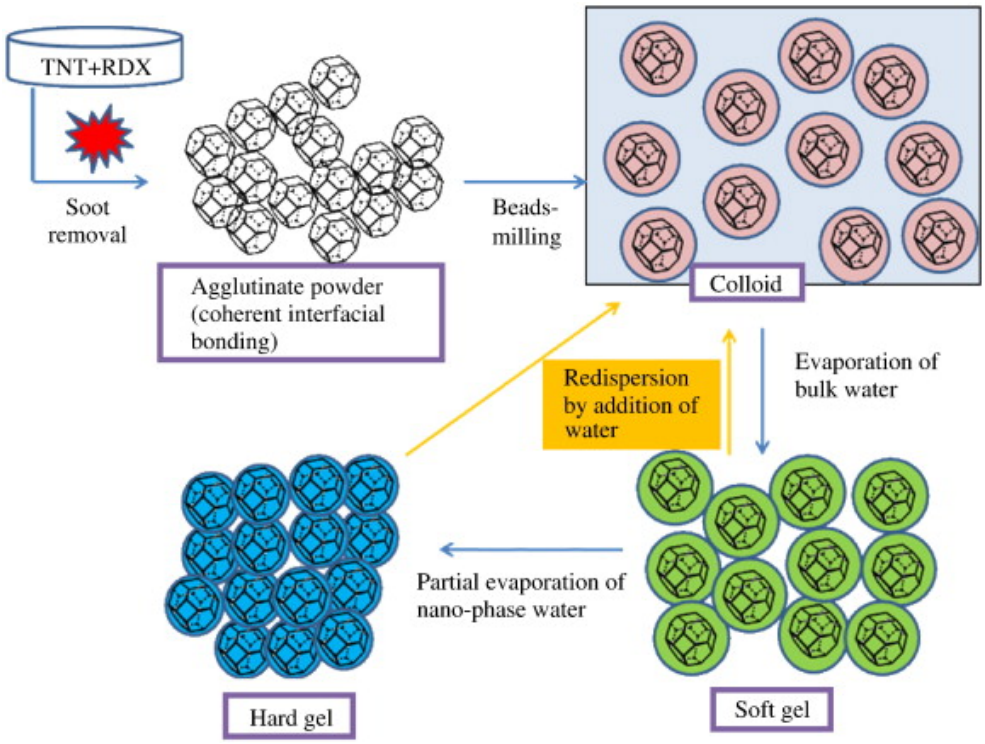

Figure 8 – formation of nanodiamonds and method to obtain a colloidal solution and soft or hard gels containg nanodiamonds.[54]

Although carbon based nanomaterials have shown great potential for medical applications they can suffer from poor solubility and are often found to be quite toxic *in vitro*[59] and are expensive and/or time consuming to obtain. Another set of nanomaterials with promising attributes for use in the life sciences is that of inorganic nanomaterials.

1.4.2 Inorganic nanomaterials

There are many different inorganic nanomaterials. One type which has shown great promise in advancing medicine is silicon-based nanoparticles. Silicon oxides are the main component of both sand and quartz and make up for 90 % of the earth's crust. It's high availability and therefore low cost along with the unique chemical and physical properties of silicon-based materials means it has been used in many applications from

construction and electrics to food and biomedical science.[60] One example of how silicon has been exploited using nanotechnology is its use in NanoceuticalsTM Microbright tooth powder. This commercial product contains nano-scaled molecular cages (1-5 nm in diameter) made of silica-mineral hydride that reduces acid that remains on the teeth from food and therefore helps to protect the enamel.[60] Mechanised mesoporous silica nanoparticles (MSNPs) have a high surface to volume ratio giving a higher surface functionalisation whilst having great porosity in which a significant amount of material can be carried whilst maintaining its stability.[61] One way in which these NPs are formed is to use a cationic surfactant as a micellular template and then condense silica around the template before removing the template to give porous particles of between 50 nm and 2 μm. The NP's can be functionalised during formation or surface functionalised afterwards. Drugs can be loaded into the porous structure and functionalisation of the MSNPs can allow targeted delivery of a drug.[61] However some studies have found some silica NPs to be toxic *in vitro*, with indications that the smaller the size and the higher the dose (up to 1 mg/ml was tested) the higher the cell mortality rate.[62]

Another well established type of inorganic NPs are gold nanoparticles. Au NP's have different properties at the nanoscale compared with bulk gold due to their size and shape. Metal NP's in general exhibit unique electronic, catalytic or optical properties depending on the metal and size of the core. Gold is of particular interest due to its localised surface plasmon resonance (LSPR), which is where the conduction-band electrons in the metal coherently oscillate when exposed to an incident light. This results in strong absorbance and scattering of the light and in the case of gold the light is emitted in the visible region when the Au core is between 3 and 200 nm in size. This gives Au NP's great potential in colorimetric sensing applications and as biological contrast agents. One example where Au NP's have been used for DNA detection is where the gold NP's have been functionalised with a single strand of oligonucleotide. These Au NP's have shown to be an effective diagnostic for *Escherichia coli* present in human urine. The NP's turn the solution red if it is present, and aggregate forming a purple solution if it is not, with a sensitivity of 54 ng.[63] The LSPR of gold NP's can also be tailed to the near-infrared region meaning they have potential application in *in vivo* imaging and photothermal treatments.[47]

Some of the most reported inorganic nanoparticles are mainly composed of silica or alumina, although the core can contain metals, metal oxides and metal sulfides. Due to

all the possible variations (size, shape, porosity etc) in inorganic nanoparticles an immeasurable number of different nanoparticles can be formed which gives them great potential as drug delivery aids. For example it has been shown that ibuprofen can be taken up by the mesoporous silica based molecular sieve MCM-41 (Mobile Crystalline Material 41) and released into body fluids after 3 days, controlling the drug's release.[64] SEM and TEM images of these can be seen in figure 9. Inorganic nanoparticles tend to be very stable across a broad range of temperatures and pH, however they do not biodegrade and have slow dissolution rates which causes concern for long term administration.[65] Some nanomaterials which have very rapid dissolution rates are polymeric-based nanomaterials formed via microemulsion.[66]

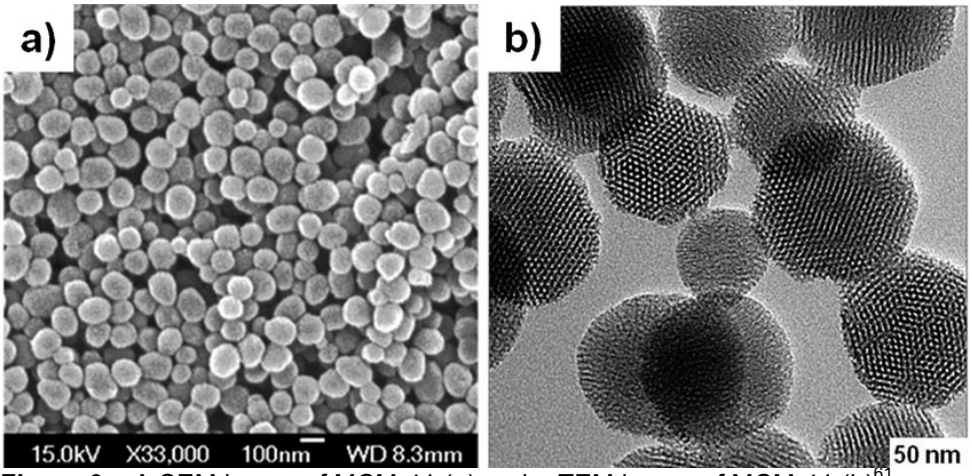

Figure 9 – A SEM image of MCM-41 (a) and a TEM image of MCM-41 (b)[61]

1.4.3 Polymeric-based nanomaterials for use in nanomedicine

Polymeric nanomaterials formed via oil in water and/or water in oil microemulsions can contain lipids, polymers and/or surfactants and have been developed for many applications. One such nanomaterial are solid lipid nanomaterials (SLN) these can be formed by using a lipid with a low melting point and forming a warm oil in water emulsion. The lipid can be loaded with an 'active' (such as a drug or tracking agent) either throughout the matrix, shown in figure 10, or in the lipid core or shell depending on how the SLN is formed.[66] Solid lipid nanoparticles can have a hydrophobic lipid core (which remains solid at both room and body temperature) with a monolayer of phospholipids surrounding them. These nanoparticles are prevented from aggregating by the addition of surfactants. The release profile of the active payload can be controlled by how much surfactant is incorporated into the nanoparticles when they are formed. Solid lipid nanoparticles biodegrade easily and are therefore less toxic than

some other nanoparticle formats.[65] SLN have been used for different applications in nanomedicine, one of which is drug delivery. Shuhendler *et al* have also found that by using solid polymer-lipid nanoparticles to deliver cancer drugs, doxorubicin and mitomycin C, resulted in a 20-30 fold decrease of drug that was required in comparison to the free drugs.[67] SLN's have been shown to increase absorption of drug when administered orally, increase drug circulation time and also increase the amount of drug crossing the blood brain barrier (BBB).[68] SNL have not only been used for drug delivery but have also been exploited in medical imaging. SLN's were developed by Gasco *et al* for use in imaging, enabling contrast agents to cross the BBB that normally do not, allowing MRI scanning of the brain.[69]

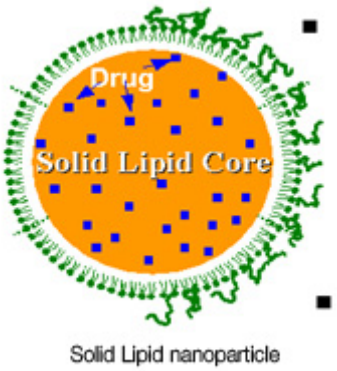

Figure 10 - A diagram of how a drug is incorporated into a solid lipid nanoparticle.[70]

Micelles and vesicles are all self-assembling polymeric nanomaterials, which have been developed over several decades. Micelles are normally formed from block-copolymers,[71] which form a monolayer with a hydrophilic head in contact with water and the hydrophobic tail, which can incorporate a hydrophobic active, on the interior, demonstrated in figure 11. An example of this are sterically stabilised micelles (SSM) which were developed to carry poorly soluble Camptothecin.[72] Micelles which are formed from synthesized co-block polymers vary in size and shape depending on their structure and the method used to form the aggregates.[73] Micelles have been evaluated for their use as permeable membranes, where co-block polymers have previously shown great potential in gas permeation and fuel cells amongst other applications. More recently micellula membranes have been formed which have acute pore size distribution and can respond to pH and temperature changes.[74] Other applications of micelles include 2D/3D coatings,[75] detection,[76] imaging[77, 78] and of course drug delivery.[77, 79-81]

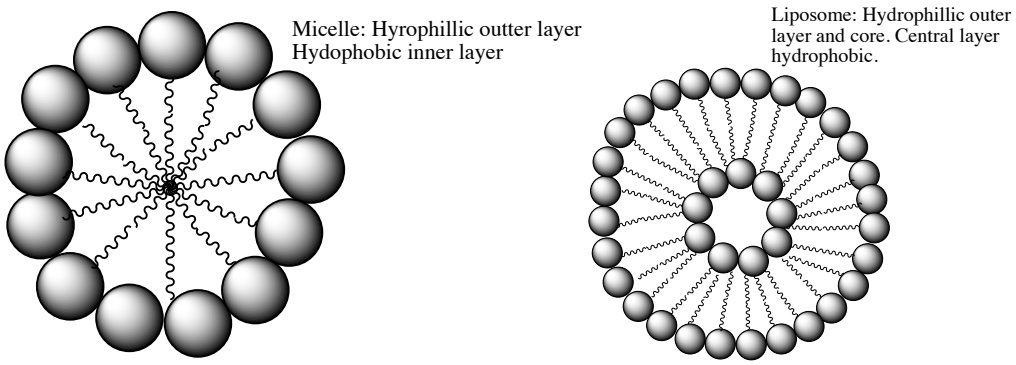

Figure 11 – Structure of a micelle and a liposome.

Liposomes are related to micelles in that they self-assemble, however unlike micelles liposomes have a bilayer, which has hydrophilic heads both inside and out and a hydrophobic layer in between the two, shown in figure 11. Liposomes are often formed from polymers and phospholipids.[82] Hydrophilic compounds can be retained in the centre of the liposomes or hydrophobic compounds can be contained within liposome wall, but these can escape encapsulation by diffusing through the phospholipid membrane.[82] Liposomes are biocompatible vesicles therefore have good potential for medical applications. One area of great interest with liposomes is drug delivery due to the potential of liposomes to increase the circulation life of proteins and peptide. Inclusion of these molecules is made possible due to their amphiphilic nature and their ease of surface modification.[65] Mirahmadi *et al* investigated using liposomes as potential carriers for cancer drugs to treat peritoneal carcinomatosis and were found to be 15.51 times more effective than the free drug.[83] Some lysosomes have been modified with polymers[84] and other substituents to help improve drug targeting and release,[85] nutrient sensing, signalling and metabolism.[86]

Another polymeric based nanomaterial with potential in nanomedicine is that of polymeric nanoparticles (PNs). PNs are formed in two ways, either using preformed polymers, or creating the polymer from its basic units, monomers. In the latter case the polymer is formed at the same time as the nanoparticles, using a 'bottom up' approach building the nanomaterial from its building blocks. Using this approach polymeric nanomaterials such as dendrimers and nanogels can be synthesised,[87] each of which have shown promise in nanomedicine. Dendrimers for example are branched polymers that are grown outwards from a central core (or in reverse starting at the periphery and polymerising to the core) to form a 'spherical' polymer. Depending on how many fragments are attached to form the dendrimer, the dendrimer is grown to a certain generation, often to a 3rd or 4th generation (3G, 4G). These have shown promise in for

use as contrast agents in MRI imaging,[88] delivering agents to stem cells to aid their proliferation and differentiation,[89] for use in microbiocides for HIV and STI prevention[87, 90] and also in drug delivery.[91]

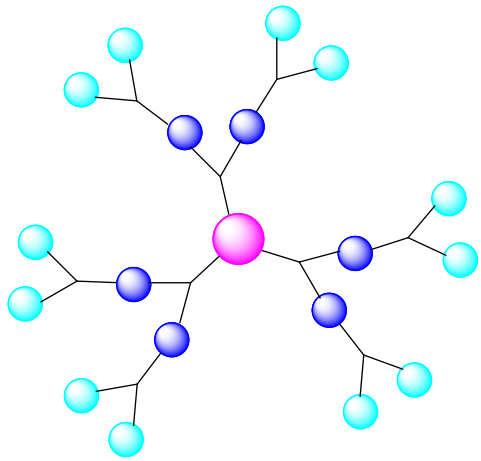

Figure 12 – structure of a dendrimer

Using preformed polymers to create nanoparticle dispersions can also be achieved. In this method the polymers are dissolved in a solvent (such as water) and the drug is dissolved in a solvent, which is immiscible to the first solvent (such as chloroform), an emulsion is then formed either spontaneously (depending on the solvents used and method chosen) or with intense mixing for example with a sonicatior. In some cases nanoparticles remain in the emulsion, in others the organic solvent is removed to leave a dispersion in water (if that is one of the original solvents) and finally both solvents can be removed (for example by freeze drying or spray drying the emulsion),[92] leaving a solid which when re-dispersed in water gives a nanoparticulate solution. These all produce particles where the active is suspended in a solution stabilised with polymers and surfactants to prevent the particles from aggregating.[93]

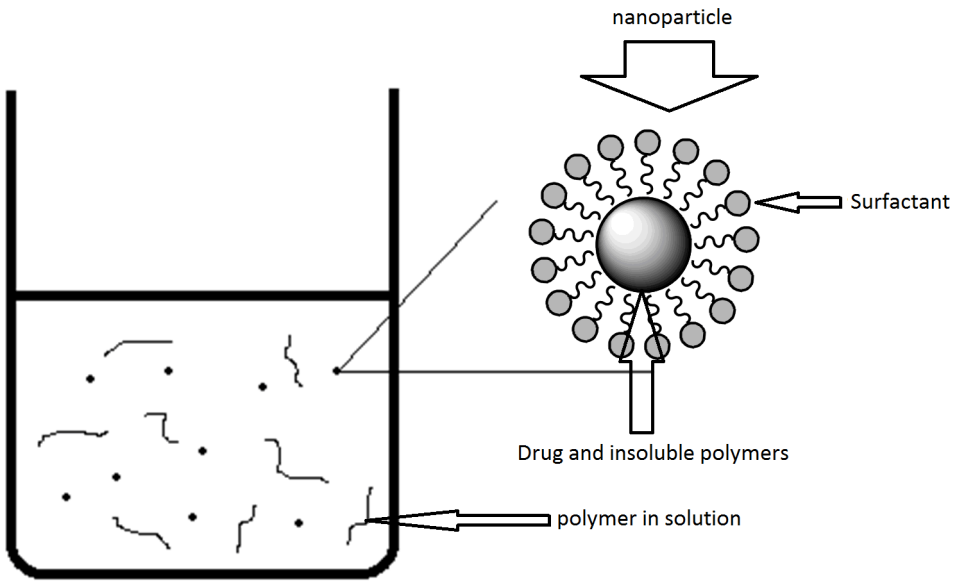

Figure 13 - How organic nanoparticles are stabilized when they are re-dispersed in water.

Another method involves monomers, such as methyl cyanoacrylate, being dispersed in an acidic aqueous medium with a surfactant and no initiator. This dispersion is added to an aqueous solution of surface-active agent containing the active ingredient and stirred vigorously to induce polymerisation. This gives mixed particles of active and polymer. The mixture is centrifuged to remove the surfactant and any excess of monomer or active.[93] These polymeric nanoparticles have been developed for use in biomedical imaging[94] and drug delivery.[95] Many of these nanomaterials have shown potential application in drug delivery due to their unique properties.

1.5 Nanoparticles and their use in drug delivery

Drugs have obvious benefits for improving and sustaining life and much research has been carried out to develop more and more drugs to combat an ever increasing number of illnesses. However, many drugs produced, although proven *in vitro* to have positive effects in fighting the disease, have difficulties when administered to the body. For example some drugs are not water soluble and therefore injecting them into the body becomes very difficult. Other drugs can be administered but once in the body have poor bioavailability. In order to compensate for the lack of uptake of the drug the patient is in effect given an overdose of the drug to ensure enough of the medicine is present within the body to obtain the desired effect on the diseased tissue. It is therefore becoming increasingly important to find not just new drugs but also new delivery methods which can overcome these problems that hinder otherwise very

promising medicines. Due to this gap between possibly life saving treatments and the ability to deliver them effectively to the body huge efforts have been put into generating synthetic materials, such as micelles and polymer nanoparticles.

Materials for drug delivery are normally considered to be suitable if their size is ≤200 nm due to the width of microcapillaries in the body.[96] This allows the drug to be carried in the blood stream to any location within the body. Most research in this area has been focussed on naturally and synthetically derived polymeric nanoparticles due to their high stability and because surface modification can be carried out easily. Different polymer nanoparticle formats have been or are being developed to exhibit different required properties such as controlled release, sustained release, disease specific localisation, to accumulate at specific site (for example in tumours), improve bioavailability and/or solubilise drugs for systemic delivery.[19, 96] Nanoparticles have advantages over microparticles in drug delivery due to their small size. Nanoparticles are not only taken up by cells more efficiently but are also taken up by a wider variety of cells and intracellular components more than microparticles. Nanoparticles also open up the possibility of carrying drugs to difficult locations in the body such as crossing the blood-brain barrier. [96]

Once the drug has been loaded onto the nanoparticle and been delivered to the required site it is important that the carrier is then degraded or excreted from the body. This is to avoid the nanoparticles from building up inside the body, where they may become toxic over time and cause problems in the long term, particularly in drugs that are administered over a prolonged period. Biodegradable polymers for drug delivery systems have been researched for several decades. These are often polymers that degrade or are catabolised down to carbon dioxide and water by naturally occurring microorganisms such as bacteria and fungi.

Nanoparticles have great potential in nanomedicine for controlling drug release, targeting drugs to specific sites and also protecting labile molecules from degrading (such as proteins, peptides and DNA).[96] Drug delivery systems consist of a nano-matrix, which acts as a delivery system by dissolving, entrapping, adsorbing, attaching and/or encapsulating the drug. Each type of interaction has its advantages and each delivery system is constructed to give different properties and release mechanisms in order to achieve the best or most suitable delivery or encapsulation of the particular drug.

There are many nanomaterials that are in various stages of development and licenced for drug delivery purposes, some of the most important discoveries, as reported by the Institute of Nanotechnology in 2008, are shown in table 1.

Nanomaterial	Drug	Applications	Prooduct names
Dendrimers	Astodrimer sodium	Microbicide	Vivagel
Liposomes	Doxorubicin	Breast cancer	Doxil
	Daunorubicin	Anthracyline antitumor antibiotic	DaunoXome
	Amphotericin B	Fungal infections, *Cryptococcal* Meningitis in HIV-infected patients	AmBisome
	Amphotericin B	invasive aspergillosis	Amphotec
	Prostaglandin E1	Vasodilator and platelet inhibitor	liprostin
	Vincristine	Acute lymphoblastic leukemia,	Marqibo
	Paclitaxel	Anticancer drug	Taxol
	Canfosfamide	Ovarian cancer and non small cell lung cancer	Telcyta
	Paclitaxel	Anticancer drug	Taxosomes
	Docetaxel	Anticancer drug	ATI-1123
	Docetaxel	Anticancer drug	Taxotere
Micelles	Paclitaxel	non small cell lung cancer	Genexol
	Paclitaxel	Breast cancer	Nanoxel
	Estradiol	Menopausal hot flushes	Estrasorb
	Cisplatin	Pancreatic cancer	Nanoplatin
	N/A	Anti-viral	Nanoviricide
	Insulin	Diabetes	Basulin
Nanocrystal	Sirolimus	Immunosuppressant	Rapamune
	Aprepitant	Prevent nausea/vomiting side effects of chemotherapies	Emend
	Fenofibrate	Reduces cholesterol	TriCor
	Megestrol acetate	Helps gain weight	Megace ES
	Amphotericin B	Invasive fungal infections	Abelcet
	Fenofibrate	Reduces cholesterol	Triglide
	Cyclosporine	Immunosuppressant	Bioral
Nanoporous silicon	32-Phosphorus	Brachytherapy	BrachySil
Nanopowder	Gentamicin	Inhalable antibiotic	NanoGENT
Polymer nanoparticles	Camptothecin	Anticancer drug	IT-101
	Paclitaxel	Breast cancer	Abraxane
	Miconazole	Antifungal	Loramyc
	SiRNA	Solid tumours	CALAA-01

Table 1 - Licenced nanotechology enabled drugs and applications that were in development in 2008.[19]

As can be seen the majority of currently licenced nanomaterials are polymeric based, this being due to their high biocompatibility and ease of modification. As mentioned above, creating a drug delivery system is useful for many different reasons including

increasing bioavailability, controlling drug release, targeting drugs to specific locations and overcoming solubility or patient compliance issues. However, before a delivery system can be used in a clinical setting, gathering knowledge on the safety and efficacy of the nanomaterial over free drug alternatives is legally required. In order to do this being able to monitor a drug delivery system *in vitro* and *in vivo* is of high importance.

1.6 Monitoring NP distribution (imaging of NP's)

Multifunctional nanoparticles are of high interest in nanomedicine with the distinct advantage of being able to deliver a drug whilst monitoring the nanoparticle's dissemination and localisation within the body. Thus drug delivery systems, which can improve pharmacokinetics of a drug, while controlling the drug's release rate and location, all with the ability to track the delivery system anatomically are sought after.[97]

For imaging, the agent used is required to provide a high signal to noise ratio, be active in biological media, and have good pharmacokinetic/pharmacodynamic behaviour to enable prolonged viewing where required without compromising the performance of the tracker.[98] To track nanomaterials different methods are utilised, and the ability to track them is especially relevant when researching their ability to target specific locations in the body. Tracking nanoparticles has enabled imaging of specific diseased tissues such as tumours,[99] liver fibrosis,[100] and inflamed cardiovascular tissue.[101] One method by Rolfe *et al*, which has enabled targeting nanomaterials to melanoma cells and imaging them via ^{19}F MRI (magnetic resonance imaging). There is minimal fluorine occurring naturally in the body and therefore detection of the fluorine moieties gives excellent signal with almost zero background noise.[98] Although targeting the nanoparticles to specific tissues can increase concentrations of the ^{19}F at target locations, making detection easier, using ^{19}F for imaging has shown to take several hours scanning time and therefore using this technique for some things such as imaging of blood pooling, would not be suitable.[102]

Another agent used for tracking nanomaterials is that of quantum dots (QDs). Quantum dots are made of semiconductor materials (such as CdSe/ZnS)[103] or materials whose fluorescence is related to their size and shape, with the intensity of fluorescence increasing as size decreases. Quantum dots consist of just a few hundred or thousand atoms and are just 2-10 nm in size, which is similar to the size of large proteins.[104] This small size gives them several benefits such as the ability to swap with both inorganic

and organic nanoparticle cores to study the behaviour of the material in question. QDs can also be incorporated into much larger nanomaterials without having a substantial impact on the carrier, enabling monitoring of their intracellular movement and distribution. Not only this but QDs can also be used for mimicking release from a nanomaterial to show distribution and final clearance of a potential drug.[104] However quantum dots, such as cadmium based QD's, have shown to have high levels of toxicity, giving them limited direct use in drug delivery.

Fluorescence itself is a highly utilised agent for tracking and imaging nanomaterials. Fluorophores are molecules that contain aromatic regions, which, when excited at specific wavelengths fluoresce. Fluorophores have many advantages including high sensitivity, robustness, ease of use, and they have undergone significant use in past and current research, continually enriching our knowledge of their potential and characteristics.[105] Many different fluorophores and incorporating techniques have been used to load the fluorophore onto respective nanomaterials. One such approach is that of aggregation induced emission (AIE) where the fluorophore gives off strong emission when it is in high concentration encapsulated in the nanomaterial, however once it is released from the nanomaterial it is highly diluted and a signal can no longer been seen.[106, 107] This is the inverse of many organic fluorescent molecules which can suffer from aggregation-caused quenching (ACQ) where they show high fluorescence at lower concentrations.[108] In the case of AIE fluorophores highly fluorescent nanoparticles can be obtained by encapsulating the fluorophore in high quantities in the matrix of the material. Such nanoparticles have the advantage of high fluorescence emission, ease of production and low toxicity. Their disadvantage is that they can have quite high particle sizes of 400-600 nm[106] which would be too big for use in drug delivery. Because of the latter characteristic, the impact of the fluorophore on the nanomaterial should be carefully considered.

In a very different approach Wang *et al* conjugated a fluorophore to their co-block polymers with which they formed micelles. The fluorophore used significantly amplified its fluorescence in environments with lower pH (present in tumour cells) thus enabling visual detection of tumour sites by contrast with healthy tissues.[109] By conjugating the fluorophore to the nanoparticle, it is possible to prevent bleeding of the fluorophore from the nanoparticle, which is of high importance when using the fluorophore to track the nanoparticle distribution.[110]

The quantum yield of a fluorophore is an important measure to consider when incorporating one into a nanomaterial as a fluorescent tracer. Strong emission is required to be able to detect the fluorescent tag at low concentrations. The quantum yield of a fluorophore can be obtained by measuring the number of photons emitted and the number of photons that are absorbed and dividing the first by the latter[111]. Therefore if a fluorescent molecule was 100 % efficient every photon absorbed would result in a photon being emitted and fluorescence being seen. However even molecules with a quantum yield of 0.1 are considered to be relatively fluorescent.

Photobleaching is also an important phenomenon that needs to be evaluated when choosing the molecule to be used for a specific application. Photobleaching occurs during the observation of almost all fluorescent molecules. It is where an irreversible photochemical change takes place in the molecule preventing it from fluorescing any more.[112] How the photochemical change takes place is not established, although one theory involves interactions between excited fluorophores and other molecules in the local environment. Fluorescence occurs when a fluorescent molecule is illuminated at a certain wavelength, its excitation wavelength, which is peculiar to each fluorescent molecule. An electron is excited from the ground state energy level (S^0) to the excited state energy level (S*). The excited electron can then either return to the ground state via the release of a photon – which is seen as fluorescence, or via an intersystem crossing where the electron moves to the excited triplet state (T*), this radiationless transition can give rise to phosphorescence which has a much longer life time, milliseconds, rather than nanoseconds, which is true of fluorescence. This is due to the transition from the T* state to the S^0 state being “forbidden,” therefore kinetically unfavoured and in turn taking much longer to occur.[112]

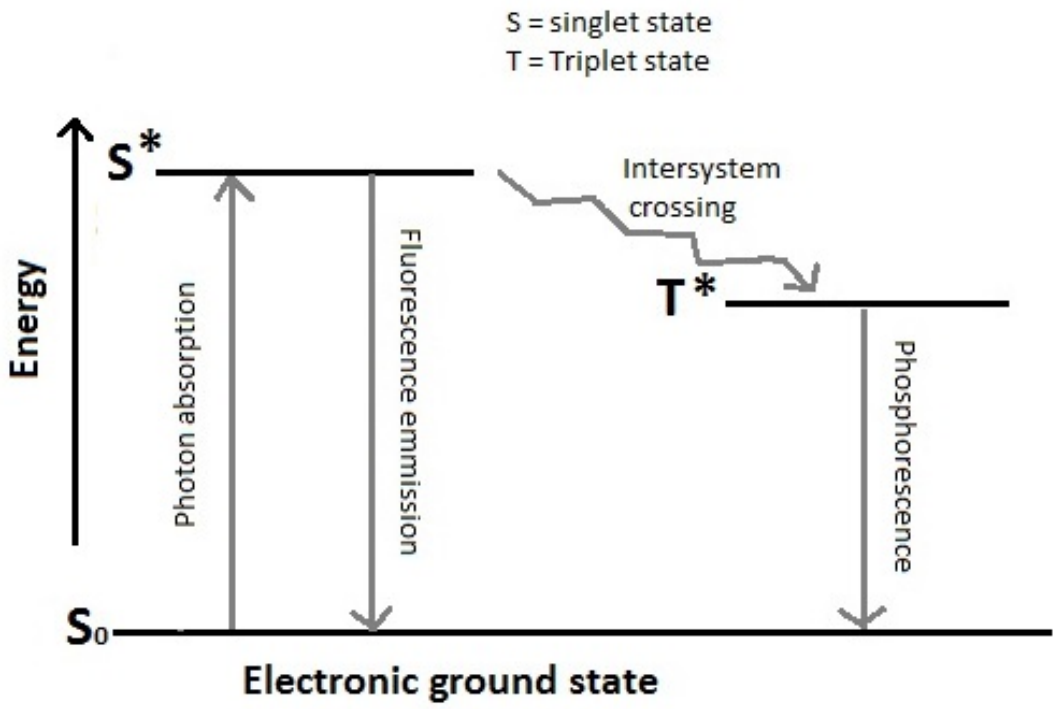

Figure 14- This Jblonski diagram represents the movement of excited photons, which release of fluorescence or phosphorescence on their return to the ground state.

If a molecule has a high quantum yield for intersystem crossing then more molecules are likely to cross from the S* excited state to the T* Triplet state. When in the T* triplet state the molecules interact with their environment for a much longer period of time, compared to those which remain in the S* before returning to S^0. Therefore it is possible that due to the molecule being highly reactive when it is in the excited triplet state it may undergo irreversible reactions with molecules in its environment, preventing anymore photons from being emitted. It is therefore highly likely that both the fluorescent molecule and its environment have an effect on how many photons are emitted before the fluorophore is destroyed.[112] It follows that fluorophores that suffer heavily from photobleaching should be avoided in order to prevent undesired loss of fluorescence.

The properties of a fluorophore need to be carefully considered and their impact on the nanoparticle matrix should be taken into account. The size of a nanoparticle in nanomedicine is key and should be taken into consideration when incorporating the fluorescent tag into the nanogel matrix. For drug delivery the desirable particle size depends on the final target, however particles below 200 nm are more suitable[95] to ensure passage through capillaries.[96] Particles below 5.5 nm in diameter should be

avoided as work by Choi *et al* found particles of this size were rapidly cleared by the renal system.[113] Having a narrow distribution of particles sizes is also important as large size variations can have a negative impact on pharmacokinetics. This is because different sized fractions will release their drug payloads at significantly different rates.[95]

The impact of the morphology of the nanoparticle matrix is not the only characteristic to consider. Although the use of fluorophores is wide-spread in nanomedicine ensuring the fluorophore is chemically bonded to the nanoparticle is essential, as leaking of the fluorophore from the nanoparticle is common,[110] at which point the fluorophore loses its purpose. Another advantage of using a polymeric-based nanoparticle is that there are many fluorescent monomers commercially available and/or synthetic procedures already established to modify other fluorescent molecules into polymerisable equivalents, thus enabling easy addition of a fluorophore to a polymer matrix with a strong covalent bond.[110]

Using nanomaterials to aid the delivery of drugs clearly has many advantages and is a fast growing and popular area of pharmaceutical research. Polymeric-based nanoparticles have shown great promise with respects to their biocompatibility and ease of modification, this combined with the excellent features of fluorophores to enable a drug delivery system to be continually monitored whilst delivering a drug load make them an ideal combination for creating a multifunctional drug delivery system. It is in this specific context that this thesis has been developed.

1.7 Aim and objectives

The aim of this project is to synthesise novel polymeric nanoparticles characterized by low toxicity and tagged with a fluorescent label that will allow in vivo monitoring of drug delivery. The work was organised in 3 main objectives:

1. Synthesis and characterisation of the fluorescent nanoparticles.
2. *In vitro* and *in vivo* toxicity studies, using zebrafish.
3. Preliminary evolution of drug uploading and release both *in vitro* and *in vivo*.

In order to simplify the discussion of the results, each objective is covered in a dedicated chapter, here below summarized.

Chapter 2 focuses on the development of a novel drug delivery system based on organic polymeric nanoparticles using high dilution radical polymerisation. Different fluorescent labels, were evaluated and their polymerisable derivative prepared. The chemical structures of the labels were confirmed by ^{1}H-NMR and ^{13}C-NMR. The incorporation of the fluorescent labels into the nanogels was analysed and their impact on the morphology was evaluated. The nanogels were further developed, by altering the polymerisation parameters, to obtain the best possible properties for their end application of drug delivery. Coumarin labeled fluorescent nanogels were obtained with good yields, small particle size of <150nm and with sufficient solubility to be taken to the next step. The particle size of the nanogels is characterised by dynamic light scattering and transmission electron microscopy. Incorporation of the fluorescent tags was evaluated by UV-Vis spectroscopy and the fluorescence intensity was monitored via a spectrofluorimeter.

Chapter 3 focuses on the evaluation of the toxicity of the coumarin labeled nanogels. Initially the nanogels were studied for their toxicity in vitro, using several different assays namely Alamer blue, MTT, LDH and cellular uptake. This work was carried out in collaboration with Dr. Diana Velluto at Queen Mary's School of medicine and Dr. Zhu and Claudia Mioa at Cranfield University. Following this work the nanogels were analysed *in vivo,* in *Danio rerio*, better known as zebrafish as the model. The nanogels were administered via two different routes, initially their distribution was evaluated via oral delivery and secondly via intravenous delivery. During these studies the zebrafish were monitored via microscope and confocal microscope and injected using microinjection in collaboration with Dr. Caroline Brennan at Queen Mary's School of

biological and chemical sciences. This work was carried out under my personal fish license (70/24303), Dr. Brennan's project license (70/7452) at the Queen Mary Fish Facility.

The final chapter of the results and discussion, chapter 4, covers the work carried out on the upload and release of tamoxifen both *in vitro* and *in vivo*. Tamoxifen, a therapy used for breast cancer, was loaded into the nanogels using the molecular imprinting approach. Acrylic acid was used to interact with tamoxifen via an ionic bond (analysed via H^1NMR), allowing release at reduced pH, which was a characteristic of cancerous cells. The upload and release of tamoxifen was analysed via HPLC. Finally the nanogels were administered to transgenic *ubi*:switch zebrafish, which triggers a fluorescence change in the fish on exposure to tamoxifen. The fish were analysed for a change in fluorescence using a fluorescent microscope and again carried out in collaboration with Dr. Brennan.

As this project was multi-interdisciplinary in order to facilitate the reading of this thesis a short introduction to specific topics has been included at the beginning of each of the results and discussion chapters.

CHAPTER 2:
Nanomaterial Preparation and Characterisation

2 Nanomaterial preparation and characterisation introduction

This first chapter of the results and discussion will centre on the synthesis and characterisation of fluorescent-tagged nanogels, describing the different fluorophores that were evaluated as well as the synthesis of the nanoparticles, focusing in particular on the optimisation of the polymerisation conditions.

2.1 Nanogels as drug delivery carriers

Although polymeric materials were initially developed in the early 1900's,[114] their potential applications as drug delivery systems have only been studied in the last 20 years, thanks to the significant advances in the area of nanotechnology, in particular nanomaterials, that have led to the preparation of a large number of nano systems.[115]

Among the most interesting ones that have been evaluated in great depth there are, micelles, lysosomes and solid-lipid nanoparticles, all of which are described in detail in the introduction (section 1.4.3). These systems are all characterised by the fact that they are self-assembled systems. All three types of materials offer substantial advantages, such as increasing bioavailability of drugs, increasing drug deposition in diseased tissues and reducing side effects associated with the drug and in many cases the materials have reached the clinical trial stage and commercialisation.[116] Currently approximately 600 clinical trials are being carried out using lipid-particle drug delivery systems[116]. One particularly successful case is that of SP1049C, which is a polymeric micelle formulation loaded with the cancer drug, doxorubicin.[117] SP1049C has been shown to overcome drug resistance in doxorubicin resistant cells and has passed phase II clinical trials and is currently in phase III[118]. However, despite the interesting potential of these self-assembled systems, a number of issues, including physical chemical instability in certain solvent systems and ability to deliver a drug mainly through diffusion remain unsolved, therefore limiting their applications as drug delivery vehicles.[119] This has led to exploration of different materials for use as carriers of pharmacologically active molecules, such as polymeric nanoparticles.

Polymeric nanomaterials are characterised by high stability, as a direct result of the presence of a strong network of covalent bonds. Among these are nanogels, which have particular potential, given their ability to support stable colloidal solutions.[120] Nanogels are commonly defined as polymeric cross-linked particles forming a 3

dimensional network[121] where at least one dimension measures between 1 and 100 nm.[122] It is the ability to cross-link between polymer chains that gives nanogels a significant advantage over simple block co-polymers. No longer relying on self-assembly (section 1.4.3), the stability of these materials is higher due to their cross-links and they have an increased polymer density, as a direct result. The size of polymeric gel can be controlled, from micrometres (microgel) to nanometres (nanogel) by simple alteration of the experimental conditions under which the preparation is made[123]. Nanogels in particular are characterised by a high surface to volume ratio, which makes them very suitable as hosts for molecules. Their large surface area also makes multivalent bioconjugation feasible and biomolecules can be incorporated into their porous interior network.[124, 125] Furthermore these polymeric gels can be prepared to respond to specific external stimuli, that induce physical changes in their structure, by using specific functional monomers. The polymers can respond to changes in pH and temperatures and trigger the relase of the incorporated molecules. This makes them particularly attractive as drug delivery systems.[126]

The first example of polymeric gels used for drug delivery refers to water soluble cross-linked polymers termed 'hydrogels'. Hydrogels were first developed for medical applications by Witchterle and Lím in the 1950's.[127] They used 2-hydroxyethyl methacrylate and ethylene dimethacrylate to form a co-monomer hydrogel. It was these hydrogels that were used for the production of the first soft contact lenses, and due to their enormous commercial success, created great interest in developing the material for other medical applications.[128]

The selection of components used for the nanogel preparation is responsible for its characteristics: the use of monomers with a high degree of hydrophilicity (such as acrylic acid) produces a nanogel with a high affinity for water.[129] This permits the water to seep in between the polymer chains inducing swelling of the polymer. Such nanogels provide an ideal vehicle for drug delivery because the high hydrophilicity of the carrier facilitates administration of otherwise insoluble drugs. Other advantages of hydrogels towards drug delivery include biocompatibility, their ability to be stimulus-responsive and the ease with which they can be chemically modified during polymerisation[129].

A number of different approaches for the synthesis of nanogels have been developed over the past two decades. One method commonly used is precipitation polymerisation. This method involves dissolving the selected monomers in the required

solvent alongside a surfactant, adding them to a flask under nitrogen with an initiator and heating the solution for several hours to initiate polymerisation. The resulting nanogels are, by contrast, insoluble in the solvent used and therefore when polymerisation takes place they precipitate and can be isolated by filtering them off from the solution.[130, 131] This method requires the use of surfactants, such as sodium dodecyl sulfate (SDS), which can be toxic and therefore ensuring their complete removal after polymerisation is a substantial concern before the nanogels can be considered for use in nanomedicine.[132]

One of the most utilized is the inverse micro emulsion method, which has been used to form acrylate-based nanogels. In this example laureth-3 surfactant is used to form water swollen surfactant micelles in the continuous oil phase. All the monomers are dissolved in the aqueous phase and the crosslinking occurs inside the water micro droplets. Shaking the mixture until a single, transparent phase is obtained forms the emulsion. The initiator is injected into the emulsion during removal of dissolved oxygen.[133] After polymerisation, extraction and dialysis are required to remove the surfactant and solvent (heptane). In another system tween 80 and span 80 were used as the surfactants for an inverse emulsion which again required washing with hexane and water as well as centrifuging to remove the surfactants, before the nanogels could be isolated.[129]

The emulsion polymerisation method is reliable and has been used for a variety of applications such as food[134] and drug delivery.[135] However, the use of surfactants is required, an additional component to the polymerisation solution that is bound to have an impact. Surfactants are surface-active agents, which congregate at the surface and interfaces to alter the surface properties.[136] Surfactants are composed of two parts, one which interacts with the aqueous phase, often referred to as the hydrophilic head and the other, which interacts with the solvent, known as the hydrophobic tail. Due to their dual characteristics, these surface active amphiphillic molecules adsorb at the interfaces and can also lead to the formation of micelles in order to reduce free energy of the system.[137] This is because when the hydrophobic section of the molecule is in contact with the water it distorts the ‘normal’ structure of the liquid, increasing the overall energy in the system. By accumulating at surfaces, interfaces and in micelles it minimises the interaction of the hydrophobic section with the aqueous medium, and the liquid can return to the normal structure.[137] This is due to the hydrophobic sections of the surfactant accumulating together either at surfaces or in the formation of micelles

minimising their interaction with the aqueous liquid. This can be seen more clearly in figure 15.

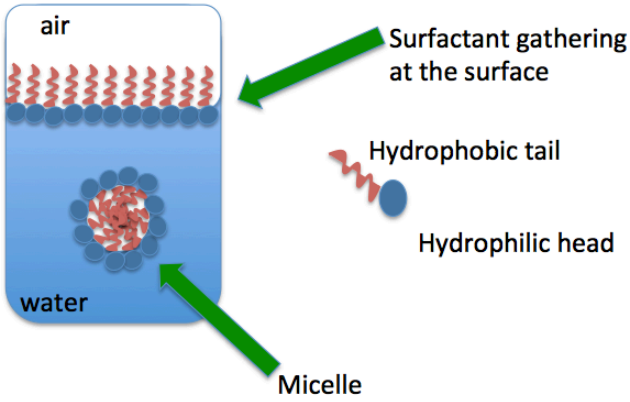

Figure 15 – A diagram of the acumulation of surfactant at the surface and forming a micelle.

Surfactants are well known to stabilise colloidal systems by surrounding the particles with one or two layers of the surfactant, which also prevents aggregation via steric hindrance. Although highly useful in stabilising systems, surfactants can be highly toxic[132] and are an extra, undesired material added to the final product, which can be difficult to remove. In this project it was decided to consider an alternative approach for the synthesis of nanogels: the high dilution radical polymerisation method, which does not require the use of surfactants. The next section will provide more details about this system and how it was applied.

2.1.1 High dilution radical polymerisation

High dilution radical polymerisation or solution polymerisation was initially developed and explored by Graham and his group in 1998.[123] It is based on the principle that a radical reaction at high dilution prevents particle-particle interaction, and therefore inhibits the formation of larger units. The use of high dilution relinquishes the need for surfactants, although the extent of the dilution is dependent on the chemical structure of the monomers used and the solvating power of the porogen in the polymerisation solution. Given a set of monomers and cross-linker, the chosen solvent must ensure that the polymer-solvent interactions are stronger than the intra-polymer attractive forces, in order to prevent the polymer chains contracting and interacting with one another. Linear polymers have a natural tendency to coil, in order to achieve the conformation of lowest energy, and although many different variations occur, the difference in energy between the conformations is so small that the polymer can easily

change from one conformation to another.[138] According to Einstein's viscosity law equation, if the viscosity of the solution is divided by the viscosity of the solvent, the viscosity of the solvent is directly proportional to the volume fraction that the sphere (or in this case polymer) occupies.[139] If a long linear polymer is obtained, when it is solvated the chains interact with the solvent, occupying a larger volume fraction of the solvent, therefore increasing its viscosity. In the case of nanogels, as a result of the presence of intramolecular crosslinking, the nanopolymers cannot uncoil and therefore do not expand in the same way as a linear polymer, meaning they behave more as a sphere and occupy a much smaller fraction of the solvent and therefore have correspondingly little effect on the viscosity of the solvent.[138]

$$\eta_r = \frac{\eta}{\eta_s} = 1 + 2.5\Phi$$ **Equation 1**

Einstein's viscosity law, where η_r = relative viscosity, η_s = viscosity of the solvent, η = viscosity of the solution, and Φ = volume fraction that the sphere's occupy

Although nanogels when formed behave more like 'Einstein' sphere's than a linear polymer, 'dead chains'[123] of polymer will occur in the nanogel, which will help to stabilise the nanogel in solution. This is referred to as the 'auto-steric stabilisation' effect in the literature.[140] When a 'good' solvent for the 'dead chains' at the surface of the particle is selected, the chains will swell and lead to strong repulsive forces between individual particles. If however a poor solvent is chosen, these chains contract, weakening the repulsive forces and giving rise to intermolecular cross-linking and ultimately macrogelation.

The high dilution radical polymerisation methodology has a number of advantages: i) there is no need for the use of surfactants, therefore reducing the number of components in the solution and simplifying the purification step as a result; ii) the reduction in the time required to isolate the polymers; iii) reduced costs; iv) highly homogenous particles sizes with low polydispersity; v) the ability to control the particle size by altering the parameters, giving a highly flexible system that can be tailored to form a nanogel with the desired characteristics.

2.2 Nanomaterial characterisation results and discussion

2.2.1 Choice of monomers, cross-linker and solvent

The polymers developed in this project were intended for use in aqueous solutions, and therefore there was a clear need for monomers that could form polymers that have good solubility in water. Amide bonds have a relatively good affinity to water, due to

hydrogen bonding, and are also abundant in the human body as a result of peptide bonds. Acrylamide (structure shown in figure 16) was therefore selected as the backbone monomer for this work as previous data suggested that acrylamide based nanogels show good solubility in aqueous solutions. The cross-linker is an essential requirement for the preparation of stable nanogels, in order to allow the formation of the three dimensional structure and the specific cavities. The chemical structure of the cross-linker and its proportion in relation to other monomers in the system are also key factors that impact the morphology and physicochemical characteristics of the materials, therefore careful studies were required in each system to identify the most suitable set of conditions. In addition, given that the radical polymerisation is a random process, it was important that the incorporation of the different monomers and the cross-linker in the final matrix reflected the ratios that were used in the prepolymerisation mixture.

Different monomers have different reaction rates, as a result of their varied chemical structures and hence stability of the corresponding radicals, as in the case of a styrene units versus acrylic acid, where the former forms a radical that can be stabilised by resonance. A method to estimate reactivity for a variety of monomers was developed by Alfrey and Price in 1996[141] and tables of reaction rates can be found in the literature. Therefore careful consideration of the structure of co-monomers and cross-linkers should be given when carrying out radical polymerisation reactions. The more similar the chemical structure of the polymerisable unit of the monomers and the cross-linker, the more likely it is that their incorporation in the polymeric matrix will reflect the ratios used in the prepolymerisation solution.

Given the previous considerations, two cross-linkers containing acrylamide bonds were selected for consideration, ethylene bis acrylamide and methylene bis acrylamide, these structures are presented in figure 16.

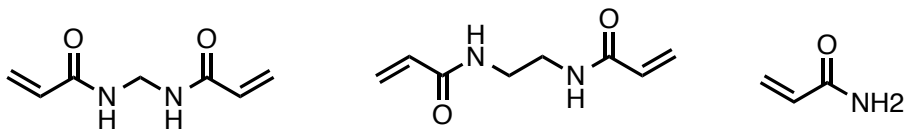

Figure 16– Structures of the cross-linkers MBA (1), EBA (2) and the monomer acrylamide (3).

Past research on the synthesis of nanogels in the Resmini group had primarily focused on their use in catalysis,[142, 143] Ania Servant successfully imprinted a vinyl pyridine-

EDGMA based nanogel, with indole, for use as a catalyst for the Kemp elimination. In this system the rebinding and release of the target analyte was the primary focus in order to facilitate the reaction. In this project the nanogels' application was completely different and therefore their solubility in water had a much higher priority. The substantial change from using methacrylate systems to acrylamide ones should increase their solubility and increase their potential as a drug delivery carrier. Several points, including the ability to solubilise these chosen acrylamide-based monomers need to be taken into consideration when choosing a solvent for HDRP.

CHOICE OF SOLVENT

The solvent should completely dissolve all the monomer components required to form the nanogel, so that a homogeneous solution can be obtained. Given the choice of acrylamide based monomers, a strongly polar solvent was required. Water is an obvious polar solvent, and as the final nanogel was required to be dissolved in water it might on first examination seem like an ideal candidate. However water could cause several problems. Firstly, if a hydrophobic drug is to be uploaded onto the nanogels, it will by its nature not solvate in water. This would prevent interaction between the nanogel and the drug, if the drug is loaded onto the nanogel during polymerisation. Not only this but water is also a protic solvent and could interfere with hydrogen bonding that may be used as the interaction between the drug and the nanogel. Other protic solvents, such as methanol and ethanol, were eliminated for the same reasons, leading to the conclusion that an aprotic polar solvent would be better suited for the purpose. After a number of evaluations DMSO was shown to be a good solvent for the polymerisation due to its highly polar aprotic nature.[144] It was also shown to have the ability to solvate both polar and non-polar compounds, even highly aromatic compounds,[145] enabling both polar monomers and a non-polar drug such as tamoxifen, to be solvated. This solvent had been extensively used in the Resmini group[146] for the preparation of acrylamide based microgels and nanogels. DMSO was chosen as the solvent for this project and preliminary experiments confirmed it to be the most suitable solvent for this type of acrylamide based polymers, allowing the formation of microgels and nanogels in good yields.

Given a set of monomers, the polarity of the solvent will determine the maximum monomer concentration that can be used to obtain micro / nanogels without observing any macrogelation. A plot of the type shown in figure 17, that shows the dependence of the initial monomer concentration on the solvating power of the solvent, measured by

the solubility parameter, can be obtained experimentally. Micro/ nanogels are obtained when the Initial Monomer Concentration (IMC) is below the critical gelation concentration (CGC), while higher values of the IMC will lead to macrogelation. If concentrations of monomer closer to the CGC line are used microgels are obtained, however if concentrations closer to the base line are used nanogels can be obtained.

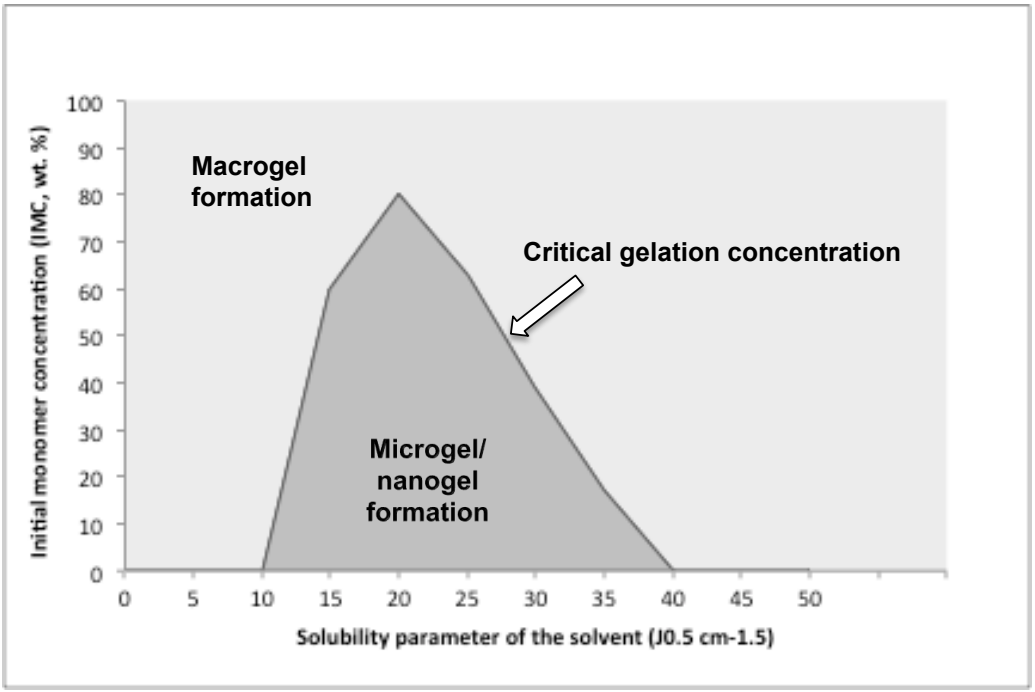

Figure 17- An example of a microgel/ nanogel formation plot.

At the end of the polymerisation reaction, if a micro/ nanogel is formed, the solution appears as a low viscosity transparent liquid, otherwise if high viscous liquid or lumps of gelatinous type materials can be observed, macrogelation has occurred. Even with a relatively high concentration of monomers (C_M) such as 20 %, a free flowing micro/ nanogel 'solution' can be obtained. This so called solution is in fact a colloidal dispersion of polymer nanoparticles, which behave more like Einstein spheres than dissolved linear polymer coils.[123] To analyse this theory three nanogels were set up each containing 80% Ethylene bis acrylamide and 20 % Acrylamide using DMSO as the solvent, the only variable was the C_M, which was set at 2, 1.5 and 0.5%. The gels obtained can be seen in figure 18.

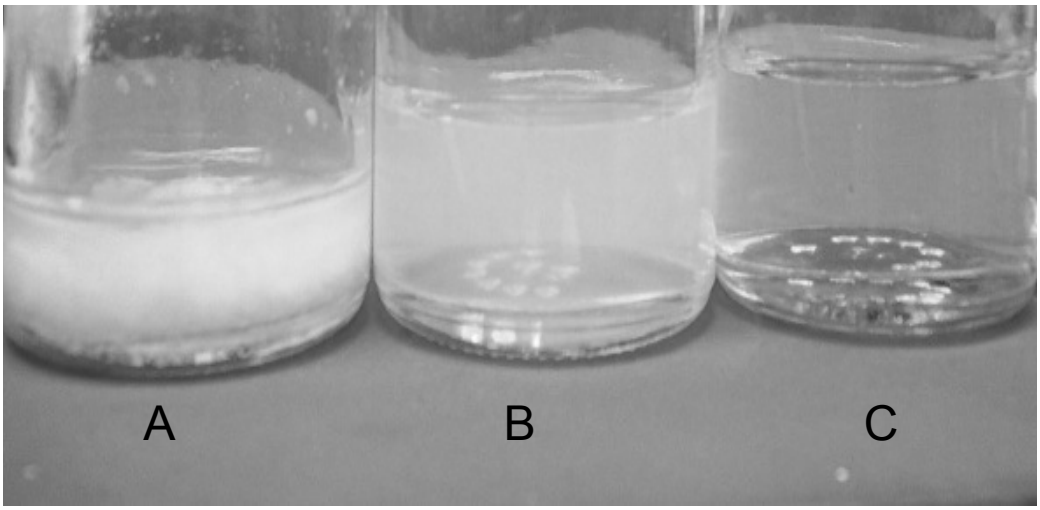

Figure 18 – Photograph of nanogels at different stages of macrogelation, a) macrogelation C_M=2, b) nanogel beginning to macrogelise, lying on the CGC line, C_M=1.5 c) microgel or nanogel, C_M=1.

This experiment showed the C_M needed to be set at 1% or below to obtain micro/nanogels. Another advantage of this polymerisation method is that the size of the particles obtained can be easily controlled by altering the experimental parameters of the preparation. The lower the concentration of monomers (C_M) is kept from the critical gelation limit, the smaller the size of the particles formed and the more homogeneous the preparation tends to be. Using this approach it is possible to form particles of size between 1 and 100 nm, normally referred to as nanogels. Having established the solvent and cross-linker to be used in this nanogel synthesis, focus then turned to the initiator of the polymerisation.

INITIATOR OF CHOICE

In order for polymerisation to take place an initiator must be used to begin the chain reaction. The initiator is required to firstly dissociate into two radicals and then react with a monomer from which the radical can then continue its polymerisation through propagation. The rate of dissociation relies both on the nature of the solvent and the temperature at which the reaction takes place. The dissociation can be triggered by either heat or irradiation such as UV light or γ rays. Initiators for free radical polymerisation require a labile group such as azo (-N=N-) disulphide (-S-S-) or peroxide (-O-O-) group for the dissociation to take place.[147] One well known initiator which thermally decomposes to form cyanisopropyl radicals and release nitrogen gas is 2,2'-azobis(isobutyronitrile), (AIBN, **4,** structure presented in figure 19). This initiator had proven to be very effective in previous research within the group, and was therefore a reliable choice for initiating the polymerisation of the nanogels. The amount

of AIBN added was set at 1% of all double bonds in the prepolymerisation mixture, based on previous work and literature data.[148, 149]

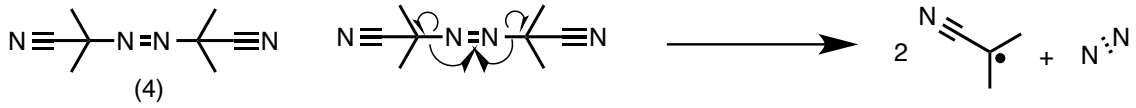

Figure 19– Structure and decomposition of AIBN (4).

The use of AIBN to initiate the polymerisation of acrylamide based monomers in DMSO forms a suitable base on which to develop nanogels as a drug delivery system. However in order to monitor the nanogels during analysis of the material's toxicity, incorporating an agent with which monitoring the nanogels becomes viable is required. It was noted in section 1.6 of the introduction that the use of fluorophores for monitoring nanomaterials is highly utilised, giving vast data on potentially suitable tags with which to tag the nanogels. Therefore identifying a suitable fluorescent monomer was a substantial part of this section of this project.

2.3 Selection of fluorescent monomer

In this section the work carried out for the identification of a suitable fluorescent monomer to be incorporated into the nanogels is described. A fluorescent tracker is required in the nanogel to enable *in vitro* and *in vivo* monitoring of the particles. A number of fluorescent monomers were examined as potential tags for inclusion in the nanogels, via covalent bond during the polymerisation reaction, or uploading post-polymerisation. For the nanogel to be suitable for this purpose the incorporated fluorophore needs to have a reasonable quantum yield to limit the quantity required in the nanogel but still be detectable at concentrations required for administration. The structure of the fluorophore was also important to ensure good incorporation into the nanogel without having a negative impact on the nanogel size, solubility and stability.

2.3.1 Introduction

Section 1.6 of the introduction gave an overview of the important features the fluorescent tag in the nanogel should possess. The fluorescent tag should not significantly alter the morphology of the nanogels as this could impact their solubility and/or stability, seriously limiting their potential applications.

Particle size and distribution of the nanogel also influences the colloidal stability and therefore the overall solubility of the nanogel. Brownian motion occurs in all colloidal

systems and is defined as the movement of particles in a system, whereby the particles move randomly due to collisions between the particles and the molecules in the solvent.[150] When a solution is not homogenously dispersed, smaller particles are attracted to the larger one, destabilising the system and causing aggregation and ultimately resulting in precipitation.[137] One significant feature of a drug delivery system, over a free drug is its ability to deliver a hydrophobic drug in a water-soluble carrier,[151] therefore it is important that the fluorescent tag should not negatively impact on the solubility of the nanogel.

In section 2.1.2 the effect of the chemical structure of the monomers on the polymerisation rate was mentioned. A similar concept also applies to the fluorescent tag. In order for the tag to be incorporated successfully and with the expected monomer-tag ratio, the fluorescent monomer was designed to contain an acrylamide-based group, to ensure that a similar reaction rate to the cross-linker and acrylamide could be achieved. In addition it was important to ensure that the bond between the fluorophore and the polymer matrix was stable under the physiological conditions required for drug delivery to avoid the risk that the fluorophore could become detached from the nanogels during the experiments.

Finally, given that these nanogels would have to be used in experiments *in vivo* using Zebrafish, it was essential to avoid having fluorescence emissions in the two wavelength bands 430-450 nm and 570-630 nm[152] where the zebrafish have a strong autofluorescence.

2.3.2 Dansyl as a fluorescent tag

Initial screening of the literature identified Dansyl as an interesting fluorescent tag. It had previously been used as a fluorescent switch when conjugated to a thrombin binding aptamer (TBA). Thrombin is an enzyme responsible for many homeostasis mechanisms in the body. In particularly it plays a major role in coagulation. Titio *et al* used dansyl and cyclodextrin attached to a TBA to create a dual-purpose thrombin inhibitor which both blocks the binding site and the dansyl fluorephore switches on, creating a fluorescent signal. Dansyl does not inhibit the aptamer by altering its morphology, crucial for rebinding, and the dansyl tagged TBA remains soluble in water.[153] On this basis dansyl was considered a good candidate as a fluorescent tracker for the nanogels.

A dansyl based fluorophore had been previously used in a nanosensor by Arduini *et al*[154] (using dansyl as the sensor for Pb+ ions). In their system the fluorescence was quenched on contact with the lead ions. As dansyl had high enough fluorescence intensity to be used for detection it was thought that this molecule could also have high enough intensity for tracking, and could be applied to our system. Dansyl contains both a tertiary amine group and a sulfide group both of which increase the solubility of the compound. The structure of dansyl is also relatively small and therefore would have less impact on the final morphology of the nanogel. Added to these significant advantages dansyl can be acquired at a low cost and a synthetic procedure for creating a monomer had already been established in the literature. The protocol for synthesising dansyl amino ethylene acrylamide was published by Yin *et al.*[155] The synthesis was obtained in two steps, the reaction scheme is given in figure 20. Initially adding ethylenediamine to dansylchloride, enabed an acrylamide group to be formed at the end of the molecule in the second step. The acrylamide group provides a strong amide bond to the nanogel that would not be cleaved by hydrolysis. The presence of the acrylamide functional group should also ensure a similar reaction rate to the rest of the monomers raising the reasonable assumption that the percentage of tag added to the prepolymerisation system should be similar to the percentage incorporated in the final nanogel. To form the fluorescent tag dansyl chloride was added dropwise to a THF solution of ethylenediamine at 0 °C under nitrogen before being worked up to obtain 89% yield of the yellow product dansylaminoethylamine. Dansylamioethylamide was further reacted with acryloyl chloride in presence of triethylamine in ice under nitrogen and after 24 hours at room temperature the product was isolated via flash chromatography to give a 65% yield of the pale yellow/green solid product, dansylaminoethylacrylamide.

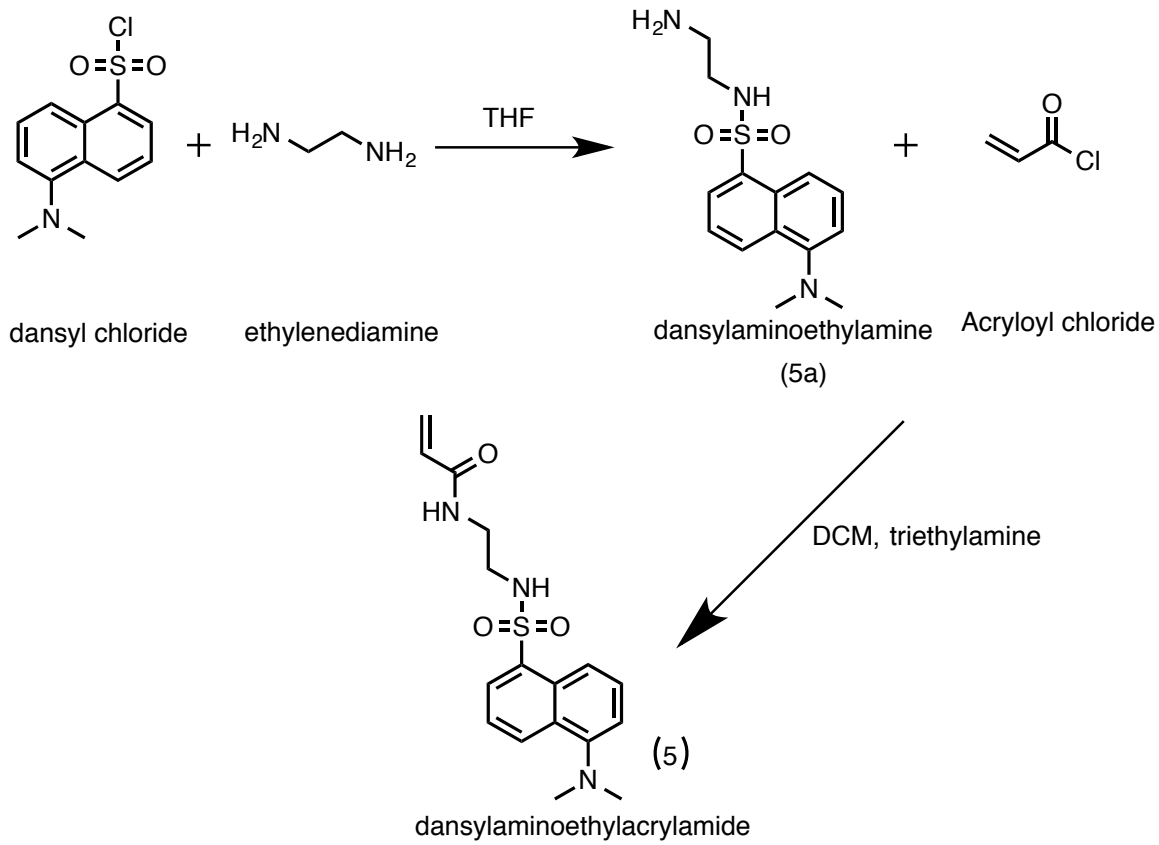

Figure 20- A reaction scheme detailing the reactants required for the two step synthesis to form dansyl amino ethyl acrylamide.

Having successfully synthesised the dansyl tag and characterised it via ^{1}H-NMR and ^{13}C-NMR the tag was incorporated into the nanogel formulation. The amount of dansyl tag in the prepolymerisation mixture was varied from 20 % to 60 % to evaluate how it would impact the nanogel's solubility.

Nanogel	Dansyl monomer (%)	Cross-linker (EBA) (%)	Yield of nanogel (%)	n_{FM} /mg of nanogel (exp) (mol/mg)	n_{FM} /mg of nanogel (theo) (mol/mg)	Incorporation (%)
JRP09	20	80	88	$7.20*10^{-7}$	$9.04*10^{-7}$	80
JRP13	40	60	43	$1.17*10^{-6}$	$1.59*10^{-6}$	74
JRP14	60	40	68	$1.59*10^{-6}$	$2.12*10^{-6}$	75

Table 2 – incorporation results of the dansyl monomer into the nanogel. EBA is ethylene bis acrylamide, C_M: Concentration of monomers. n_{FM}= number of moles. exp = experimental result. theo = theoretical result. The yield of nanogel is the percentage of nanogel collected compared to the mass of monomers put in the prepolymerisation mixture.

2.3.2.1 Stability and solubility of the dansyl tagged nanogels

Three nanogels containing varying amounts of the dansyl tag, **5,** were prepared, namely JRP09, JRP14 and JRP15 (table 2). The first set of experiments concentrated on studying the solubility of the polymers in water, an essential feature given the envisaged application as drug delivery systems. In addition it was important to achieve sufficient solubility to allow the *in vivo* experiments to be carried out using zebrafish as the model. The nanogels were not soluble in 100 % water, however they were soluble in 94% water with 6% DMSO (V/V) at the concentration of 0.01 mg/ml of polymer and in 85% water with 15% DMSO (V/V) at the concentration of 0.1 mg/ml. Although some DMSO was required to completely solubilise the nanogels, the solubility achieved was high enough for initial studies to be carried out. Therefore the quantification of the fluorescent tag into the nanogel was evaluated to ensure a reliable and reproducibly tagged nanogel was formed.

2.3.2.2 Incorporation of the dansyl monomer into the nanogel

The quantification of the fluorescent tag incorporated in the nanogel was important to ensure that it was consistent with the ratio of monomers used in the polymerisation. Quantification was achieved by UV-Vis spectroscopy by using a reference line and the Lambert-Beer law that directly correlates absorbance against concentration at a fixed wavelength.[156] Dansylaminoethylamide was used to create a reference line for the dansyl monomer incorporation rather than the final monomer dansylaminoethylacrylamide, (**5a**) because once the monomer is incorporated into the nanogel the double bond of the monomer ceases to exist and the absorption peak of the molecule with and without the double bond present would be different. Nevertheless a minor error between the precursor molecule (**5a**) and the dansyl tag (**5**) incorporated into the nanogel would exist. Therefore a nanogel solution in DMSO was initially scanned for its absorption wavelength when the dansyl tag was incorporated into the nanogel matrix and then varying concentrations of dansylaminoethylamine were evaluated for their absorbance at this wavelength (339 nm). Three different stock solutions of dansylaminoethyl amine were prepared at different concentrations in DMSO using volumetric flasks. Each solution was cross-diluted three times producing 9 solutions with different concentrations ranging from 0.02 mM to 0.23 mM. By preparing 3 different stock solutions by weight and cross-diluting, experimental errors can be easily identified and corroboration of actual concentrations is easily achieved. The absorbance maximum of each solution was obtained at 339 nm and plotted against the corresponding concentrations of dansylaminoethylamine, **5a**.

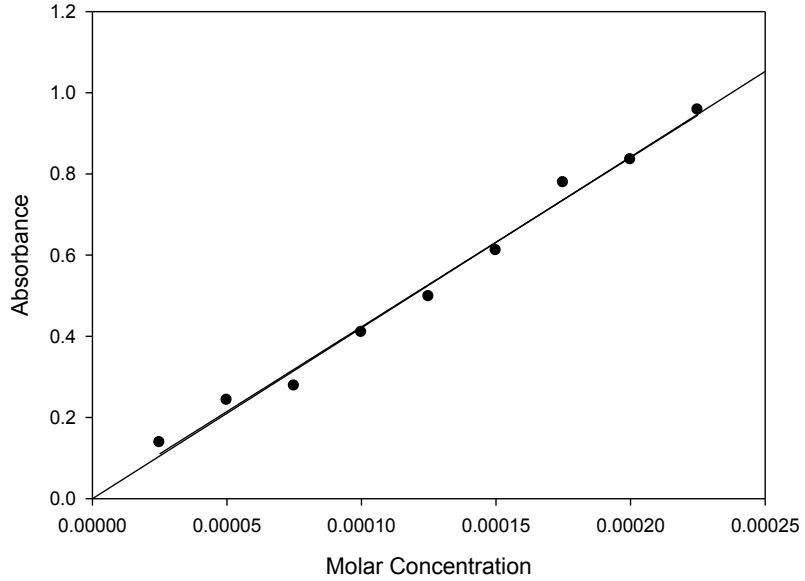

Figure 21– Calibration curve of dansylaminoethylamine, 5a, in 100% DMSO. The absorbance value for each concentration was obtained by a UV-Vis spectrometer, using the crossdilution method.

The molar absorption coefficient (also referred to as extinction coefficient) can be determined from the calibration curve using equation 2. Where ε is the molar absorption coefficient, A is the absorbance, c is the concentration and l is the path length of the cell. The molar absorption coefficient was calculated from the reference line to be 4173 $M^{-1}cm^{-1}$ (S.E.) with a R^2 value of 0.9949.

$A = \varepsilon cl$ **Equation 2**

The molar absorption coefficient obtained from the reference line was then used to calculate the incorporation of the monomer into the nanogels by measuring the absorption of known concentrations of nanogel and comparing them to theoretical values taking into account the chemical yield of nanogel obtained. As the concentration of a sample is directly related to its absorbance, the concentration of an unknown sample can easily be obtained. The incorporation data are presented in table 2 above.

On analysis of the results it can be seen that a relatively high proportion of the dansylaminoethylacrylamide monomer was incorporated into the nanogels. JRP09 with 20 % dansyl tag in the prepolymerisation mixture had an incorporation of 80 %. Nanogel JRP13 with 40 % dansyl tag had an incorporation of 74% and JRP14 with 60% dansyl tag had an incorporation of 75% (table 2). This indicated that the reaction rates were comparable and that the reasonable assumption that the final nanogel consisted of the desired fractions of the polymer (which were initially disposed) were

verified. To establish what percentage of fluorescence tag was required in the nanogel formulation for detection, the emission of the nanogels was evaluated.

2.3.2.3 Fluorescent studies with the dansyl tagged nanogels

Having demonstrated the successful incorporation of the dansyl based monomer into the nanogel matrix, the next step focused on determining the minimum concentration of tag required to ensure optimal tracking of the polymers. Previous *in vivo* studies using zebrafish have used concentrations of approximately 0.1 mg/ml.[157] To be absolutely sure the nanogels could be detected at the levels anticipated as being required *in vivo,* it was decided to assess the nanoparticles for fluorescence at 0.01mg/ml. Solutions of three dansyl containing nanogels (JRP09, JRP13 and JRP14, table 2) were prepared at 0.01 mg/ml, in 100 % ethanol and measured for their fluorescence at an excitation of 339 nm. All three nanogels showed fluorescence emission, figure 22, however only JRP13 and JRP14 could be considered sufficiently fluorescent for use *in vivo*. JRP9, which contained only 20 % of the fluorescent tag showed a much lower fluorescence emission, however there appeared to be no correlation in the emission between JRP13 and JRP14 and the amounts of dansyl tag that was used in the preparation.

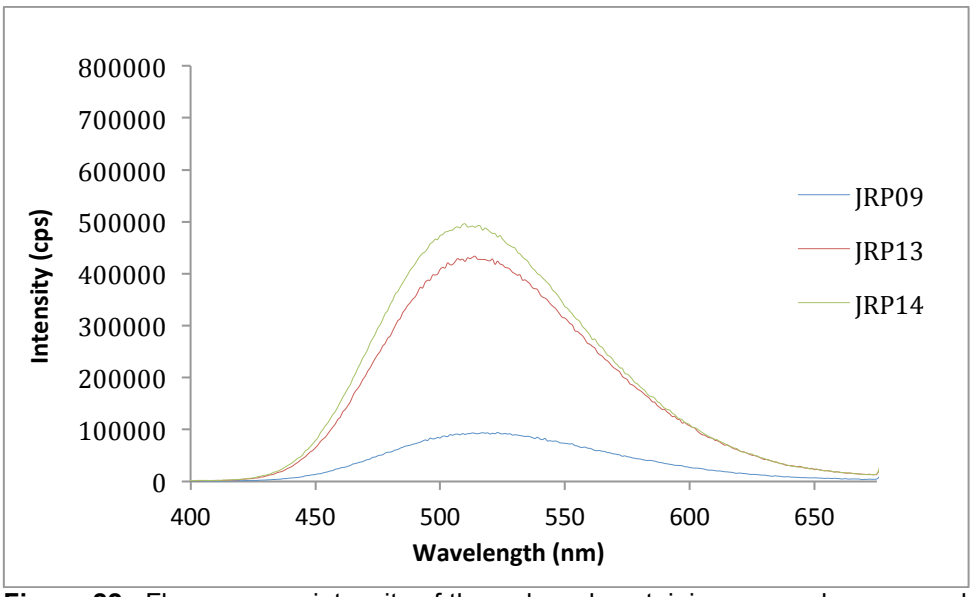

Figure 22– Fluorescence intensity of three dansyl containing nanogels measured at 0.01 mg/ml in ethanol. Measured at excitation 339 nm, emmission 470 nm.

The dansyl moiety however contains hydrophobic features and there was concern that a very high incorporation of the tag would have significant impact on the solubility of the nanogels. Nanoparticles reported in the literature contain as little as 2% (wt) of fluorescent tag compared to the total polymer,[158] with a much lower fluorescence

intensity than that of JRP09 therefore suggesting that the values obtained with JRP09 would be sufficient for in vivo monitoring.

2.3.2.4 Particle size studies with the dansyl tagged nanogels

Efficient drug delivery systems should ideally have a particle size smaller than 200 nm, to allow easy passage through capillaries and to avoid being removed by the spleen[126]. In addition small particle sizes are known to lead to stable colloidal solutions, preventing aggregation and sedimentation. Nanogels formed using the dansyl monomer, **5**, were all made with a C_M=1 (JRP09, JRP13 and JRP14), a concentration that is considered to be on the high side but one that ensures good yields of polymers. As the C_M was closer to the solubility limit of the monomer in DMSO, the risk of obtaining larger microgels rather than desired nanogels was higher. The particle size was evaluated by dissolving the nanogels in 100% DMSO with sonication, with a concentration of 0.1 mg/ml nanogel. The sample was sonicated once more before analysis on the zetasier via dynamic light scattering (DLS).

Polymer	C_M (%)	Dansyl monomer, **5** (%)	EBA (%)	Ave. diameter (nm)	Yield (%)
JRP09	1	20	80	35±2.1	88
JRP13	1	40	60	Mixture of 8±1.9 250±209 (M)	43
JRP14	1	60	40	190±69	68

Table 3 – nanogel preparations with dansyl as the fluorescent tag. EBA is ethylene bis acrylamide, C_M: Concentration of monomers. Ave diameter: the average particle size taken from a distribution of particles, measured on the DLS Zetasizer in 1% DMSO 99% water at a concentration of 0.1 mg/ml.

JRP09 contained the largest amount of cross-linker and had the least polydispersed and smallest particle size of the three samples, shown in table 3. This is because the cross-linker tightens the structure into a small compact particle, preventing the nanogels from interacting with each other and aggregating. JRP13 had a significantly reduced yield compared to the others. This abnormality could be due to the particles with the small particle size being lost during dialysis. The nanogels were isolated using a 35000 daltons dialysis tube to remove the solvent and any small material remaining after polymerisation. As the particle size of JRP13 is mainly 8 nm a greater quantity of smaller, material is likely to have also been formed and been lost during the dialysis, having a negative effect on the yield. As can be seen in figure 23 the distribution of particle size was multimodal and much larger material than the average (35 nm) indicates, was also obtained. A multimodal system is much more likely to suffer from

flocculation, than one with a monodispersed system. Due to the polydispersed system lowering the C_M was investigated to see if a monodispersed system could be obtained. However, this had a negative effect on the yield. This could be due to a significant decrease in molecular weight of the material and therefore loss of the material through dialysis. Due to the polydispersity of the dansyl systems, and the likely influence of Brownian motion, the nanogels were highly likely to suffer from poor stability.

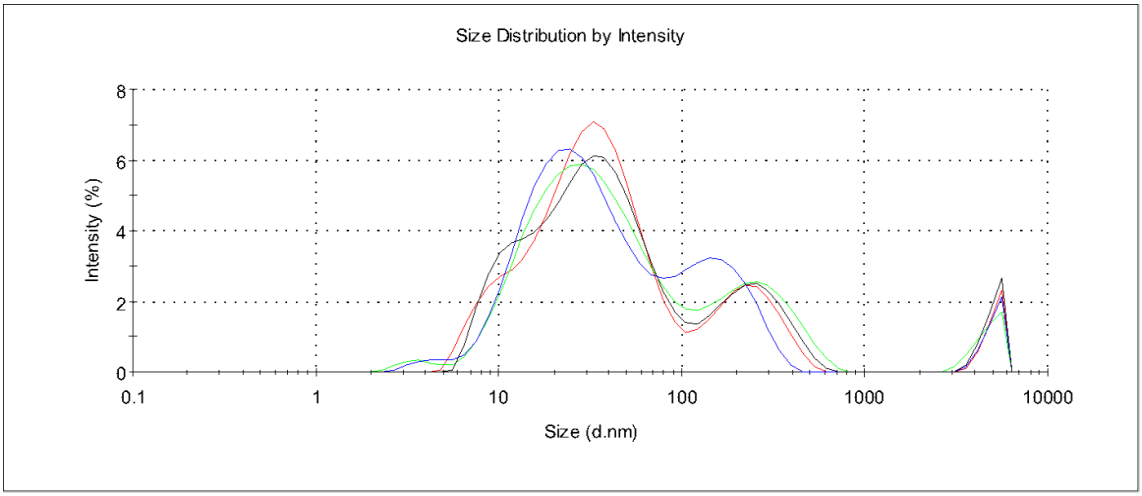

Figure 23 - The average particle size trace of a nanogel containing the dansyl fluorescent tag
A particle size trace of JRP09 at 0.1 mg/ml in 100 % DMSO. Fourty scans of the nanogel were carried out with each line (in different colours) representing the average particle size of the sample over 10 scans.

Over the course of these studies further investigations did confirm that the colloidal solutions were not stable over a long period of time. The nanogel precipitated out of solution after just a few hours. Due to the poor stability of these nanogels, long-term suspension required for toxicity studies would be extremely difficult to achieve, even with parameter changes to the nanogel system. Therefore other fluorescent molecules were explored as possible candidates. As fluorescein is often used as a fluorescent tracker in biological[159] and medical applications,[160, 161] it was next to be evaluated as a potential tracker.

2.3.3 Fluorescein as a fluorescent tag

Fluorescein has been used for many applications including immunoassays,[160] biological imaging,[159] measuring blood volume,[162] and drug delivery[163] to name a few. Its hydrophilicity and low detection limit[160] are two of its greatest advantages and therefore supported its selection as the next candidate for tracking our nanogels. Fluorescein *O*-methacrylate (structure shown in figure 24) has a number of oxygens increasing its water solubility. Whereas dansyl has negligible water solubility,

fluorescein has a water solubility of 80 g/L.[164] In addition fluorescein also has a much higher quantum yield (Φ = 0.95[165]) than that of dansyl (Φ =0.5[166]). This would also potentially reduce the amount of fluorescent tag required in the nanogel. The fluorescein tag has an emission wavelength of 537 nm, which again is outside the auto-fluorescence ranges of the *in vivo* model. Although different from the other acrylamide-based monomers, the methacrylate group should have a similar reaction rate to the acrylamide groups as the charge can still be delocalised across both oxygens. In addition this fluorescent monomer is readily available and inexpensive to use.

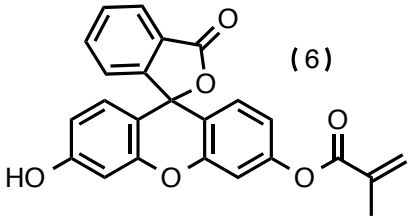

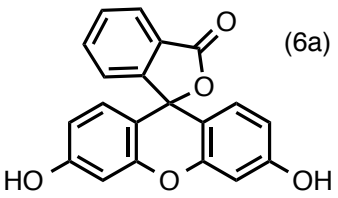

Figure 24 – Fluorescein *O*-methacrylate, (6), the structure of the next potential fluorescent tag for our nanogels, and free fluorescein, (6a).

Nanogels were synthesized using the fluorescein monomer; these nanogels are described in table 4 (page 66). The yields of these nanogels were significantly less than those obtained with the dansyl fluorescent tag. This could have been due to a number of causes, one of which could be the poor incorporation of the fluorescein monomer into the nanogel. This was further explored by evaluating the nanogels in a series of investigations. As previously, one of the first steps was the evaluation of the solubility of the fluorescein tagged nanogels.

2.3.3.1 Solubility of the fluorescein tagged nanogels

Solubility of the fluorescein tagged nanogels in water, as with the previous nanogels, is a key factor for the final application of drug delivery, as well as for use in the toxicity studies. Analysis showed that these fluorescent nanogels were soluble in ethanol, DMF and DMSO alongside ACN and acetone when they were combined with water at concentrations up to 0.1 mg/ml. However, for the *in vivo* studies it was necessary that the nanogels were soluble in water with as little solvent as possible, if not pure water. The fluorescein tagged nanogels were not soluble in 100 % distilled water but they were soluble with just 1% DMSO and 99% water (V/V) at concentrations up to 0.1 mg/ml. Therefore the nanogels with fluorescein as their fluorescent tag had much better solubility characteristics than the dansyl tagged nanogels. This result was not unexpected due to the more polar structure of fluorescein compared to dansyl. As their

solubility was considered to be sufficient, evaluation of the fluorescein incorporation into the nanogels was subsequently investigated.

2.3.3.2 Incorporation of fluorescein monomer into the nanogels

Establishing and quantifying the incorporation of fluorescein *O*-methacrylate into the system was important, to ensure the final polymer had a reproducible and reliable composition of units that clearly reflected the prepolymerisation mixture. As previously with dansyl, investigations were made in order to obtain a reference line for the fluorescein monomer, however the resulting data were not satisfying. A satisfying calibration line could not be obtained (figure 25) and the plotted data appear to form a curve, initially giving a linear curve (until ~60 µM) however due to the large errors in the data establishing reliable incorporation rates of the Fluorescein *O*-methacrylate monomer in the nanogels could not be achieved when the Lambert Beer law was applied.

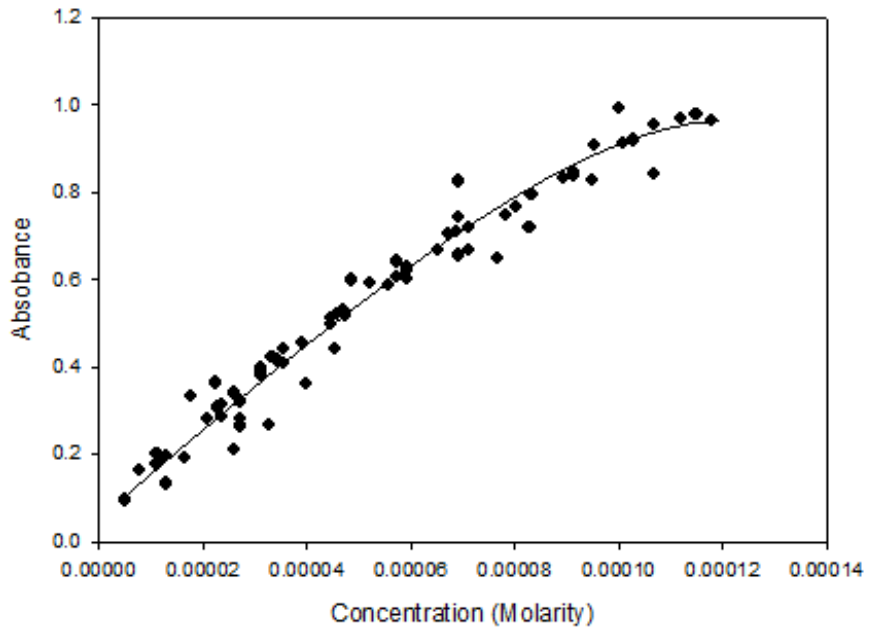

Figure 25 – A graph showing the relationship between the concentration of fluorescein and its absorbance. Measured at 490nm absorbance.

Nanogel preparation	C_M (%)	fluorescein *O*-methacrylate (%)	Cross-linker (%)	Average diameter DLS (nm)	% yield
JRP03	1	20	80	210±2.57	20
JRP04	1	40	60	330±5.1	46
JRP05	1	60	40	350±9.6	45
JRP06	1	80	20	290±8.2	57

Table 4 – nanogel preparations with fluorescein as the fluorescent tag. C_M: Concentration of monomers. EBA is ethylene bis acrylamide, C_M: Concentration of monomers. Ave diameter: the

average particle size taken from a distribution of particles, measured on the DLS Zetasizer in 1% DMSO 99% water at a concentration of 0.1 mg/ml.

Table 4 shows the data relating to the fluorescein nanogels synthesis and characterisation. The chemical yields were overall lower than the ones obtained with the dansyl monomer and the particles sizes were overall larger. Interestingly it would appear that the yield increased with the percentage of fluorescein but not proportionally. This was concerning and potentially indicated that incorporation of the fluorescein monomer into the nanogels matrix was not consistent giving rise to unpredictable variation in behaviour during polymerisation, significantly reducing their reproducibility. The methacrylate nature of the fluorescein monomer could have led to a different reaction rate from the acrylamide cross-linker. Although both contain a stabilising group, the difference could be enough to prevent interaction between the cross-linker and the monomer, thus creating much smaller and tighter nanogels consisting mainly of cross-linker, which would be lost during dialysis. To establish if enough fluorescein was incorporated into the nanogels for tracking, the fluorescence of the nanogels was evaluated.

2.3.3.3 Fluorescent studies with fluorescein tagged nanogels

Establishing the fluorescence intensity of the nanogels was a key step, as the incorporation of fluorescein into the nanogels by UV spectroscopy could not be determined. The fluorescein monomer had been introduced into the nanogel system for the sole reason of tracking the nanogel, therefore detecting reasonable fluorescence from these nanogels was central, if fluorescein was to be a successful tag. Nanogels JRP03 to JRP06 were polymerised with 20-80 % fluorescein *O*-methacrylate respectively (table 4). All nanogels had intense fluorescence, and even with just 20% fluorophore in the prepolymerisation, the mixture appeared to be fluorescent enough to be tracked, with the potential possibility of lowering the percentage of the fluorescent monomer even further.

Figure 26 shows that all the fluorescein containing nanogels were emitting fluorescence at an excitation of 490 nm. There was no correlation between the amount of fluorophore in the nanogels and the emission. As JRP03 and JRP04 had 20-40% fluorescein in the polymerisation and had higher emission values than JRP05 and JRP06, which contained 60-80%flophore and had the lower two emission intensities. This could be due to the nanogels reaching a plateau due to the high quantum yield of fluorescein. However, coupled with the unexpected trend of increasing yield on

increasing % of fluorecein in the nanogel polymerisation, it is more likely that there was a problem during polymerisation of the nanogels. To investigate what effect the fluorescein tag had on the nanogels, the particle size was measured via DLS.

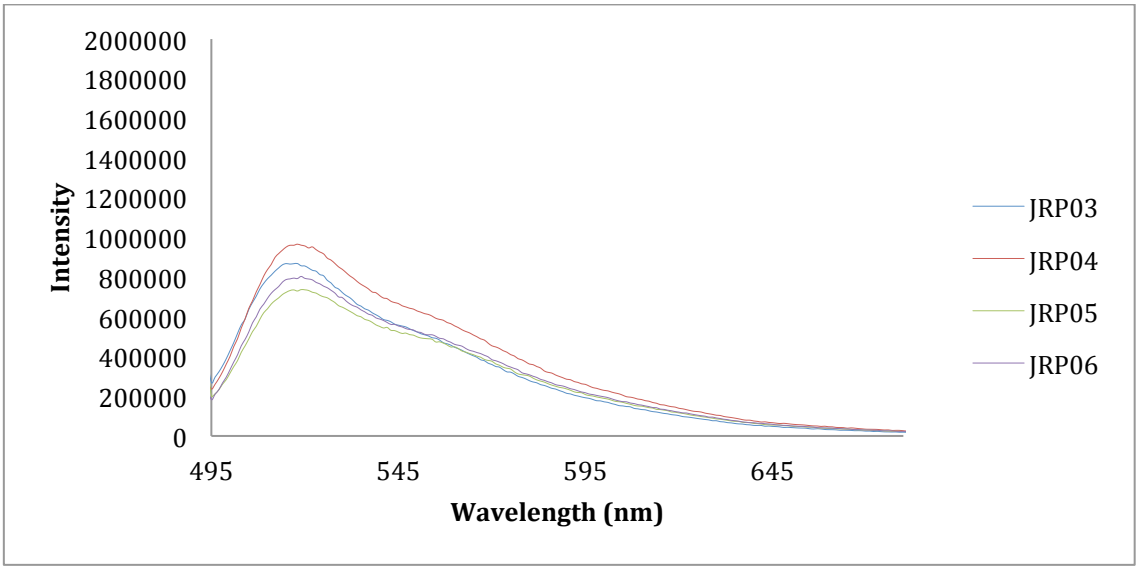

Figure 26 – Fluorescence intensity of 4 fluorescein containing nanogels measured at 0.01 mg/ml in ethanol at an excitation of 490 nm.

2.3.3.4 Particle size for fluorescein tagged nanogels

The effect of the fluorescein tag on the particle size of the nanogels was investigated, as the nanogel needed to be ≤200 nm to be suitable for drug delivery[120]. All nanogels were measured at 0.1 mg/ml in 1% DMSO, 99% water (V/V). All of the particle size traces were much more uniform and giving much narrower distributions than those containing the dansyl tag. The dynamic light scattering particle size trace of JRP03 is given in figure 27. Although very stable, these particle sizes are too big to be eligible for drug delivery, as they would struggle to pass through capillaries. However this could be addressed by altering other parameters of the nanogel preparation at a later date.

Fluorescein has a larger chemical structure than the dansyl group, and it is therefore expected to negatively impact the size of the nanogels. Data obtained with this fluorescent tag indeed showed that an increase in the percentage of fluorescein monomer used in the polymerization mixture resulted in a significant increase in particle size. JRP03 with just 20 % fluorescein had the smallest particle size of just 210 nm, JRP04 with 40 % fluorescein tag was 330 nm and JRP05 with 60 % increased in size to 350 nm. However JRP06 with 80 % fluorescein in its polymerisation mixture had a particle size of 290 nm. These data clearly indicated that there were a number of

factors that were contributing to the inconsistency of the results, leading to a study to evaluate the stability of the nanogels in a variety of solvents.

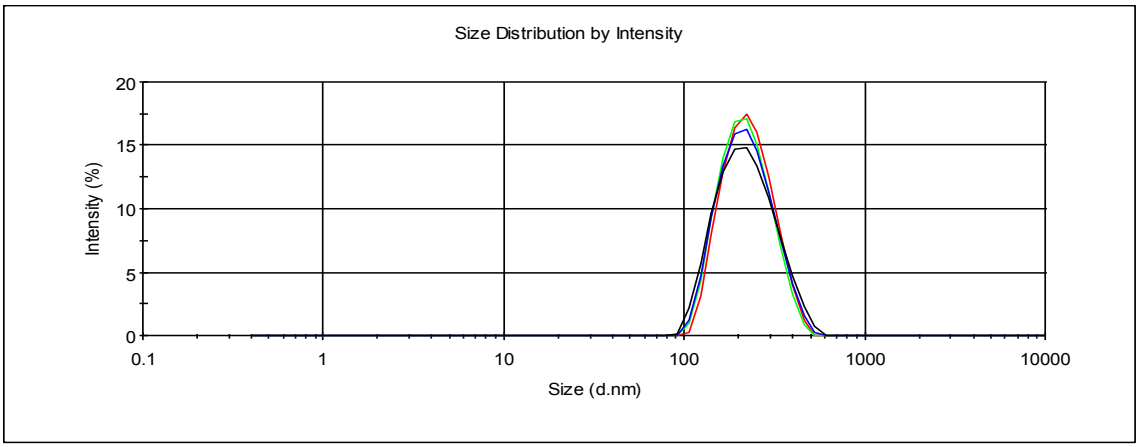

Figure 27 – The particle size distribution of fluorescein containing nanogel JRP03 at 0.1 mg/ml in 1% DMSO 99% water. Fourty scans of the nanogel were carried out with each line (in different colours) representing the average particle size of the sample over 10 scans.

2.3.3.5 Stability of the fluorescein tagged nanogels

A major concern of using fluorescein *O*-methacrylate was the stability of the ester bond, i.e. whether the fluorescein molecule would hydrolyse when exposed to water. This would be a major issue as during isolation of the nanogels, via dialysis, and for the toxicity studies, as the nanogels would have to be exposed to water for long periods of time.

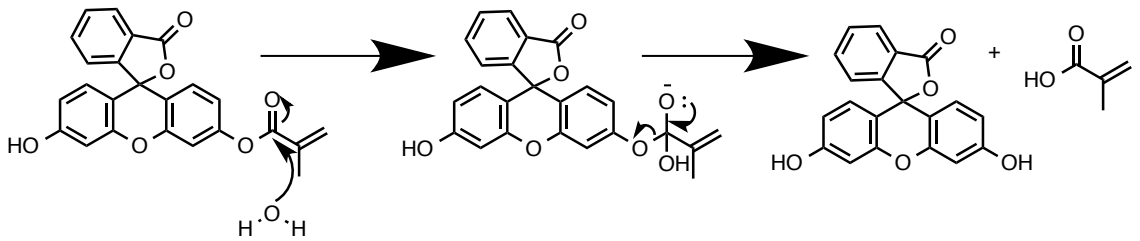

Figure 28 – Mechanism of the hydrolysis of Fluorescein *O*-Methacrylate

The nanogels' stability was analysed via thin layer chromatography (TLC) during polymerisation, dialysis and also after the nanogels were isolated via freeze-drying. Analysis showed that the fluorescent tag was slowly hydrolysed even during the polymerisation process, far too early for its practical use. It appeared that the DMSO was promoting hydrolysis of the ester bond as the spot of free fluorescein was present in the TLC plate when analysed during the polymerisation process. In addition the experiments confirmed that isolation via dialysis in water was not effective at removing the excess fluorescein molecules, which were not soluble in water and therefore precipitated in the dialysis tubing and remained there throughout dialysis. To

counteract this, dialysis was attempted using 50 % acetone, 50 % water (V/V) in which fluorescein was soluble. When the dialysis eluent was altered, hardly any fluorescein was detected in the nanogels, indicating therefore that incorporation of the fluorescein tag into the nanogel matrix had been very poor.

Further studies were carried out to establish a better solvent system in which to prepare the polymers, however each attempt did not lead to any improvement. DCM gave the least amount of fluorescein release from the nanogel, however AIBN required an activation temperature of 60 °C and with a boiling point of 40 °C it was not a viable combination. Other solvents, (ACN and DMF) were tried with a much lower C_M of 0.5% however these solutions led to macrogelation. Even if a viable polymerisation system could have been attained, it was highly likely that the fluorophore would have been released during the dialysis phase or the toxicity studies. Therefore it was decided to investigate other potential fluorescent monomers with a more stable bond between the fluorophore and the nanogel.

2.3.4 Coumarin as a fluorescent tag

A new fluorescent tag that was evaluated was trifluoromethylcoumarin acrylamide (TCA), which has an amide bond that can be used to link the coumarin unit to the nanogel. TCA is also a smaller molecule than fluorescein and would therefore have less impact on the final size of the nanogel. Coumarin derivatives have been used previously to tag PEG based block polymers, which self assemble to form micelles. In this application the coumarin does not prevent solubility of the polymer in water to at least 1 mg/ml. In addition, only one unit of coumarin is used per block polymer which remains fluorescent enough to detect at concentrations as low as 8 µg/ml[167]. As coumarin has been incorporated into another polymeric nanomaterial (micelles) well, without having a negative impact on the material's characteristics and also had the benefit of being readily available, coumarin was the next fluorophore set for analysis.

7-[4-(Trifluoromethyl)coumarin] acrylamide (TCA) (structure is displayed in figure 29) is a very interesting fluorescent molecule, it has a nice compact chemical structure, with an aromatic system that can contribute to hydrophobic interactions, the acrylamide polymerisable unit which ensures high stability of the tag-nanogel link and the presence of the trifuoromethyl unit with high dipole characteristics, that should help with the overall solubility. In terms of fluorescence emission, with its maximum around 430 nm. although it is outside one of the zebrafish autofluorescence zones, it does fall in the middle of the second autofluorescence band, typical of when the cells die. This issue

was identified as having the potential to disrupt analysis of the nanogels *in vivo*, however advice was given that this problem could be circumvented, by maintaining the settings on the confocal microscope, the smart gain was maintained at 729 and the UV light intensity was set at 60 %. The presence of the acrylamide group, would also allow us to expect a good yield in tag incorporation in the acrylamide-based nanogels.

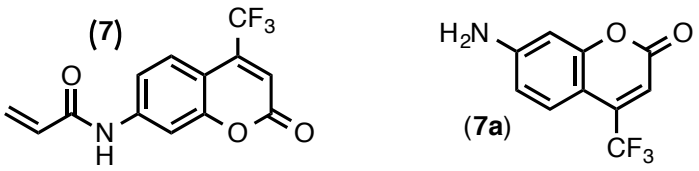

Figure 29 – Structure of 7-[4-(Trifluoromethyl)coumarin] acrylamide, (**7**) and 7-amino-4-(trifluoromethyl) coumarin, (**7a**).

Three nanogels were initially prepared, with the aim to carry out some preliminary studies that would help evaluate whether this monomer was a viable option (table 5).

Nanogel preparation	C_M	TCA (%)	A (%)	XL (EBA) (%)	Ave. diameter (nm)	Yield (%)
JRP29	1	10	20	70	72±0.47	48
JRP30	1	20	20	60	62±0.84	37
JRP31	1	30	20	50	61±1.9	17

Table 5– Nanogel preparations with coumarin as the fluorescent tag. C_M: Concentration of monomers. Ave diameter: the average particle size taken from a distribution of particles, measured on the DLS Zetasizer in 1% DMSO 99% water at a concentration of 0.1 mg/ml. Where A is acrylamide, EBA is ethylenebisacrylamide and TCA is 7-[4-(Trifluoromethyl)coumarin] acrylamide.

The yields of the TCA tagged nanogels were all fairly low, less than 50%. In fact the yield appeared to decrease with increase of 7-[4-(Trifluoromethyl)coumarin] acrylamide in the formulation. JRP29 has 48% yield with just 10 % TCA content, JRP30, with 20 % TCA content, has a yield of 37%. The yield of JRP31, with the highest content of TCA at 30 %, is just 17%, which is a drop in yield of 54% compared with JRP30. as the drop in chemical yield is proportional to the concentration of TCA, and this phenomena had not been observed before, it was concluded that the TCA was likely to be quenching the radicals produced by the AIBN initiator and therefore reducing the overall yield. This hypothesis was actually supported by literature data.

Quinones, which contain two conjugated oxygens, are known to quench radicals due to stabilisation of the radical over several resonance structures[168]. The radical is then stabilised, making it less reactive and stalling the active chain radical, which prevents

further addition of monomer. Trifluoromethyl coumarin has a semi-quinone structure and therefore has the potential to inhibit the radical polymerisation. Some coumarin derivatives have been exploited for this trait and used to actively scavenge free-radicals in the body to prevent oxidative damage[169, 170]. Therefore although it may initially impact on the polymerisation process, the incorporation of the coumarin monomer into the nanogel could have a beneficial side effect whilst circulating within the body. This radical-inhibitory effect can be counteracted by an increase in AIBN, so this result was not of a huge concern. Of higher priority were investigations into the impact of the hydrophobicity of coumarin on the nanogel's overall solubility.

2.3.4.1 Solubility of coumarin tagged nanogels

The application of these nanogels as a drug delivery system requires them to have sufficient solubility in water, both for administration purposes of the end product but also in the short term for enabling the *in vitro* and *in vivo* studies. All the monomers in the nanogel preparation were chosen with their suitability for solubility in mind. However, finding a fluorescent monomer with good fluorescent properties and high water solubility is challenging due to the opposing characteristics. Fluorescence occurs in molecules with conjugated systems, which tend to be highly hydrophobic. Coumarin itself is a hydrophobic molecule and could therefore limit the solubility of the nanogels tagged with TCA. Due to the presence of the coumarin unit the nanogels were not 100% soluble in water at 0.1 mg/ml but the coumarin containing nanogels were soluble at 0.1 mg/ml in just 1% DMSO with the remaining 99% being made up with distilled water (V/V) which was an acceptable ratio for this stage of the process. This increase in water solubility over the dansyl tag, and the more stable amide bonds linking the coumarin to the nanogel were promising results. The next step focused on the evaluation of the coumarin incorporation in the nanogels.

2.3.4.2 Incorporation of the coumarin monomer into the nanogel

In order to estimate the incorporation of coumarin into the nanogels, the molar absorption coefficient of the coumarin monomer needs to be determined. Estimating the incorporation of TCA into the system is important, to ensure the final polymer has a reproducible and reliable composition of units that clearly reflect the prepolymerisation mixture. Therefore a precursor to the coumarin acrylamide monomer was sort after, in order to perform UV anlysis and gain a reference line for the fluorophore. One molecule, which was commercially available and therefore highly advantageous to use, was that of 7-amino-4-(trifluoromethyl) coumarin (TMAC). TMAC does not contain the

double bond present in TCA but also loses the carbonyl group, which will have an impact on the molar absorption coefficient. Therefore to analyse the difference between the two molecules the UV spectra of the two molecules were compared with the spectra of JRP29.

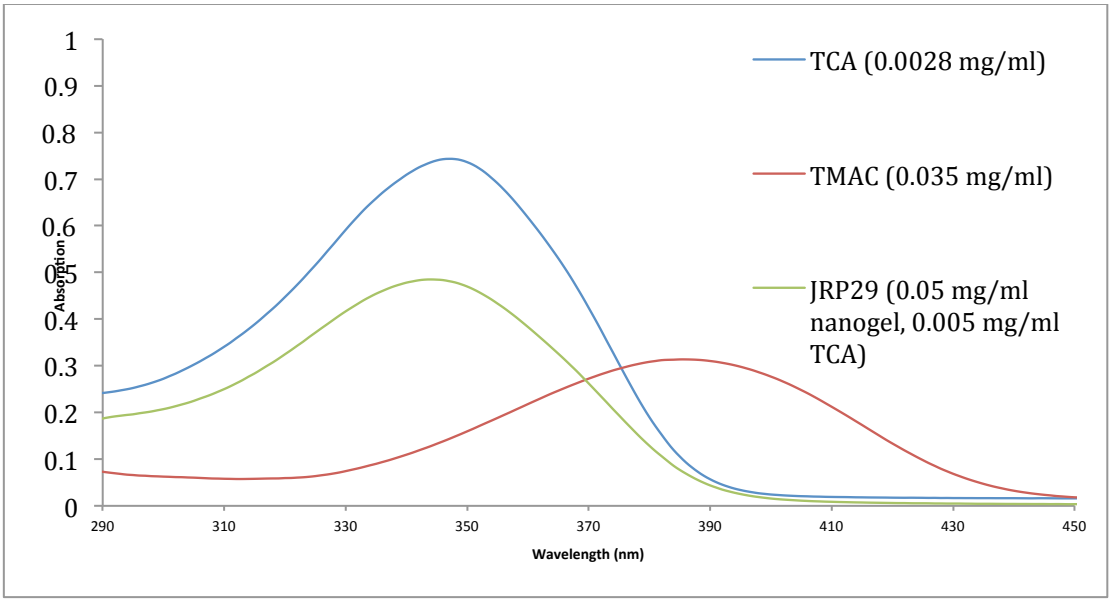

Figure 30 - The UV-Vis spectra of TCA, TMAC and nanogel JRP29 in 100 % DMSO. Where TCA is 7-[4-(Trifluoromethyl)coumarin] acrylamide, (7) and TMAC is 7-amino-4-(trifluoromethyl) coumarin, (7a).

TMAC clearly has a significant peak shift to the right compared to TCA and the absorption value of TMAC is significantly lower than TCA, despite the concentration of TMAC being higher than that used for TCA. The TCA peak for JRP29 can be seen to lie directly beneath the peak in the TCA Spectra and therefore gave a much better comparative for the nanogels. The use of TCA with the saturated bond being hydrated would have been a better choice, however as TCA was commercially available, it had excellent solubility in DMSO and the fluorophore was ultimately just to enable tracing of the nanogel for toxicity studies, it was considered to be within close enough range, despite the double bond, to allow an insight into the incorporation of the monomer into the nanogel. Therefore a reference line was obtained using TCA, to which the absorbance of known concentrations of the various nanogel preparations, were compared. The reference line, figure 31, was established by using the cross-dilution method, measuring the absorbance of the TCA solutions at 345 nm (which was previously established to be the absorption peak of TCA in JRP29) at varying concentrations.

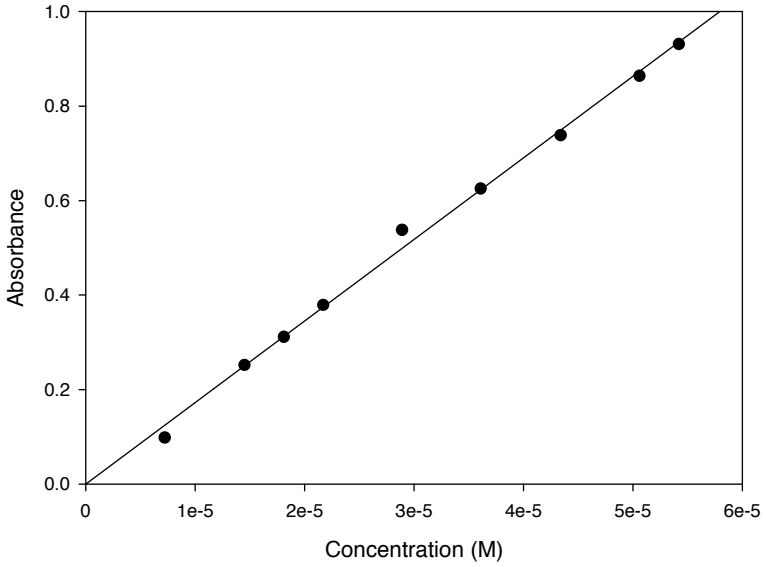

Figure 31 - A calibration curve of TCA in 100 % DMSO. Absorbance measured at 345 nm. The extension co-efficient is 16821 and the R^2 value is 0.9964.

Once the calibration curve for TCA was established, several different concentrations of the coumarin tagged nanogels were analysed via UV-Vis spectrometry and the absorbance was determined for each concentration. Several coumarin containing nanogels were evaluated, with approximately 0.35 mg of each polymer added to 2 ml of DMSO. Various dilutions, between 0.015 and 0.06 mg/ml, were formed of each stock solution and each of the dilutions was measured for their absorbance at 345nm. The number of moles of TCA was calculated using the molar absorption coefficient and compared to the concentration of the nanogel. The results of the experimental number of moles of TCA in each nanogel were calculated for every dilution and the results were averaged. These were cross-referenced with the calibration curve and theoretical incorporation to obtain the incorporation of coumarin in each nanogel.

Nanogel	TCA (%)	A (%)	XL (EBA) (%)	Yield (%)	n_{FM} /mg of nanogel (exp) (mol/mg)	n_{FM} /mg of nanogel (theo) (mol/mg)	Incorporation (%)
JRP29	10	20	70	48	$5.09*10^{-7}$	$6.24*10^{-7}$	86
JRP30	20	20	60	37	$1.30*10^{-6}$	$1.95*10^{-6}$	>99
JRP31	30	20	50	17	$1.35*10^{-6}$	$1.21*10^{-6}$	>99

Table 6 – incorporation results of the coumarin monomer into the nanogel. A= acrylamide, EBA = ethylene bis acrylamide. n_{FM}= number of moles. exp = experimental result. theo = theoretical result.

The data confirmed that the TCA monomer was incorporated with a good ratio. JRP29 has the lowest incorporation of 86%, this nanogel has the lowest amount of coumarin monomer in the polymer and has the highest yield. The poor chemical yields in nanogel synthesis have already been discussed together with the radical quenching role of coumarin. This characteristic is also expected to impact the incorporation. With higher amounts of coumarin in the polymerisation, more of the radicals will be stabilised, suspending the polymerisation faster, without much incorporation of the cross-linker. Therefore the higher the amount of coumarin in the mixture, the lower the overall yield and the higher the incorporation value.

On close analysis, the results appear to indicate a very good incorporation of the tag into the polymers, with over 99% of monomer estimated to be incorporated into JRP30 and JRP31. However, if this fluorophore was chosen, investigations into increasing the amount of initiator would be necessary to ensure nanogels are composed of the desired monomer ratios. Before in depth nanogel studies were carried out, establishing the size of these nanogels was required to assess their suitability for a nanodelivery system.

2.3.4.3 Particle size of coumarin tagged nanogel

As mentioned previously, efficient drug delivery systems should ideally have a particle size smaller than 200 nm[126]. All coumarin tagged nanogels were measured at 0.1 mg/ml in 1% DMSO, 99% water (V/V). All of the particle size traces were much more uniform and giving much narrower distributions than those containing the dansyl or fluorescein tags. The size of the nanogel reduces slightly on increase of the amount of coumarin present (table 6). JRP29 with just 10 % TCA has a particle size of 72 nm, JRP230 with 20 % TCA has a particle size of 62 nm and JRP231 has a particle size of 61 nm and contains 30 % TCA. The hydrophobicity of the nanogel increased as the coumarin content increased, thus reducing the swelling of the nanogel and maintaining a more compact structure. An example of the particle size distribution of JRP29 coumarin nanogel is shown in figure 32.

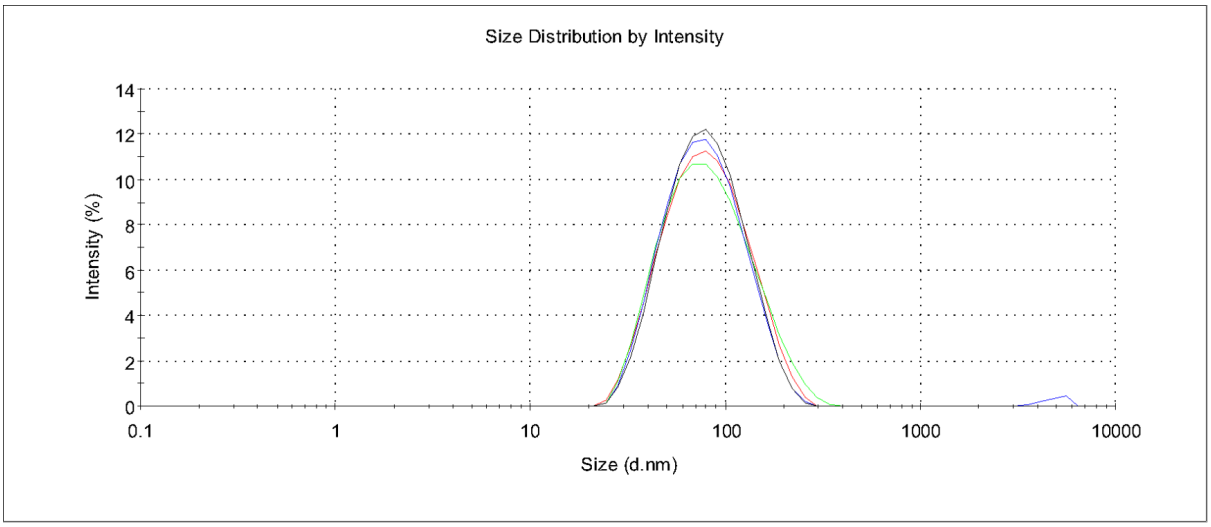

Figure 32 - The particle size distribution of coumarin containing nanogel JRP29 at 0.1 mg/ml in 1% DMSO 99% water. Fourty scans of the nanogel were carried out with each line (in different colours) representing the average particle size of the sample over 10 scans.

At this stage the nanogels were obtained, with with particle sizes in the desired range, and they also displayed a good water solubility and incorporation of the fluorophore, therefore the only outstanding issue to be evaluated related to the fluorescence emission and whether this could be considered high enough to study the incorporation and toxicity of the nanogels both *in vitro* and *in vivo*.

2.3.4.4 Fluorescent studies with coumarin tagged nanogels

The primary function of the fluorophore is to enable tracking of the nanogel during *in vitro* and *in vivo* experiments. One of the nanogels (JRP29) was evaluated for its fluorescence at the required concentrations for the toxicity studies of 0.1 and 0.01 mg/ml. Figure 33 shows that the nanogel containing coumarin was emitting fluorescence at an excitation of 377 nm; therefore TCA had successfully been incorporated into the nanogel. The fluorescence was evaluated at two different concentrations for JRP29, 0.1mg/ml and 0.01mg/ml. Both solutions clearly show strong fluorescence emission, with a good dependence on concentration.

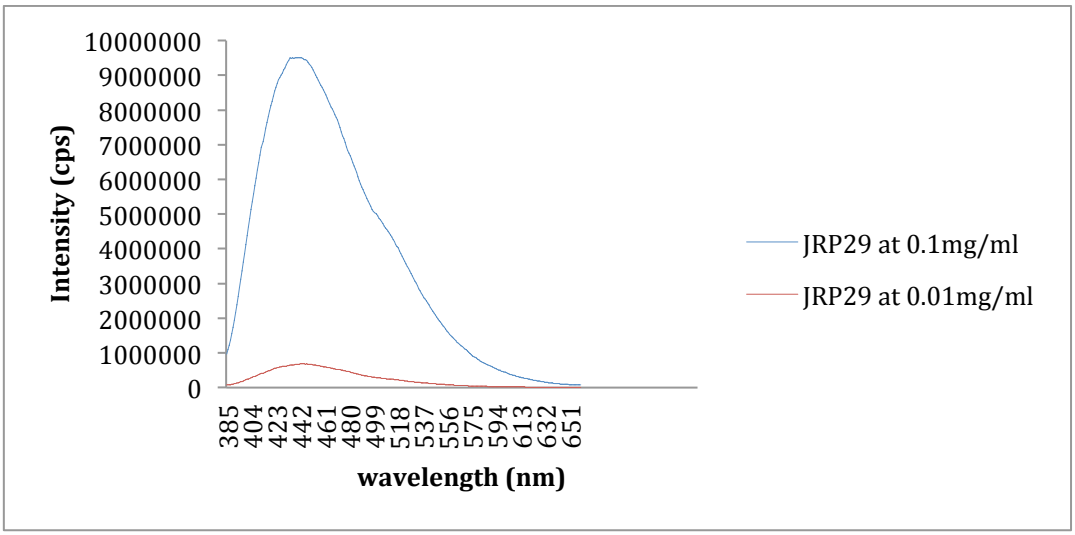

Figure 33 – Fluorescence intensity of the coumarin tagged nanogel JRP29 at 0.1 mg/ml and 0.01mg/ml in ethanol. Excitation is 377 nm and emmission is 445 nm.

The TCA tagged nanogels had a small, narrow particle size, reasonable fluorescence emission, a stable amide bond and therefore good chemical stability, reasonable solubility and good incorporation thus warranted further investigation. Two slight concerns with the nanogels needed to be addressed, the first was the likely quenching of the free radicals by the coumarin monomer which has a negative impact on the yield and the second is the need for complete water solubility, for which the overall drive during the following studies is to increase the water solubility.

2.4 Synthesis of soluble fluorescent nanogels

In the next stage of the project the focus was the optimisation of the nanogel formulation with the aim of obtaining nanoparticles with ideal characteristics for the application in drug delivery. In order to achieve this, the work concentrated on improving the chemical yield, and obtaining particles with smaller size and also considerably increasing the water solubility.

2.4.1 Addition of acrylic acid

The coumarin tagged nanogel described in the previous section showed good solubility, although this was not deemed sufficient to carry out preliminary studies of toxicity, therefore the addition of a comonomer was required, that would increase the hydrophillic nature of the nanogel. One monomer that has been widely used to increase solubility of many materials is acrylic acid. Acrylic acid has been used to make even highly hydrophobic material, such as carbon nanofibres, hydrophilic by attaching acrylic acid to their surface[171]. Acrylic acid has also been used as a co-monomer in

many different polymer preparations due to its hydrophilic nature, including block co-polymers[172], hydrogels[173] and nanogels[174]. Acrylic acid contains two oxygen atoms in its small structure, which significantly increases the water interaction of the nanogel when it is incorporated.

Acrylic acid has a pKa of 4.25[175] which at neutral pH carries a negative charge as the acid is largely dissociated. Therefore the negatively charged oxygen will form ionic interactions with H+ ions present in water, alongside those which are undissociated interacting with water through hydrogen bonds, both of these features aiding the solubility of the nanogels. Not only does acrylic acid substantially increase the hydrophilic nature of the nanogels, it also introduces a negative charge. This therefore gives a secondary use for the co-monomer by potentially using the carboxylic acid group to interact with a drug. Acrylic acid (AA) was introduced into the nanogel at 10% of the prepolymerisation mixture to evaluate its effect on these acrylamide-based nanogels. There was a significant increase in solubility, where before 1% of DMSO was required to solubilise the nanogel, on addition of AA the nanogel was 100% water soluble at 0.1mg/ml. Not only this, with the addition of AA the yield of the nanogel also increased by over 18%. Due to this positive result, acrylic acid was included on all further nanogel preparations to aid their solubility in water.

Nanogel preparation	TCA (%)	XL (%)	AA (%)	A (%)	CM (%)	AIBN (%)	Yield (%)	Solubility in 100% water (mg/ml)	Soluble in 1%DMSO 99%water (mg/ml)
JRP29	10	70		20	1	1	48	No	1
JRP2105	10	70	10	10	1	1	61	0.1	>1

Table 7 – Nanogel preparations showing the effect of addition of acrylic acid. JRP29 and JRP2105 were polymerised for 4 days at 70°C using Ethylene bis acrylamide as the cross-linker (XL) and JRP254 and JRP2106 were polymerised for 4 days at 70°C, using Methylene bis acrylamide as the cross-linker (XL).

[This project was interrupted after 1 year of study to undertake a placement as part of a Marie Curie IAPP project in a company, Polyintell, in France. During the suspension of studies optimisation of polymerisation parameters by other members of the group led to significant findings.] Firstly, methylene-bis-acrylamide was identified as a better cross-linker for the nanogels, reducing hydrophobicity due to the reduction in carbon atoms between the acrylamide groups and therefore also leading to a tighter more compact structure. Secondly it was shown that reduction of the total monomer concentration (C_M) from 1% to 0.5% led to nanogels with smaller particle size and lower polydispersity. Furthermore data suggested that reduction of the polymerisation time from 4 days to 2

days did not significantly impact on the chemical yields, while improving the overall time required to obtain each preparation.

As a result of the data obtained in the group, it was agreed that the changes could also be implemented in this project, as better results were expected. Therefore a series of experiments were carried out following my return to QMUL using MBA as the cross-linker, Cm = 0.5% and a polymerisation time of 2 days. The next section describes the results obtained.

2.4.2 Cross-linker choice and content

As the research in the group showed methylene bis acrylamide as a better cross-linker for nanogel formulations, its use in this acrylamide-based system was considered a high priority. In addition, research by Ken Shea had proven that nanogels could be obtained using concentrations of cross-linker as low as 5%[176]. Therefore investigations were carried out not only to evaluate which of the two cross-linkers would afford better nanogels, but also to establish the lower limit for the cross-linker concentration that would still lead to nanogels. The work was entirely driven by the objective of significantly increasing the water solubility of the nanogels, by partially offsetting the presence of the highly hydrophobic fluorescent tag.

The first step was to lower the total concentration of the monomers, to a value of C_M equal to 0.5%, shown to be optimal. The acrylic acid concentration was maintained to 10 %, as before, to retain the solubility, while the concentration of trifluoromethylcoumarin acrylamide (TCA), was dropped to 5%, to further aid hydrophilicity of the nanogels. In previous studies TCA was shown to have a high intensity of fluorescence, so it was expected not to impact significantly on the tracking of the nanogels.

Nanogel preparation	TCA (%)	EBA (%)	MBA (%)	AA (%)	A (%)	C_M (%)	Yield (%)	Average diameter By DLS (nm)
JRP255	5	20		10	65	0.5	25	295±18
JRP257	5	50		10	35	0.5	27	352±22 (M)
JRP259	5	70		10	15	0.5	51	509±34 (M)
JRP241	5		20	10	65	0.5	30	107±4
JRP251	5		50	10	35	0.5	58	130±16
JRP253	5		70	10	15	0.5	51	255±45 (M)

Table 8 – Nanogel preparations for cross-linker comparisons. Polymerisation was carried out at 70 °C for 2 days in DMSO. JRP251 and JRP253 were measured in 1%DMSO at 0.1mg/ml for DLS, all others measured in 100% water 0.1mg/ml. M=multimodal.

Analysis of the data, gathered in table 8, indicates that the choice of MBA or EBA does not have any significant impact on the chemical yields of the nanogels. However the concentration of cross-linker in the polymer solution appears to positively impact the yield, with higher percentages leading to better yields. For example JRP255 with 20 % EBA has a yield of just 25% however when the EBA is increased to 70 % the yield is increased to over 50 %. The loss of material is likely due to loss of smaller material during the dialysis step used for the isolation of the nanogel. This is also confirmed by the fact that the higher the percentage of cross-linker and the larger the particles tend to be. This is true for both cross-linkers, however the MBA nanogels have a much smaller particle size than those containing EBA. For example JRP255 with 20% EBA, has an average particle size of almost 300nm whereas the equivalent MBA nanogel, JRP241 has a particle size of just 107nm. MBA has just one CH_2 group between the acrylamide groups, instead of the two in EBA, thus reducing the size of the cross-liner and creating a tighter more compact nanogel. This therefore gives an overall smaller and less polydispersed particle size. Taking into consideration both the yields and average particle sizes, the MBA is incorporated into the nanogel more effectively, losing similar amounts of material with half the particle size of equivalents containing EBA.

Due to the significant improvement in the nanogels, MBA was chosen as the final cross-linker and its percentage maintained below 50 molar percent of the prepolymerisation mixture. The C_M fixed at 0.5% was giving particle sizes in the ideal range therefore further preparations were all formed using a total monomer concentration of 0.5%.

2.4.3 Amount of initiator required

Traditionally the percentage of initiator used for the nanogels synthesis in the group has always been kept at 1% of all the double bonds in the mixture. However, as the yields were still less than 50%, it was decided to investigate whether an increase in initiator content would help increase the overall yield. Termination of the radical polymerisation reaction can happen via three mechanisms: firstly, termination by combination, whereby two radicals react to form a bond, combining the two polymer chains; secondly termination by disproportiation, where two radicals react but the two polymers chains remain separated, leaving a saturated bond on the end of one and an unsaturated bond on the other; lastly chain transfer can occur, in which case a hydrogen is scavenged from another molecule (which could also be the solvent) and

termination of that polymer occurs although another radical is yielded[147]. These three processes are affected by the monomers in the system and their reactivities. Therefore the amount of initiator tailored for a particular system needs to be identified, in order to achieve optimal yields of polymer without promoting particle-particle reactions. In this particular case the presence of the semiquinone structre in the fluorescent tag and its ability to promote quenching required additional experiments, where the concentration of initiator was varied to maximise the nanogel yields.

A small set of experiments was carried out where the concentration of AIBN was varied between 1% and 3% while maintaining all the other parameters unaltered.

Nanogel preparation	TCA (%)	XL (%)	AA (%)	A (%)	AIBN (%)	Yield (%)	Average diameter By DLS (nm)
JRP216	5	35	10	50	1	48	191±6
JRP217	5	35	10	50	2	69	110±4
JRP218	5	35	10	50	3	83	>1000

Table 9 – Nanogel preparations; carried out at 70 °C for 2 days with a C_M of 0.5% in DMSO. Particle sizes all carried out in 100% water at 0.1 mg/ml.

The results, presented in table 9, confirmed as expected, that the yield did increase as a result of the initiator increase. JRP216 with just 1% AIBN had a yield of 48%, when AIBN was increased to 2% in nanogel JRP217 the yield increased by 43% to give 69% and also reduced the particle size of the nanogel. By introducing more initiator into the system, more radicals will be formed initially, forming many more, but smaller nanogels, which would reduce their average particle size overall. However on further increase of AIBN to 3% (JRP218) the yield increases by 20 % but there is a significant undesired increase in particle size, and in fact formed a microgel. This increase in initiator was a step too far, creating an excessive number of radicals promoting inter-particle polymerisation, forming much larger polymer gels. From the positive results obtained when the initiator was increased to 2% of the bonds, 2% AIBN was chosen as the default concentration for the initiator.

2.4.4 Polymerisation time

Nanogels obtained during the studies to identify the most suitable fluorescent tag were all polymerised for four days, as this was considered to be the optimal length of time in the group. In order to establish whether this timeframe could be improved to shorten the overall length of time required for the polymerisation, a number of experiments

were carried out. Table 10 shows the data relative to three nanogel preparations, all done under the same set of experimental conditions, only differing in polymerisation time. Due to the improvement seen with MBA over EBA when analysing cross-linkers in section 2.3.1, MBA was used in these nanogels. 20 % MBA cross-linker was chosen due to the reduced particle size obtained in comparison to the nanogels containing 35, 50 or 70 % MBA cross-linker. MBA was used as cross-linker in a concentration of 20 %. Although this is low and the yield was expected to be less than 40 % based on previous work, it was chosen nevertheless because the particle sizes, determined by DLS were all in the range considered to be valuable for drug delivery (particle size less than 150 nm)

Nanogel preparation	TCA (%)	MBA (%)	AA (%)	A (%)	Polymerisation time	Yield (%)	Average diameter By DLS (nm)	Solubility in water (mg/ml)
JRP232	5	20	10	65	1 day	32	141±26	>1
JRP241	5	20	10	65	2 days	30	107±4	>1
JRP238	5	20	10	65	3 days	33	188±2 (M*)	>1

Table 10 – Nanogel preparations carried out at 70 °C, at a CM of 0.5% in DMSO. M* = multimodel distribution. Particle sizes all carried out in 100% water at 0.1 mg/ml.

Analysis of the data indicate that effectively there is no significant change in the percentage yield of nanogel obtained as a result of changing the polymerisation time. There seems to be a more substantial variation in particle size, as a result of variations in polymerisation times, however as these were not really significant and did not appear to have a trend, it was decided to use a 2 day polymerisation time to reduce preparation time.

2.4.5 Concentration of fluorescent tag

Trifluoromethylcoumarin acrylamide (TCA) was set at 5% of the nanogel monomers in the initial studies to investigate other parameters and their effect on the nanogel. Having decided on the limits for the other variables, the final parameter to investigate was the effect of TCA on the nanogel. Previous studies (section 2.2.4.2) showed that TCA incorporation was very good, and 10-30 % of the nanogel composition had been TCA content. However, the solubility of these nanogels was still not sufficient as they required 1% DMSO in order to be solubilised. Since the initial investigations into using TCA as a fluorophore, the protocols for the preparation of the nanogels had changed significantly, with the addition of acrylic acid, the use of MBA instead of EBA and

changes to its concentration, shorter polymerisation times and high amount of initator. Therefore new nanogels were prepared with TCA concentrations ranging between 2.5 and 10 % in the polymerisation mixture.

Nanogel preparation	TCA (%)	MBA (%)	AA (%)	A (%)	C_M (%)	Yield (%)	Average diameter By DLS (nm)	Solubility in water
JRP234	2.5	20	10	67.5	0.5	40	171±41	>10mg/ml
JRP235	5	20	10	65	0.5	31	123±2	10mg/ml
JRP236	10	20	10	60	0.5	30	153±3	0.1mg/ml

Table 11 – Nanogel preparations with varying amounts of fluorescent tag. Particle sizes all carried out in 100% water at 0.1 mg/ml.

Three nanogel preparations were obtained, all again using 20% MBA as cross-linker. The percentage yields were essentially unaffected by the variations in concentrations of the fluorescent tag and the particle size (carried out in water at 0.1 mg/ml) was also not significantly altered and it was comprised between 100 and 200 nm. However the most significant change that was observed related to the solubility of the isolated nanogels. The variation in hydrophilicity is very substantial when going from 10% TCA to 2.5%, with a 100-fold increase in solubility, results shown in table 11.

In order to analyse the nanogels using fluorescence spectroscopy with as much accuracy as possible, samples of the polymers were prepared with similar concentration of coumarin tag, with each of the nanogels prepared to form a $1x10^{-5}$ mM TCA solution. Therefore twice the mass of JRP234 (2.24 mg in 2 ml) was used to that of JRP235 (1.12 mg in 2 ml) and half as much mass was used for JRP236 (0.56 mg in 2 ml). These solutions were measured for their fluorescence at an excitation of 345nm. The emissions (measured at 445 nm) of the nanogel solutions are presented in table 12. JRP234 (2.5% TCA) contains half the amount of TCA than JRP235 (5%) and should therefore produce twice the fluorescence intensity over JRP234. A significant increase in fluorescence was seen between that of JRP234 and JRP235, at the same concentration of nanogel. JRP235 however does not improve its emission over JRP234 even though the coumarin content has once again increased, from 5% in JRP235 to 10 % in JRP236 as its emission would be their emission would be roughly the same at the same concentration of nanogel. Therefore both a significant decrease in solubility of the nanogels is seen, when 10 % coumarin tag is used, and no benefit seen from the increased amount of fluorophore. This could be due to self-quenching, if the molecules are in too close contact (which by an increase in content in the nanogel preparation

could be made possible) and collide with each other it is possible the excited molecules, on collision, lose their energy[177].

Nanogel	% TCA in nanogel	Conc of nanogel (µg/ml)	Emission intensity of sample (cps)	Theoretical Emission at 57 µg/ml (cps)	TCA incorporation (%)
JRP234	2.5	57	2084681	2084681	>99
JRP235	5	23.5	1694161	3388322	>99
JRP236	10	11.8	845320	3381280	>99

Table 12 – Fluorescence emission at 445 nm (excitation 345 nm) of coumarin incorporated nanogels and the percentage of incorporation.

Nanogels containing just 2.5-5% coumarin in their formulation produce yields comaparative or higher to those containing higher quantities of coumarin tag. The solubility is significantly increased (100 fold) when the coumarin content was dropped from 10 % to 5 or 2.5%, which was the major focus in these latter investigations. Having just 5% TCA or less in the nanogel polymerisation yielded the best results, therefore JRP234 and JRP235 were utilised moving forward.

2.4.6 Final Nanogel preparation and characterisation

To ensure reproducibility subsequent sets of nanogels were prepared following an identical protocol to JRP234 and JRP235. JRP240 and JRP241 gave very similar results to their predecessor equivalents, reinforcing their potential as drug delivery system. Therefore the general procedure was identified as 10 % acrylic acid 2.5-5% TCA with just 20 % MBA cross-linking, the remainder of the nanogel being composed of acrylamide. The monomers were polymerised at 70 °C for 2 days with 2% AIBN using a C_M of 0.5% in DMSO. The nanogels used for the toxicity studies are listed in table 13.

Nanogel	TCA (%)	MBA (%)	AA (%)	A (%)	C_M (%)	Yield (%)	Average diameter By DLS (nm)	Solubility in water (mg/ml)	Nanogel formulation and batch no.
JRP234	2.5	20	10	67.5	0.5	40	171±41	>10	NG1 (batch1)
JRP235	5	20	10	65	0.5	31	123±2	10	NG2 (batch1)
JRP240	2.5	20	10	67.5	0.5	25	123±56	>10	NG1 (batch2)
JRP241	5	20	10	65	0.5	31	107±4	10	NG2 (batch2)

Table 13 – final nanogel preparations for toxicity testing, all nanogels were polymerised for 2 days at 70 °C with 2% AIBN.

The solubility and size of the nanogels are consistent between the equivalent nanogels and very similar particle size distributions were obtained. There was a slight drop in

percentage yield for JRP240, which was due to material being lost during dialysis. As these nanogels proved to be reliable and reproducible, the nanogels were fully characterised by dynamic light scattering and TEM before moving on to investigate their toxicity. To facilitate the reading of this thesis from now on the nanogels will be referred to as NG1 and NG2 according to their formulation with the batch number associated with that formulation (see table 13). The two formulations can be viewed in table 14. As JRP29 was also required for further analysis in chapter 3, this has also been given the preparation name NG3, no batch number is associated with this as only one batch was produced.

Nanogel preparation	NG1	NG2	NG3
TCA	2.5	5	10
Acrylic acid	10	10	0
Acrylamide	67.5	65	20
Methylene bis acrylamide	20	20	0
Ethylene bis acrylamide	0	0	70
AIBN	2%	2%	1%
C_M	0.5	0.5	1
Polymerisation time	2 days	2 days	4 days

Table 14 – The three different nanogel preparations used for further studies showing the ratio of the monomers in the system, C_M is the concentration of monomers.

2.4.6.1 Particle size via dynamic light scattering using a Malvern Zetasizer

Throughout this chapter dynamic light scattering (DLS) has been touched upon as a method of obtaining an average particle size or average diameter of a nanoparticle. DLS, also referred to as Photon Correlation Spectroscopy (PCS) provides the hydrodynamic radius of particles. The technique exploits the Brownian motion theory and relates the size of particles to their motion in suspension. Samples are analysed by illuminating them with light, in this case a laser, and measuring the scattered light. Particles that are ≤ 250 nm in size scatter light in every direction; however, when a group of particles is present constructive and destructive interferences will occur and consequently the scattered light intensity will vary. As these particles are in solution they are constantly moving, therefore the light intensity is constantly rising and depleting over time forming intensity fluctuations[178]. A detector is placed at 90 to the beam to avoid detection of reflected light and the intensity is recorded as a function of time. The random movement of the particles results in broadening of the signal. The rate of these light intensity fluctuations is measured on the Zetasizer and the similarity of two signals in a particular time frame τ (1 μs) are correlated. An auto-correlation function $G(\tau)$ (the function with a time shift) can be defined as:

$G(\tau) = G_0 e^{-DA\tau}$ **Equation 3**

Where D is the translational diffusion coefficient

The movement rate of particles is dependant on their size, larger particles will move slower and smaller ones faster. Therefore measuring the light fluctuations and correlating them to their rate of fluctuation can indicate the size of particles. The hydrodynamic radius d(H) can be calculated using the Stoke-Einstein equation (equation 4) once the speed of fluctuation has been quantified using the translational diffusion coefficient (D).

$d(H) = \frac{kT}{3\pi\eta D}$ **Equation 4**

Where k is the Boltzman constant, T is the temperature in Kelvin and η is the viscosity.

Although the hydrodynamic radius d(H) gives a good indication of the size of particles, it is dependent on the nature of the solvent, how the particles swell in that solvent and the viscosity of the sample and therefore not an accurate representation of the real core particle size[179]. Therefore there are often discrepancies between the particle size obtained via DLS and particle sizes obtained via other methods such as Transmission electron microscopy.

The standard size distribution of a sample given by the zetasizer is in light intensity, a volume distribution of particle size can be extrapolated from the light intensity using the refraction index of the solvent and polymer investigated. From the volume distribution a number distribution can also be calculated. However, small errors in collected or correlated data can give large errors in the final hydrodynamic radius. For example, if a solution contains two different sized populations of particles equal in number, some of 5 nm and some with 50 nm, three very different graphs would be given (figure 34).

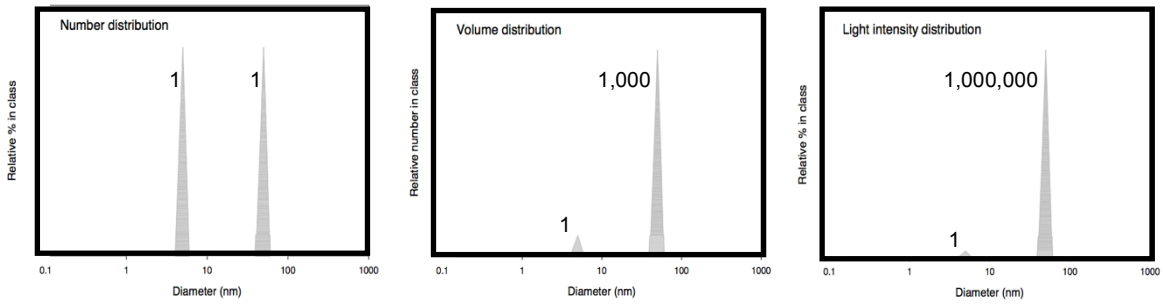

Figure 34 – Number, Volume and light intensity distributions of a sample containing two populations of particles, one with 5 nm and one with 50 nm diameters[178].

As the number of particles in each of the two populations was equal, peaks of equal size can be seen in the number distribution. However, when observing the volume distribution of the particles the peak for those at 50 nm is 1000 times larger than that of those at 5 nm as would be expected according to the volume of a sphere ($4/3\ \pi r^3$). The light intensity for the 50 nm particles is larger still, with an increase of 10^6. This can be explained by Rayleigh light scattering as larger particles scatter more light than smaller ones. The Rayleigh scattering equation shows there is a direct relationship between the diameter of a particle and the amount of light scattered to the power of 6, equation 5.

$$I = I_0 \frac{1+\cos(\theta)}{2R^2}\left(\frac{2\pi}{\lambda}\right)^4\left(\frac{n^2-1}{n^2-2}\right)^2\left(\frac{d}{2}\right)^6 \qquad \textbf{Equation 5}$$

Where λ is the wavelength, I_0 is intensity of the beam of light, θ is the scattering angle, *n* is the refractive index of the particle and *d* is the diameter of the particle.

Taking this into account and looking in depth at the particle size distribution of JRP240 using all three distributions, it can bee seen that the particle size given by light intensity is in this case confirmed by those by volume and number. The distribution of both volume and number are slightly skewed to the left, indicating that more of the particle population is slightly below 100nm than above. These particle size distributions can be seen in figure 35.

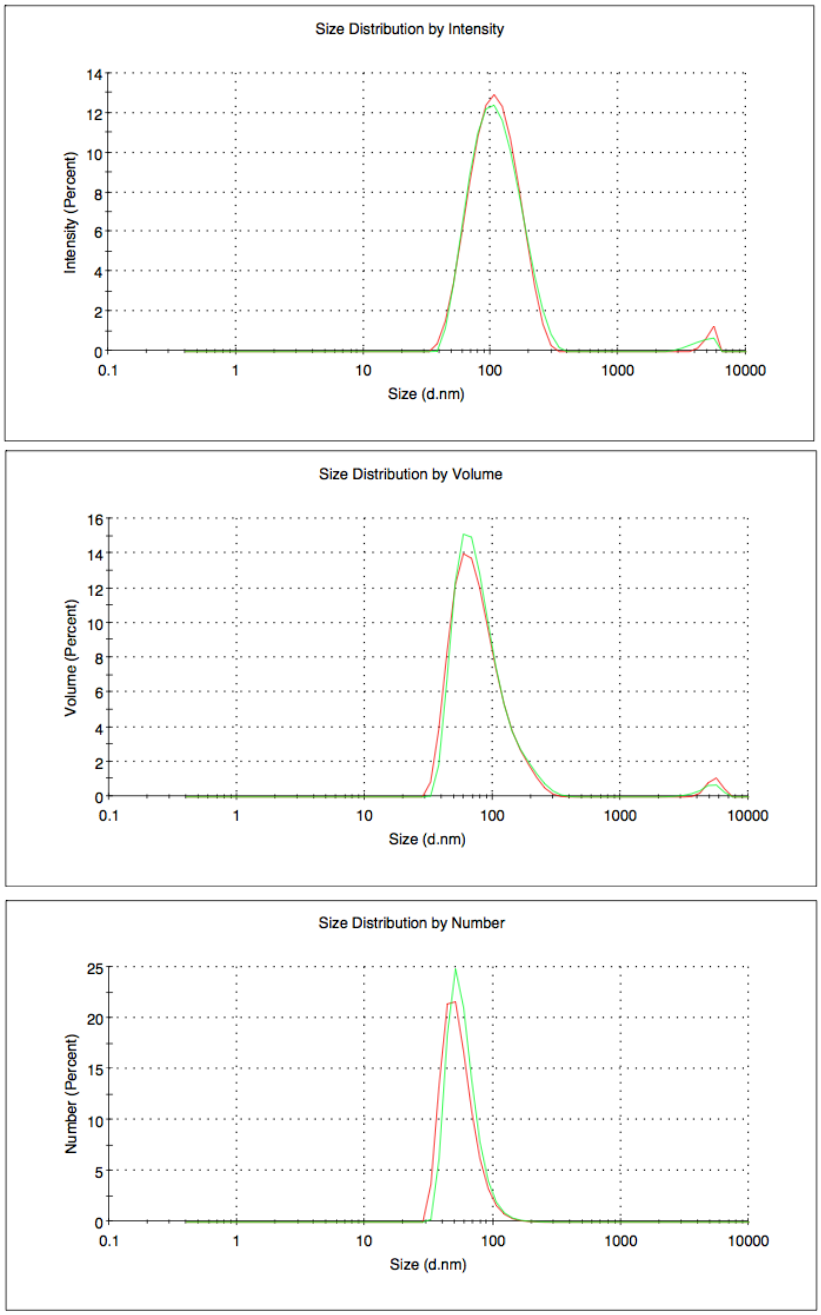

Figure 35 – Particle size distributions of JRP240 at 0.1 mg/ml in water using light intensity, volume of the particles and number of particles. Twenty scans of the nanogel were carried out with each line (in different colours) representing the average particle size of the sample over 10 scans.

2.4.6.2 Particle size conformation via TEM imaging

JRP240 was further analysed by TEM to visually support the DLS average particle size obtained. Transmission electron microscopy (TEM) is a very powerful technique, highly exploited in the field of nanomaterials, which allows imaging diffraction and chemical analysis of solid materials[180]. Material can be magnified to more than 10000 times by

use of the electron microscope. The electron beam gives high resolution images which give the TEM a significant advantage over a simple light microscopy. Electromagnetic lenses can magnify the image portrayed by the electron beam, which can be converged and focused on a detection surface (such as a fluorescent screen, photographic film or a CCD camera) by adjusting these lenses. TEM images are obtained with light and dark areas, which differentiate between materials of different densities by accounting for the amount of transmitted electrons passing through the material. Therefore the contrast of the image is dependant on the density of the sample analysed; for less dense samples a staining agent may be required to gain an image with good contrast and resolution.

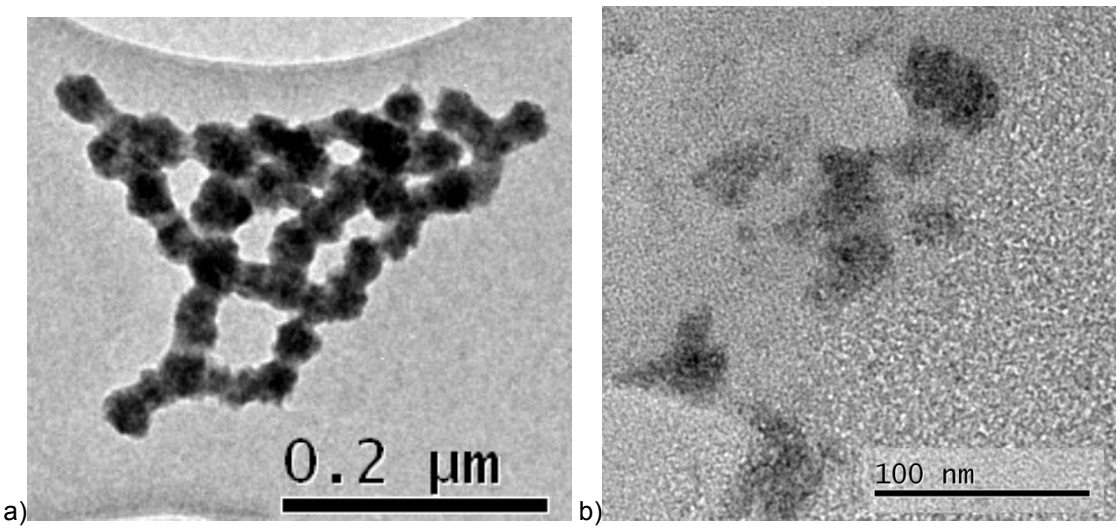

Figure 36 – TEM images of JRP240.

The TEM image of JRP240 shows the nanogels at around 40-50nm in size. This is not unexpected as nanogels swell in water, therefore their diameter in aqueous solution is likely to be larger than when dry. The DLS particle size trace does have an average of 123 nm. This can be accounted for the irregular shape of the nanogels seen in figure 36b where some of the nanogels are longer in one direction than in another. These images confirm that the particle size of the nanogels are less than 200 nm and therefore suitable for drug delivery.

2.5 Nanogel preparation conclusions

Nanogels were identified as a suitable polymeric nanomaterial for drug delivery with their significant advantage of intermolecular cross-linking, mainting a small structure with high surface to volume ratio and their flexibility to adapt the nanogel for the desired purpose. High dilution radical polymerisation was found to be a promising method for

the nanogel synthesis, eliminating the need for surfactants and giving good control of the size of the nanogel given by the ability to change various parameters. An acrylamide-based nanogel was decided upon due to the hydrophilic nature of acrylamide.

Having established the material and method of choice for this drug delivery system, three fluorescent tags were evaluated for their use as a tag to track the nanogels. A dansyl based tag was eliminated due to stability issues once incorporated into the nanogels and Fluorescein was eliminated due to the tag being released from the nanogels via hydrolysis. Trifluoromethylcouamrin acrylamide was identified as the fluorophore with the best properties for tagging the nanogels. It's high fluorescencent emission and good incorporation coupled with the amide bond between itself and the nanogel proved to be a reliable combination.

The initial nanogels had limited solubility therefore further investigations found acrylic acid significantly increased their solubility. Use of Methylene bis acrylamide as the cross-linker was determined to give the most suitable nanogels when used at 20% of the polymerisation mixture. The concentration of monomers was lowered to 0.5% to maintain a small and narrow particle size and the polymerisation was discovered to go to completion within 48 hours at 70 °C. An increase of the initiator, AIBN from 1 to 2% of all double bonds in the polymerisation was found to counteract the slight inhibition of the free radicals by the coumarin monomer. Finally investigations into the amount of TCA required in the nanogel formulation identified that TCA accounting for ≤5% of the total monomers gave best results with respect to particle size, solubility and fluorescence.

Nanogels containing TCA, together with acrylamide, acrylic acid and methylene bisacrylamide cross-linker, were successfully obtained and had a diameter of less than 200 nm. These nanogels also contained enough fluorophore to be tracked *in vitro* and *in vivo*, whilst maintaining high solubility (10 mg/ml) in water. These nanogels therefore have the ideal characteristics for testing the nanogels safety, and therefore shall be used to assess the safety of acrylamide-based nanogels via toxicity testing in the following results and discussion chapter.

CHAPTER 3:
Safety Studies

3. Safety Studies

Achievements in the area of nanomaterials have significantly advanced research in the development of novel drug delivery systems. Previously the focus was primarily on the synthesis and development of new drugs and their delivery was very much a secondary and expensive area of research. However, in the past few decades nanotechnology has enabled advances in medicine that previously could not have been imagined. There is still very little research that goes from bench to *in vivo* studies and on to clinical studies due to the high costs entailed[181]. Research in pharmaceutical applications was forecast to grow to 18 billion US Dollars this year with less than 4% of the FDA budget being allocated to nanoparticle safety. The effects of long term and chronic exposure to nanoparticles are still unclear and this is a cause for concern. In particular correlative and predictive *in vitro* and *in vivo* data on nanotoxicity is still lacking. As a result, finding methods and *in vivo* models for the evaluation of toxicity with substantially reduced time and costs is of high interest, particularly for the pharmaceutical industry[182, 183].

The previous chapter described the successful synthesis of a water-soluble nanocarrier tagged with a fluorophore. The next section reports on the investigation of the safety of the nanogels, an essential feature if these nanomaterials are to be further developed for medical applications. In general terms there are three major concerns over the toxicity of nanomaterials: (i) short term effect in the body; (ii) accretion inside the body over the medium-long term; (iii) effect on the environment when excreted. There are many novel nanomaterials that are developed everyday and for each of these systematic studies of toxicity are required. There is a clear need for information that can provide a more general picture on the impact of these nanoparticles[184]. Not only this, the acrylamide monomer used to create these nanogels has previously been identified as a neurotoxicant which inactivates proteins leading to disruption of terminal processes and impaired neurotransmissions. Acylamide has also shown signs of reducing fertility and causing tumours in animals.[185] Therefore any remaining monomer that remained in the nanogel after isolation could be of concern. In this results and discussion chapter, the nanogels safety studies are described and interpreted. Initial experiments were carried out *in vitro* using several assays for validation, however the main results were on the safety of the nanogels *in vivo* using *Danio rerio* as the animal model.

3.1 Establishing a suitable method for preliminary experiments in determining the toxicity of acrylamide based nanogels

3.1.1 The legalities of drug control and animal testing

The toxicity of drugs has been known for many centuries, it was Paracelsus (1493-1541) who said "The right dose differentiates a poison and a remedy."

However control of drugs and proving their safety is of relatively recent concern. It was less than 100 years ago, in 1937, when sulphanilamide was successfully used to treat streptococcal infections in tablet form. However, on demand for a liquid form of the drug, pharmacists found sulphanilamide to be soluble in diethylene glycol and sold the dissolved drug as sulphanilamide elixir, which caused severe kidney damage and 70 deaths[186]. On reaction to this the US FDA (Food and Drug Administration) introduced the first regulatory act to prove the safety of drugs prior to marketing in 1938. This required drugs to be tested on two animal species with histopathological examination. The thalidomide debacle of 1957 in Germany, which led to 15,000 foetuses to be born deformed, and causing the death of a significant number of those, led to regulatory acts in Europe and the need to prove efficacy of drugs, not just their safety[186, 187]. Since then drug legislation and regulation has developed and refined, not only to protect humans from the dangers of unproven exposure to new therapeutics, but also to protect animals from unnecessary dosages and pain in the testing laboratories.

One of the more recent acts with regards to animal welfare in science in the UK is the 1986 Animals (scientific procedures) Act, which came into force on 1st January 1987. This law requires trained personnel to obtain licences for carrying out procedures on animals, a licence for the project in which the animals will be used and also a licence for designated establishments where the animals are housed and experimented on[188]. All countries in the European Union were required to transpose their existing laws on the use of animals for scientific purposes over to a new European directive, 2010/63/EU by 1st January 2013. This law brought all countries in line to maintain a high standard of animal welfare in science across Europe[189]. It requires the implementation of the 3R's initially laid out by Russell and Birch in 1959, Replacement, Reduction and Refinement[190]. **Replacement**, where possible, expects that studies should be carried out by non-animal means, such as *in vitro* testing, computer modelling, chemical methods and statistical assessment,. **Reduction** seeks to keep the number of number of animals used to an absolute minimum, through: the use of the

most appropriate species and strain; attention to experimental design with appropriate statistical methods; limited sample variation by use of inbreeding and finally the use of animals with a scientifically controlled state of health. **Refinement** provides a reduction in the amount of stress an animal is exposed to by: maintaining enriched environments; good handling; the use of less invasive techniques wherever possible and effective pain control with efficient nursing care. It was therefore essential that all of the above requirements were adhered to during the research carried out for this project and that careful consideration and planning of the experiments took place.

In view of the above regulatory requirements and safety standards it was necessary to review the methods that are currently used to assess toxicity of nanoparticles and their reliability, and to understand the levels of toxicity that are currently considered acceptable by general scientific consensus.

3.1.2 Review of *in vitro* techniques, cell types used and concentration of the nanoparticle to use for the *in vitro* studies

In alignment with the **Replacement** principle discussed above of keeping the use of animal testing to an absolute minimum, *in vitro* testing is the first logical step in establishing the efficacy of any new therapy. In order to establish a thorough assessment of the nanogels' toxicity *in vitro*, previous studies were analysed to determine assays that would be consistent with other relevant research. One of the most common assays, to evaluate the toxicity of polymer-based nanoparticles *in vitro,* is the MTT (3-(4,5-dimethylthiazol-2-yl)-2,5-diphenyl tetrazoliumbromide) assay[191], a colorimetric test for the assessment of cell viability. NAD(P)H-dependent cellular oxidoreductase enzymes may, under defined conditions, reflect the number of viable cells present. These enzymes are capable of reducing the tetrazolium dye MTT 3-(4,5-dimethylthiazol-2-yl)-2,5-diphenyltetrazolium bromide to its insoluble and blue coloured formazan. Other cell viability assays include the XTT[192], sulforhodamine B[193], neutral red[194] and the alamar blue assay[195], which are all fundementally different, measuring different defects in the cell to determine cell viability. One assay often used for cell viability and that works in reverse to the MTT assay mentioned above, is the LDH assay[196]. This measures the lactase dehydrogenase released when the cell membrane is disrupted and cell death occurs. Although it is reported less frequently than the MTT assay, it is still regarded as a reliable method[194]. It is clear that different assays give different cytotoxicity results as they rely on different functions in the cell. As a result, it

is prudent to carry out more than one cytotoxicity analysis in order to get a more comprehensive view of the material's toxicity[194].

Cell viability assays are often combined with a cellular uptake assay, normally, but not only, performed by using flow cytometry[197]. Cytometry is a laser-based, biophysical technology employed in cell counting, cell sorting, biomarker detection and protein engineering, by suspending cells in a stream of fluid and passing them by an electronic detection apparatus where fluorescent cells are detected and counted. Cellular uptake can also be analysed via visual analysis using optical fluorescent microscopy[196]. In the latter method it is also possible to locate where in the cell the fluorescently tagged material has gone.

It is consistent with good practice to carry out both a cell viability assay, to establish the toxicity level of the therapy to healthy cells, and also a cellular uptake assay, to establish that it is actually entering the cells in order for the therapy to have its effect. However many polymeric nanoparticles, produced for a drug delivery application, are not tested for their cell viability or cellular uptake and even fewer go on to *in vivo* studies. This gives rise to a lack of consistent advance/promotion from bench to *in vivo* studies and on to clinical studies[181].

Of those materials that are analysed for their toxicity at the *in vitro* level, it is important to establish the cell type and concentration of polymeric nanoparticles applied in order to evaluate the final nanogel results. The type of cells used in these assays often varies according to the end application of the drug delivery system[193, 197, 198]. Many therapies developed for cancer treatments are tested on malignant cells such as MCF-7 cells, (breast cancer cells)[199-201]. In this way the researchers can assess both the toxicity of the nanocarrier and the therapeutic effect of the loaded drug[202]. Burts *et al* used this kind of cell to assess how effective their nanoparticles were at releasing the drug, doxorubicin, on application of UV light (the trigger). They used concentrations of up to 100 μM of drug, at a loading of 10% drug onto the nanoparticle. This assay gave Burts very positive results, seeing the cell viability drop to less than 10 % when the drug release was triggered, but without this significant change when the drug wasn't loaded (as part of the control)[203].

Keratinocytes, (skin cells) are commonly used for *in vitro* assays. These are frequently used, because they are quite resilient, due to their protective nature; they differentiate and proliferate well *in vitro*, reducing variation between lines. One study by Payyappilly

into the development of self-assembling block co-polymer micelles used keratinocyte HaCat cells to evaluate their cytotoxicity[204]. The nanomaterial was applied to the cells at 1-5 mg/ml. Other research by Teixeira *et al* however looked at the cytotoxicity of their nanomaterials at concentrations up to 1 mg/ml, focussing on lower concentrations[205]. The concentrations (1-5 mg/ml) used in the above two assays are comparatively high compared to the concentrations that were decided upon for the nanogels used in this project. Although the nanomaterials created in the studies above were both created with drug delivery in mind, they had different end applications to the nanogels produced in this project.

Having established that more than one cell viability test and a cellular uptake test would be necessary to determine the preliminary *in vitro* toxicity of the nanogels, focus turned to the selection of the best *in vivo* model with which to to proceed, keeping in mind replacement, reduction and refinement. Analysis of extant literature suggests that mice are the most commonly selected species for initial *in vivo* experimentation [206].

3.1.3 Discussion of *in vivo* models

In vivo testing allows the evaluation of effect of the materials across a much wider range of cells and enables analysis of its distribution. Initial *in vivo* studies are normally carried out on small rodents such as rats[207, 208], hamsters[209], gerbils[210] and guinea pigs[211], sometimes with comparisons being made of observed differences of effect between species[211]. By far the most utilised *in vivo* model is mice[206]. These are commonly used as an initial *in vivo* model as they are cost effective and have physiological similarities to humans. Not only this, more than a thousand mutant loci have been discovered which occur either spontaneously or are formed via radiation or chemical modifications. The discovery of these mutant loci has given rise to many potential models of different human diseases[206]. The ability to create new mouse models has been significantly increased through the better knowledge of the mouse genome and transgenic technologies, which allow modifications to virtually any gene. There are many mouse models with a homologous gene, which mutates in both mice and humans, where the mouse phenotype is highly similar to that of the human one. This enables relevant *in vivo* study of the disease development in question and provides a suitable model for testing treatments and preventative medicines[212].

Mice have been used to analyse the effect of many nanomaterials including nanotubes[213], PEG based nanoparticles[214], solid lipid nanoparticles[215], micelles[216], lysosomes[217], and many more[217-220]. In fact for a new therapeutic to pass through to

clinical trials, the first step of pre-clinical trials is that the material must be evaluated in a rodent species. For the development of a new drug, preclinical trials require dose-escalation, animal scale up with both rodents and non-rodent species as well as repeated administration studies with the final formulation. Dogs, often beagles, are used to study the drug's toxicity when repeatedly administered as well as observing the pharmacokinetics and pharmacological effects[221]. Once these steps have been completed, and the toxic levels and efficacy of the materials have been evaluated in animals, the material can then progress to clinical trials in humans. The use of a good *in vivo* model for use as an initial high throughput model with easy stage identification of good candidates is highly advantageous. Because of this, finding ways to eliminate poorer performing drugs and drug delivery systems with reduced cost is highly desirable, and would potentially increase the success rate once entering rodent studies.

3.1.3.1 Zebrafish as an in vivo model

A relatively new and highly interesting *in vivo* model emerging as an initial high throughput system for toxicity testing is that of *Danio rerio*, better known as zebrafish[222]. *In vitro* assays using cell cultures are useful for giving an initial indication of toxicity however they frequently have significant differences from *in vivo* results. This is due to the drug encountering many different processes including absorption, distribution, metabolism and excretion in the *in vivo* model which cannot all be accounted for in cell culture experiments. Advancing the drug development process using *in vivo* tests on zebrafish is an increasingly popular choice, as it allows the quantification of materials' toxicity before embarking on a costly mammalian study[223]. There are often large discrepancies between results found in *in vitro* and *in vivo* models when mammalian models are used[224]. By analysing toxicity in another animal species before embarking on a rodent trial, provides a clear advantage: if lack of toxicity is observed in both fish and rodents then further analysis in preclinical and clinical trials can go ahead with a predictably better success rate.

Zebrafish have many advantages for assessing the preliminary toxicity of a drug delivery carrier. They are very small, with adult fish being around 3cm long and their larvae being between 1 and 4 mm long, making them cheap and easy to maintain. Zebrafish reproduce in large numbers with a single clutch of eggs normally containing 100-200 eggs with a single larva being able to survive in one well of a 96 well plate for up to 7 days, thus enabling testing of large numbers of materials at once[223]. Drugs

and/or their carriers can easily be administered to the zebrafish embryos as at an early stage they can absorb material in their surrounding environment through their skin and gills. From 72 hpf (hours post fertilisation) they begin to swallow and at 5 dpf (days post fertilisation) they begin to actively feed and therefore the material in question can be administered orally. It is also possible to inject the material into the yolk of the zebrafish sinus venous or blood circulation of the zebrafish, giving an intravenous route of administration[223], although this method can be time consuming.

Zebrafish embryos are relatively large and for the first 24 hours of development the zebrafish embryos are completely transparent, allowing easy analysis of the embryo and any defects seen. Recent advances in targeting genetic modifications in the embryos allow breaks in their genome that are locus-specific and double stranded. This permits the generation of many mutant alleles that replicate human disease loci[222]. Zebrafish have been genetically modified to produce many different strains including an albino line (also known as Casper's), which remain transparent throughout their adolescence and in fact never develop the pigmentation seen in wild type. The transparency and speedy development of these fish make them a particularly suitable species for *in vivo* imaging[222].

The following diagram[225] (figure 37) shows a time course of zebrafish embryo development when incubated at 28.5ºC. Embryo development times vary according to the incubation temperature[226].

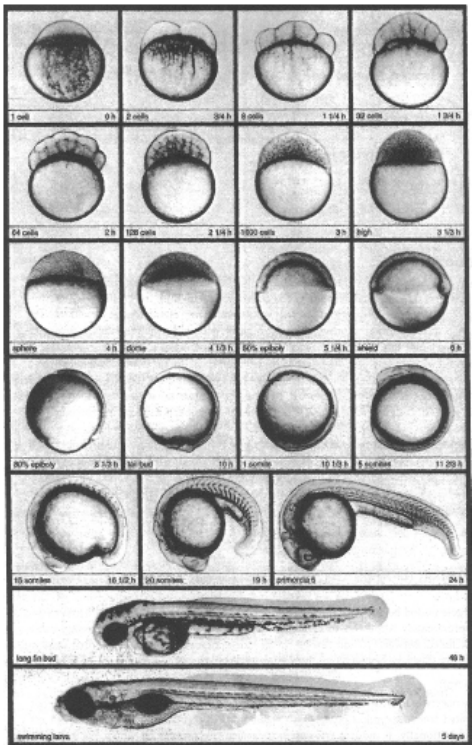

Figure 37 – Development stages of a zebrafish embryo from fertilisation to 5 days post fertilisation.

As zebrafish are a relatively new species for in vivo analysis of drug delivery systems, there are only a few published studies. Fako and Furgeson reviewed zebrafish as a correlative and predictive model for the assessment of biomaterial focussing on the toxicity of PAMAM dendrimers, fullerenes, carbon nanotubes, metal oxide and copper nanoparticles [183] . They concluded that zebrafish provide a useful system for bridging the gap between *in vitro* cell culture assays and rodent *in vivo* studies. Of the few published studies one or two groups have looked at fullerenes [227] and nanotubes [228]. Most other nanotoxicology studies have been on metals and metal oxides for example both Lubick [229] and Griffitt *et al* [230] looked at copper and metallic nanoparticles[230, 231] and Zhu et al studied metal oxides [232].

One group which used zebrafish for in depth analysis of a polymeric nanomaterial was Heiden *et al* [233], who investigated the toxicity of PANAM dendrimers. In this experiment zebrafish embryos were exposed to 0.2-20 μM dendrimer solutions at 6 hpf both continually for 114hrs (to 120 hpf) for prolonged exposure and some for a short burst of 1.5 hrs. 24 hpf embryos were also analysed to evaluate the effects of the dendrimers once many of the main features of the zebrafish had been established. The larvae were analysed for both signs of toxicity such as altered body axis, malformations of the eye, jaw, heart, fins, yolk sack, slowed growth, failure to inflate the swim bladder and

oedema as well as general developmental progression such as gastrulation completion (early embryo development, 5-10 hpf), somite formation (10-24 hpf developmental stages), heart beat and spontaneous movement. They graded the larvae every 24 hours on a scale of 0-4 of toxicity, 0 apparent health, 1 minor (1 morphological malformation), 2-moderate (2 morphological malformations), 3-severe (3 morphological malformations) and 4 death. This graduation enabled a more precise discussion of the toxic effects of the dendrimers. The toxicity was found to be dependent on the generation of dendrimer formed. 4^{th} generation dendrimers were found to cause death to between 50% and 94% of embryos within the first 24 hours regardless of the various exposure times used. However when applied at 24 hpf the embryos had a better survival rate, which may have been due to the embryo being further developed or due to the fact that the membrane[233] (normally referred to as their chorion) surrounding the embryo becomes less permeable at 12 hpf (as the embryos were only immersed in the dendrimer solutions for 18 hrs, to 42 hpf, and hence remained inside their chorion). For the purposes of studying the effects of a material administered at a later stage of development, exposing the embryos to the solution beyond dechorionation (when the embryo breaks through it's chorion) would provide valuable and relevant data.

In another study Kumar *et al*[197] evaluated the acute toxicity of their poly 2-(hydroxyl ethyl methacrylate) nanoparticles in zebrafish. They administered the nanoparticles at concentrations of between 5 and 100 μM via immersion of the embryos, for 96 hours. The age of the zebrafish embryos was not specified. In this study the authors analysed the embryos for dechorionation retardation, oedema and bent trunk and tail malformations, of which they found no evidence, even at the highest concentration[197].

Using a different method He *et al*[218] evaluated the toxicity of their coordination polymer nanoparticles in zebrafish embryos of less than 1 hpf. Between 50 and 100 pg of nanoparticles were injected into the yolk at the 4-cell stage and evaluated the embryos development at 6, 28, 52, 76 and 100 hpf. These nanoparticles slowed epiboly development, caused the embryos to have smaller heads, shorter bodies and caused pericardial oedemas. Even if it is time consuming, this method does ensure that the nanoparticles penetrate the embryo, as an alternative to the immersion technique, should the latter fail to demonstrate uptake of the nanogels.

Evidence from the literature clearly suggests that once *in vitro* studies have provided promising results, analysis of the nanogels *in vivo* in zebrafish is a cheap and relatively fast option that generates a large quantity of data. It was concluded that the best

scientific procedure to adopt was an initial immersion of the zebrafish in the nanogel solutions, as this method is much less time consuming, with a lower threshold for error, and is a more commonly used technique, offering greater cross comparison.

3.2 *In Vitro* toxicity results

In this section each of the cell viability and cellular uptake assays are described and discussed. In order to establish the maximum concentration of nanogel required for a drug delivery application, it was necessary to evaluate current dosages of the drug prescribed in order to predict the higher end concentrations that may be required. The model drug chosen for this project was tamoxifen. Current medical forms of Tamoxifen such as Nolvadex are prescribed as either a one-tablet dose of 20 mg or a twice-daily dose of 10 mg. This has a blood circulation peak concentration of 20 ng/ml 5 hours after administration, with a requirement of $\geq$70 ng/ml steady state concentration to see a clinical response[234]. 65% of tamoxifen entering the body is excreted in the faeces[235]. To circulate tamoxifen at 100 ng/ml in the blood, with a target loading of 10% tamoxifen on the nanogels, these would need to circulate at a concentration of 1 µg/ml of blood. It follows that, to remain safe, the nanogel should not prove toxic at 1 µg/ml, If intravenously (as opposed to orally) administered, this stock solution could be much more concentrated therefore concentrations of up to at least 200 µg/ml nanogel was explored in our assays.

Both cancerous cells and keratinocytes offer sound bases for analysing the cytotoxicity of these nanogels. Keratinocytes were chosen for assessing the nanogel's cytotoxicity for several reasons: the ease of line maintenance and therefore reduction in variability; keratinocyte cell lines were readily available at Queen Mary's medical school and Cranfield University; whilst cell lines in general vary widely as to their cytotoxicity results, Nogueira *et al* found that, when comparing cancerous cell lines to keratinocytes, the latter were found to have greater sensitivity to cytotoxicity. They also suggested using more than one cell line when analysing cytotoxicity, to gain more reliable results[236]. Alamar blue and MTT assays were selected as both had proven to be effective in evaluating cell proliferation in keratinocytes[237], along side the LDH assay.

3.2.1 Alamar Blue Assay

Initially the alamar blue assay was carried out at Queen Mary's Medical school to give an indication of the level of cytotoxicity of the nanogels before embarking on full *in vitro*

analysis. The alamar blue assay is a cell proliferation assay which works by the reduction of resazurin (a non-fluorescent dye[195]), to resorufin (abs 570 nm, ex 560 nm, em 590nm) a compound that emits in the red channel. The reduction of resazurin only happens in living, metabolically active cells. At the end of the test, only cells that are still viable produce the fluorescent dye, thus giving a quantifiable result. In this way the target cells are treated with the combination of the non-toxic, cell-permeable resazurin (acting as an indicator of continued metabolic activity) and the material of which the toxicity is unknown (which may or may not kill the cells, affecting the indication), and control cells are treated with just resazurin. This allows clear and quantifiable analysis of the metabolic activity in the two groups of cells through observation of fluorescence after varying the timescales of treatment. These results then serve to indicate the cytotoxicity of the material under observation.

In this study just one nanogel, NG1 (batch 2), with 2.5% coumarin fluorescent tag was analysed to get an initial assessment of the nanogel's cytotoxicity. NG1 (batch 2) was chosen as it contained the least amount of fluorescent tag, which was likely to be the most toxic component of the nanogels. Initial investigations used comparatively low concentrations (up to 50 µg/ml) as Hamid *et al* had found alamar blue to be slightly more sensitive than MTT at lower concentrations[237]. This assay was carried out over over 5 days to obtain toxicity data for sustained exposure of nanogel, NG1 (batch 2). NG1 (batch 2) was applied to N-tert keratinocyte cells at concentrations of 1 µg/ml, 5 µg/ml and 10 µg/ml for 48hrs, results displayed in figure 38a. As As these experiments did not show any apparent cytotoxicity to N-tert cells, the concentration of nanogels was increased to 50 µg/ml and the experiment was repeated over 5 days, figure 38b. The alamar blue assay confirmed that the nanogel had no significant impact on the cell viability with a >95% cell survival rate.

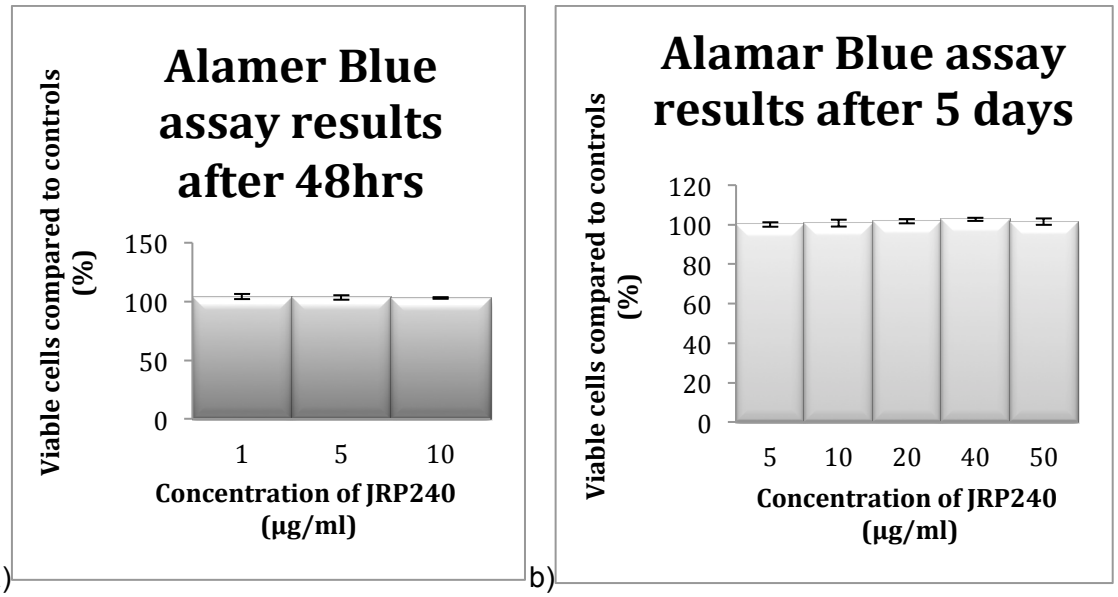

a) b)

Figure 38 – Cytotoxicity results of nanogel NG1 (batch 2) in N-tert karetinocytes at concentrations of 1-50 µg/ml after a) 48hrs incubation, b) 5 days incubation. Three replicates were carried and the error given is the standard deviation between the replicates.

3.2.2 MTT Assay

To assess the toxicity of these nanogels, the MTT assay was performed, as this assay is used extensively for cell viability[194]. It was originally published by Mosimann but further developed by Denizot and Lang in 1986[238] as well as many others since. It works on the basic principle of the reduction of MTT (3-(4,5-dimethylthiazol-2-yl)-2,5-diphenyl tetrazoliumbromide), which is yellow in colour, by mitochondrial succinic dehydrogenase in living cells, to a blue coloured formazan product[238]. The living cells can then be quantified by measuring the amount of absorbance per mm^2 of sample and comparing treated cells to negative controls (untreated cells).

As the alamar blue assay had shown promising results with concentrations up to 50 µg/ml, the MTT assay was carried out at this concentration but also at higher concentrations, up to to 200 µg/ml to ensure the nanogels would not be cytotoxic at these higher levels. In this assay HaCat Keratinocyte cells were used as the experiment was carried out in collaboration with Cranfield University and these were the cells available.

The MTT assay was carried out on HaCaT cells, with two nanogels, NG1 (batch 1) and NG2 (batch 1), neither of which showed significant toxicity after 3 days up to 200 µg/ml. 97±4.2% of the cells treated with NG1 and 92±6.6% of those treated with NG2 were

viable after 3 days incubation at 200 µg/ml compared to the negative control. In the case of the positive control, hydrogen peroxide, there was a very significant impact on the number of viable cells even at the lower concentration. In fact in the first 24 hours the cell lines treated with either nanogel showed so much improved cell viability to that of the control cells that it indicated a positive effect on their proliferation by appearing to act as a nutrient resource. The study was carried out for 72 hours in total to ensure that the cells had stabilised and the cell proliferation was maintained and not reducing in comparison to the controls, which would have indicated a damaging, toxic effect. In fact the cells did stabilize by 72 hours and no significant apoptosis was seen in comparison to the negative control. The destructive effect of the hydrogen peroxide load in the positive control could be seen with 66±2.2% of cells surviving at the lower concentration (25 µg/ml) and less than 37±1.5% cell survival at the higher concentration of 50 µg/ml.

a)

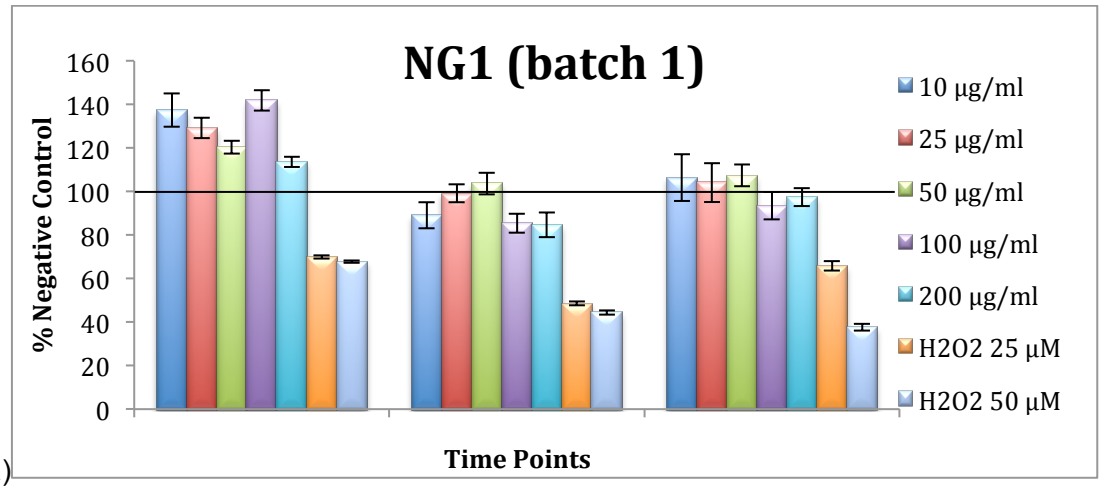

b)

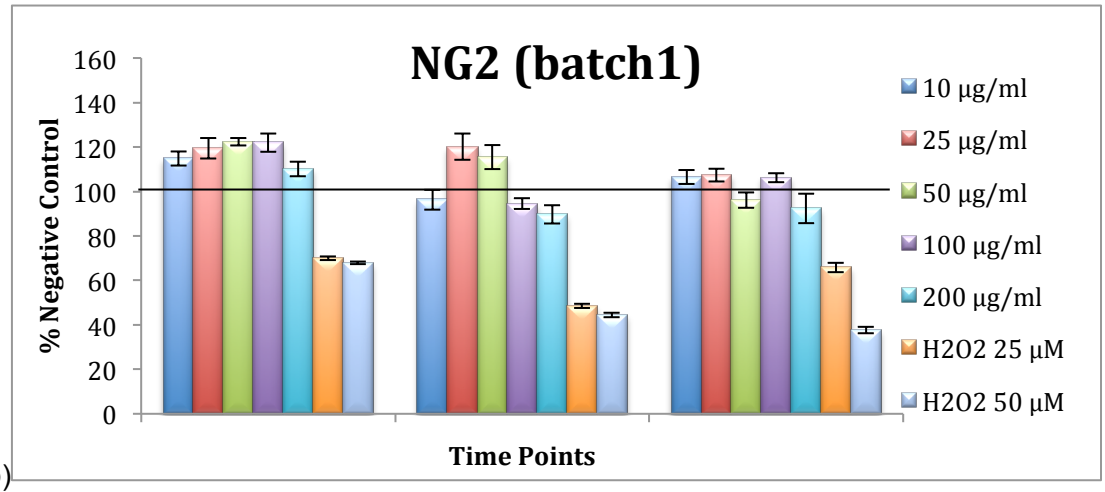

Figure 39 – MTT assay results for the nanogels at varying concentrations of nanogel after 24, 48 and 72 hrs incubation with a) NG1 (batch 1) b) NG2 (batch 1). Three replicates were carried and the error given is the standard deviation between the replicates.

3.2.3 LDH Assay

To confirm the results found with the MTT test, the LDH assay was carried out which works on an inverse method to MTT: it measures the amount of lactate dehydrogenase present in the media surrounding the cells. Lactate dehydrogenase is released into the extracellular medium when a cell dies as a result of irreversible damage to the cell membrane [194]. If LDH has been released it aids the formation of pyruvate from lactate which at the same time reduces NAD+ (nicotinamide adenine dinucleotides) to NADH. It is the NADH produced by the first reaction that is used to convert a colourless tetrazolium salt (INT, 2-p-iodophenyl-3-p-nitrophenyl-5-phenyl tetrazolium chloride) to a red formazan product. It follows that the amount of LDH present (therefore the quantity of dead cells) is directly proportional to the amount of formazan product detected.

When analysing the short term data at 4 and 8 hours no significant cytotoxicity was seen either with the nanogels or the positive control. However the LDH assay is well proven to need longer timeframes to be able to establish cytotoxicity[194]. After 24 hours the positive controls showed significant signs of toxicity and studying the cells at 48 and 72 hrs the toxicity substantially increased, confirming this trend, see figure 40. The LDH assay was carried out on NG1 (batch 1) and NG2 (batch 1), neither of which showed any significant increase in the amount of LDH present over a 72 hour period, most significantly in comparison to the hydrogen peroxide positive control. At 48 hours the level of toxicity of the nanogels peaked with the highest seen in 200 µg/ml, which had a 31±0.34% increase of LDH for NG1 and 30±0.76% increase for NG2. However, this was significantly lower than the positive control which increased by 120±0.45% at the lower concentration. Furthermore the data was inconsistent with concentration, for example in the experiment using NG1 at 48hrs, 10 µg/ml had a higher amount of LDH, 11±0.16% than the nanogel at 50 µg/ml which was 3±0.19%. However by 72 hours no significant toxicity could be seen in any of the nanogel concentrations with maximum increase in LDH at 200 µg/ml of 6±0.77% for NG1 and 19±0.94% for NG2. The data clearly indicate that the LDH levels return to normal values within 72 hours of incubation, suggesting that the slight increase in LDH over the shorter period was not of concern.

a)

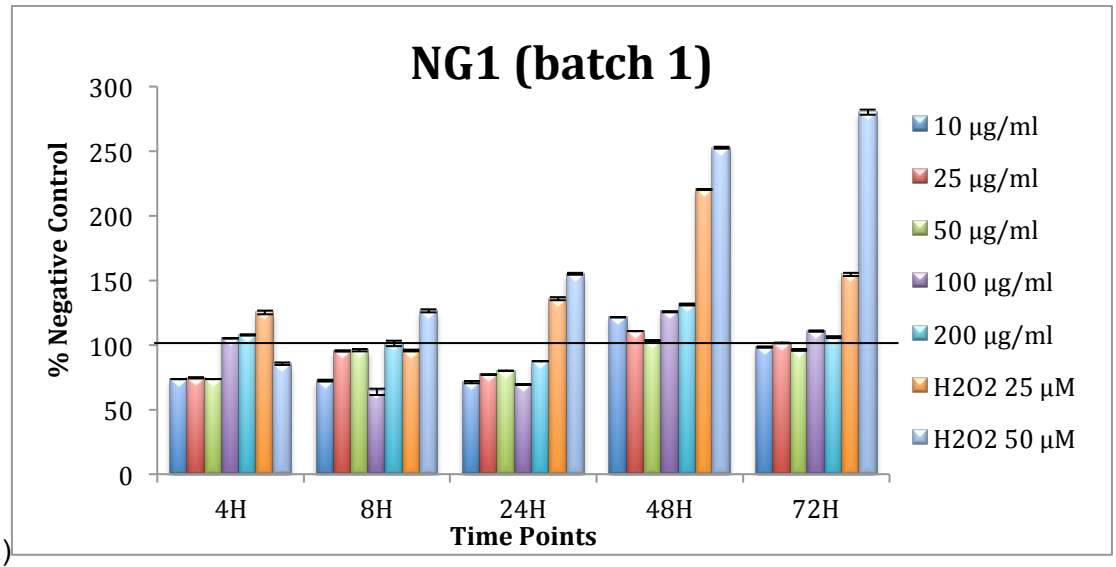

b)

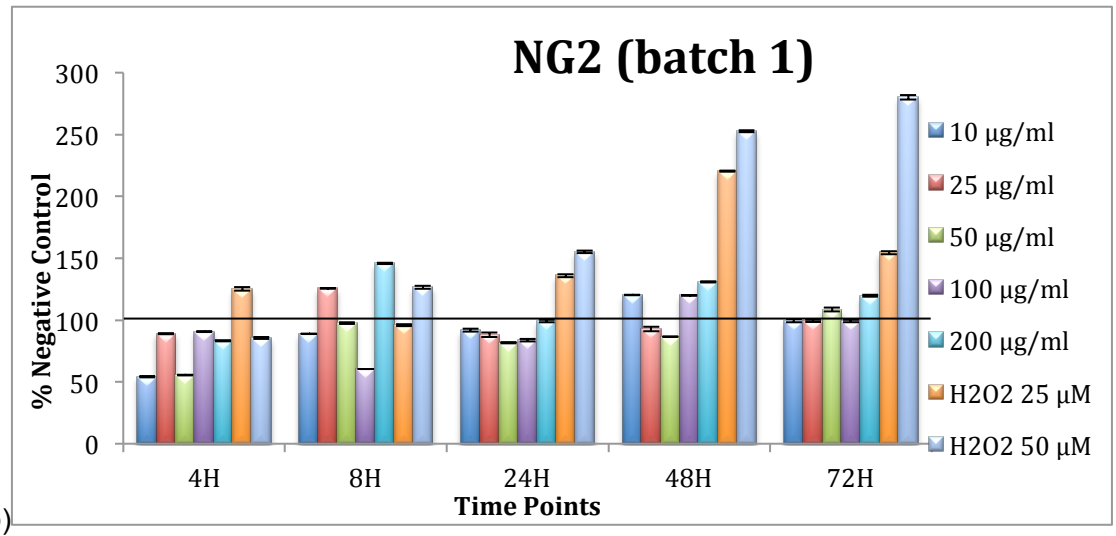

Figure 40 – Cell viability via the LDH assay at 4, 8, 24, 48 and 72 hours of incubation with varying amounts of a) NG1 (batch 1) (2.5% coumarin tag) and b) NG2 (batch 1) (5% coumarin tag). Three replicates were carried and the error given is the standard deviation between the replicates.

Potential differences in cell cytotoxicity between cell lines has been well documented[236], however all three assays gave no evidence of toxicity of the nanogels despite differences in cell lines used. Having carried out 3 different cell viability assays and found no preliminary evidence of cytotoxicity in keratinocyte cells, in the next stage it was important to establish that the cells were internalising the nanogels. At this stage, it was deemed appropriate to proceed to carry out *in vitro* investigations, specifically with a cellular uptake assay where the cells were analysed by confocal microscopy for visual analysis of the nanogels in the cell structures.

3.2.4 Cellular uptake of nanogels

As no cell toxicity was observed using any of the *in vitro* tests so far, it was important to establish that the cells were taking up the nanogels. To ensure a potential application of these nanoparticles, where the therapeutic drug could be delivered into cells using them as a carrier system. This was analysed via two methods. The first was by flow cytometry using emission at 450 nm. Two different nanogels were used for examination: NG1 (batch 2) (2.5% coumarin tag) and NG2 (batch 2) (5% coumarin tag), together with a negative control control sample. For reliable indication of cellular uptake, the nanogels loaded with the coumarin tags should emit fluorescence and therefore a peak in fluorescence intensity should be detected at 450 nm wavelength.

In this method the N-tert-1 keratinocyte cells were incubated with the fluorescent nanogels NG1 (batch 2) (2.5% coumarin tag) and NG2 (batch 2) (5% coumarin tag) at 50 µg/ml for two hours before being washed with PBS. The remaining cell suspension was added to a stream of liquid, thus diluting the solution so there was as close to one cell per droplet of liquid as possible. Just before the droplet formed, the fluorescence of the liquid stream was measured for every cell passing through. A control sample was also measured for fluorescence and the sample was then compared to the control. The results for nanogels NG1 (batch 2) and NG2 (batch 2) against a control can be seen in figure 41. Cells exposed to both nanogels exhibited fluorescence at 450 nm showing uptake of the nanogels into the N-tert-1 cells. The cells exposed to NG2 (batch 2) contained far more fluorescence than those exposed to NG1 (batch 2). This is explained by the fact that NG1 (batch 2) contained half as much fluorophore (2.5% coumarin monomer) compared to nanogel NG2 (batch 2) (5% coumarin monomer), therefore the fluorescence intensity seen in NG1 (batch 2) was far lower than that exhibited by NG2 (batch 2). This gave a clear indication that the nanogels were being taken up by the skin cells. However, to visualise the cellular uptake, and provide further positive confirmation of it, the cells were analysed via confocal microscopy.

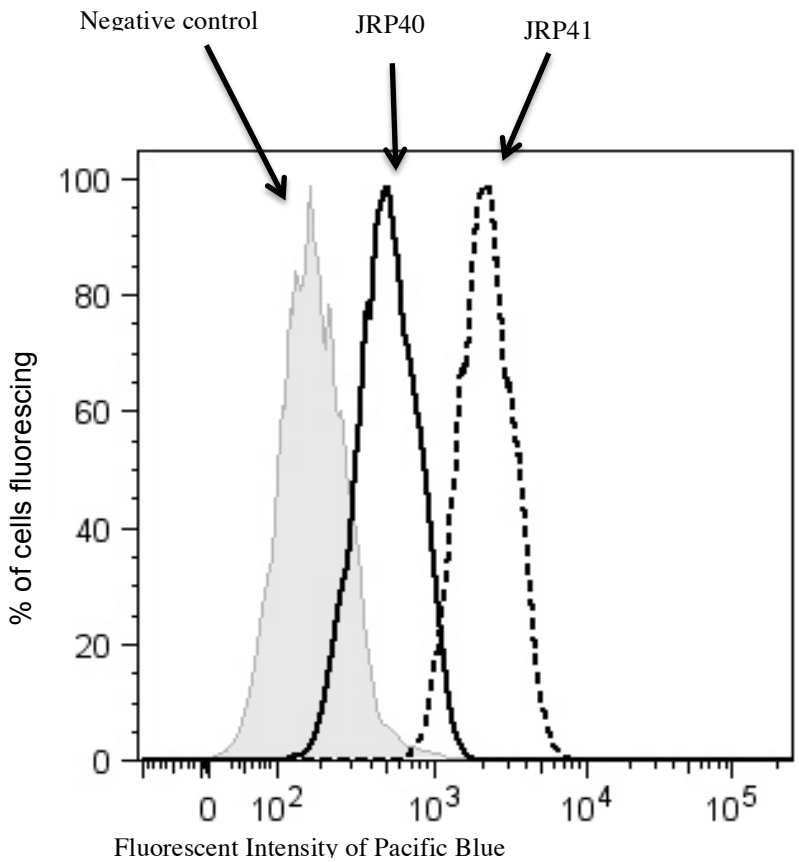

Figure 41 – FACS results of the cellular uptake of NG1 (batch 2) and NG2 (batch 2) into N-Tert-1 keratinocytes analysed by flow cytometry.

The cells prepared for the visualisation experiment were incubated at 37 °C in the relevant nanogel solution for 2 hours at 50 µg/ml before being washed with PBS, and fixed with 4% paraformaldehyde. The cells were then analysed for fluorescence using a Zeiss 510 confocal microscope. In the images from using the confocal microscope presented in figure 42 the nanogel can be clearly seen in the cytoplasm of the cells, showing that the nanogels successfully entered the keratinocyte cells. Preliminary experiments had already shown that the cells had taken up the nanogels and moreover that the latter did not appear to be cytotoxic in keratinocyte cells at concentrations up to and including 200 µg/ml in three complementary cell viability assays. Consequently, it was considered safe and prudent to continue and expand on the toxicity studies *in vivo* using zebrafish.

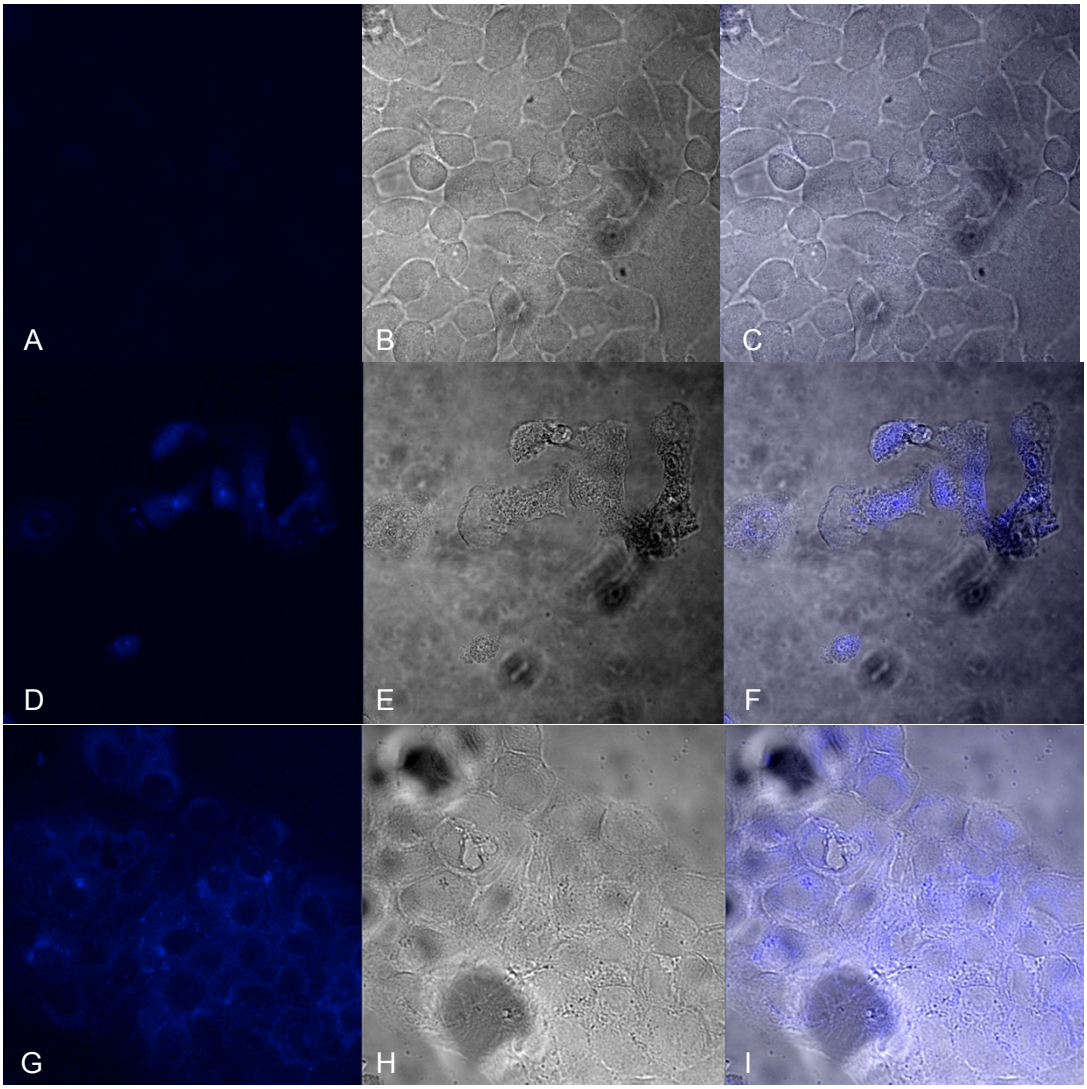

Figure 42 – Confocal images of the nanogels' cellular uptake in the cells. A-C are controls, D-F are treated withNG1 (batch 2), G-I are treated with NG2 (batch 2). A, D and G show the fluorescence, B, E and H are the bright field and C, F and I are the two overlaid.

3.3 *In Vivo* toxicity results

The purpose of the work described here was to evaluate any impact that the nanomaterial would have *in vivo* and allow study of their effect on a range of different cell types to which the nanogels would potentially be exposed.

There are three areas of concern with nanoparticles and their potential toxicity. These are the safety of the NPs to the patient, the user (producer) and environmental safety. Through analysis of the toxicity of these nanogels in zebrafish preliminary data on their direct effect can be established: when applied in the short term; on excretion (if, indeed

they are excreted by the zebrafish); long term build up (if excretion is low) and consequent toxicity levels. Furthermore, given that zebrafish are a species of fish, these results would provide an additional indicator of potential hazards to aquatic species as a result of nanoparticles arriving in the sea through sewage routes (via watercourses and land run-off) when excreted from humans and/or animals after administration.

3.3.1 Nanogel immersion evaluation

One of the most common approaches used to assess the toxicity of nanomaterials in zebrafish, involves the suspension of the material under investigation in the zebrafish's environment[239-241]. The OECD (organisation for Economic Co-operation and Development) recommends that zebrafish embryos should be used for acute toxic analysis screening before the blastula period begins (at 2.5 hours post fertilisation, hpf)[242]. Active feeding, however, does not begin until the larvae are 5 days old[225] therefore two sets of data need to be collected: that from immersion at the time point recommended by the OECD and that found at the later stage of development when the larvae begin to feed. Therefore both the 2 hpf stage and 48 hpf stage of development were evaluated in this study, with the fish being maintained in the nanogel environment beyond 5 dpf (days post fertilisation) to enable toxicity evaluation via active feeding. When analysing the zebrafish embryos at 2 hpf the emphasis was on whether the nanogels were toxic when passing through the chorion, the acelluar membrane surrounding the embryo, to the embryo itself. Initial experiments were carried out on embryos at 2 hpf, with both nanogels at 0.1 and 1 mg/ml each. Analysis of the fish for change in morphology and oedemas was noted along side the death of embryos.

As the *in vitro* results had not shown any evidence of toxicity in concentrations up to 200 µg/ml, it was decided to use two concentrations of the nanogel, one below the limit of that tested *in vitro* and one substantially higher, to see the impact of a such a high dose on the zebrafish embryos. In these experiments a genetically modified strain of zebrafish was used, often referred to as Caspers, due to their transparent nature throughout their development with the mature fish having transparent skin allowing visual analysis of organs and cellular activity[222]. This mutated strain has the advantage of not requiring the addition of PTU (1-phenyl-2-thiourea) in order for optimal analysis. PTU is used to prevent pigmentation in the fish, which can interfere with visual analysis of the zebrafish embryos, however, it is itself toxic at high doses. Injection of the

nanogels into the zebrafish could be considered at a second stage of the nanogels' toxicity evaluation.

To carry out these preliminary investigations the nanogels were 'dissolved' in fish water (0.03% salts) at 1 and 0.1 mg/ml and 10 embryos at 2 hpf (hours post fertilisation) and 48 hpf were added to the different solutions. The embryos were added to the nanogel solutions at 2 hpf when they were at the 8-16 cell stage. Using this stage of embryo allowed investigation of effects on very early stages of development. These embryos were removed from the nanogel solutions after 24 hours exposure and returned to fresh fish water. After just 6 hours a significant death rate in the higher concentration of both nanogels was seen. 40±5.8% of embryos had died in 1 mg/ml NG1 (batch 2) that contained 2.5% coumarin monomer and 50±11.5% of those in the same concentration of NG2 (batch 2) with 5% coumarin monomer. However at the lower concentrations the survival rate was more promising with a 70±5.8 and 80±5.8% survival respectively. After 24 hrs, all embryos exposed to the nanogels at the higher concentrations had died, as had those in 0.1 mg/ml NG2 (batch 2). However no further embryos had died in 0.1 mg/ml NG1 (batch 2), which also contained less coumarin monomer. See figure 43.

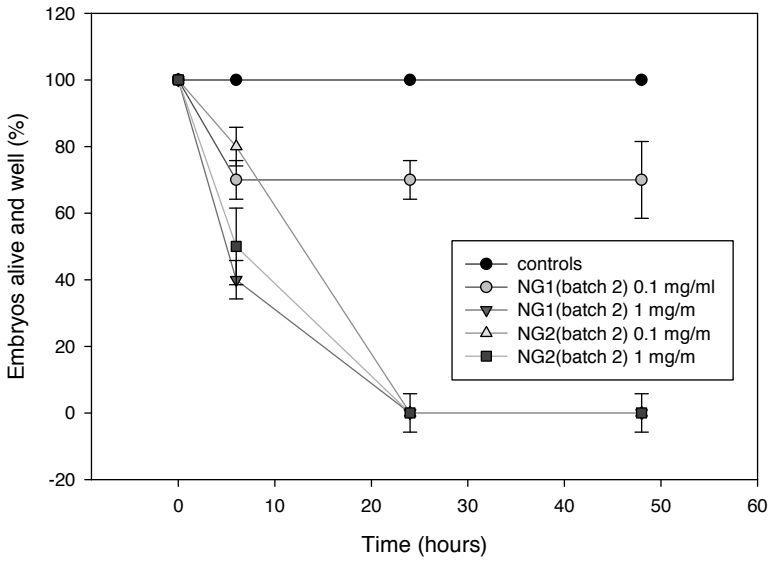

Figure 43 – Initial in vivo experiment carried out on 2hpf (hours post fertilisation) zebrafish embryos. Nanogel NG1 (batch 2) contained 2.5% coumarin monomer and NG2 (batch 2) contained 5% coumarin monomer. 10 zebrafish were exposed to the relevant solution for 24hrs before being returned to fresh fish water. For each replicate 10 embryos were placed in each solution and the experiment was carried out 3 times, the error bars give the standard deviation between the three experiemtents.

These experiments were highly preliminary and the first set carried out within the research group, therefore little knowledge was known on the number of embryos required per solution analysed and lethal concentration levels required to be established. Since obtaining these results it has been noted that when repeating these studies establishing a 10%, 50% and a no effect level of the nanogels on zebrafish ebryos would be required in order to establish a the margin of safety of the nanogels with using a minimum of 20 embryos per solution used.

The experiemental results displayed in figure 43 show that after 48 hours 70±11.5% of the zebrafish survived in the lowest concentration, 0.1 mg/ml, of nanogel NG1 (batch 2). All embryos (±5.8%) died within 24 hours exposure to NG2 (batch 2) at the same concentration, 0.1 mg/ml. NG1 (batch 2) contains half the amount of coumarin monomer (2.5%) compared to NG2 (batch 2) (5% coumarin). As the only significant difference between the two nanogels is the coumarin tag content, it could be that the coumarin tag itself is toxic to the zebrafish at very early developmental stages. Therefore to investigate whether the coumarin monomer may be impacting on the nanogel's toxcicity at this stage of development, 2 hpf embryos were exposed to trifluoromethyl acetyl coumarin (TMAC, 7a chapter 2). TMAC is highly similar in structure to the monomer (TCA, 7, chapter 2) used, but without the terminating double bond which has already shown to be acutely toxicity[243] and the double bond no longer exists once polymerisation has taken place. 2 hpf embryos were placed in solutions of TMAC 0.01 mg/ml (in 1% DMSO, 99% fish water v/v), nanogel NG3 at 0.075 and 0.025 mg/ml (containing 10% coumarin monomer, in 1% DMSO, 99% fish water v/v) and controls in fresh fish water. The use of DMSO was required as a result of the low solubility of TMAC in water. NG3 was used as it contained a higher amount of coumarin monomer allowing lower concentrations of nanogel to be analysed yet producing high enough fluorescence to be tracked. A 24 well plate was used with 2 ml of the relevant solution being placed in each well, including fresh fish water for the controls. A single embryo was placed in each well and the well plate was studied at 24 hour intervals under a microscope for signs of toxicity such as curvature of the notochord, oedema or death. All the embryos were maintained in their relevant solution for 3 days before being returned to fresh fish water.

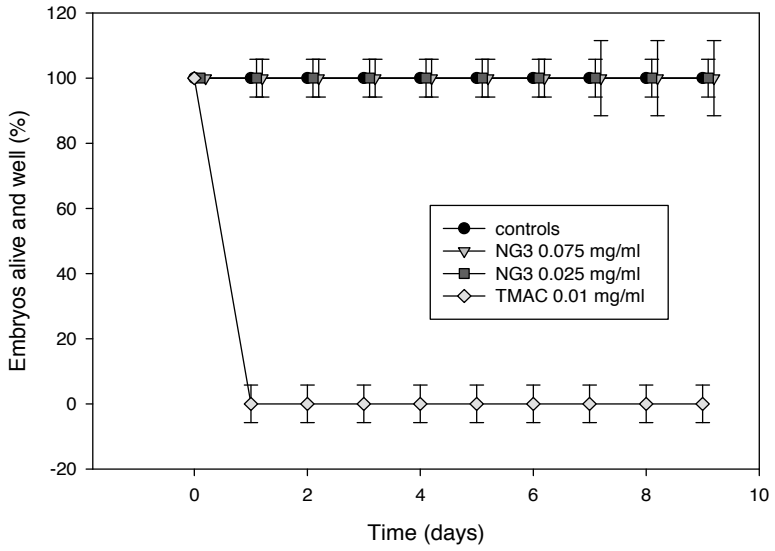

Figure 44 – Results of a zebrafish experiment evaluating the toxicity of TMAC. Where TMAC is trifluoromethyl acetyl coumarin, NG3 is a nanogel containing 10% TCA. All solutions were formed with 1% DMSO in fish water (v/v) except the control with is 100 % fish water. Between 5 and 8 Embryos were maintained in the relevant solution from 2 hpf for 3 days before returning to fresh fish water. For each replicate 8 embryos were placed in each solution and the experiment was carried out 3 times, the error bars give the standard deviation between the three experiemtents.

This experiment showed that the TMAC alone was highly toxic to 2 hpf embryos all of which died within 24 hours of exposure. However the young embryos tolerated the nanogels at lower concentrations. Effectively NG3 at 0.025 mg/ml contained 0.0025 mg/ml coumain monomer and NG3 (10% coumarin monomer) at 0.075 mg/ml contained 0.0075 mg/ml coumarin monomer. These concentrations of coumarin are lower than those used in the first experiement where NG1 containing 2.5 % couamrin was used at concentrations of 1 mg/ml and 0.1 mg/ml, effectively having concentrations of 0.025 and 0.0025 mg/ml couamrin tag and NG2 containing 5% coumain used at the same concetrations of nanogel, effectively dosing the embryos at 0.05 and 0.005 mg/ml coumarin tag. Evidently these concentrations were too high therefore much lower concentrations of nanogel were used to compare with free coumarin. In this experiement 0.01 mg/ml of free couamrin (TMAC) was chosen as it was a lower dose of couamrin tag than that administered in the initial set of experiement but higher than that in the nanogels solutions of this experiement. However in hindsight dosing the nanogel at 1 mg/ml (0.01 mg/ml coumarin tag) would have been a sensible addition for a more direct comparison. In reality TMAC is a small molecule which will behave differently to the nanogels and likely be absorbed efficiently

across the gills of the zebrafish and therefore unless both nanogel and TMAC were directly injected into the zebrafish it is difficult to make a direct comparison. It does however show that if the fluorescent tag is at any point released from the nanogel it would cause toxicity, giving indication that the nanogel remains attached to the nanogel. In this second (TMAC) experiment, figure 44, No zebrafish in the nanogel solutions appeared to have severe deformities such as curvature of the notochord or oedema (images of these deformities can be seen in figure 47). By contrast both Heiden *et al* and He *et al* found these deformities occurred when zebrafish embryos were immersed in some of their nanomaterials[233, 244], leading to the conclusion that these acrylamide gels were showing a much lower degree of toxicity at concentrations of 0.025 to 0.075 mg/ml, and could be safely used in that range[218].

To analyse the effect of the nanogels on zebrafish at the later stage of development, the same protocol used for the 2 hpf zebrafish embryos was repeated with 48 hpf zebrafish. After 48 hours post fertilisation the zebrafish have developed the majority of their organs, having completed morphogenesis, and their development is known to slow down rapidly[225]. The effect of the nanogels on more stable juvenile larvae could thus be contrasted with that on those undergoing rapid early development process. The nanogels were developed to carry tamoxifen to treat breast cancer, not to treat growing foetus' therefore analysing the effect of the nanogels on a more fully formed organism is a more representative model. Not only this, at 2 hpf zebrafish do not actively feed therefore any nanogel that had entered the 2 hpf embryos had done so through diffusion rather than through potential oral administration. Therefore to establish if toxicity was present at a later stage of development and the effect of the nanogels on more fully formed zebrafish fry, nanogels NG1 (batch 2) and NG2 (batch 2) were dissolved at concentrations of 0.1 and 1 mg/ml, and 48 hpf embryos were placed in the solutions along side embryos in fresh fish water as controls. The embryos were studied under fluorescent microscope every 24 hours to evaluate nanogel intake and distribution and their toxic effects.

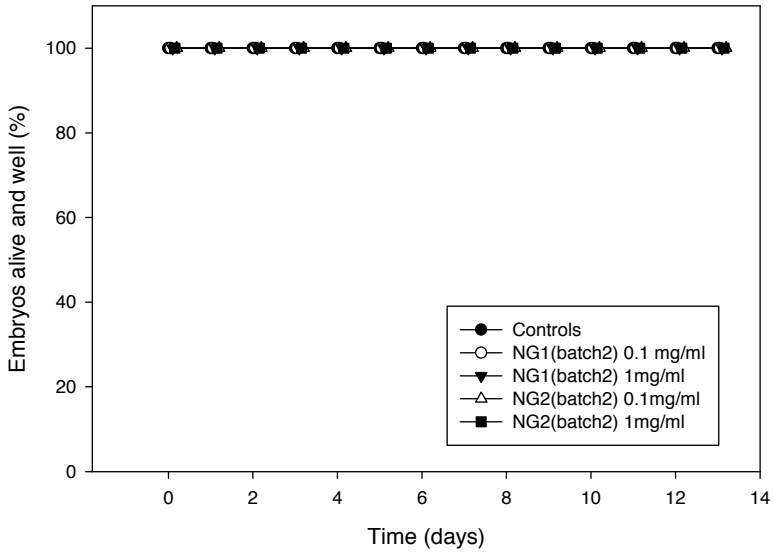

Figure 45 – Effect of nanogels on 48hpf (hours post fertilisation) zebrafish embryos. Nanogel NG1 (batch 2) contained 2.5% coumarin monomer and NG2 (batch 2) contained 5% coumarin monomer. The zebrafish were exposed to the relevant solution for 7 days before being returned to fresh fish water. The experiment was carried out in triplicate, but no variation in results was seen.

This experiment gave strong evidence of better tolerance of the nanogels by the fry. This time they were exposed to the nanogel solutions for 7 days, as no impact on survival was seen, figure 45. 4 days after being immersed in their solutions, nanogel could be seen in the intestine of the zebrafish immersed in the solutions at the highest concentrations of nanogel (1 mg/ml) although it was very weak. As a consequence, the zebrafish were maintained in their nanogel solutions for a further 2 days when the fluorescence was more intense. At this point the zebrafish were analysed on the confocal microscope and images were obtained showing the nanogel present in the intestine, shown in figure 46b. On day 7 the zebrafish were removed from their relevant solutions and returned to fresh fish water. 5 days after being removed from their nanogel solutions the fluorescence could no longer be seen. During this period, the coumarin could be seen being excreted from the zebrafish in their faeces. No visible signs of toxicity were seen in the zebrafish such as oedema, bent tail or death during the two week period, therefore making it likely that the coumarin was still attached to the nanogels and the nanogels were still intact as if coumarin had been released, high levels of toxicity would have been expected and if the coumarin had be metabolised it would no longer be fluorescing. At this point the experiment was terminated. It cannot be fully established whether the nanogels entered the zebrafish via the gills or across

the body surface and gathered in the intestine or whether the nanogels entered the zebrafish through their drinking source. The latter is a possibility as zebrafish drink ~2µl g^{-1} fish per hour therefore in 6 days the fish would have drank ~80nl of nanogel solution. This volume of solution would allow for enough of the coumarin tagged nanogels (~80ng) to gather in the GI tract and therefore making it possible that the zebrafish have imbibed the nanogels.

One concern when viewing the zebrafish, which was mensioned in the second chapter (section 2.2.4), was the fact that the emission of the coumarin monomer is close to the wavelength at which the zebrafish naturally show autofluoresence when the cells die. To overcome this problem control zebrafish (subjected to no nanogel solution) were analysed under the microscope in order to set the intensity of the fluorescent lamp at a point where no autofluorescence could be detected. Keeping these settings, a zebrafish that had been subject to the nanogel was then examined. This would ensure that any fluorescence detected would be the result of the nanogels present.

The nanogels could be seen in the intestine of the zebrafish within 4 days exposure to the nanogels, but they could not be observed in the surrounding tissues of the fish. The lack of seeing them in surrounding tissues could be due to reduced concentration and therefore not being able to detect the coumarin. Therefore it was possible that the nanogels were not passing through the lining of the intestine. This experiment showed that the nanogels successfully entered the zebrafish, causing no visible signs of damage or distress to the fish and was also excreted by the fish, leaving no damage or risk of further toxicity if it had remained and accrued inside the body. The fish were immersed in the nanogels for 7 days, indicating that prolonged treatment, even at relatively high concentrations (~40 pg $ng^{-1}day^{-1}$ zebrafish which is equivalent to ~40 mg $g^{-1}day^{-1}$ for a mouse or ~30g $kg^{-1}day^{-1}$ for a human) did not adversely affect the 48 hpf fry. In spite of high tolerance of the presence of nanogels passing through the alimentary canal, the nanogels had not likely been exposed to the bloodstream or to the main tissues inside the zebrafish, if indeed the nanogels have been imbibed. Because of this, and because many drugs are delivered directly into the bloodstream for transport round the body, further investigation would be required to establish their safety there.

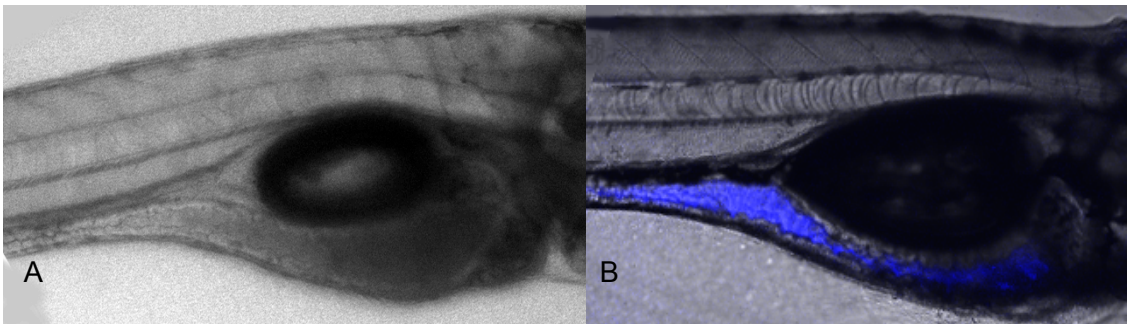

Figure 46 – Confocal images of Casper zebrafish A is a control and B is 6 days after exposure to NG1 (batch 2) (8 dpf).

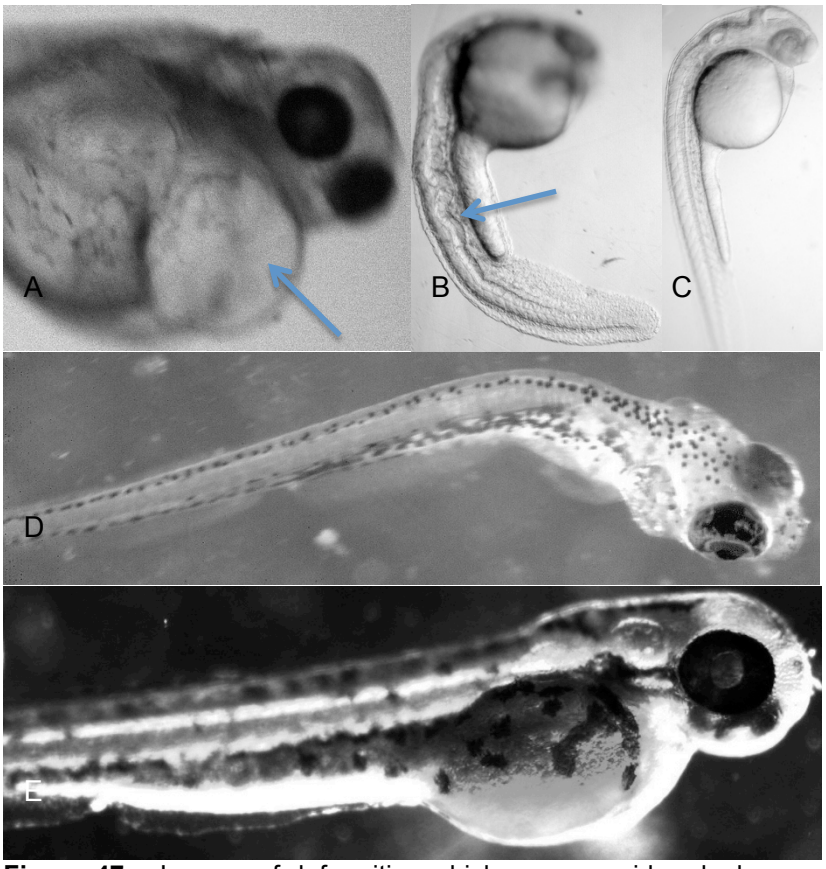

Figure 47 – Images of deformities which were considered when analysing toxic effects of the nanogels on juvenile zebrafish (NG2 1 mg/ml). A – oedeoma, B – curvature of the nortichord, C – healthy control 12 hpf, D – curvature of the nortichord at 5dpf, E – healthy control at 48-72 hpf.

To investigate whether the free coumarin, TMAC, was also toxic at this later stage of development a new experiment was carried out with 48 hpf larvae. A 12 well plate was prepared with each well containing either 4 ml of 0.01 mg/ml TMAC solution or fresh fish water and one 48 hpf embryo was placed in each well. The embryos were analysed every 24 hours via microscope to check for any deformities (figure 47) or mortality.

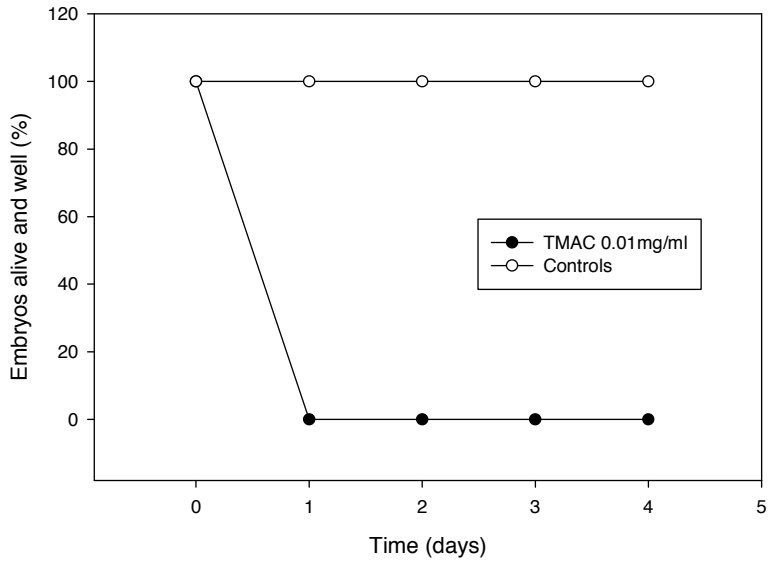

Figure 48 - Effect of the free coumarin, TMAC (7-amino-4-(trifluoromethyl) coumarin), on 48 hpf (hours post fertilisation) zebrafish embryos. 6 zebrafish were exposed to each solution. The experiment was carried out in triplicate, but no variation in results was seen.

As with the younger embryos these 48 hpf larvae showed sensitivity to TMAC within the first 24 hour period, with all embryos exposed to it unable to survive, shown in figure 48. This experiment confirmed that the free monomer was highly toxic to 48 hpf zebrafish embryos when administered at a lower concentration, 0.01 mg/ml, than was incorporated into the nanogels, which at the higher concentrations, 1 mg/ml, (containing 0.025 and 0.05 mg/ml coumarin monomer for NG1 and NG2 respectively) showed no acute toxicity. Although it should still be noted that the TMAC, being a small molecule, may have entered the zebrafish through a different route potentially exposing the zebrafish to a different concentration of TMAC to the nanogels internally. This experiment, along side the experiment carried out with TMAC on the embryos at 2 hpf, also gave indication that the fluorophore was still likely to be linked to the nanogel with the acrylamide bond successfully resisting hydrolysis. Had hydrolysis occurred, the fish would have died from the toxicity of the coumarin monomer, following its release.

Initial studies of the coumarin tagged nanogels (JPR240 and JPRP241) showed no acute toxicity when administered through immersion. Free coumarin, TMAC, was also found to be acutely toxic to the zebrafish, indicating that the fluorophore was not being released via motabolisation of the nanogels *in vivo* as this would have rapidly killed the fish. However, it was highly likely that the nanogels were not passing through the lining of the intestine and therefore not reaching internal cells. A study of the effect of intravenous administration of the nanogels was required, in order to determine the toxicity of the nanogels when circulating in the blood.

3.3.2 Intravenous administration

The intravenous administration of substances to zebrafish is an alternative technique used when systemic circulation is required. Intravenous administration has been used previously for studies involving mutagenesis[225] and toxicity evaluation[228]. The majority of microinjection into zebrafish occurs at very early embryo development stages during the cell division stage[228, 245, 246]. However, some groups have injected into zebrafish embryos at a later development stage. Of those that inject into embryos beyond the epiboly stage, where the embryos are not longer a blastodisc cell mound, the majority inject into the yolk of the embryo[247-249]. Injection into the yolk would not lead to the circulation of the nanogels in the bloodstream, as it would just be adding to the zebrafish's nutrient source (although likely not benificially), effectively taking a secondary route into the bloodstream. Therefore the direct microinjection into the bloodstream was selected for this work, to ensure direct and provable circulation of the nanogels. Injection into the caudal vein at 28 hpf has been achieved before by Veneman *et al* who studied the bacterial proliferation of *staphylococcus epidermidis* in zebrafish through multiple exposure techniques[249]. Another study by McLeish *et al* also evaluated the toxicity of nanoparticles, this time on microinjection into the venial blood pool below the yolk at 48 hpf[240].

In order to select the optimal opportunity for intravenous injection of the nanogel sample, it was necessary to take account of the following features of early development in zebrafish. During the pharyngula development stage (24-48 hpf) the cardiovascular system evolves. All the chambers of the heart develop early on in this period of development and blood can be seen circulating in the closed system of arteries and veins. At around 36 hpf (hours post fertilisation) the caudal vein can be clearly identified across the yolk sack feeding into the heart, at which time the vein is still in the process of forming, is wide and less rigid, creating an optimal point of entry

for microinjection penetration into the blood stream. Therefore 36 hpf was the point in time chosen to inject the embryos. To ensure visual monitoring of the nanogel in circulation, a concentrated solution of 10mg/ml NG1 (batch 2) (2.5% coumarin tag) was formed and injected into the fish using a microinjector. Approximately 54 ng of nanogel was injected into 6 Casper zebrafish at 36 hpf. When injected successfully the nanogel could be seen under a DAPI filter being pumped into the heart and around the cardiovascular system immediately after injection, image displayed in figure 49b.

The fish were further observed on a confocal microscope showing that the nanogel was clearly circulating in the bloodstream after one 1hr, shown in figure 50. After 5hrs the nanogel could be seen concentrating in the hindbrain (displayed in figure 51), a result that would indicate interesting applications of nanogels for neural drug delivery. However as the blood brain barrier is not fully formed in the zebrafish at 36hpf, further experiment would be required with older fish to validate these results. After 12 hours post injection the nanogel could no longer be seen in the zebrafish. To demonstrate that this was not the result of any fluorescence quenching of the tag, a specific experiments was carried out. 100 µl of NG1 (batch 2) and NG2 (batch 2) (1mg/ml) were each incubated with proteins from 36 hpf homogenised embryos in a multiwell plate and mixed thoroughly at 28 °C. After 24hrs analysis of the plate indicated that fluorescence emission was unchanged, therefore providing evidence that the fluorescent nanogels were stable and that the tag was not altered in any way. The likely explanation the loss of fluorescence in the experiment above is that the fluorescent nanogels are motabolised by the zebrafish.

One week after injection the same batch of fry used for the experiments previously described were still alive and well with no signs of curvature of the spine or oedema, at which point the experiment was terminated. In summary, the nanogels were successfully injected into the zebrafish at 36 hpf, could be seen circulating their blood stream and had no observable acute toxic effect on the fry. A short experiment was attempted aiming to evaluate the ability of the nanogels to cross the blood brain barrier, by injecting the larva at 8 dpf (days post fertilisation). Despite a number of attempts the difficulty of the injections, as a result of the more mature vessel system, resulted in significantly less nanogel being able to enter the system. Although the nanogel could be visualised at the time of injection, 20 minutes later it could be no longer detected, and no difference could be seen between the injected fry and the control, most likely as a result of higher dilution. Nanogels with increased fluorescence intensity will be

required to explore this line of research. As a result of limited time and facilities this was not pursued any further in this project.

The work presented here has achieved far more than what many zebrafish *in vivo* studies do, in the evaluation of the toxicity of nanomaterials, by complementing the data obtained via immersion administration with results obtained via injection[197, 233].

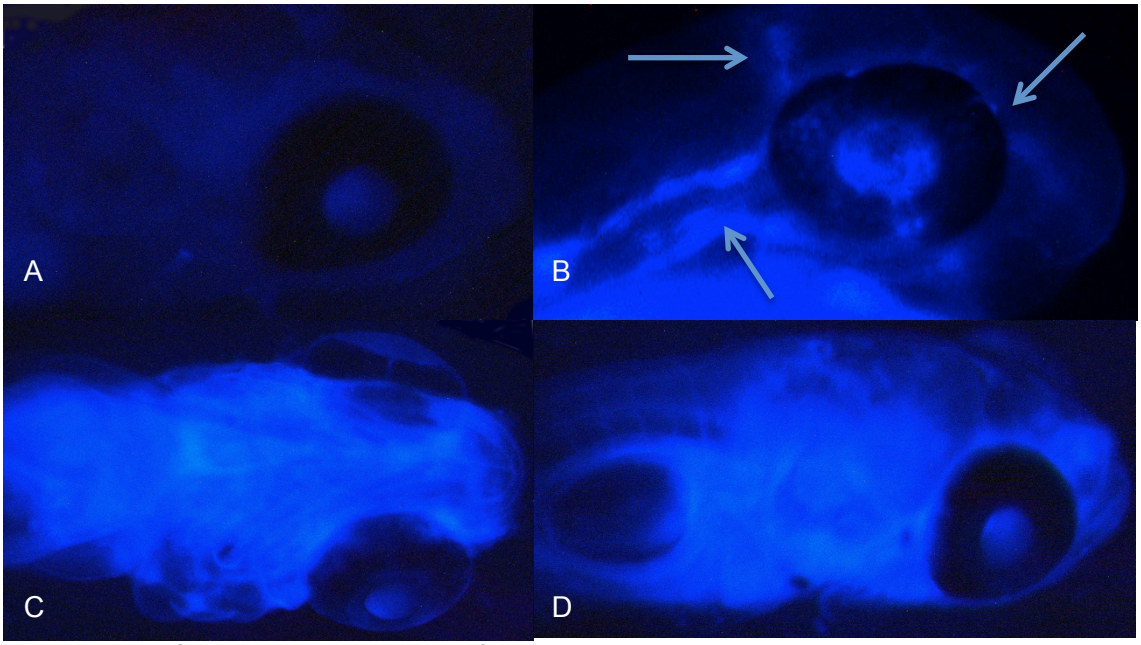

Figure 49 A) Control, B) immediately after injection, nanogel seen in the blood vessels (some blood vessels indicated by the arrows), C) Nanogel dispersed into the cells of the zebrafish, medial view, D) Nanogel dispersed into the cells of the zebrafish, lateral view.

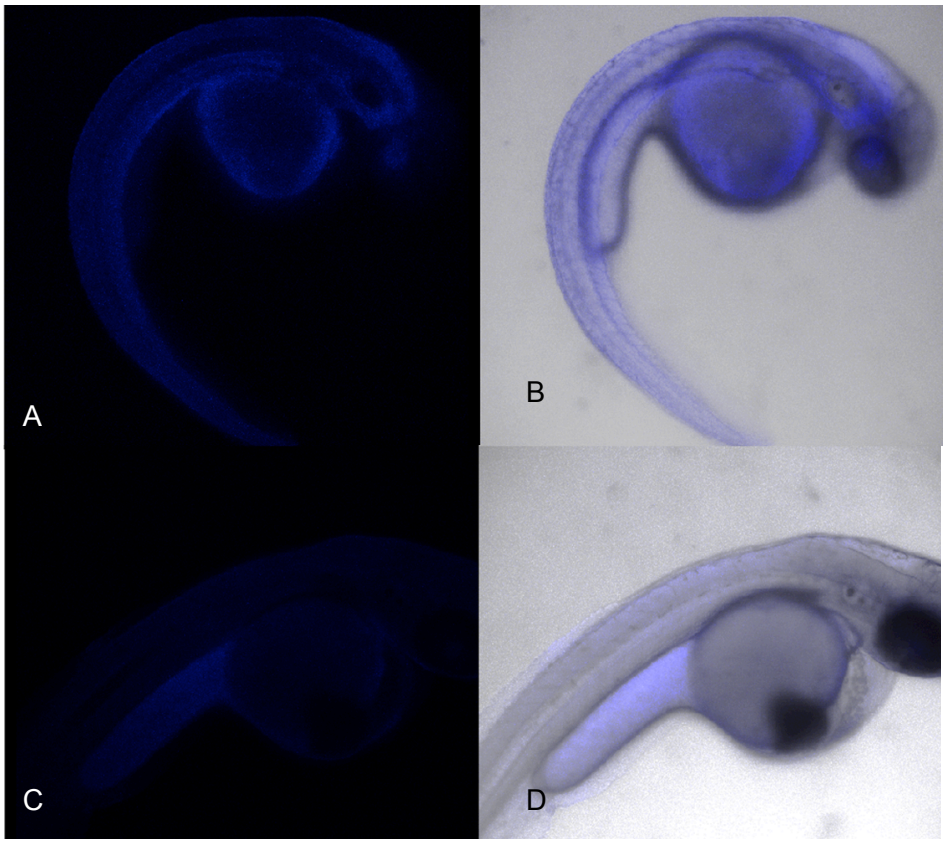

Figure 50 – Images taken 1 hour after injection on confocal microscope. A) Control fluorescence only, B) control fluorescence overlaid with bright field, C) Injected fluorescence only D) injected fluorescence overlaid with bright field.

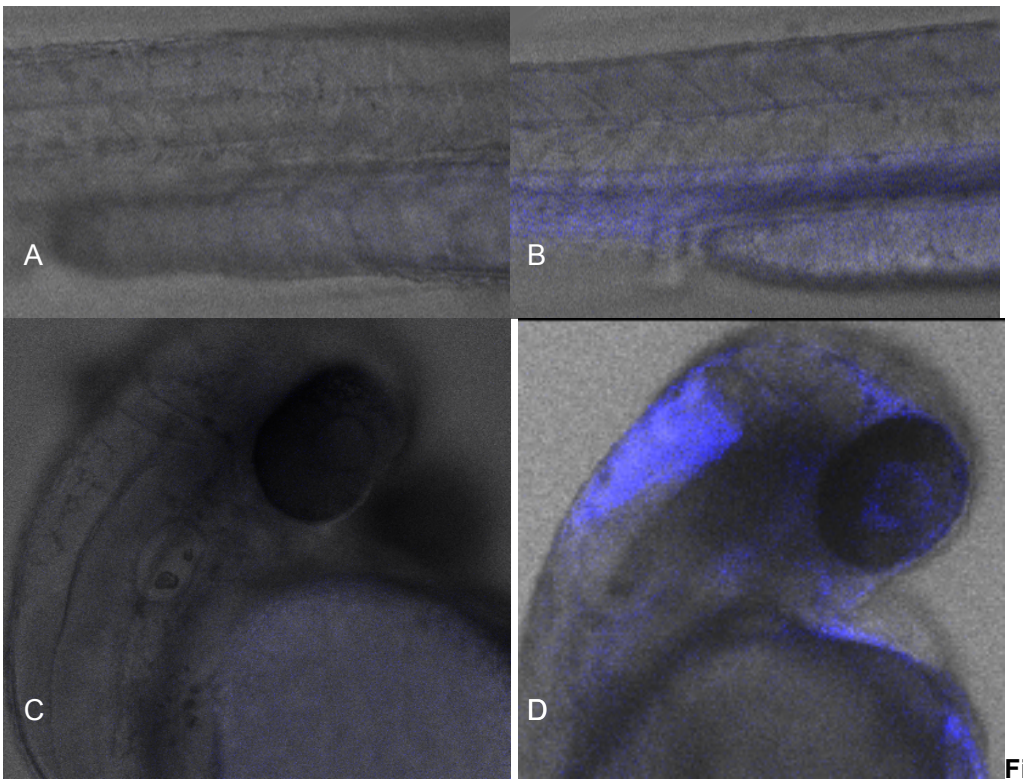

Figure 51 – images taken 5 hours after injection. Nanogel can be seen circulating the cardiovascular system (B) and gathering in the hindbrain (D). A and C are controls.

3.4 **Conclusions**

Preliminary analysis of the nanogels synthesised in chapter 2 have shown no toxicity up to 200 g/ml in MTT and LDH assays. The nanogels have also been shown to be taken up by the cells using both FACS and microscopic imaging. Having obtained successful initial analysis with limited toxicity and good uptake, the nanogels were administered through immersion to 2 hpf zebrafish embryos at concentrations up to 1 mg/ml. Though at higher concentrations the nanogels proved to be fatal at this age, at 0.1 mg/ml the nanogels were less cytotoxic to the early stage development embryos. After analysis of the effect of the coumarin monomer itself, it was clear the fluorescent tag was toxic and could be hindering the evaluation of the nanogel's toxicity. When the nanogels were orally fed to 48 hpf zebrafish for 5 days no acute toxicity (curvature of the notochord, oedema, death) was seen. Nanogel was clearly seen in the intestine of the zebrafish and yet it could not be seen to have passed through the lining of the intestine and entered internal cells of the zebrafish. Nanogel NG1 (batch 2) was injected into the caudal vein of the 36 hpf zebrafish where it could be seen immediately being pumped around the cardiovascular system and shortly afterwards diffusing throughout the zebrafish. 5 hours after injection the nanogel could be seen gathering in the hindbrain. No trace of the nanogel could be seen in the zebrafish 12 hours after injection. No adverse side effects could be seen 7 days after injection. This combination of preliminary toxicity analyses of the nanogel carrier itself, characterised by positive, non-toxic effects, gave strong evidence in favour of its use as a safe carrier for a therapeutic drug. Not only this, the study indicates that although the acrylamide monomer, which has proven toxicity, shows no preliminary toxicity in zebrafish once incorporated in the nanogel polymer, showing that any remaining monomer after polymerisation was highly likely to have been removed during the isolation process. Therefore the next step focused on the uploading of the drug. Tamoxifen was incorporated into these nanogels for further analysis of their efficacy as part of a drug delivery system.

CHAPTER 4:

Applying nanogels to drug delivery

4. Applying nanogels to drug delivery

In this final chapter of the results and discussion, the results relating to the incorporation of tamoxifen into the coumarin-tagged nanogels are presented and discussed. European legislation requires that novel therapeutic agents are shown to be highly efficient and safe, before they can be used in clinical trials. The previous chapter focussed on measuring the toxicity and hence the safety of the nanogels as part of a drug delivery system. In this chapter the efficacy of the nanogel as a carrier is evaluated both *in vitro,* through chemical analysis, and *in vivo,* using a genetically modified strain of zebrafish that changes colour on detection of tamoxifen.

4.1 Uploading the drug on to the nanogels

The uploading of a drug on nanocarriers has been achieved via different approaches, including surface interactions, covalent links and encapsulation techniques.[250] When deciding which uploading method to use, it is important to consider the ultimate application and purpose of the drug delivery system. If increasing bioavailability or masking foul tastes of therapies is the focus, simple encapsulation techniques are can be used[250]. However, when targeting specific tissues or attempting delivery to precise locations in the body, more complex methods are required.[251-253]

4.1.1 Different approaches to uploading drugs onto drug delivery systems

Encapsulation is often achieved by absorption of the drug into the delivery system,[254] or by coating or surrounding drug particles in polymers and/or surfactants and subsequent evaporation of the solvents used in the process.[255] The latter method has significant advantages, including the achievement of very high loadings of the selected drug and the creation of highly stable dispersions, both of which significantly increase bioavailability, and patient compliance.[250] However, simple encapsulation of the drug often doesn't target a drug to a specific location, which means there is no control over where the drug is released. Therefore drug leakage from the delivery system in random locations occurs as a direct consequence of this, leading to undesired side effects.

Another approach to loading drugs on to a carrier is to use non-specific interactions between the drug delivery system and the drug itself. Moorthy *et al* loaded two drugs onto their Mesoporous Organosilica Hybrid Microcarrier, using hydrogen bonding and electrostatic interactions. In this system the two drugs loaded were ibuprofen, an anti-inflammatory drug and 5-fluorouracil, a cancer therapeutic. They reported substantially

increased release of ibuprofen at higher pH (7.4), which was much slower at reduced pH (5.5) and the reverse for 5-fluorouracil. The reason for this was the difference in solubility of each of the drugs at different pH values: the cancer therapeutic, more soluble at the lower pH, being delivered to tumour cells which inherently have a lower pH, and ibuprofen, more soluble at the higher pH, being released in healthy cells, where the pH typically has a higher value. Their model effectively demonstrated delivery of two different drugs only to locations where they were required[256].

In some cases the drug is covalently linked to the drug delivery system through chemical bonds that can be broken through certain physiological conditions or during specified physiological processes. One example of this is a copolymer, *N*-(2-hydroxypropyl) methacrylamide (HPMA), formed by Li *et al* who loaded a cancer therapeutic (doxorubicin) onto it using a hydrazone link. The link was broken and the drug released only in conditions where the pH was significantly lower, typically those found in the endo/lysosomal compartment of tumour cells[257].

Although the formation of generic interactions allows the drug to be loaded onto the carrier, there are significant advantages in being able to use specific interactions to link the drug to the delivery systems, especially the ability to be selective and to trigger specific release. Among the different approaches that have been investigated, molecular imprinting has provided some interesting results.

4.1.2 The molecular imprinting approach

The first suggestion of imprinting was introduced by Polyakov in the early 1930s[258] when he discovered silica gels had a preference for re-binding a solvent additive when the additive was present during the gels' formation[259]. This tendency to favourably rebind the additive present during formation, under specific conditions, is the essence of 'imprinting'. This work was followed in 1949, by further research by Dickey, who imprinted analogues of methyl orange, noticing that the silica gels had an enormous preference for the dye, which was made available and present during their formation. He also highlighted that an increase in rebinding was seen, the closer the structure of the gel was to that of the analogue made present during formation[260]. However it was Wulff et al who first proposed formation of an imprinted organic bulk polymer which was able to separate a racemic mixture[261].

The molecular imprinting approach is based on the self-assembly of functional monomers around a template or target molecule. Polymerisation of the functional monomers in the presence of a cross-linker, is followed by removal of the template via specific washing. This results in the formation of a 3-D cavity whose structure is complementary to the template used. The cross-linked matrix holds the functional groups in position allowing selective recognition and rebinding of the template molecule or a target analyte, which is highly similar in structure. A template analogue is often used for creating the MIP, which differs slightly in structure to that of the target analyte desired to be rebound. This can be for several reasons, one such reason is to prevent bleeding of the target analyte from the MIP once the template has been removed, for example in extraction techniques[262]. The molecular imprinting approach is schematically depicted in figure 52.

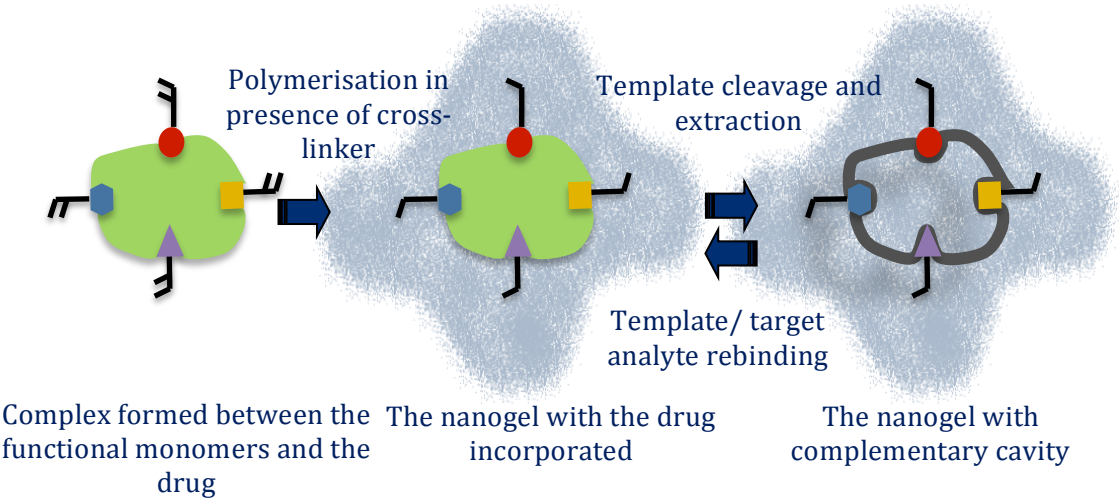

Figure 52 – A systematic illustration of the molecular imprinting process.

The key feature of this approach is the interaction between the template and the functional monomer. The stronger and more defined the interaction the higher is the selectivity and the imprinting efficiency of the resulting polymer. A number of different approaches based on different type of interactions have been investigated, which include covalent, semi-covalent and non-covalent. Despite the covalent approach being the one giving the best outcomes, non-covalent interaction examples dominate the literature. This is mainly due to the considerably higher availability of suitable functional monomers and the wider applicability of the approach to a variety of templates[263]. The next sections will provide more details about the different potential system.

4.1.2.1 Monomer – template interaction

The monomer – template interaction for molecular imprinting is of high importance. There are several different methods of forming monomer – template complexes to imprint into the polymer matrix. The first is the 'covalent approach' introduced by Wulff *et al*[259]. In this method a covalent bond (bond energy of ~85 kcal/mol) is formed between the template and the monomer that can be broken and reformed in a specific environment[264]. This has the positive advantage of lending high stability to the complex. The functional groups normally used for this form of imprinting are alcohols, aldehydes, amines or carboxylic acids, directly limiting the possible number of template molecules available. Furthermore, it should be noted that the release of these molecules is mainly through hydrolysis, meaning such release could happen anywhere within the human body, thus losing the ability to target specific cells such as cancer cells.

Another approach that has had significant success is the 'semi-covalent approach'. Here, the template molecule is initially bound via a covalent bond, sometimes with the use of a spacer molecule. However, once the template is released, the target molecule re-binds to the polymer matrix via non-covalent interactions[265]. This approach could be feasible but it would require an extra step of polymerisation with the template, releasing the template and allowing rebinding of the target molecule/ model drug. If the drug can be directly used for the final monomer – template interaction without such need for template release and drug rebinding, it would reduce the preparation time as well as cost of preparation.

The most widely used method in molecular imprinting is certainly the 'non-covalent approach' where strong interactions such as ionic bonds (bond energy of ~5 kcal/mol) or hydrogen bonds (bond energy of ~3 kcal/mol[266]), complemented by dipole – dipole interactions (bond energy of ~1.4 kcal/mol[266]), and Van der Waals (bond energy of 1-0.5 kcal/mol[266]), take place between the functional monomers and the template molecules. In this instance re-binding of the template (or drug) occurs using the same non-covalent interactions used to form the complex initially as opposed to the semi-covalent method, which creates the imprint using covalent interactions, and rebinds the template/target analyte using non-covalent interactions. By using this approach, targeting a drug to a specific location becomes feasible. If an ionic interaction between a drug and the drug delivery system is used, which is disrupted at a suitable pH, then the drug can only be released under these specific conditions. Thus preventing leakage in healthy cells and in turn reducing side effects and increasing drug deposition at the required site of action. The weakness of this method is that there is limited control over

the complex self-assembly, giving rise to heterogeneous rebinding sites. However for present purposes this could be an advantage. This is because the intention is to imprint the drug directly (effectively using the drug as the template), during polymerisation and to focus on the release mechanism allowing delivery of the therapeutic drug to a specific location in the body. As different arrangements of the 'self-assembled complex will collapse at different rates, there is the potential for some variation in release times. The same feature could help prevent undesirable rebinding of the drug after the entire load has been released. However it is important to study the template (drug) – monomer interaction to ensure that experimental conditions are identified that maximise and favour the complex formation.

4.1.3 Molecular imprinting and its application for drug delivery

The molecular imprinting approach has been exploited in many areas of science[267] including sensors[268], biosensors[269], solid phase extraction[270], chiral separation[271] and catalysis[272]. However, their application in drug delivery is of particular interest. There are many natural processes in living organisms that rely on molecular recognition, from information transfer and reaction catalysis to fighting disease. These processes rely on a macromolecular 'hosts' to identify and interact with specific molecules of low molecular weight to function. Therefore it is of no surprise that being able to mimic these processes using synthetic materials could reap huge benefits when applied to drug delivery[259].

One application of molecular imprinting in drug delivery has been in ocular therapy. Ophthalmic drugs in general are known to have poor patient compliance and ≤ 5% of the drug reaches the tissue required when administered correctly. Molecularly imprinted hydrogel/silicone composites have been successfully produced which release antibiotic, ciproflaxin, over several days[273]. These contact lenses, due to their ability to allow enough oxygen exchange to prevent hypoxia when warn through the night, allow sustained delivery of the drug over 14 days. These imprinted lenses released a consistently higher amount of drug, over a non-imprinted control when low loadings were used. Therefore these ciproflaxin imprinted contact lenses could significantly improve patient compliance over repeat administration of eye drops.

There are several molecularly imprinted polymers that have been developed for controlled release of a drug[274-276]. Salian and Byrne inprinted poly(HEMA-co-DEAEM-co-PEG200DMA) with the anti-inflammatory diclofenac sodium, via two different polymerisation techniques. They found that when living radical polymerisation (in which

a reversible termination step is introduced, creating a dormant species that can be re-activated to continue the polymerisation as desired[277]) was used to form the polymer, a slower release rate of the drug was obtained which was more independent of concentration of the drug inside the polymer than when free radical polymerisation (where the polymerisation termination is fixed) was used[278]. Thus the drug transport succumbed less to Fick's law of diffusion, which states the flux will flow from high concentration to low concentration. Javanbakht et al have also developed a molecularly imprinted polymer for the sustained steady release of dipyridamole, which prevents clotting of the blood and induces vasodilation. Their MIP (molecularly imprinted polymer) showed a slower release profile over their NIP (non-imprinted polymer), with the NIP releasing the full drug load within 20 hrs in acidic conditions and the MIP taking 65 hrs for complete drug release[279].

Research into cancer therapies attracts considerable attention in general, due to it being the leading cause of death in adults in the US. Moreover problems associated with diagnosis' and treatments, often given too late, along side the fact that the delivery of the majority of current oncology treatments are non-specific, create systemic toxicity and cause adverse effects[280]. Although focus has been given to researching cancer therapies using nanoscale technologies, in the case of molecular imprinting, very little is reported. However one MIP of tocopherol succinate, an analogue of vitamin E, which has shown to be selectively effective against malignant tumour cells, whilst harmless to healthy cells, has been formed and investigated[281]. This MIP proved to selectively rebind the target analyte over a non-imprinted polymer. However, no release profile of the drug was shown. The successful upload of a drug on to a drug delivery system solves only half of the problem: the precision of control over release of the drug and consequent targeting to a specific location is vital both to provide efficient load delivery and to prevent accidental leakage of the drug in undesired areas of the body.

4.2 **Drug template and functional monomer**

Loading the drug onto a drug delivery system is not the only consideration required when attempting to deliver a drug to specific locations in the body, the method of release is also of high priority. Molecular imprinting introduces an interaction between a functional monomer and drug template, which is critical in holding the drug in place. However disruption of this interaction is required to release the drug and careful consideration into the interaction used and therefore the environment required to disrupt it should be considered if a controlled and/or targeted release is to be achieved.

Before a functional monomer offering optimised interaction with the model drug could be chosen, investigation of the release mechanisms of drugs in current drug delivery devices was required.

4.2.1 Mechanisms for release of a drug from a drug delivery system

One of the benefits of using molecular imprinting for uploading and releasing a drug from a drug delivery system is the ability to target the drug toward specific (diseased) tissues. For example, as discussed before, by introducing an ionic interaction between the drug and carrier which is disrupted with reduced pH, prevalent in cancerous cells. In general, there are two well-documented ways of targeting a drug, the first is passive targeting. In this approach the anatomical differences between diseased and healthy tissues[282] are exploited (such as a difference in temperature) allowing direction of the drugs to the tissues requiring them. By contrast, active targeting exploits the selectivity between a receptor and a ligand, giving rise to site-specific targeting. Active targeting can be achieved using receptor-ligand or antigen-antibody recognition, or by using aptamers (chemical equivalents of antibodies, they can specifically bind proteins or other cellular targets[283])[284]. In either approach the release of the drug can be triggered directly by the recognition event, or the targeting moiety can be independent to that of the drug release. In the case of the latter leakage of the drug is common and can reduce the overall therapeutic effect and side effects may still be observed[285]. Therefore ensuring the release mechanism is triggered by the environment where the drug is required is highly desired. To gain insight into the potential of molecular imprinting as an approach for the release of a drug at a diseased site, reviewing other methods currently used for releasing drugs from drug delivery systems was of interest for comparison.

One release mechanism that is highly utilised is that of simple diffusion. For example the majority of drugs encapsulated in micelles are released via diffusion and often rely on passive targeting such as the enhanced permeation and retention (EPR) effect, when used for delivery of drugs to tumours[286]. The EPR effect occurs due to the leaky vascular tissue formed surrounding tumours, allowing a higher amount of drug to be delivered to tumour cells over healthy cells. This is due to the higher permeability of the leaky vascular tissue surrounding tumours, over healthy tissues, allowing a higher does of nanomaterials to penetrate the tumour cells[287]. Reduced lymphatic drainage also allows retention of the drug in the tumour tissues[252]. Another method that has been reported is drug release via osmosis. In this case the encapsulated drug is solubilised

by the flow of water into the carrier, creating a water gradient. As water continues to flow into the carrier to dilute the drug and restore osmotic balance, it causes 'microcracks' in the carrier, allowing slow release of the drug, and ultimately bursting the carrier releasing the final payload[288]. Another favourable system for delivering drugs are degradable drug delivery systems. This is because of their ability to break down in to biodegradable and biocompatible materials, relinquishing the concern of an accretion of the material in question in the body during sustained delivery. The use of a biodegradable drug delivery system was investigated by Young et al, who aimed to slow the release of drugs for bone repair. By altering the proportion of the A block in their lactic acid (A block) propylene glycol (B block) block co-polymer they were able to control the degradation of the transport polymer and ultimately the release of the drug[289]. However, loss of drug through diffusion (thus poor control over accurate targeting and consequent inappropriate leakage) was still apparent which is a common occurrence in degradable drug delivery systems[284].

All of these methods exhibit controlled release, releasing the drug over a sustained period. However, both these release methods also lead to leakage of the drug from the carrier in undesired locations. This is due to the drug being released from the carrier continually, regardless of location and relies on localisation of the drug delivery system at the desired location, thus localisation of the drug delivery system at the diseased site is independent to that off the release of the drug resulting in leakage in undesired healthy tissues. Leakage of the drug not only affects the efficacy of the therapy but can also lead to side effects due to the effects of the drug on normal healthy cells[285].

By actively targeting diseased tissues and coupling that to the release of drugs at desired locations reduces the risk of drug release outside of desired tissues. One example of an actively targeted drug delivery system is Ligand-based vascular targeting agents (VTAs) which selectively bind to tumour blood vessels rather than normal ones, allowing coagulating drugs to be dispensed in the vascular structure of a tumour, blocking the blood vessels and cutting off the blood (and therefore oxygen) supply to the tumour[290]. One example of this is an antibody to VCAM-1 (vascular cell adhesion molecule -1, present in tumour vascular cells) which is covalently linked to human tissue factor, which is a gene which encodes for a coagulation factor. The gene is not triggered unless the anti-body binds the VCAM-1 and therefore formation of the coagulation factor to coagulate the blood is not triggered unless bound to tumor vascular cells[291]. This resulted in necrosis of 95% of the tumour cells. The remaining tumour cells were at the periphery of the tumour and often respond well to

antiproliferative antitumour therapies. For this drug active targeting was essential as cutting of blood supply to healthy tissues would result in very serious side effects if not death of the patient. However, the process of establishing suitable antibodies or peptide markers to target and encompassing that into a trigger on a drug delivery device is time consuming and expensive.

Another interesting approach for releasing drugs is the one where a stimuli leads to a physical change in the conformation/structure of the delivery system, which results in the release. Examples of these include response to temperature and pHs. The use of pH as a trigger in drug delivery systems has been a widely investigated[174, 256, 292, 293] approach due to the pH of tumour tissues being acidic when compared with normal tissues[294]. The pH of healthy cells is normally 7.4[295] whereas tumour tissues can have a pH as low as 5.7[294]. Using this pH change as a trigger retains the drug in the drug delivery system until the target location is reached. This protects healthy cells from potentially toxic drugs (avoiding drug leakage) and targets tumour tissues (providing efficient drug release only where it is required). Min *et al* found that by targeting their micelles to tumour cells, by using the collapse of their micelles with a change in pH, the drug accumulated in much higher doses in the tumour tissue than in normal healthy tissues when administered *in vivo* in mice[295].

In order to prevent leakage of a drug, connecting the triggering event to the release of the drug is fundamental. Cancer therapies are notorious for their undesirable side effects such as hair loss and vomiting. Targeting a drug to tumour cells would have huge benefits by increasing drug deposits at the required site, providing a reduction in unwanted side effects, an increase in precisely controlled bioavailability and therefore eventual reduction in the total drug dose required[284, 285]. Molecular imprinting has been shown to have the ability to prevent unwanted drug release until an activation source is detected. The pH of tumour cells is proven to be much lower than that of normal healthy cells[294] and this change in pH can be exploited by molecularly imprinted nanogels, which on detection of reduced pH trigger the release of the drug. A candidate anti-cancer drug, often used for the treatment of breast cancer, is Tamoxifen.

4.2.2 Tamoxifen

Tamoxifen, structure displayed in figure 53, is used medically to treat breast cancer as it competitively binds to the oestrogen receptor and prevents further production of breast tissue, effectively stopping the growth of tumours. More specifically, tamoxifen is a selective oestrogen receptor modulator (SERM), which acts as an agonist, binding to

the receptor, triggering a response in bones and the uterus. However, tamoxifen acts as an antagonist in breast tissue, binding to the oestrogen receptor in the breast tissue cells preventing it from binding oestrogen and triggering excessive reproduction of breast tissue[296]. A study in the Cancer Research journal in 1987 found that when MCF-7 breast cancer cells were denied the oestrogen hormone, they adapted and continued to grow. However, when an anti-oestrogen was present growth of the cells was suppressed[297]. Cole *et al* were the first to prove clinical efficacy in 1971[234] and since then tamoxifen has become a widely used drug to both treat and prevent breast cancer, at all stages of development.[298, 299] However, tamoxifen has limited bioavailability and takes 4-8 weeks to reach steady state concentration, together with one of its metabolites *N*-desmethyltamoxifen.[234] Moreover, tamoxifen also exhibits serious side effects such as endometrial cancers and drug resistance can occur when administered long-term.[298] Creation of a drug delivery system that delivers tamoxifen only to the target tissues would increase the amount absorbed by the desired tissue, dramatically reduce its exposure to other undesired tissues and help prevent these side effects.[298]

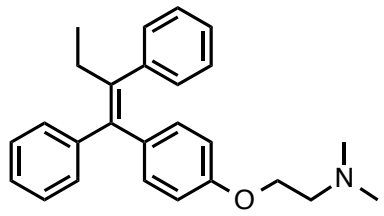

Figure 53 - Structure of tamoxifen.

4.2.3 Tamoxifen – acetic acid interaction

Tatavarati *et al* found that by incorporating an acidic monomer into a polymeric matrix can aid release of a weakly basic drug when the monomer forms a complex with the drug. Enhanced drug release only occurs providing the pKa of the drug's conjugated acid is above that of the pH of the environment in which drug release is desired[300]. The pKa of tamoxifen's conjugated acid in aqueous solution is approximately 11 according to Loftsson *et al* who investigated drug-cyclodextrin complexes[301]. This is well above the pH of tumour cells and therefore had good potential for release when complexed with an acidic monomer.

One acidic monomer that has already been incorporated into the nanogels, originally to aid its solubility, is that of acrylic acid. Acrylic acid monomer has a pKa of 4.25[175] and when incorporated into a polymer has a pKa of 4.75[302] in aqueous environments. This

increase in pKa can be accredited to the increased stabilisation in the monomer due to the double bond, which disappears once polymerised and therefore the acid is slightly more easily dissociated in the monomer form than the polymer.

Tamoxifen has an exposed tertiary amine group, which can interact with the acrylic acid. The carboxylic acid group on the acrylic acid is partially dissociated at normal pH, and the amine on the tamoxifen is reduced, allowing an ionic bond to form between the two. However, as the pH of the solution containing acrylic acid is reduced, as would occur when the complex reaches the malignant tissue, the interaction with tamoxifen will be disrupted and the tamoxifen will be released. The ionic interaction can be viewed in **figure 54.**

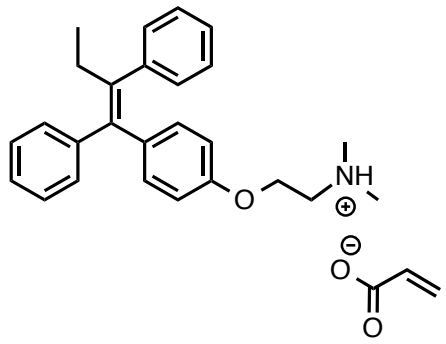

Figure 54 – Tamoxifen – acrylic acid complex, forming an ionic interaction.

4.2.4 ^{1}H NMR study of complex interaction

Analysis of the ionic complex interaction can be carried out using nuclear magnetic resonance spectroscopy (NMR). This technique has been carried out many times previously for determination of binding constants and investigations of complex formation. Proton NMR in particular is of use for this study as it is highly sensitive to the proton environments, even when non-covalent interactions are of interest.

In these studies acetic acid was used to study the interaction between the functional monomer and the drug in place of acrylic acid. This is due to acetic acid having a pKa of 4.76[303], which is much closer to the pKa of the acrylic acid (4.75[302]) after polymerisation and therefore can be a better mimic of the interaction between tamoxifen and the functional monomer in complex once polymerised in the nanogel, than the acrylic acid monomer (pKa 4.25[175]).

In the complex formed here between tamoxifen, which is the ‘guest’, and acetic acid, the ‘host’ is presumed to be through a non-covalent ionic interaction. This interaction is

between the protonated tertiary amine nitrogen on the tamoxifen and the dissociated alcohol oxygen on the acetic acid. This interaction will decrease the positivity of the nitrogen on tamoxifen, theoretically shifting the hydrogens on the adjoining carbons downfield. Knowledge of the non-covalent interaction between a host (H) and a guest (G) in a complex ultimately comes down to binding constants. Analysis of binding constants, allow quantification of the association between two molecules. In the system reported here it was expected that the interaction would be 1:1, therefore only one binding site would have been given by each molecule of acetic acid to bind the tamoxifen. If true, stoichiometry would not come into play and the reaction of complex formation can be written as in Equation 6[304].

$H + G \rightleftharpoons HG$ **Equation 6**

Where, H is the Host, G is the guest and HG is the complex formed. From this the association constant (K_A) can be written as:

$K_A = \frac{[HG]}{[H][G]}$ **Equation 7**

By substituting [H] = $[H]_0$ – [HG] into equation 7, $X_{HG}=\frac{[hG]}{[H]+[HG]}$ (where X_{HG} is the amount of host in complex with the guest) can be re-arranged to give:

$\frac{[HG]}{[H]_0} = \frac{K_A[G]}{1+K_A[G]} = X_{HG}$ **Equation 8**

It can be assumed that the chemical shift (δ) of interest is the weighted average of the free host (H) and the complexed host (HG) for a 1:1 system. As the total amount of host in the system (X_{Htot}, free host + complexed host) cannot exceed 1 ($X_{Htot}=X_H+X_{HG}=1$) the observed chemical shift can be written as seen in equation 9.

$\delta_{obs} = X_H\delta_H + X_{HG}\delta_{HG}$ **Equation 9**

Where δ_{obs} is the observed chemical shift, X_H is the amount of free host, X_{HG} is the amount of complexed host, δ_H is the chemical shift of the free host and, δ_{HG} is the chemical shift of the complexed host. As $X_H = 1 - X_{HG}$ equation 10 can be obtained.

$\Delta\delta \equiv \delta_{obs} - \delta_H = X_{HG}(\delta_{HG} - \delta_H)$ **Equation 10**

Equation 8 can then be substituted into equation 10, to give equation 11.

$\Delta\delta = \frac{\Delta\delta_{tot}K_A[G]}{1+K_A[G]}$ **Equation 11**

Where Δδ is the change in chemical shift, $\Delta\delta_{tot}$ is the maximum change in chemical shift, K_A is the association constant and [G] is the concentration of guest in the system.

This method can then be applied to determine the binding constant between tamoxifen and acetic acid by using NMR spectrometry.

4.2.4.1 The tamoxifen – acetic acid complex

In the first set of experiments tamoxifen was reacted with increasing amounts of acetic acid and each time a ^{1}H-NMR spectrum was recorded. The aim was to identify which protons would have their chemicals shifts affected by the interaction with the acid and to attempt to quantify the shift. Initially the proton environments affected by the ionic bond were required to be identified. The protons on adjacent carbons to the amine in complex (H_{ta} and H_{tb}) with the acetic acid would both be affected by the effect of the ionic interaction, these hydrogens are indicated in figure 55.

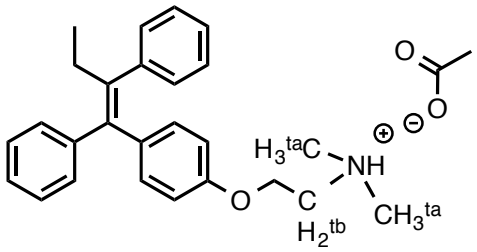

Figure 55 – Interaction of Tamoxifen and acetic acid with labels marking those protons affected by the interaction.

Tamoxifen and acetic acid were dissolved in d6-DMSO and ^{1}H-NMR carried out. The complex was formed and analysed in d6-DMSO. DMSO was required for solubility of the drug and monomers for polymerisation and therefore analysis of the interaction was required under the same conditions. However DMSO is not the ideal solvent in which to study the interaction due to its high dielectric constant (49), which inhibits the ionic interaction as it forms a stronger screening effect between charge carriers and counter ions reducing Coulomb interaction[305]. The singlet peak for the CH_3 groups on the tertiary amine (H_{ta}) and the triplet peak for the CH_2 group (H_{tb}) attached to the amine could be seen to shift in ppm downfield, this is displayed in figure 56.

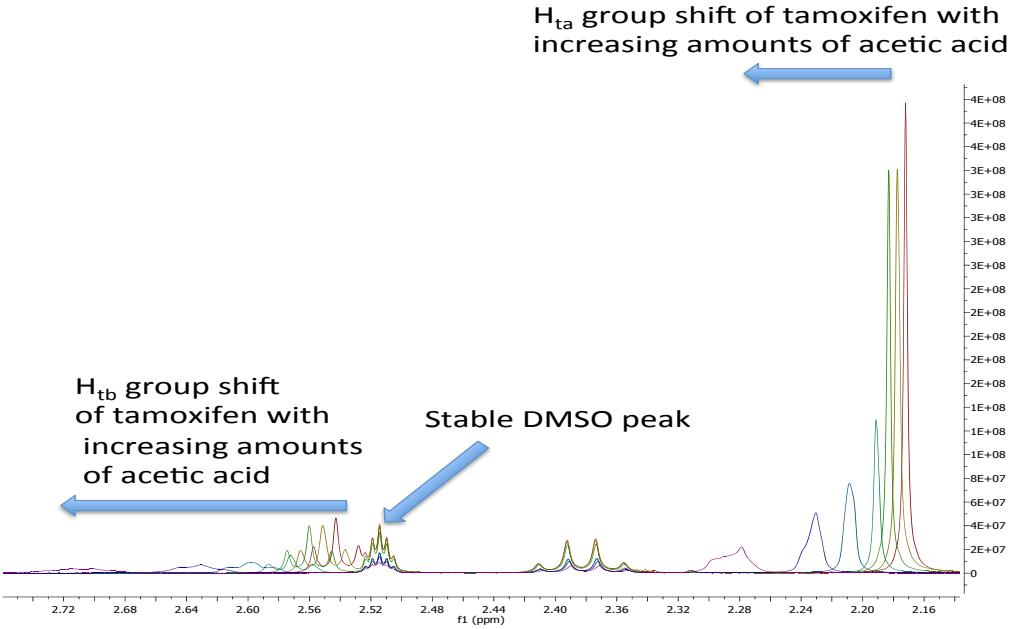

Figure 56 – Stacked NMR spectrums of Tamoxifen a) alone, red b) with 0.5eq AA, yellow, c) with 1eq AA, green, d) with 2eq AA, turquoise, e) with 4eq, blue, f) with 8eq AA, purple and g) with 12eq AA, pink. Where AA=acetic acid.

Analysis continued with the H_{ta} peak to try to obtain the association constant, as it was a clear singlet that could more accurately be evaluated for its ppm shift. The values of change in chemical shift in function of acetic acid concentration can be seen in table 15.

[Acetic acid] (M)	δ_{Hta} in d6-DMSO (ppm)	$\Delta\delta_{Hta}$ in d6-DMSO (ppm)
0.0000	2.172	0.0000
0.0355	2.177	0.0080
0.0710	2.183	0.0170
0.1420	2.191	0.0290
0.2840	2.209	0.0550
0.5680	2.230	0.0880
0.8520	2.279	0.1720
1.1360	2.321	0.2190
2.2700	2.426	0.3690
3.4100	2.604	0.4320
3.9800	2.615	0.4430
4.5400	2.637	0.4650

Table 15 – Values of chemical shift (δ_{Hta}) and of their variation ($\Delta\delta_{Hta}$) in function of acetic acid concentration in d6-DMSO using H^1NMR (400MHz). The chemical shifts are in ppm and relative to TMS (tetramethylsilane).

When analysing the change in chemical shifts of the two peaks H_{ta} and H_{tb}, the variation in chemical shift of Hta can be seen to increase from 0.008 ppm (0.5 eq) to

0.465 ppm (128 eq) as concentration increases. When the chemical shift of H_{ta} protons on Tamoxifen, compared to H_{ta} in uncomplexed tamoxifen, in function of the concentration of Acetic acid added was plotted a clear curvature could be seen which plateaued at 32 equivalents.

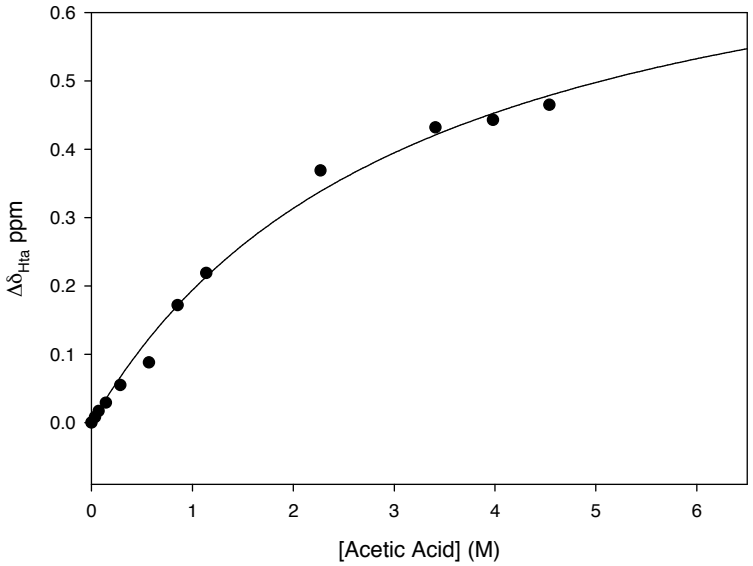

Figure 57 – Plot of the variation of chemical shifts $\Delta\delta_{Hta}$ of the protons H_{ta} in complexed tamoxifen corrected from the value of the chemical shift of H_{ta} in uncomplexed tamoxifen verses the concentration of acetic acid in d6-DMSO.

The association constant was calculated using equation 11, which establishes the relationship between the change in shift of the Hta peak of Tamoxifen and the concentration of acetic acid. The data presented in figure 57 is fitted to a hyperbola using a ligand-binding model in sigma 8.0 data analysis software.

$$y = \frac{a * x}{1 + b * x} \qquad \textbf{Equation 12}$$

Where y= the change in chemical shift of the H_{ta} proton, a is the total chemical shift multiplied by the association constant, x is the concentration of acetic acid and b = K_A which is the association constant of the complex.

As a plateau was reached, the equilibrium was quantified and the association constant was determined to be $0.31M^{-1}$. This association constant is quite low, which was predicted due to the high dielectric constant of DMSO inhibiting the interaction. In DMSO acetic acid has a pKa value of acetic acid is approximately 12.6 and the tertiary amine of tamoxifen would have a pKa value of 41-42. This therefore means acetic acid effectively becomes a much weaker acid in DMSO, meaning a much higher proportion of the acetic acid was present as the undissociated acid and therefore inhibiting its

interaction with the tertiary amine on tamoxifen. This in turn means a much higher proportion of acetic acid needed to be present to obtain a good degree of complexation of the tamoxifen (128 equivalents was required for 65% of tamoxifen to be complexed). However this would be true if only the ionic interaction was considered. The tamoxifen molecule and the coumarin molecule (in the nanogel) both contain aromatic rings, therefore the ionic interaction between the tamoxifen and the acrylic acid is not the only interaction taking place. In fact π-π stacking of the aromatic rings (which have bond energies of 2-3 Kcal/mol) in the two molecules will also be occurring: this is well documented for polymers containing coumarin molecules[167, 306]. DMSO was used to help solubilise the drug, however it has high dielectric constant, which works against the formation of the ion pair. Therefore to try to maintain as much specific interaction between the tamoxifen and acetic acid as possible, and to reduce the non-specific interactions (which would cause bleeding of the drug in undesired areas) as far as possible, a 1:1 ratio of tamoxifen to acrylic acid was selected.

4.3 Uploading drug into the nanogels and *in vitro* release studies

The ionic interaction, along side the π-π stacking, between tamoxifen and acetic acid confirmed via ^{1}H-NMR studies was discussed in section 4.2.4.1. This interaction was exploited in the nanogels, to create a drug delivery system that would prevent leakage of the drug while the carrier is moving towards its target location. Furthermore the ionic bond would be expected to be disrupted when the nanogels are internalised in tumorous cells, which are characterised by a reduced pH, leading to a pH triggered release.

4.3.1 Formation of MIP/ NIP nanogels

Having established that a good interaction between tamoxifen and acetic acid can be achieved, the drug was loaded into the nanogels at a ratio of 1:1, 0.5:1 and 0.25:1 tamoxifen to functional monomer. The amount of tamoxifen was varied to analyse its effect on the system, without going above the crucial 1:1 ratio to avoid unspecific binding. The nanogels were prepared using the same method as the non-imprinted nanogels obtained in chapter 2, except that, in this case, the drug was present in the polymerisation solution. For every MIP formed a corresponding NIP (non-imprinted polymer) was also synthesised, as a control. The nanogels were then characterised for their size and solubility and the data is presented in table 16.

Nanogel	MIP/ NIP	Ratio Fm:Tam	% TCA (%)	% A (%)	% yield (%)	Ave. diameter (nm)	Solubility in water (mg/ml)
NG1 (BATCH 3)	NIP	N/A	2.5	67.5	40	230 ±15	10
NG1A	MIP	1:1	2.5	67.5	54	154 ±2	0.1
NG1B	MIP	1:0.5	2.5	67.5	38	167 ±3	0.1
NG1C	MIP	1:0.25	2.5	67.5	44	168 ±3	0.5
NG2 (BATCH 3)	NIP	N/A	5	65	50	217 ±18	10
NG2A	MIP	1:1	5	65	54	104 ±7	0.1
NG2B	MIP	1:0.5	5	65	52	130 ±2	0.1
NG2C	MIP	1:0.25	5	65	45	112 ±1	0.1

Table 16 – Molecularly imprinted nanogels prepared. MIP/NIP nanogels contained 20 % MBA and 10 % AA and polymerised at 70 °C in DMSO with a C_M of 0.5%, using AIBN at 2% of all double bonds by mol. All particle sizes were carried out at 0.1 mg/ml in 1% DMSO in water. Where TCA is trifluoromethyl coumarin acrylamide acrylamide, MBA is methylbisacrylamide, AA is acrylic acid and A is acrylamide.

The addition of tamoxifen considerably reduced the solubility of the nanogel, however when both the amount of TCA in the formulation was decreased and the amount of tamoxifen was decreased a transparent solution could be obtained at 0.5 mg/ml. Tamoxifen is highly hydrophobic due to its three phenyl rings and coumarin is also hydrophobic due to its hydrophobic rings. It naturally followed that the solubility decreased with an increase of either of these molecules.

The presence of tamoxifen appeared to have a significant impact on the particle size reducing it by approximately 70-80nm in all cases. The drug loaded nanogels also appeared to be more monodispersed, giving more narrow particle size distributions. The drug loaded nanogels containing 2.5% coumarin were all roughly 50 nm bigger than the 5% coumarin equivalent. This could be the result of strong hydrophobic interactions such as the π-π stacking, which would be holding the nanogels in a more tightly compact and rigid structure, also justifying the reduced solubility. The higher the content of coumarin tag in the formulation, the more π-π interactions taking place and the more tightly held is the polymer structure, which in turn increases the hydrophobicity of the nanogel. The more narrow particle size distribution of tamoxifen loaded NG1A compared to the unloaded NG1 (batch2) nanogel and are displayed in figure 58.

a)

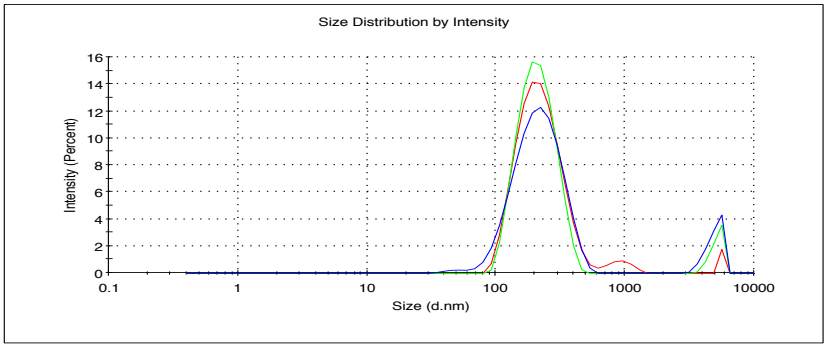

b)

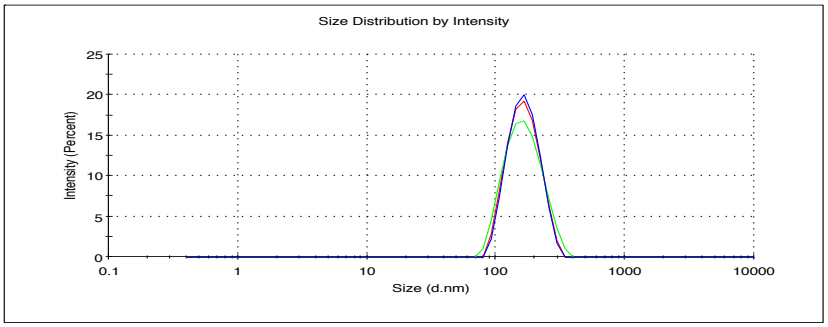

Figure 58- DLS traces of a) NG1(batch 2) with no tamoxifen loaded and b)NG1A with 0.42eq tamoxifen loaded. Both samples meaured at 0.1 mg/ml in water.

Surprisingly, no significant difference was observed in the particle size with increasing amount of tamoxifen incorporated in the nanogels. A possible explanation for this is the overall low concentration of the drug in the nanogel solution; this could change if much higher amounts of tamoxifen were used. Following the successful incorporation of tamoxifen in the nanogels the next step focussed on characterising the loaded nanoparticle and evaluating the drug release.

4.3.2 Tamoxifen uploading on to the nanogels

Drug loading on carriers can vary a lot, with some carriers managing to load up to almost 2 equivalents of drug per carrier[307]. However, this is not the norm, when reviewing polymer-based nanocarriers, loadings up to 0.2 equivalents are more frequently encountered[308-310]. The percentage of drug successfully loaded on to a drug delivery system is dependent on variables such as the upload method, structure of the carrier and release mechanism. Work by Yan et al produced polymer-based nanospheres, which were passively tumour-targeted using sulfadiazine and loaded with between 0.1 and 0.25 equivalents of drug to carrier depending on the uploading method used and their nanosphere composition[308, 311]. More complex systems, such as those with active targeting moieties often have a lower drug loadings due to the multifunction and more complex nature of the drug delivery system[312].

Establishing the entrapment efficiency enables the comparison of the uploading technique used for these nanogels compared to those reported in the literature. The drug entrapment efficiency can be calculated via equation 13.

$$Entrapment\ efficiency = \frac{Actual\ drug\ loaded}{Theoretial\ drug\ loaded}\ x\ 100 \qquad \textbf{Equation 13}$$

Sun *et al* obtained a maximum entrapment efficiency of 84% when loading upto 0.14 eq drug onto their nanoparticles[313] and Tavassolian *et al* had a maximum entrapment efficiency of 79% when loading 0.5 eq of drug onto their micelles[312]. Yigitoglu *et al* managed to achieve exceptionally good results with their alginate polyvinylpyrrolidone copolymer beads with between 0.13 and 0.5 eq drug loadings and entrapment efficiencies of 92% and above.[314]

To establish how much tamoxifen was successfully uploaded into the nanogels through molecular imprinting, the nanogels were analysed using HPLC (high performance liquid chromatography). The method involved dispersing the nanogels in a solvent, in this case ACN, where interactions between the drug and functional monomer were easily disrupted, but where the drug was highly soluble. This was followed by quantification of the drug in solution by HPLC. The optimal conditions for analysing tamoxifen in the Hichrom C18 25mm column were found to be 5:95 water acidified with 0.5% acetic acid to Acetonitrile at a flow rate of 1.5 ml/min, which gave a pressure of approximately 80 bar. This gave a peak at around 7 minutes. Initially a reference line of Tamoxifen, figure 59, in dissolved in ACN (acetonitrile) was established.

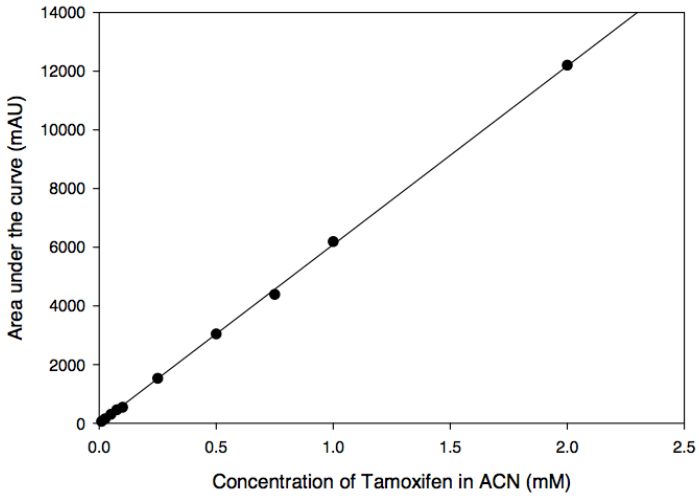

Figure 59 –Calibration curve of the area under the curve obtained via HPLC against the concentration of tamoxifen injected. 20 µl were injections performed in acetonitrile measuring the absorbance at 291nm. Flow rater was 1.5 ml/min using 95% ACN, 5% water acidified with 0.5% acetic acid.

Once the calibration curve was obtained the nanogels were dissolved in ACN (at 1 mg/ml) and mixed for 5 minutes. This process was established as the best method to extract all the tamoxifen from the nanogels as the tamoxifen is highly soluble in ACN, whereas the nanogels are insoluble in ACN, disrupting the ionic interaction and the drug was released. After 5 minutes stirring the mixture was filtered with a 20 nm filter to remove the nanogel from the mixture and 20 µl were injected into the HPLC. The data can be seen in table 17.

Nanogel	Ratio Fm:Tam (by mols)	TCA content (%)	Entrapment efficiency (%)	Final Ratio of drug to carrier
NG1A	1:1	2.5	> 99.9	0.42:1
NG1B	1:0.5	2.5	92	0.19:1
NG2A	1:1	5	95	0.38:1
NG2B	1:0.5	5	96	0.19:1

Table 17 – The entrapment efficiency and final drug loadings of some of the molecularly imprinted nanogels prepared. MIP nanogels contained 20 % MBA and 10 % AA with the remained of the nanogels comprised of acrylamide. All nanogels were polymerised at 70 °C in DMSO with a C_M of 0.5%, using AIBN at 2% of all double bonds by mol. Where TCA is trifluoromethyl coumarin acrylamide and Fm is functional monomer.

A high drug loading of tamoxifen into the nanogels was achieved, with nearly 100% entrapment efficiency. In NG1A and NG2A with a 1:1 ratio of acrylic acid to tamoxifen, there are 0.42 equivalents of Tamoxifen to nanogel. This is a relatively high loading of drug for a drug delivery with excellent entrapment efficiencies of between 92 and > 99% compared to those found in the literature.[210, 313, 314] Having confirmed that molecular imprinting can be an efficient method for the uploading of tamoxifen onto the nanogels, an analysis of the pH-triggered release of the drug *in vitro* was the next investigation.

4.3.3 Diffusion verses triggered release

To assess the efficacy of these nanogels in terms of their qualities as potential drug carriers, *in vitro* analysis of the drug release was required, as mentioned above. The aim of this investigation was to minimise drug release via diffusion, and ensure that the drug release only occurs when an environment with reduced pH is encountered, in order to increase drug dosage at the required site (here, breast tumour cells) and reduce healthy cell exposure to the drug. At pH 3, below the pKa value of acrylic acid, which is 4.25, the acid is undissociated[303] and therefore retains its hydrogen, and no longer maintains the ionic interaction with tamoxifen . This is on the assumption that the polymer matrix in water does not significantly alter the pKa values of the functional

monomer. Analysis of the nanogel tamoxifen content at pH 3 enabled evaluation of the maximum amount of drug available for release in an aqueous environment, giving the limit of the system. Although the maximum amount of tamoxifen loaded onto the nanogels was established, it is likely that some of the tamoxifen is imprinted deep into the core of the nanogel, which under physiological conditions would not be accessible for release. Therefore to determine the maximum drug available for release in an acidic aqueous environment the nanogels were exposed to aqueous solutions at pH 3.

The nanogels were re-suspended in water acidified with HCl to pH=3 and dialysed for 2 days, with 4 water exchanges (the final water exchange was with pH neutral water) and freeze dried once again. The nanogels were worked up in the same way as described previously, dissolved at 1mg/ml in ACN, stirred for 5 min, filtered and injected into the HPLC. The area under the curve was compared to that of the nanogel without the extraction process and the percentage of drug retained in the nanogel after pH reduced extraction was recorded in table 18.

Nanogel	Ratio Fm:Tam	TCA (%)	Entrapment efficiency (%)	Tamoxifen retained by the nanogel in water at pH 3 (%)	Ratio of drug to carrier available for release in aqueous conditions.
NG1A	1:1	2.5	>99.9	20	0.34:1
NG1B	1:0.5	2.5	92	5	0.17:1
NG2A	1:1	5	95	4	0.35:1
NG2B	1:0.5	5	96	7	0.17:1

Table 18- Tamoxifen available for release in acidic aqueous environment from some of the molecularly imprinted nanogels. MIP nanogels contained 20 % MBA and 10 % AA with the remained of the nanogels comprised of acrylamide. All nanogels were polymerised at 70 °C in DMSO with a C_M of 0.5%, using AIBN at 2% of all double bonds by mol. Where TCA is trifluoromethyl coumarin acrylamide and Fm is functional monomer.

The amount of tamoxifen remaining in the nanogels is a very small percentage of between 4 and 7% for the majority of the nanogels (NG1B, NG2A and NG2B). NG1A had a larger proportion of loaded tamoxifen unavailable for release with 20% being retained in the polymer matrix, however due to the initial high loading of tamoxifen in the nanogel (0.42 eq) it maintained a comparatively high drug load which was available for release. Therefore NG1A effectively had a 0.35:1 drug (available for release) to nanogel ratio, higher than the majority reported in the literature.[308, 312, 313] If both the entrapment efficiency and the drug available for release are considered, then between 80 % (NG1A) and 91% (NG2A) of drug loaded onto the nanogels is available for release.

4.3.4 Drug release

The data obtained so far clearly suggested that the molecular imprinting approach had allowed the upload of very good quantities of tamoxifen in the nanogels. This was the result of the combination of the imprinting approach together with the use of the acrylic acid as a functional monomer to specifically 'anchor' the drug to the polymeric matrix. The nature of this acid-base interaction could therefore be further exploited to induce a stimuli-controlled release of the drug. The next set of experiments focussed on measuring the impact of the pH in triggering the release of the drug from the tamoxifen-loaded nanogels.

Data in the literature report different values of pHs for tumorous cells, varying. from 6.8 for extracellular tumour tissue pH, to pH 4.5 in some of cellular compartments (such as pH 6.5-5.0 in endosomes and pH 5.0-4.5 in lysosomes)[315, 316]. Breast tumour cells themselves vary in pH with drug resistant breast tumour tissues having lower pH than their non-resistant counter parts[317]. pH 5.5 is conventionally used when analysing novel materials as proof of principle[256, 318-320]. Therefore investigations into the release of tamoxifen from the nanogels were carried out at pH 5.5 to mimic tumour environments in general.

In order to analyse the drug release from the nanogels, the nanoparticles loaded with tamoxifen were dissolved in the aqueous phase and dialysed against a buffer solution being stirred at 37 °C to mimic the dynamic equilibrium *in vivo*. In this way any drug released from the polymer would be removed from the carrier by passing through the dialysis membrane, as it would in the body, reducing the likelihood of rebinding and therefore allowing the evaluation of continued drug release. In a closed system whereby the carrier is simply dissolved in the relevant buffer and continually mixed, the carrier is in continual contact with any free drug which would not be the case *in vivo*, as the drug would be released and used for it's intended purpose, preventing rebinding. The amount of drug released as a function of time was determined by quantification of the drug remaining incorporated in the nanogel. The first step involved analysing the drug release at pH 5.5 using 1mM acetate buffer. When the drug was removed during dialysis at pH 3 it was noticed that a significant increase in water solubility of the nanogel itself was obtained. This indicated that sedimentation at pH 5.5 was unlikely as the more drug was removed, the more soluble the nanogel became in water. Therefore NG1A (6 mg) was dissolved in buffer at 2 mg/ml and suspended on dialysis in acetate buffer (1 L, 1 mM) and at each time point the dialysis tube was inverted several times

to ensure a representative sample was removed. At the required time points 100 µl of the nanogel solution were removed, 100 µl of ACN were added to facilitate the release of the drug from the polymer matrix, the solution was vortexed for 30 seconds, filtered and injected (20 µl) into the HPLC. This allowed for many time points to be assessed. This was repeated in triplicate to obtain reliable data. The results can be seen in figure 60.

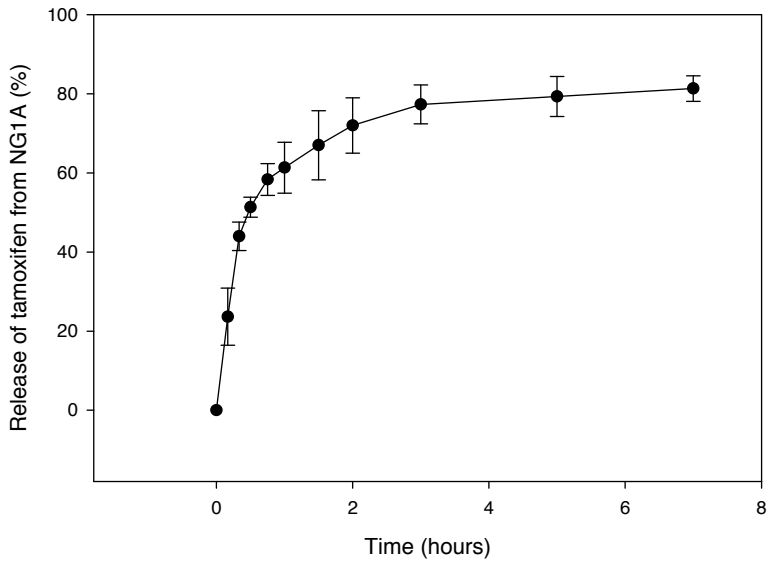

Figure 60 - Tamoxifen released from nanogel NG1A in acetate buffer (pH 5.5) over 7 hours. Analysis carried out using HPLC, eluent used was 95% acetonitrile to 5% water acidified with 0.5% acetic acid at a flow rate of 1.5 ml/min.

The data clearly indicated that the drug was released successfully at pH 5.5. A very rapid release was observed and the payload totally dispensed within the first 2 hours. This could be advantageous as depositing a high payload of drug, only at the site of the intended target could have a beneficial effect on preventing the rapid replication of breast tissue cells. As these nanogels are <200 nm in size they will be retained at the tumour site by the EPR effect (explained in section 4.2.1) and therefore the drug would theoretically be released over a 2 hour period only at the target site. However to establish that the drug was only released at acidified pH, analysis of tamoxifen release from the nanogels at physiological pH (pH 7.4[295]) was also evaluated. Leakage of the drug outside of its required location increases the systemic toxicity and reduces the appropriate bioavailability of the drug, as less accumulates at the lesion site[285].

To evaluate drug leakage at pH 7.4, NG1A was dissolved in water at 2 mg/ml and placed in 1000 dalton dialysis tubing. As mentioned above, NG1A was less soluble at higher concentrations; as such this was a cloudy solution. To prevent artefacts in the

data due to sedimentation of the nanogels, individual 'parcels' of nanogel containing 500 µl of the nanogel solution were each put in a separate section of dialysis tube, but each parcel was placed in the same dialysis solution. In this case the dialysis solution was 1 litre of 1 mM PBS buffer, adjusted to pH 7.4. A parcel was removed at each relevant time point, all contents removed and diluted (to 1 mg/ml) with 500 µl of ACN, vortexed for 30 seconds, filtered using a 20nm PTFE filter and injected (20 µl) into the HPLC. This was carried out in triplicate for accuracy and the results are presented in figure 61.

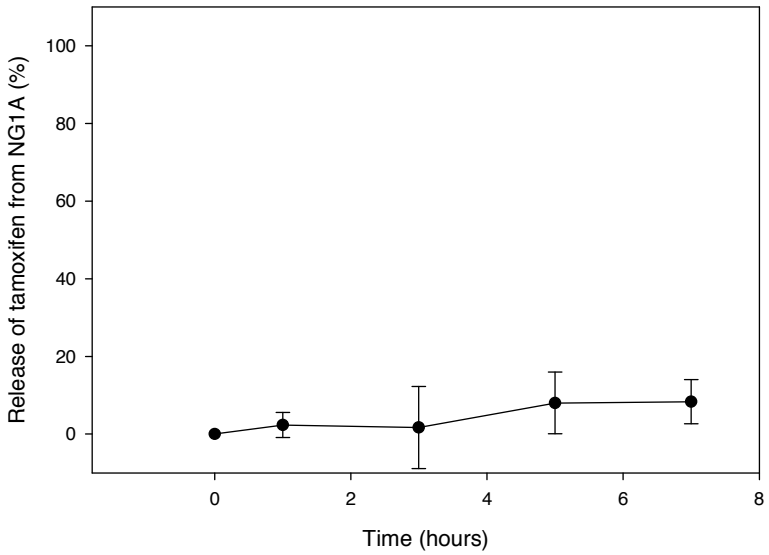

Figure 61 – Tamoxifen released from nanogel NG1A in PBS buffer (pH 7.4) over 7 hours. Analysis carried out using HPLC, eluent used was 95% acetonitrile to 5% water acidified with 0.5% acetic acid at a flow rate of 1.5 ml/min.

Figure 61 shows that less than 10 % of the drug was released in 7 hours. In the case of pH 5.5 80% of the drug was released, suggesting only a very small amount of drug would be leaked whilst the nanogel circulated inside the body. The data suggests that the nanogels have released the drug in high dosage at a pH of around 5.5 and retain the drug at physiological pH. This feature makes the nanogels attractive as a drug delivery system as it may significantly reduce side effects of the drug.

The release response of the drug delivery carrier at reduced pH was rapid, releasing the majority of the payload within the first 2 hours. This would be beneficial for an immediate response for a growing tumour, however for prevention of breast cancer and a more sustained delivery of tamoxifen a slower more controlled release would be desirable. Several studies have attempted to show controlled release however when

the nanoparticles reach their trigger the tamoxifen payload is often released within the first 2-3hours, as with the nanogels under test[321, 322]. One study by Vivek *et al* has more successfully controlled the release of tamoxifen from the nanoparticles (with loadings of up to 28%) releasing steadily over 6 hours[323]. However more drug was released at pH 7.4 (~20% within 6 hours) than the nanogels produced in this project. Moreover, at pH 4 the reported maximum drug release was 68% and at pH 6 just 43% of the reported drug load was released by 48 hours[323], whereas in the current study, the nanogels released >80% of the loaded drug. To investigate whether a reduced payload would release more slowly, for a more controlled release, the nanogels previously prepared with varying loading (section 4.3.1) were analysed over a longer period of time for their drug release.

To investigate the effect of reducing the loading of the drug in the nanogel on the release timescale NG1A, NG1B and NG1C were analysed for their release over a 48 hour period.

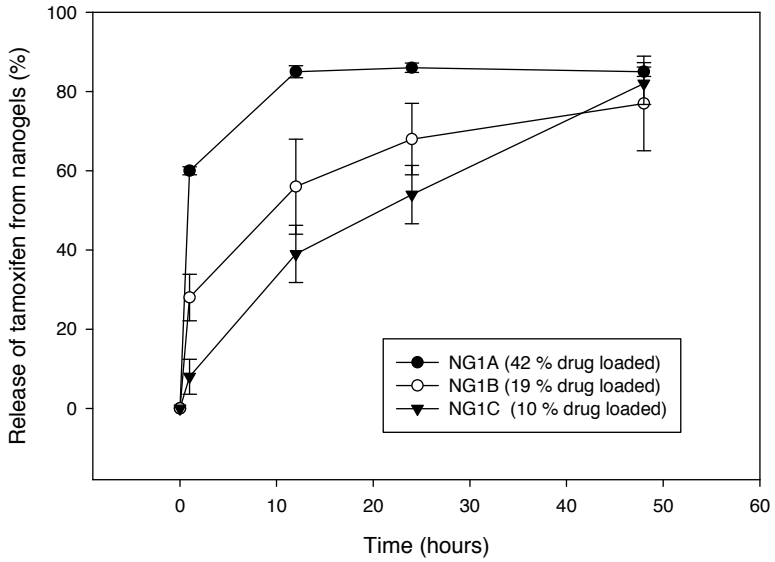

Figure 62 - Tamoxifen released from nanogel NG1A, NG1B and NG1C in PBS buffer (pH 7.4) over 7 hours. Analysis carried out using HPLC, eluent used was 95% acetonitrile to 5% water acidified with 0.5% acetic acid at a flow rate of 1.5 ml/min.

As can be seen in figure 62, when the loading of tamoxifen is less (10 %, NG1C) a much slower release profile is seen, with tamoxifen being released more steadily and evenly over the 48 hour period. Even at double this drug loading as in JRP103 (20 % drug loading) the drug is steadily released over a 24 hour period. It follows that this system can be tailored for either a slower release of a drug at lower concentrations, which is ideal for preventative care, or for a faster release with a higher payload when

treating tumours. In all circumstances the payload is mainly released at reduced pH, targeting the specific target lesions and protecting healthy cells from substantial side effects. As the *in vitro* studies have shown positive results with regard to the efficacy of these nanogels, an analysis *in vivo*, using a genetically modified line of zebrafish was carried out.

4.4 In vivo drug release

The *in vitro* release of the drug at pH 5.5 proved to be very successful. In the next section the data related to the testing of the release mechanism of the selected nanogels *in vivo*, using a transgenic line of zebrafish are presented, which demonstrate that the same release mechanism can be shown to occur *in vivo*. Zebrafish tamoxifen reporter line ubi:loxP-EGFP-loxP-mCherry (ubi:switch), acquired from University College London fish facility, were used for these studies.

4.4.1 The LoxP-CreERT system

An advantage of mice and zebrafish is the ability to generate transgenic reporter lines. One of the many reasons mice are often used as an *in* vivo model is the ability to create new mouse models due to better knowledge of their genome and transgenic technologies[206]. One such system that has been exploited in both mouse models and zebrafish is the loxP-creERT system. Using the loxP-creERT system DNA modifications can be made. For this project the loxP-creERT system has been exploited to visualise a colour change in zebrafish in presence of tamoxifen. Therefore when tamoxifen is not present the zebrafish fluoresce green (GFP) fluorescence. When tamoxifen is present, an enzyme (cre recombinase) is triggered and the fish DNA encoding for the green fluorescence is deleted and the fish instead produce red (mcherry) fluorescence.

The cre/lox system is a well known biological process that has been used for the past 15 years to artificially control gene expression (the process of reading the information of a gene and synthesising the gene product, which is normally a protein although can be the formation of functional RNA). Cyclization recombination (cre) is a gene that encodes site specific DNA recombinase, thus allowing recombination of specific DNA sites when the cre protein is present. The specific sites that the cre protein can cut, and then recombine the DNA surrounding it, is a 'locus of-X over P1' or loxP sequence. LoxP sequences are 34 base pairs long and from a bacterial virus, 'P1 bacteriophage'[324, 325]. The loxP DNA excised from the virus is not found in animals or plants. Therefore the loxP sequence can be artificially inserted into an animal or plants

DNA without the risk of excision of undesired areas of their genome. A representative diagram of how the cre/loxP system works can be seen in figure 63.[309]

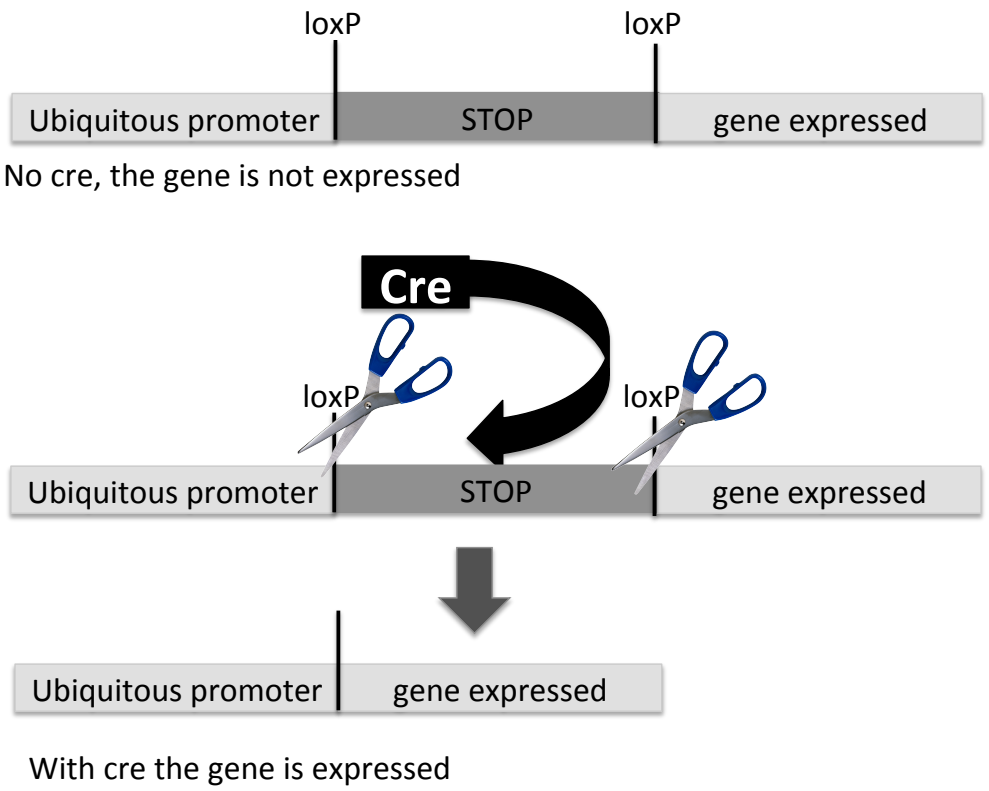

Figure 63- A systematic diagram of Cre mediated loxP recombination where the gene is only expressed when Cre recombinase is released and deletes the STOP coding.

For a gene to be expressed, a promoter is required to initiate the multi-step process required for the protein production. To gain control over the expression of a particular gene/protein a STOP coding DNA sequence is surrounded by loxP sequences and inserted between the promoter and the gene. The promoter needs to be 'ubiquitous' to enable the switch to be present in all cells at all stages of development[326]. Only when the loxP sequences are cut, removing the stop coding, can the protein be produced and therefore gene expression occurs.

To produce an *in vivo* model containing this gene control a transgenic line containing the cre recombinase and a separate transgenic line containing the loxP-flanked gene must be produced. In the resulting offspring, those that inherit both genes, the coding between the loxP sequences will be excised and no longer function, and gene expression will occur in tissues where cre is present[327]. However where cre is not

present and the code between loxP sites will remain and function as normal and in the gene would not be expressed.

4.4.2 LoxP –creERT induced by tamoxifen zebrafish

Work carried out in 2009 by Hans *et al* introduced a tamoxifen inducible cre^{ERT2} mediated loxP recombination in zebrafish[328]. They found loxP excision was dose dependant and occurred within 2-4 hours of administration of tamoxifen or its 4-hydroxytamxifen metabolite when applied at mid-gastrulation period of development (~8 hpf). However Hans used *EF1α* promoter to drive the transgene expression, which was ubiquitous for zebrafish embryos during gastrulation (5½-10 hpf) and mid-somitogenesis (10-24 hpf) stages. They found expression was only strongly retained in the retina and hindbrain beyond 24 hpf[328]. It was Mosimann *et al* who used *ubiquitin* (*ubi*) as the promoter for the cre/loxP system in zebrafish[326]. They found that *ubi* promoter drove transgene expression ubiquitously in the vast majority of cells starting at mid-blastula (2-5 hpf) development and remaining through all stages of development. Therefore using *ubi* promoter Mosimann created a *ubi*:switch line of zebrafish which emitted GFP fluorescence. When their loxP flanked line were crossed with the cre^{ERT2} line and the resulting embryos were exposed to tamoxifen, mcherry (red) fluorescence was expressed[326]. A systematic diagram of the transgene expression can be seen in figure 64.

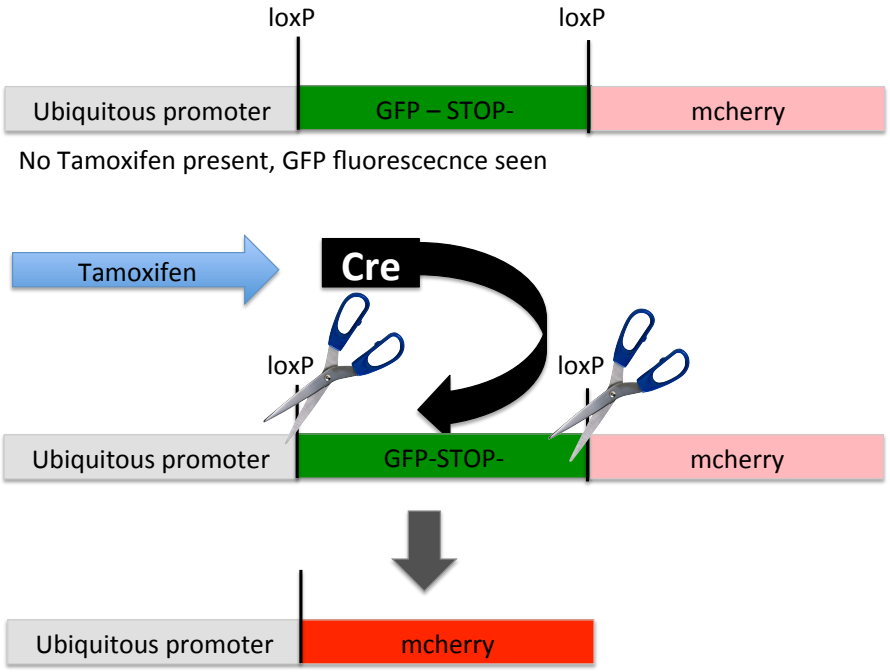

Figure 64 – A systematic diagram of tamoxifen induced creERT2 mediated loxP recombination where GFP fluorescence is seen in absence of tamoxifen, and mcherry fluorescence is seen in presence of tamoxifen.

In this model two zebrafish lines are created, the first containing the loxP sequences, which emit GFP fluorescence ubiquitously from 24 hpf. The second line contains the cyclization recombinase and express GFP fluorescence in the heart at 48 hpf. It is possible to create homozygous cre and loxP containing zebrafish, by crossing two heterozygous zebrafish. From this two heterozygous offspring (+/-), and two homozygous offspring, one containing no cre recombinase or loxP (-/-) and one containing both genes of either cre or loxP (+/+), of which 3 will express GFP fluorescence, can be obtained. The one containing both alleles will emit slightly stronger GFP fluorescence, although this can be difficult to identify. By crossing a homozygous cre transgenic zebrafish with a homozygous loxP transgenic zebrafish all offspring produced would contain one loxP allele and one cre recombinase allele, therefore all offspring would contain the *ubi*:switch. However the fish obtained for this project were acquired from University College London's fish facility, where the transgenic zebrafish is maintained as a heterozygous line. In practical terms, to avoid the need to put in place a breeding program over several generations(which itself is highly time consuming as zebrafish take 3 months to become sexually active) it was decided to use the heterozygous fish obtained.

Both genes generate visible fluorophores with a single allele and therefore fish used to create embryos containing the loxP/cre system were heterozygous (+/-), forming four different offspring (+/-, +/+, -/+, -/-), of which only one (+/+) will contain the *ubi*:switch mechanism required for detecting tamoxifen. At 24 hpf it is possible to isolate those embryos which have not inherited the loxP sequences (-/+, -/-), as they do not emit GFP fluorescence throughout their body and can therefore be remove from the sample. However only 50 % of the embryos that remain will contain the *ubi*:switch (+/+). Therefore when analysing effects of tamoxifen it is important to remember that not all embryos in a sample group will express mcherry fluorescence, even if tamoxifen is present. A schematic illustrating the generation of ubi:switch ubi:loxP-EGFP-loxP-mCherry embryos can be seen in figure 65.

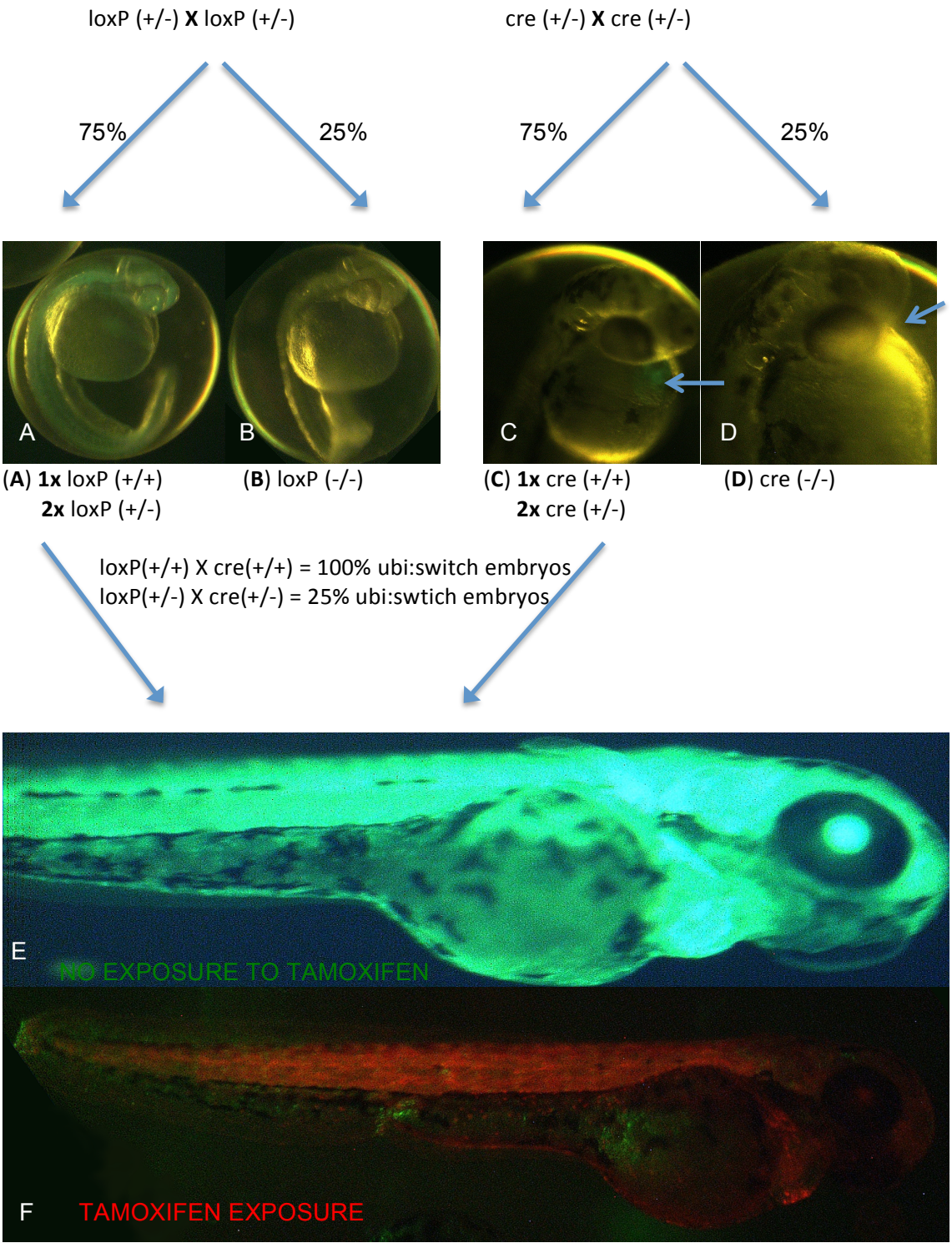

Figure 65 – Schematic of zebrafish embryos allele inheritance to form a *ubi*:switch transgenic zebrafish. A) hetro/homozygous embryo which has inherited loxP, showing all over GFP fluorescence at 24hpf. B) homozygous embryo which has not inherited loxP, showing no GFP fluorescence at 24hpf C) hetro/homozygous embryo which has inherited cre, showing GFP fluorescence ain the heart at 48hpf. B) homozygous embryo which has not inherited cre, showing no GFP fluorescence in the heart at 48hpf E) *ubi*:switch ubi:loxP-EGFP-loxP-mCherry zebrafish before exposure to tamoxifen (GFP fluorescence) F) *ubi*:switch ubi:loxP-EGFP-loxP-mCherry zebrafish after exposure to tamoxifen (mcherry fluorescence).

4.4.3 Tamoxifen release studies in loxP zebrafish

The development of the 'ubi:switch transgenic zebrafish' line enables reliable visual evaluation of the release of tamoxifen from the nanogels *in vivo*. Transgenic zebrafish have previously been used to establish preliminary efficacy of drug delivery systems. Lui *et al* found that piperlongumine loaded onto their polymer micelles inhibited tumour growth in transgenic zebrafish through inhibiting angiogenesis (prevention of forming new blood vessels)[329]. FLK-1 premoter EGFP transgenic zebrafish were used, whose blood vessels emit GFP fluorescence and hence allowed monitoring of intersegmental blood vessel growth.

Mosimann had already shown that a short application (15 minutes) of tamoxifen was enough to induce the fluorescence change in the ubi:switch zebrafish, although it took 3 days for results to be visually perceived. He also found the longer the fish were left to develop their colour, the more intense the fluorescence seen. However the age at which he was using the transgenic fish was much younger, 8 and 24 hpf[326]. To ensure the nanogels were entering the zebrafish, immersing them in the nanogel solutions beyond 5 dpf was preferable. At 24 hpf Mosimann found a higher intensity of fluorescence was seen with proportionately higher concentrations (1 µM compared to 5 µM) of drug administered and that 10 µM was a lethal concentration, however he did not administer tamoxifen at later stages of development. Zebrafish are considerably bigger at 5 dpf compared to 24 hpf[225] and therefore lethal concentrations of tamoxifen and concentrations high enough to trigger the cre recombinase in enough cells to visualise the colour change by microscope remained unobserved at 5 dpf and beyond. Investigations were required to use concentrations above and below 10 µM of tamoxifen, to ensure enough drug is present to visualise any release without administering a toxic dose.

To evaluate the effect of the drug over different timescales and in varying concentrations, three different experiments were set up, each with distinct groups of zebrafish. The first group were fed tamoxifen-loaded nanogel NG1A (2.5% coumarin tag) at a concentration of 24 µg/ml, which contains tamoxifen at 10 µg/ml (27 µM), for 30 minutes before returning to fresh fish water. The second group were fed NG1A at a concentration of 2.4 µg/ml, which contains tamoxifen at 1 µg/ml (2.7 µM), for 2 hours before returning to fresh fish water. And the final group were fed NG1A at a concentration of 0.24 µg/ml, which contains tamoxifen at 0.1 µg/ml (0.27 µM) for 12 hours before returning to fresh fish water. Along side each of these groups, 3 control

groups were also maintained under the same conditions in 6 well plates. Firstly a parallel control group was placed in a tamoxifen citrate solution (effectively the free drug) of the same concentration of tamoxifen for the same length of time. The second control was non tamoxifen loaded nanogel, NG1 (Batch 2), at the same concentration of nanogel as NG1A. The final standard negative control were zebrafish in fresh fish water, the experiment set up can be seen in figure 66. Twelve 6 dpf *ubi*:switch zebrafish were placed in each solution, the fish were previously sorted for GFP fluorescence at 24 hours, removing any fish who did not inherit systemic fluorescence and therefore the loxP allele. Therefore the embryos that remained either contained the full loxP-creERT system, which turn mcherry on exposure to tamoxifen or just the loxP allele which would remain GFP fluorescent regardless of exposure to tamoxifen.

Drug loaded nanogel NG1A (34 µg/ml) 24 µg/ml nanogel 10 µg/ml tamoxifen	**Free Drug** Tamoxifen citrate (15 µg/ml) 10 µg/ml tamoxifen	Treated for 30 minutes
Controls in fish water	**Non-drug loaded nanogels** NG1 (batch 2) (24 µg/ml) 24 µg/ml nanogel	

Drug loaded nanogel NG1A (3.4 µg/ml) 2.4 µg/ml nanogel 1 µg/ml tamoxifen	**Free Drug** Tamoxifen citrate (1.5 µg/ml) 1 µg/ml tamoxifen	Treated for 2 hours
Controls in fish water	**Non-drug loaded nanogels** NG1 (batch 2) (2.4 µg/ml) 2.4 µg/ml nanogel	

Drug loaded nanogel NG1A (0.34 µg/ml) 0.24 µg/ml nanogel 0.1 µg/ml tamoxifen	**Free Drug** Tamoxifen citrate (0.15 µg/ml) 0.1 µg/ml tamoxifen	Treated for 12 hours
Controls in fish water	**Non-drug loaded nanogels** NG1 (batch 2) (0.24 µg/ml) 0.24 µg/ml nanogel	

Figure 66- Experiement layout for investigating the release of tamoxifen in juvenile *ubi*:switch zebrafish.

After 24 hours one fish in the strongest solution of NG1A containing 10 µg/ml tamoxifen had died but otherwise all other fish were alive and well. However, no mcherry fluorescence could be seen in any of the zebrafish except for the remaining yolk which was fluorescing red in every fish at every timeframe. The single fish may have died due to a rapid and concentrated internal release of tamoxifen. The lack of mcherry fluorescence was not an immediate concern as Mosimann reported a time delay before detecting the fluorescence change and only presented images taken 3 days after

tamoxifen exposure[326]. After 48 hours still no mcherry fluorescence was seen in any of the samples. However 3 days after the initial exposure to tamoxifen all fish remaining were alive and well and 50 % of zebrafish exposed to tamoxifen citrate or NG1A contained varying degrees of mcherry fluorescence. This was expected as, statistically, half of the fish would have inherited both the cre and loxP alleles required. None of the fish exposed to the non-loaded nanogel were expressing mcherry fluorescence and neither were any of those maintained in fish water, except the yolk, which was fluorescing red in every fish at every timeframe. Images of the fish can be seen in figure 67 for the lower two concentrations of tamoxifen, and in figure 68 for the higher concentration. This experiement was not fully balanced as not all concentrations were administered for the all the timeframes (due to the project deadline) therefore further experiments would be required showing the effects of all the variables to fully validate these results. In general fish in all three concentrations of the tamoxifen-loaded nanogel showed a stronger mcherry fluorescence than the fish exposed to the free tamoxifen citrate at equivalent concentrations. This suggests tamoxifen loaded nanogels had successfully triggered the cre recombinase release in the cells more successfully than the free drug, therefore improving its bioavailability and confirming it's release. However what triggered the release of the tamoxifen was not clearly identified. It is possible that the tamoxifen was released when the nanogels reached the stomach of the zebrafish which itself may have a reduced pH, however no information could be retrieved on the pH of the stomach. (Although potential reduced pH of the stomach could be enabling release of the drug from the nanogels in this *in vivo* experiment, in final use of this nanogel delivery system, the nanogels would be required to be injected otherwise tamoxifen would be immediately released when the nanogels reached the stomach.) The pH of the zebrafish water was measured before, during and after the experiment, and it remained consistently at neutral pH. Zebrafish buffer their own pH to maintain neutral pH in cells[330]. To establish if tamoxifen was released in fish water solution, an *in vitro* experiment was carried out, suspending NG1A in fish water over a 24 hour period.

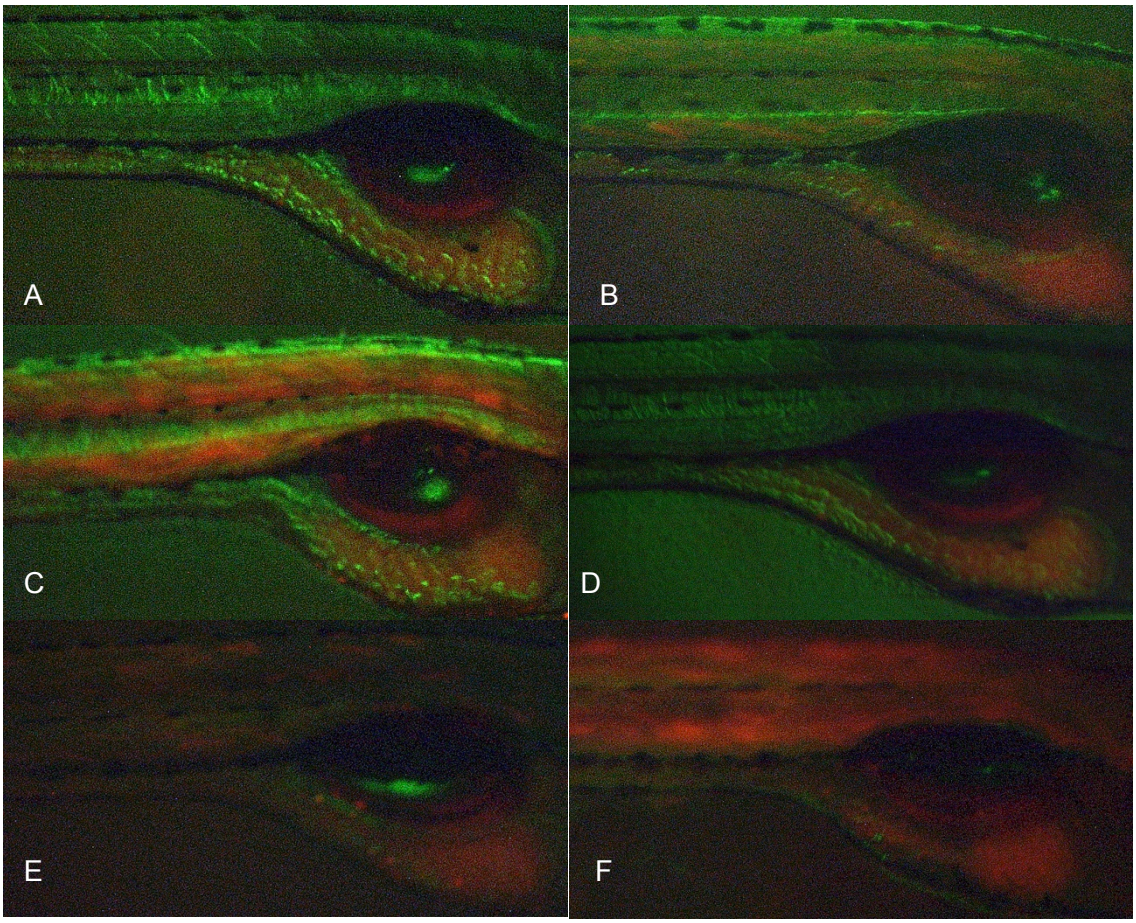

Figure 67 - *ubi*:switch zebrafish treated for 12 hours at 0.1 µg/ml tamoxifen, viewed 3 days after exposure, A) control immersed in fish water, B) immersed in Tamoxifen citrate, C) immersed in NG1A, 0.1 µg/ml tamoxifen loaded nanogel. *ubi*:switch zebrafish treated for 2 hrs at 1 µg/ml tamoxifen, viewed 3 days after exposure, immersed in, D) fish water (control), E) tamoxifen citrate and F) NG1A tamoxifen (1 µg/ml) loaded nanogels.

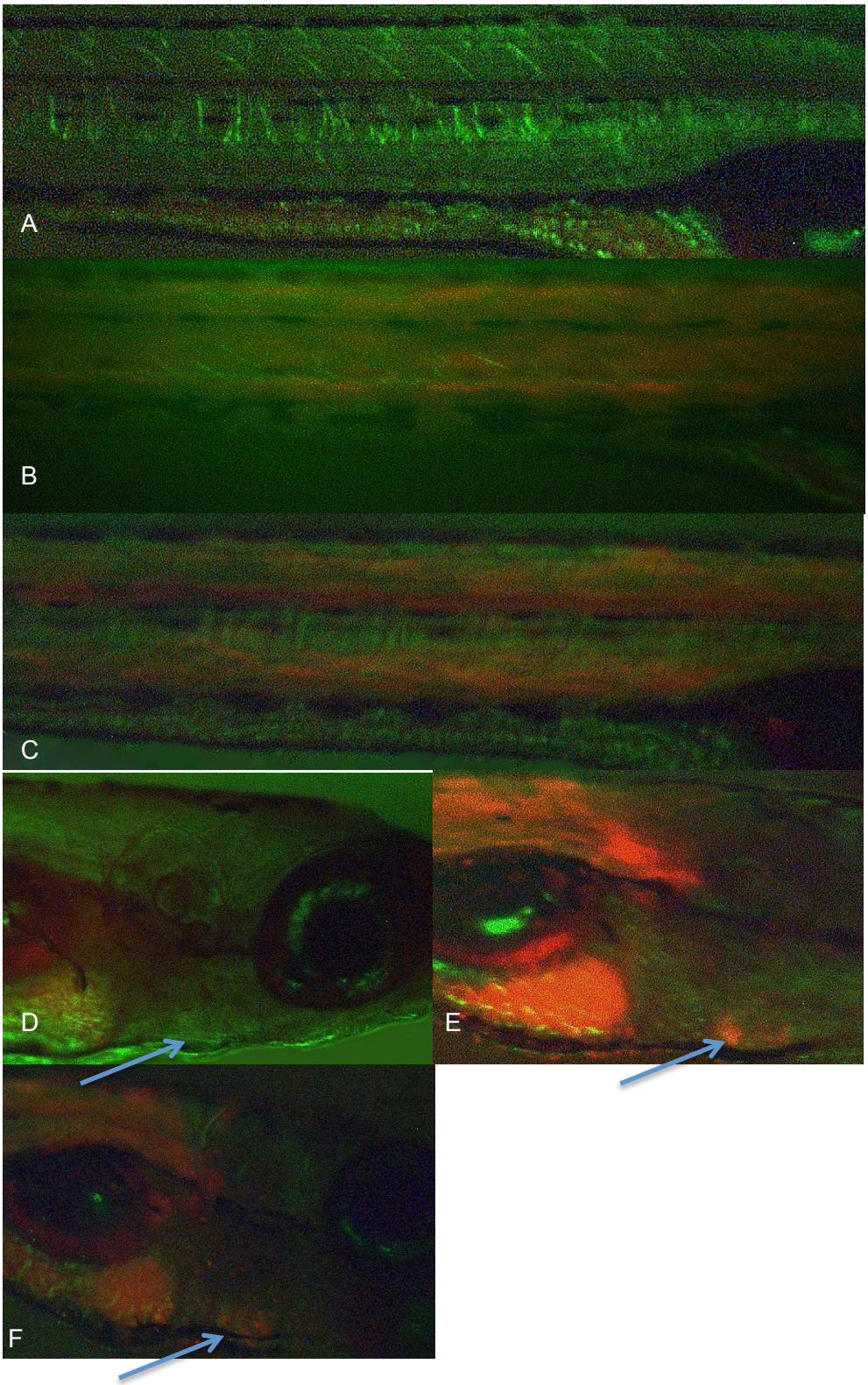

Figure 68 – *ubi*:switch zebrafish treated for 30 minutes at 10 µg/ml tamoxifen citrate, viewed 3 days after exposure, A and D) control, no mcherry fluorescence seen in the body or heart, B and E) Tamoxifen citrate, mcherry fluorescence seen everywhere including in the heart, C and F) NG1A tamoxifen loaded nanogels, mcherry fluorescence seen everywhere including in the heart as indicated by the arrows.

4.4.3.1 Release of tamoxifen from NG1A in fish water

The preliminary data indicated that tamoxifen loaded nanogels were releasing the drug in transgenic zebrafish. However clearly establishing the release trigger required further investigation. To eliminate the water required for healthy fish survival as a potential release trigger and therefore to confirm that a mechanism operating inside the zebrafish was causing the release of the tamoxifen from the nanogel, the nanogel was suspended in fish water solution. Using the same method as studying the tamoxifen release at pH 7.4, ~6 mg nanogel was dissolved in fish water at 2 mg/ml, divided into 500 µl dialysis parcels and placed in 1 l of fish water. At the relevant time point one parcel was removed, 500 µl ACN was added, the solution was vortexed for 30 seconds and 20 µl was injected into the HPLC using exactly the same conditions as before. The area under the peak was analysed according to the calibration curve (figure 58) obtained in section 4.3.2 and the data point plotted. This data is presented in figure 69.

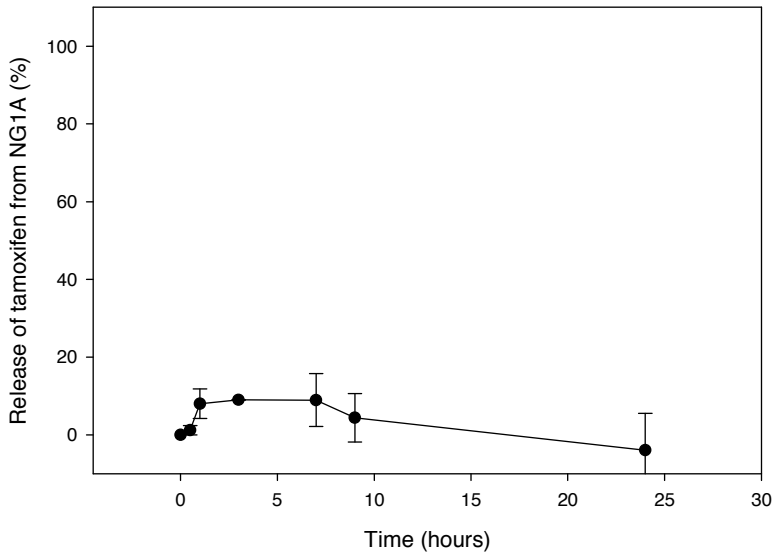

Figure 69 – Tamoxifen released from nanogel in fish water (0.75g sodium biocarbonate, 0.18g marine salts and 0.08g calcium sulphate per 10L water) over 7 hours. Analysis carried out using HPLC, eluent used was 95% acetonitrile to 5% water acidified with 0.5% acetic acid at a flow rate of 1.5 ml/min.

This experiment showed no significant amount of tamoxifen being released in the fish water from the nanogel and therefore it confirmed that the drug was not being released before the nanogel entered the zebrafish. It remained to be investigated whether the (possibly) reduced pH in the stomach of the zebrafish, or enzymes in the zebrafish, caused release of the tamoxifen from the nanogel. In order to prove release and

accumulation of the drug at a target lesion site, the nanogels would need to be administered in a mouse model.

4.4.4 Comparison of the therapeutic effect of tamoxifen loaded nanogels over the free drug

Zebrafish have no breast tissue and therefore analysing real therapeutic effect is not possible. However, tamoxifen is lethal to zebrafish and monitoring the time it takes for a lethal dose of tamoxifen to cause signs of toxicity to the fish is a valid way to establish how quickly the tamoxifen is taken up by the zebrafish. To analyse the potential bioavailability of tamoxifen when loaded onto the nanogels over the free drug *in vivo, ubi*:switch zebrafish were exposed to tamoxifen citrate and NG1A at a lethal concentration of tamoxifen (27 µM). For the test sample, NG1A (24 µg/ml, 2.5% coumarin tag) containing a 43% loading of tamoxifen, dosed at 10 µg/ml (27 µM) tamoxifen was used. In the first control sample, tamoxifen citrate was used as a free drug dosed at 10 µg/ml (27 µM) of tamoxifen. A further control sample was devised, having the nanogel (not loaded with tamoxifen) NG1 (batch 2) (2.5% coumarin tag) at 24 µg/ml.

Twelve 7 dpf zebrafish were placed in each of the 4 solutions, including the controls, in a 6 well plate maintained at 28.5 °C and were monitored regularly under microscope, for conventional signs of toxicity such as lack of movement, lying on their side, lack of response to touch and death. After 1.5 hours the fish exposed to tamoxifen-loaded nanogel, NG1A, were all floating in their solution and were unresponsive to touch, showing severe signs of toxicity. Those in all other solutions including that of tamoxifen citrate were all healthy showing no signs of toxicity. It was not until 16 hours after immersion in the solutions that the fish in tamoxifen citrate showed the same reactions to toxicity as those after just 1.5 hours exposure in the tamoxifen-imprinted NG1A. All zebrafish in fresh fish water and control nanogel with no loaded tamoxifen, NG1 (batch 2), were healthy, swimming and highly responsive to touch at 16 hours after exposure. These results potentially show that the imprinting of tamoxifen on the nanogel both increased the bioavailability (and subsequently, the therapeutic effect) of the drug and significantly decreased the lag time before such therapeutic effect was seen in the zebrafish. However uptake of the free drug and the nanogel bound drug may have been via different routes (and therefore having potentially different therapeutic effects.) Therefore although preliminary experiments seem promising, giving indication that these NPs should be taken on into further in depth mammalian studies, no final

conclusions on the drug carrier and its efficacy over the free drug can be made. If the increased bioavailablilty of the drug when bound to the nanogel is true, along side the pH stimulated release, this drug delivery system would provide more precise targeting of the drug, with reduced doses of drug required (when loaded onto the nanogels) in order for the same therapeutic effect to occur by comparison with larger doses conventionally used when administering the 'free drug'. To pursue these investigations in greater depth, and with a closer analogue to human reaction, analysis of the effect of these loaded nanogels on both MFC-7 breast cancer cells *in vitro* and in a mouse model with breast tumour growth would be required.

4.5 **Final Conclusions and further work**

Acrylamide based nanogels were identified as a potential drug delivery system, with high dilution radical polymerisation giving a practical approach to their formation, in particular allowing control over particle size without the need for surfactants. Evidence showed that trifluoromethyl coumarin acrylamide could be successfully incorporated in the acrylamide nanogels, giving good levels of fluorescence emission without having significant negative effects on particle size or water solubility. Acrylamide based water-soluble nanogels containing a trifluoromethyl coumarin acrylamide with an average particle size of less than 200 nm were successfully synthesised.

These nanogels were found to be not acutely toxic in keratinocyte cells using several different *in vitro* assays. Uptake of the nanogels into the skin cells was also seen visually using confocal microscopy alongside evidence given by flow cytometry. Further analysis of the nanogels *in vivo* in 48 hpf zebrafish embryos showed no acute toxicity when administered orally (up to 1mg/ml). Immersion of 2 hpf zebrafish embryos in nanogel solutions showed acute toxicity at 1 mg/ml, however this was demonstrably due to the high concentration of coumarin which showed acute toxicity to both 2 hpf and 48 hpf zebrafish embryos when the free tag was administered. At concentrations of 0.075-0.025 mg/ml nanogel no acute toxicity was seen on the 2 hpf zebrafish embryos. Nanogel did not appear to pass through the lining of the intestine of the zebrafish when the immersion technique was applied, at either 2 hpf or 48 hpf. Therefore 36hpf zebrafish embryos were injected into the cardinal vein with a 10 mg/ml nanogel solution (54 ng per fish), which saw the nanogel circulating the bloodstream of the zebrafish before dispersing into the cells. 5 hours after injection the nanogels could be seen gathering in the hindbrain of the zebrafish, no nanogel could be seen circulating the

zebrafish 12 hours after injection and all fish were alive showing no evidence of acute toxicity 7 days after injection.

Molecular imprinting was identified as a suitable method for the uploading of the drug onto the nanogels whilst maintaining control over its release. The ionic interaction introduced between tamoxifen and acrylic acid as the functional monomer, evaluated by ^{1}H-NMR studies, allowed release of the drug at reduced pH. The drug was successfully loaded onto the nanogels with relatively high drug loadings of 19-42%, which had excellent encapsulation efficiencies of 92-99.5%. Little drug release from the loaded nanogels was observed at physiological pH (7.4 using PBS buffer) whilst excellent release was seen at pH 5.5 (in acetate buffer), enabling targeted release in tumour cells which have a similarly reduced pH. When the drug-loaded nanogels were administered orally to 6dpf transgenic *ubi*:switch zebrafish, drug release was seen by a colour change in fluorescence (from GFP to mcherry). The mechanism of release is not yet completely understood. However, release due to the fish water required for their survival was ruled out. Zebrafish showed signs of response to toxicity from the tamoxifen 14.5 hours sooner, when immersed in nanogel solutions loaded with tamoxifen than when the free drug was administered, showing a much faster response, and therefore a better therapeutic effect in zebrafish. Although these studies gave promising very preliminary results and showed the drug was released in zebrafish, this gives no real indication to the release of tamoxifen from the nanogels or the system's therapeutic effect in humans. This system would need to be administered intravenously to ensure the nanogels bypassed the stomach (where they would be released immediately due to the low pH), therefore the next stage to asses release of the tamoxifen from the nanogels in a more in depth study would be to inject the nanogels into a mouse model.

4.5.1 Further work

The next step for these nanogels would be to carryout *in vivo* testing on a small mammal such as mice. As transgenic mice have also been developed with loxP-creERT system[228] this could prove useful in detecting tamoxifen release and identifying tissues in which the drug is released. Efficacy can also be further tested in mice as they have breast tissue. It would be possible to grow analogues of breast tumours on mice to see if the nanogels continued to show a significant advantage over the free drug in reducing the tumours and preventing further growth.

These preliminary studies have shown promising results, however there are some areas of the system that could be extended. The solubility of the nanogels with the drug loaded, is considerably less than those without. This issue needs to be addressed, possibly by adding more acetic acid or another highly soluble monomer. Core-shell nanogels have been formed using RAFT (reversible addition fragmentation chain transfer) polymerisation[135], whereby macro chain transfer agents (CTA's) are formed initially and then the macro-CTA's are polymerised together using a cross-linker. This method could be used to load the drug in the centre of the nanogel and putting highly soluble groups on the shell aiding the overall solubility and potentially addressing the quick release of the drug at the same time.

The nanogels should also be evaluated for their release at higher pH such as 6.8 for tumour cell extracellular environment and the pH's consistent with both resistant and non-resistant breast cancer cells. At this higher pH the drug may also be released at a slower rate, giving greater control over its release and giving a more prolonged delivery of the drug. Not only this, the molecular imprinting technique could be exploited to develop a polymer which contains both a recognition site for a specific ligand or antigen which is coupled to an imprinted drug. This could actively target the drug delivery carrier to the target site and trigger the release more accurately. In doing this, it may also further help control and slow down the release of the drug, achieving a more sustained delivery.

The initial intravenous zebrafish toxicity studies showed the nanogels gathering in the hindbrain of the zebrafish, further experiments should be carried out on the zebrafish at 8 dpf as this is the age when the blood brain barrier is formed. Crossing the blood brain barrier is notoriously difficult and therefore, these nanogels could prove to be highly beneficial for delivery of drugs to the brain if they do indeed cross the blood brain barrier.

CHAPTER 5:
Materials and methods

5. Materials and methods

5.1 Materials

5.1.1 Chemicals for the synthesis of dansyl amioethyl acrylamide

Ethylene diamine (99%), Dansyl chloride (99%), triethylamine (99%) and acryloyl chloride (Fluka, 96%) were all purchased from Aldrich Chemical Co. (Gillingham, Dorset, UK). Dry Solvents dichloromethane (CH2Cl2) and tetrahydrofuran (THF) were supplied from MBRAUN MB SPS-800 solvent purification system. Reactions were carried out under an inert atmosphere of nitrogen, at the temperature stated. All glassware was oven dried and flamed prior to experimental use. Flash column chromatography was performed on reaction mixtures using Fluka silica gel 60 (220-240 mesh) (Brockmann 2-3). Analytical thin layer chromatography (TLC) was carried out using pre-coated aluminium or glass backed plates with Merck Kieselgel 60 F254 and the plates were visualized under an ultraviolet lamp at λ = 254/365 nm.

5.1.2 Chemicals and materials for nanogel synthesis and drug incorporated

Ethylene bisacrylamide (99%), methylene bisacrylamide (99%), acrylamide (99%), and Acrylic acid (99%) were all purchased from Aldrich Chemical Co. (Gillingham, Dorset, UK). 2,2-azobisisobutyronitrile (AIBN, 98%) was purchased from Acros Fisher Scientific UK (Loughborough, Leicestershire) and recrystallized from methanol before use. Tamoxifen citrate (98%) was purchased from Cambridge Bioscience (Cambridge, UK). Dialysis membrane for nanogel isolation was purchased from Medicell International Ltd, 22 mm diameter and molecular cut off 3500 Daltons. Biotech CE membrane dialysis tubing used for drug release studies was purchased from VWR (Leicester, UK) with a diameter of 16 mm and molecular cut off of 550-1000 Daltons.

5.1.3 Chemicals for interaction studies via 1H-NMR (400MHz)

All deuterated solvents for NMR studies were purchased from Cambridge Isotope Laboratories Inc. All other solvents used for polymerisation and analytical experiments were of analytical grade.

5.1.4 Chemicals and materials for the kinetic assays

Anotop™ 10 Plus 0,02 µm syringe filter with a 10 mm diameter and water (HPLC grade, BDH Prolabo) were purchased from VWR. Acetonitrile (HPLC grade) was purchased from Acros Fischer Scientific UK (Loughborough, Leicestershire, UK).

5.1.5 Chemicals for the *in vitro* studies

The DMEM/F12, Penicillin/streptomycin solution, FBS and Trypsin/EDTA cell culture were purchased from Acros Fisher Scientific UK (Loughborough, Leicestershire). Phosphate buffered saline solution, thiazolyl Blue Tertrazolium Bromide (98%), dimethyl sulfoxide (99.5%), Lactic Dehydrogenase in vitro toxicity assay kit and CellBLIND 96 well plates were all purchased from Aldrich Chemical Co. (Gillingham, Dorset, UK). Trypan Blue Stain (0.4%) and Countless Cell counting Chamber Slides were purchased from Invitrogen (paisley, UK).

5.1.6 Chemicals for the *in vivo* studies

Sodium bicarbonate and calcium sulphate were purchased from VWR (Leicester, UK). Marine salts were purchased from MBK installations limited. PTU, Tricaine methanesulfonate (MS-222) and methyl cellulose were all purchased from Aldrich Chemical Co. (Gillingham, Dorset, UK).

5.1.7 Micros-pipettes/ Hamilton syringes:

Eppendorf micropipettes with volumes ranging from 2-20 µl, 10-200 µl, 100-1000 µl, 1-5 ml and 1-10 ml were used for forming nanogel solutions for DLS analysis and for fish experiments. The accuracy of the volume measured was verified by weight and found to be ±1%. Hamilton syringes of 1-10 µl, 5-50 µl, 10-100 µl, 20-250 µl and 50-500 µl were used for forming solutions for UV-VIS and Fluorescent spectroscopy experiments and used for measuring volumes for drug upload and release studies.

5.1.8 Instruments

5.1.8.1 NMR Spectroscopy:

^{1}H and ^{13}C NMR spectra were recorded on a Bruker AV400 NMR spectrometer. Chemical shifts in NMR spectra are reported in δ (ppm) relative to residual solvent signals: $CDCl_3$ δ_H = 7.26 ppm; δ_c = 77.23 ppm or d_6-DMSO δ_H = 2.50; δ_c = 39.51. H1NMR peak multiplicity were reported as follows = singlet, d = doublet, t = triplet, q = quartet, m = multiplet). Coupling constants (*J*) were measured in hertz. NMR data are presented as follows: chemical shift δ (in parts per million (ppm)) integration, multiplicity, coupling constant *J* (in Hz) and assignment.

5.1.8.2 UV-VIS Spectroscopy:

UV-Vis samples were analysed using Varian Cary 300 BIO UV_Vis Spectrophotometer, equipped with an internal thermostat.

5.1.8.3 Fluorescent Spectroscopy:

All fluorescence data was accomplished on a Flouromax-3.

5.1.8.4 Zetasizer (Dynamic light scattering):

DLS measurements were performed in Queen Mary's School of Materials and Engineering on a Malvern Zetersizer Nano ZS.

5.1.8.5 Freeze-dryer:

Two freeze-dryers were used, Edwards, super Modulyo and Labcoco FreeZone 6 Litre Benchtop Freeze Dry System.

5.1.8.6 High performance liquid chromatography (HPLC):

All data was recorded on a manual injector Aglient Technologies 1220 Infinity LC fitted with a Hichrom 5 C18 250 x 4.6mm column.

5.1.8.7 Confocal Microscope:

Leica SP5 confocal laser scanning microscope

5.2 Methods

5.2.1 Synthesis of dansyl amino ethyl amine

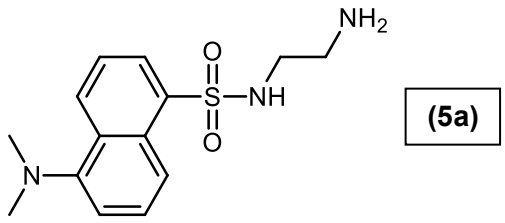

(5a)

11 ml (0.16 mol) of ethylene diamine was dissolved in 30 ml of dry THF and stirred. 1.1g (3.7 mmols) of Dansyl chloride was dissolved in approximately 15 ml of dry dichloromethane and added to the mixture drop wise over 1 hour at 0ºC (ice bath). The reaction mixture was left stirring at room temperature. TLC monitoring (DCM/Acetone: 8/2) showed the reaction to be complete after 2 hours. 10 ml of saturated NaCl solution was added to the mixture and the majority of the THF was evaporated at reduced pressure. The mixture was neutralised with HCl, before being extracted with DCM (3 x 10ml) The combined organic layers were dried of MgSO4, filtered and evaporated under reduced pressure which gave 0.97g of product (solid, pale yellow) (JR_S_07) with a yield of 89%.

$C_{14}H_{19}N_3O_2S$

^{1}H-NMR ($CDCl_3$, 400MHz) δ(ppm), *J*(Hz):**8.47** (d, *J*=8Hz, 1H, Ar*H*), **8.23** (d, *J*=12Hz, 1H, Ar*H*), **8.19** (d, *J*=8Hz, 1H, Ar*H*), **7.50** (t, *J*=16, 8Hz, 2H, Ar*H*), **7.45** (t, *J*=16, 8Hz, 1H, Ar*H*), **2.85** (t, *J*=12, 8Hz 2H, -CH_2CH_2NH_2), **2.82** (s, 6H N(CH_3)$_2$, **2.62** (t, 2H *J*=8, 12Hz, 2H, -CH_2CH_2NH_2).

^{13}C-NMR ($CDCL_3$, 100Hz) δ (ppm) **156.53, 140.59, 134.70, 134.53, 134.35, 133.58, 132.74, 127.97, 123.99, 119.90** (Napthalenyl), **50.85** (-NH*C*H_2CH_2NHS-), **50.14** (-N(*C*H_3)$_2$), **46.22** (-NHCH_2*C*H_2NHS-).

5.2.2 Synthesis of dansyl amino ethyl acrylamide

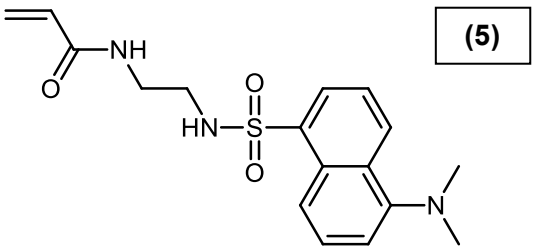

(5)

0.4g (1.37 mmols) of Dansyl amino ethyl amine (**2**) and 0.21 ml (1.50 mmols, 1.1 eq.) of triethylamine were dissolved in 40 ml of dry DCM and stirred. 0.12 ml (1.50 mmols, 1.1 eq.) of acryloyl chloride was dissolved in approximately 10 ml of dry dichloromethane and added to the mixture drop wise over 1 hour at 0ºC (ice bath). The reaction mixture was left stirring at room temperature overnight, after which TLC monitoring (DCM/Acetone: 8/2) showed the reaction to be complete. The DCM was evaporated at reduced pressure and the product was purified by flash chromatography (EtOAc/hex: 1/1) which gave 0.3g of product (solid, pale green/yellow) (**3**) with a yield of 65%.

$C_{17}H_{21}N_3O_3S$

^{1}H-NMR ($CDCl_3$, 400MHz) δ(ppm), *J*(Hz):**8.47** (d, J=12Hz, 1H, Ar*H*), **8.28** (t, *J*=16, 8.0 Hz, 2H, Ar*H*), **7.61** (t, *J*=16, 8Hz, 1H, Ar*H*), **7.56** (t, J=12, 4Hz, 1H, ArH), **7.23** (d, *J*=4Hz, 1H, Ar*H*), **6.22** (d, *J*=16Hz, 1H, -COC*H*=CH_2), **5.95** (d, *J*=12Hz, 1H, -COCH=CH_2cis), **5.91** (d, *J*=12Hz, 1H, CON*H*), **5.62** (d, *J*=8Hz, 1H, -COCH=CH_2trans), **5.36** (s, *J*=12Hz, 1H, SO_2N*H*), **3.41** (dd, *J*=8, 12Hz, 2H, -CH_2CH_2NHCO) **3.11** (dd, *J*=8, 12Hz, 2H, -CH_2CH_2NHCO) and N(CH_3)$_2$, **2.97** (s, 6H, N(CH_3)$_2$).

^{13}C-NMR ($CDCL_3$, 100Hz) δ (ppm) **166.22** (-*C*OCH=CH_2), **152.20, 134.21, 130.78, 130.03, 130.00, 129.83, 129.49, 128.68, 126.84, 123.21, 118.50, 115.33** (Napthalenyl, - CO*C*H=*C*H_2), **45.41** (-NH*C*H_2CH_2NHS-), **43.19** (-N(*C*H_3)$_2$), **39.38** (-NHCH_2*C*H_2NHS-).

^{13}C-NMR ($CDCL_3$,100Hz) δ(ppm): 166.26, 166.06 ((-*C*OCH=CH_2)$_2$), 152.28, 134.11, 131.96, 131.80, 130.75, 130.39, 130.02, 129.47, 129.04, 128.57, 126.53, 123.03, 117.80, 115.61 (Napthalenyl, (-CO*C*H=*C*H_2)$_2$), 45.61(-NH*C*H_2CH_2NHS-), 45.38 (-N(*C*H_3)$_2$), 39.42 (-NHCH_2*C*H_2NHS-).

5.2.3 General procedure of the nanogel synthesis

The standard protocol of high dilution radical polymerization was used to prepare Tamoxifen imprinted (MIP) and non-imprinted (NIP) nanogels. Both nanogels were systhesised using the same conditions. However, polymerization of imprinted nanogels took place in the presence of the drug, and the non-imprinted without it. The concentration of monomers (C_M) was fixed at 0.5% and the percentage of initiatior, AIBN, at 2% of the number of moles of double bonds in the polymerization solution. The percentage of cross-linker was set at 20 % and acrylic acid at 10 % and TCA at 2.5 or 5% of the total monomers in the prepolymerisation mixture, with the shortfall made up with acrylamide. Tamoxifen (53mg, $1.4x10^{-4}$ mol, 1 eq.) acryllic acid (10 mg, $1.4x10^{-4}$ mol, 1 eq.), TCA (20 mg, $7.1x10^{-5}$ mol), acrylamide (176 mg, $2.5x10^{-3}$ mol), MBA (98mg, $6.4x10^{-4}$ mol) and AIBN (13 mg, $7.9x10^{-5}$ mol) were dissolved in dry DMSO (60 g, 54 ml) in a 100 ml Wheaton glass serum bottle. The solution was flushed with nitrogen and heated at 70°C for 2 days. (where eq. = equivalent).

5.2.3.1 nanogel recovery

After polymerisation the nanogel solution was dialysed against non-distilled water for two days, with 2 water exchanges per day unless complete template removal was desired at which point the nanogel was dialysed against non-distilled water acidified to pH 3 with HCl, the last water exchange was with non-distilled water at normal pH). The dialysis membrane used had a pore size of 3500 Daltons. On completion of dialysis the solutions were frozen in liquid nitrogen and freeze-dried. Dry, off white to pale yellow, very lightweight powders were obtained.

5.2.4 Nanogel characterization general procedures

5.2.4.1 Zetasizer

All fluorescein tagged Nanogels were prepared as 0.1 mg/ml solutions in 1% DMSO 99% water, all the dansyl tagged nanogels were prepared as 0.1 mg/ml solutions in

100 % DMSO due to the solubility issue. All coumarin tagged nanogels were prepared as 0.1 mg/ml solutions in 100 % water where possible, those unsoluble in water were measured in 1% DMSO 99% water. Many samples were measured both with filtration (450 nm pore size PTFE filter) and without, however no difference in size was seen. Size distribution of the light intensity was calculated using the refractive index of the solvents (DMSO n_D^{25} and water n_D^{25} 1.33). Volume and number distributions were extrapolated from the intensity by adding the refractive index of polymethacrylate selected as a reference from the literature (n_D^{25} 1.4914 and dn/dλ 0.0575).

5.2.4.2 TEM

A 1 mg/ml nanogel solution was prepared to which a 4% OsO_4 solution was added at a ratio of 4:1 respectively. The combined solution was allowed to rest for 1 hour before being dialysed overnight against distilled water. to prevent interference during imaging by the presence of excess oxidant. The final solution was diluted 1 in 10 and a drop deposited on the 300 mesh carbon coated copper grid and left to dry. Images were obtained using a JEOL 1200EX (120kV) with the beam at 90°.

5.2.4.3 Fluorometer

For fluorescence analysis of the nanogels, the nanogels were dissolved in different solvents. The fluorescein containing nanogels were dissolved in 10 % ethanol and 90 % distilled water at 0.01 mg/ml. The dansyl containing nanogels were dissolved in 100 % ethanol at 0.01 mg/ml. The coumarin containing nanogel were all formed with 100 % DMSO at 1 mg/ml and 0.1 mg/ml. 2 ml of each solution was placed in a 4 sided quartz cuvette and measured for fluorescence intensity using their excitation wavelengths of 307 nm for dansyl, 490 nm for fluorescein and 345 nm for the coumarin tag. The emission of the nanogels were read at 470, 516 and 460 nm respectively.

5.2.5 Fluorescent tag incorporation studies

5.2.5.1 Calibration curves

Incorporation of fluorescent tags into the nanogels were evaluated by mean of calibration curves obtained via UV-Vis spectroscopy. Three stock solutions of dansylaminoethylamine, Fluorescein-*0*-methacrylate and trifluoromethyl coumarin amine were prepared independently by weight in DMSO. The three stock solutions were then cross-diluted to create 9 solutions of varying concentrations with a UV-Vis absorption range between 0 and 1. The absorption maximum of 1 ml (maximum

volume inside the spectrophotometric cuvette) of each solution was measured by UV-VIS spectrometry at 339 nm for dansylaminoethylamine solutions, 490 nm Fluorescein-*0*-methacrylate solutions and 386 nm for trifluoromethyl coumarin solutions. The absorptions were plotted against their relevant concentrations and where possible the data was fitted to a linear regression passing through the origin using sigma plot 8.0. The determination of the molar absorption coefficient ε_{max} at pH 14 was determined using the Beer-Lambert Law, defined by the following equation:

$A = \imath\, \varepsilon\, c$ **Equation 1**

Where A is the absorption maximum, ε is the molar absorption coefficient, l is the length of the cuvette (1 cm) and c is the concentration inside the cuvette. The molar absorption coefficient for each fluorophore was determined via the slope of the linear curve obtained.

To establish the incorporation of fluorescent tag into the nanogel, nanogels were weighed accurately at 0.35 mg and dissolved in 2 mls DMSO. 3 dilutions of the stock solution were formed and the maximum absorption were read at the same wavelength as at their respective fluophore's calibration curve (339, 490 or 386 nm). The extention coefficient from the reference curve of the relevant fluorophore was compared to the concentration of nanogel prepared in mg/ml, to establish the mole/mg of tag in the nanogel (equations 15 and 16). The theoretical value of moles of tag per mg of nanogel, if 100% incorporation had been achieved, was also calculated taking into consideration both the chemical and percentage yield (equation 17). The final incorporation of tag into the nanogel was achieved by comparing the two results (equation 18). At least 3 different samples of each nanogel were analysed and the average incorporation was reported.

$$\frac{n_{FM}}{ml} of\ nanogel\ solution = \frac{A}{\varepsilon l} x 10^{-3} \qquad \textbf{Equation 14}$$

$$c_{FM(exp)} = \frac{n_{FM/ml}}{m_{FM/ml}} \qquad \textbf{Equation 15}$$

$$c_{FM(theo)} = \frac{n_{FM} \times \%\ yield}{m_{nangel}}$$ **Equation 16**

$$\%\ incorporation = \frac{n_{FM(exp)}}{n_{FM(theo)}} \times 100$$ **Equation 17**

where n_{FM} = no. of moles of functional monomer, m_{FM} = mass of functional monomer, $C_{FM(exp)}$ = concentration of functional monomer determined experiementally, $C_{FM(theo)}$ = concentration of functional monomer determined theoretically, $m_{nanogel}$ = final mass of nanogel obtained and % yield = final percentage yield obtained of the nanogel.

5.2.6 Tamoxifen acetic acid interaction studies via ^{1}H-NMR

Proton, ^{1}H-NMR, spectra were record at 400MHz on a Bruker AV400 NMR spectrometer. A stock solution of Tamoxifen was prepared in d6-DMSO at a concentration of 7.1×10^{-2} mM. Increasing quantities of acetic acid were added to the tamoxifen solution from 0 to 128 equivalents recording the spectra after each addition. The variation in chemical shift ΔδHta of the protons of the two methyl groups bound to the nitrogen in tamoxifen was calculated and plotted against acetic acid concentration. The data obtained was fitted into a hyperbola curve using sigma plot 8.0 software and the binding constant was determined using the ligand binding equation as follows:

$$\Delta\delta_{Hta} = \frac{A*x}{1+B*x}$$ **Equation 18**

Where $\Delta\delta_{Hta}$ is the variation of chemical shift of the methyl hydrogens adjacent to the nitrogen on tamoxifen, x is the concentration of acetic acid, B is the association constant of the complex formation and A is a constant.

5.2.7 Drug upload and release experiments

5.2.7.1 Tamoxifen calibration curve achieved via HPLC

Concentrations of tamoxifen uploaded onto the nanogels was evaluated by means of calibration curve established using HPLC. Three stock solutions of tamoxifen at different concentrations were prepared independently by weight in acetonitrile. The

solutions were cross diluted to generate 9 solutions with different concentrations ranging from 0.1 to 1 mM. 20 µl of each solution was injected into the HPLC using an eluent of 95:5 acetonitrile to water acidified at 0.5% (v/v) with acetic acid at a flow rate of 1.5 ml/min (creating a pressure of approximately 86 bar). Tamoxifen eluted at approximately 7 minutes and the area under the curve was plotted against concentration to form a reference curve. Thus obtaining a value for b in the equation:

$$y=bx+c \qquad \textbf{Equation 19}$$

Where y= area under the curve, x = concentration, b = slope of the curve and due to the curve passing through the origin c=0.

5.2.7.2 Determination of tamoxifen loading

The nanogel was dissolved in acetonitrile to release the drug from the drug delivery system at a concentration of 1 mg/ml of nanogel. The solution was stirred rapidly for 5 minutes before being filtered through a 20 nm PTFE filter to remove the nanogel. 20 µl of the solution was injected into the HPLC using the same eluent and flow rate as used to obtained the calibration curve. This was carried out in triplicate with three independent samples. The area under the curve gave a value for Y in equation 19 and b could be substituted from the slope of the calibration curve hence giving the concentration of tamoxifen present in the sample.

5.2.7.3 Tamoxifen release studies

5.2.7.3.1 Establishing maximum drug release at pH 3

Drug loaded nanogels were dialysed for 2 days in water acidified to pH 3 with HCL with water exchanged 4 times within that period. The final water exchange was with distilled water at neutral pH. The nanogels were frozen in liquid nitrogen and freeze-dried. The newly isolated nanogels were dissolved in acetonitrile at 1mg/ml and stirred rapidly for 5 minutes before being filtered through a 20 nm PTFE filter and 20 µl was injected into the HPLC using the same eluent and flow rate as before. The area under the curve was once again compared to the slope of the calibration curve to give the concentration of tamoxifen that remained in the nanogels.

5.2.7.3.2 Establishing drug release at pH 5.5 in acetate buffer

643 ml sodium acetate trihydrate solution (1.36 g in 1 L, 0.01 M) was added to 357 ml acetic acid (0.01 M), diluted 1 in 10 and brought to pH 5.5 with NaOH (0.01 M) to

create a 1 mM acetate buffer solution. 1 L of the 1 mM buffer solution was heated to 37 °C. Approximately accurately 6 mg nanogel was dissolved in the buffer at a concentration of 2 mg/ml, the mixture was stirred for 30 seconds. 100 µl of the mixture was immediately removed and 100 µl of acetonitrile was added, vortexed for 30 seconds and filtered through a 20 nm PTFE filter. 20 µl was injected into the HPLC using the same eluent and flow rate as the calibration curve achieved. The remaining nanogel was placed on dialysis (tubing was 500-1000 Daltons cut off) in the heated buffer solution with samples being taken and treated in the same way as the sample taken immediately (time 0 hr) at time 20, 30 and 45 minutes and 1, 2, 3, 5 and 7 hours. Dialysis buffer was exchanged for fresh heated buffer at 4 hours. The dialysis bag was inverted several times before each sample was taken to ensure a representative sample was analysed. This was carried out in triplicate with three independent samples of each nanogel.

5.2.7.3.3 Establishing drug release at pH 7.4 in phosphate buffer

Potassium chloride (0.2 g) disodium hydrogen phosphate (1.44 g) and potassium dihydrogen phosphate (0.24 g) were dissolved in 1 L distilled water to form a 10 mM solution. The buffer was diluted 1 in 10 and brought to pH 7.4 with NaOH (0.01 M) to create a 1mM phosphate buffer solution. 1 L of the 1 mM buffer solution was heated to and maintained at 37°C. Approximately accurately 6 mg nanogel was dissolved in the buffer at a concentration of 2 mg/ml, the mixture was stirred for 30 seconds before being divided into 500 µl volumes and each being added to a separate length of dialysis tubing (500-1000 Daltons), all ‘parcels’ were added to the same heated buffer solution (except sample for time 0). At relevant time points, one ‘parcel’ of 500 µl of the mixture was removed and 500 µl of acetonitrile was added, vortexed for 30 seconds and filtered through a 20 nm PTFE filter. 20 µl was injected into the HPLC using the same eluent and flow rate as the calibration curve achieved. Samples were removed at time 0, 20, 30 and 45 minutes and 1, 2, 3, 5 and 7 hours. Dialysis buffer was exchanged for fresh heated buffer at 4 hours. This was carried out in triplicate with three independent samples of each nanogel.

5.2.7.3.4 Establishing drug release in fish water

Fish water, comprised of sodium bicarbonate (75 mg/L), marine salts (18 mg/L) and calcium sulphate (8.4 mg/L) in reverse osmosis (R/O) purified water, was formed and 1

L was heated to 37 °C. Approximately accurately 6 mg nanogel was dissolved in the fish water at a concentration of 2 mg/ml, the mixture was stirred for 30 seconds before being divided into 500 µl volumes and each being added to a separate length of dialysis tubing (500-1000 Daltons). All 'parcels' were added to the same heated buffer solution (except sample for time 0). At relevant time points one 'parcel' of 500 µl of the mixture was removed and 500 µl of acetonitrile was added, vortexed for 30 seconds and filtered through a 20 nm PTFE filter.20 µl was injected into the HPLC using the same eluent and flow rate as the calibration curve achieved. Samples were removed at time 0, 20, 30 and 45 minutes and 1, 2, 3, 5 and 7 hours.

5.2.8 In vitro assays

All the experiments were performed in triplicates.

5.2.8.1 Alamer blue assay

The immortalized human keratinocyte cell line N/Tert-1 was used as model to test the cytotoxity and the cellular uptake of JR P240 nanogel. To test the cell viability the sample P240 cells was dispersed in medium (DMEM-F12 modified) at 5, 10, 20, 40, 50 µg/ml and used to treat a minimum of $2x10^5$ cells/well previously seeded in 12-well plates. After 24, 48 and 96 hours at 37 °C AlamarBlue Assay was performed. The reagent, an oxidative-reductive indicator that fluoresces or changes colour as a result of cells growth, was added to treated and untreated cells and incubated for a minimum of 2 hours at a concentration as suggested by the vendor. The change from oxidized (non-fluorescent, blue) form to reduced (fluorescent, red) form of the indicator was monitored at 530-560 nm excitation wavelength and 590 nm emission wavelength and the results were reported as the percentages of viable cells respect to the negative control.

5.2.8.2 MTT assay

To test cell viability each sample (NG1(batch1) and NG2(batch1)) was dispersed in medium at 10, 25, 50, 100, 200 µg/ml and used to treat a minimum of 3000 cells/well previously seeded in 96-well plates. After 24, 48 and 72 hours MTT test was performed using 3-(4,5-dimethylthiazol-2-yl)-2,5-diphenyltetrazolium bromide to treat the cells for 2 hours at room temperature. The reaction was stopped using Dimethyl Sulfoxide and each assay plate was read at Thermo Scientific Varioskan Flash Multimode Reader at 570 nm. Tested samples were compared to negative controls and reported as a percentage of the negative control.

5.2.8.3 LDH assay

Membrane damage was measured at 10, 25, 50, 100, 200 µg/ml of nanogel (NG1(batch1) and NG2(batch1)) dispersed in medium which was applied to a minimum of 3000 cells/well previously seeded in 96-well plates. After 4, 8, 24, 48 and 72 hours supernatant aliquots from previously treated 96-well plates were transferred to new plates, centrifuged and used to perform Lactate Dehydogenase Assay. The samples were incubated at room temperature for 20 minutes, then emission was recorded Thermo Scientific Varioskan Flask Multimode Reader at 690 nm (background reading) and 490 nm (sample reading). Tested samples were compared to emission of negative control and reported as a percentage of emission of negative control.

5.2.8.4 Cellular uptake

The cellular uptake was observed by confocal microscopy of the fluorescent nanogels and FACS. At a concentration of 200 ug/mL, the nanogels were detected in the cytoplasm of the N/Tert keratinocytes after 2 hours of incubation in DMEM/F12 media (without phenol red present). The cells were washed with PBS before being fixed for FACS analysis, for which the Pacific blue channel (corresponding to 405 nm excitation and 455 nm emission) was used.

For confocal microscopy after 2 hours incubation and washing, the cells were seeded on cover slips in 12 well plates for confocal imaging. When the cells were 60-70% confluent, fluorescent nanogels (NG1(batch2) and NG2(batch2)) were added to the media and incubated for 2 hours. Cells were then washed with PBS and fixed with 4% paraformaldehyde and confocal microscopy imaging (Zeiss 510) was performed at 405 nm and emission read at 450 nm.

5.2.9 In Vivo experiements

All fish were maintained at 28.5 °C in 'fish water' which is a salt water solution comprised of sodium bicarbonate, marine salts and calcium sulphate in a ratio of 7.5:1.8:0.84 g in 100 L of reverse osmosis (R/O) purified water. All test solutions were formed using fish water. Adult fish were maintained on a 14 hr / 10 hr light dark cycle following standard husbandry protocols. Embryos/larvae used for *in vivo* nanogel analysis were maintained at 28.5 °C in the dark. Casper Fish were bred in-house and were generated from established casper breeders in our facility. *Ubi*:switch transgenic

zebrafish were acquired from University College London fish facility and quarantined for one month prior to use. For breeding fish were housed in pairs (1 L tanks) overnight with a clear divider separating tank-mates to facilitate identification. Embryos were collected within 2 hpf and placed in separate petri-dishes (n*40/dish). All groups were age and sex matched before testing. During this time, fish from each treatment group were housed in groups of ~10 per tank (5 L). All procedures were carried out under the Animals (Scientific Procedures) Act, 1986, and under local ethical guidelines (Queen Mary, University of London).

5.2.9.1 Immersion administration

For toxicity assessment Casper embryos were collected and sorted at 2 hpf.

5.2.9.1.1 Experiements carried out at 2 hpf

2 hpf casper embryos were placed in 2ml of test solution in a 24 well plate (one embryo per well). The embryos were monitored for signs of nanogel up take (via fluorescent microscope) and for signs of acute toxicity (such as oedema or curvature of the notochord) or death every 24 hours. The embryos were exposed to the required solutions for 24 hours (unless otherwise stated) before being returned to fresh fish water.

5.2.9.1.2 Experiments carried out at 48hpf

48 hpf casper embryos were placed in 10ml of test solution in a 6 well plate (6 embryos per well). The embryos were monitored for signs of nanogel up take (via fluorescent microscope) and for signs of acute toxicity (such as oedema or curvature of the notochord) or death every 24 hours. The embryos were exposed to the required solutions for 7 days (unless otherwise stated) before being returned to fresh fish water. When sufficient up take of the nanogels was seen, the fish were analysed live, whilst anesthetized using MS222, via confocal microscopy.

5.2.9.1.3 Fluorescence quenching studies in 36 hpf Casper embryos

100µl of 10mg/ml solutions of nanogels (NG1(batch2) and NG2(batch2)) were added to 20 homogenized 36hpf Casper zebrafish embryos in a 96 well plate, with 5 repetitions for each nanogel. The fluorescence was measured on the plate reader. After 24 hours maintained at 28.5°C the fluorescence was measured again.

5.2.9.2 Intravenous administration

Casper embryos were maintained in a petri dish until 36 hpf. The embryos were then anesthetised with MS222 and dechorionated. The embryos were immobilized on a microscope slide using a 5% methyl cellulose and injected with a 10mg/ml solution of JRP240 into the cardinal vein blood pool just above the heart using the fluorescent microscope fitted with the micro injector. The fish were monitored for the first 30 minutes using the fluorescent microscope. The fish were monitored for nanogel distribution under the confocal microscope at 1, 2.5, 4, 5, 6, 12, 18, 24 hours after injection and every 24 hours after that until the experiment was terminated at 7 days after injection. During observation under the confocal microscope, fish were anesthetised with MS222 and immobilized using methyl cellulose where necessary.

Injection concentration was calculated by measuring droplet size produced by the glass needle inserted in the micro-injector using a grid embedded in the eyepiece of the microscope. Under the same magnification a ruler was placed under the microscope to measure the size of the grids, which can then be used to calculate the radius of the droplet. The volume of the droplet could be determined using volume of a sphere:

$$\frac{4}{3}\pi r^3 \qquad \textbf{Equation 20}$$

where r = the radius of the droplet.

The mass of nanogel can then be calculated using the volume and concentration of the solution injected.

5.2.9.3 Drug release studies in transgenic zebrafish

A heterogeneous loxP (-Tg(3.5ubb:loxP-EGFP-loxP-mcherry) adult zebrafish was crossed with a heterogenous creERT2 (-Tg(3.5ubb:creERT2,my17:EGFP) zebrafish to produce *ubi*:switch embryos in a 1 L tank with a clear divider, removed immediately prior to the start of the light cycle. Embryos were collected, sorted and maintained at 28 °C. At 24 hpf fish who did not show all over GFP fluorescence were removed from the test sample. 6 dpf *ubi*:switch embryos were placed in 10ml of test solution in a 6 well plate (12 embryos per well). The three solutions used for analysis were nanogel NG1A (34 µg/ml, 10 µg/ml tamoxifen, 24 µg/ml nanogel), NG1 (24 µg/ml) and tamoxifen

citrate (15 µg/ml, 10 µg/ml tamoxifen). Where 29% of NG1A (by weight) was tamoxifen, 71% was nanogel. These were all formed in fish water and diluted with fish water to gain lower concentrations where necessary. The embryos were monitored for signs of tamoxifen exposure (via fluorescent microscope) and for signs of acute toxicity (such as oedema or curvature of the notochord) or death every 24 hours. The embryos were exposed to the required solutions for 30 minutes, 2 hours or 12 hours according to the strength of solution they were exposed to, before being returned to fresh fish water.

5.2.10 Isolation of tamoxifen from it's citrate salt

Tamoxifen citrate (2 g) was 'dissolved' in a sodium carbonate solution (160 ml, 10 mM) and extracted with chloroform (3x120 ml). The extracts were dried over MgSO4 and evaporated to dryness.

6. Bibliography

1. T. Theis, D. Parr, P. Binks, J. Ying, K. E. Drexler, E. Schepers, K. Mullis, C. Bai, J. J. Boland, R. Langer, P. Dobson, C. N. R. Rao and M. Ferrari, *Nature Nanotechnology*, 2006, **1**, 8-10.
2. I. Freestone, N. Meeks, M. Sax and C. Higget, *Gold Bulletin*, 2007, **40**, 270-277.
3. M. Faraday, *Philosophical Transactions Royal Society London*, 1857.
4. Nobelprize.org, The Nobel Prize in Physics 1965, 2013, vol. 2013.
5. E. Gazit, *Plenty of Room for Biology at the Bottom: An Introduction to Bionanotechnology*, Imperial College Press, 57 Shelton Street, Covent Garden, London, WC2H 9HE, 2007.
6. P. Samori, *Scanning Probe Microscopies Beyond Imaging, Manipulation of Molecules and Nanostructures*, Wiley-VCH, Weinheim, 2006.
7. IBM, IBM Research, 2013, vol. 2013.
8. S. Sepeur, *Nanotechnology: Technical Basics and Applications*, Vincentz Network GmbH & Co Hanover, Germany, 2008.
9. N. R. C. o. t. N. Academies, *Review of Federal Strategy for Nanotechnology-Related Environmental, Health and Saftey Research*, The National Academies Press, Washington, 2009.
10. A. Gogos, K. Knauer and T. D. Bucheli, *Journal of Agricultural and Food Chemistry*, 2012, **60**, 9781-9792.
11. L. R. Khot, S. Sankaran, J. M. Maja, R. Ehsani and E. W. Schuster, *Crop Protection*, 2012, **35**, 64-70.
12. V. Mlinar, *Nanotechnology*, 2013, **24**, 1-11.
13. W. van Sark, J. de Wild, J. K. Rath, A. Meijerink and R. E. I. Schropp, *Nanoscale Research Letters*, 2013, **8**, 81-91.
14. J. Liu, J. G. Zhang, Z. G. Yang, J. P. Lemmon, C. Imhoff, G. L. Graff, L. Y. Li, J. Z. Hu, C. M. Wang, J. Xiao, G. Xia, V. V. Viswanathan, S. Baskaran, V. Sprenkle, X. L. Li, Y. Y. Shao and B. Schwenzer, *Adv. Funct. Mater.*, 2013, **23**, 929-946.
15. L. B. Kish, *Physics Letters A*, 2002, **305**, 144-149.
16. L. Garber, *Computer*, 2013, **46**, 26-26.
17. Singularity, Stamford University, USA, 05-07-2013 http://cs.stanford.edu/people/eroberts/cs181/projects/2010-11/TechnologicalSingularity/pageviewa478.html?file=forfeasibility.html
18. O. f. L. Sciences, ed. I. a. S. Department for Buisness, Crown copyright, 2012.
19. T. Joseph and R. Moore, the Institute of Nanotechnology, 2008, p. 50.
20. T. Joseph and R. Moore, *Drug Delivery using Nanotechnology, Technologies, Markets and Competitive Environment*, the Institute of Nanotechnology, 2008.
21. R. Singh and H. S. Nalwa, *Journal of Biomedical Nanotechnology*, 2011, **7**, 489-503.

22. M. Geszke-Moritz and M. Moritz, *Materials Science & Engineering C-Materials for Biological Applications*, 2013, **33**, 1008-1021.
23. A. Darwish and A. E. Hassanien, *Sensors*, 2011, **11**, 5561-5595.
24. R. A. Freitas, *Nanomedicine*, Austin : Landes Bioscience, 1999-.
25. D. K. Kim and J. Dobson, *Journal of Materials Chemistry*, 2009, **19**, 6294-6307.
26. T. Summers, R. C. Langan, A. Nissan, B. Brucher, A. J. Bilchik, M. Protic, M. Daumer, I. Avital and A. Stojadinovic, *Journal of Cancer*, 2013, **4**, 210-216.
27. M. S. Henry, A. P. Passmore, S. Todd, B. McGuinness, D. Craig and J. A. Johnston, *International Journal of Geriatric Psychiatry*, 2013, **28**, 331-340.
28. A. O. Pasternak, V. V. Lukashov and B. Berkhout, *Retrovirology*, 2013, **10**, 41-56.
29. J. D. Siliciano and R. F. Siliciano, *Current Opinion in Hiv and Aids*, 2010, **5**, 491-497.
30. T. Derfuss, *Bmc Medicine*, 2012, **10**, 116-121.
31. J. Bates, *Insight Pharma Reports - Cancer Biomarkers Report Overview*, 2008.
32. S. Carrara, S. Ghoreishizadeh, J. Olivo, I. Taurino, C. Baj-Rossi, A. Cavallini, M. Op de Beeck, C. Dehollain, W. Burleson, F. G. Moussy, A. Guiseppi-Elie and G. De Micheli, *Sensors*, 2012, **12**, 11013-11060.
33. F. Valgimigli, F. Lucarelli, C. Scuffi, S. Morandi and I. Sposato, *Journal of diabetes science and technology*, 2010, **4**, 1182-1192.
34. B. Yu, Y. Mao, Y. Yuan, C. Yue, X. Wang, X. Mo, D. Jarjoura, M. E. Paulaitis, R. J. Lee, J. C. Byrd, L. J. Lee and N. Muthusamy, *Biomaterials*, 2013, **34**, 6185-6193
35. A. Chen and S. Chatterjee, *Chemical Society reviews*, 2013, **42**, 5425-5438.
36. P. C. Li, in *Introduction and Overview of Biosensors and Electrochemistry*, Nanobioengineering&Bioelectronics Lab, Department of Biomedical Engineering, Florida International, Florida International University, vol. 2013.
37. C. Parolo and A. Merkoci, *Chemical Society Reviews*, 2013, **42**, 450-457.
38. J. J. Willard, J. W. Drexler, A. Das, S. Roy, S. Shilo, O. Shoseyov and H. M. Powell, *Tissue engineering. Part A*, 2013, **19**, 1507-1518.
39. S. Xu, L. Sang, Y. Zhang, X. Wang and X. Li, *Materials Science & Engineering C-Materials for Biological Applications*, 2013, **33**, 648-655.
40. R. M. Boehler, J. G. Graham and L. D. Shea, *Biotechniques*, 2011, **51**, 239-59.
41. M. B. Fisher and R. L. Mauck, *Tissue Engineering Part B-Reviews*, 2013, **19**, 1-13.
42. M. J. Lysaght and J. Crager, *Tissue Engineering Part A*, 2009, **15**, 1449-1450.

43. Q. Z. Chen, S. L. Liang and G. A. Thouas, *Progress in Polymer Science*, 2013, **38**, 584-671.
44. W. H. Zimmermann, *Antioxidants & Redox Signaling*, 2009, **11**, 2011-2023.
45. E. Saiz, E. A. Zimmermann, J. S. Lee, U. G. K. Wegst and A. P. Tomsia, *Dental Materials*, 2013, **29**, 103-115.
46. W. Dunn, *Journal of Nanobiotechnology*, **2**, 1-7.
47. S. E. Lohse and C. J. Murphy, *Journal of the American Chemical Society*, 2012, **134**, 15607-15620.
48. R. Bakry, R. M. Vallant, M. Najam-Ul-Haq, M. Rainer, Z. Szabo, C. W. Huck and G. K. Bonn, *International Journal of Nanomedicine*, 2007, **2**, 639-649.
49. A. Rawsthorn, in *The New York Times*, The New York Times, New York, 12-05-2013. http://www.nytimes.com/2013/05/13/arts/design/Richard-Buckminster-Fuller-a-Gentle-Revolutionist.html?pagewanted=all&_r=0
50. V. F. Samanidou and E. G. Karageorgou, *Current Organic Chemistry*, 2012, **16**, 1645-1669.
51. Y. Zhang, Y. Bai and B. Yan, *Drug Discovery Today*, 2010, **15**, 428-435.
52. Y. Chen, A. Star and S. Vidal, *Chemical Society reviews*, 2013, **42**, 4532-4542.
53. C. Cha, S. R. Shin, N. Annabi, M. R. Dokmeci and A. Khademhosseini, *Acs Nano*, 2013, **7**, 2891-2897.
54. E. Osawa, D. A. Ho, H. J. Huang, M. V. Korobov and N. N. Rozhkova, *Diamond and Related Materials*, 2009, **18**, 904-909.
55. L. C. L. Huang and H. C. Chang, *Langmuir*, 2004, **20**, 5879-5884.
56. E. K. Chow, X.-Q. Zhang, M. Chen, R. Lam, E. Robinson, H. Huang, D. Schaffer, E. Osawa, A. Goga and D. Ho, *Science Translational Medicine*, 2011, **3,** 73-83.
57. R. A. Shimkunas, E. Robinson, R. Lam, S. Lu, X. Xu, X.-Q. Zhang, H. Huang, E. Osawa and D. Ho, *Biomaterials*, 2009, **30**, 5720-5728.
58. H. B. Man and D. Ho, *Physica Status Solidi a-Applications and Materials Science*, 2012, **209**, 1609-1618.
59. L. M. Manus, D. J. Mastarone, E. A. Waters, X.-Q. Zhang, E. A. Schultz-Sikma, K. W. MacRenaris, D. Ho and T. J. Meade, *Nano Letters*, 2010, **10**, 484-489.
60. H. Jaganathan and B. Godin, *Advanced Drug Delivery Reviews*, 2012, **64**, 1800-1819.
61. Z. X. Li, J. C. Barnes, A. Bosoy, J. F. Stoddart and J. I. Zink, *Chemical Society Reviews*, 2012, **41**, 2590-2605.
62. I. Passagne, M. Morille, M. Rousset, I. Pujalte and B. L'Azou, *Toxicology*, 2012, **299**, 112-124.
63. P. Bakthavathsalam, V. K. Rajendran and J. A. B. Mohammed, *Journal of Nanobiotechnology*, 2012, **10**, 8-18.

64. M. Vallet-Regi, A. Ramila, R. P. del Real and J. Perez-Pariente, *Chem. Mat.*, 2001, **13**, 308-311.
65. A. H. Faraji and P. Wipf, *Bioorganic & Medicinal Chemistry*, 2009, **17**, 2950-2962.
66. K. Margulis-Goshen and S. Magdassi, *Current Opinion in Colloid & Interface Science*, 2012, **17**, 290-296.
67. A. J. Shuhendler, R. Y. Cheung, J. Manias, A. Connor, A. M. Rauth and X. Y. Wu, *Breast Cancer Res. Treat.*, 2010, **119**, 255-269.
68. V. Kakkar, A. K. Mishra, K. Chuttani and I. P. Kaur, *Int. J. Pharm.*, 2013, **448**, 354-359.
69. M. R. Gasco, L. Priano and G. P. Zara, in *Nanoneuroscience and Nanoneuropharmacology*, ed. H. S. Sharma, 2009, vol. 180, pp. 181-192.
70. Solid lipid nanoparticle diagram, 11-02-2010, http://www.dailycosmetic.com/ImgData/TheDaily/200904/200904224.jpg.
71. B. P. Bastakoti, K. C. W. Wu, M. Inoue, S. Yusa, K. Nakashima and Y. Yamauchi, *Chemistry-a European Journal*, 2013, **19**, 4812-4817.
72. O. M. Y. Koo, I. Rubinstein and H. Onyuksel, *Journal of Nanoscience and Nanotechnology*, 2006, **6**, 2996-3000.
73. D. Velluto, S. N. Thomas, E. Simeoni, M. A. Swartz and J. A. Hubbell, *Biomaterials*, 2011, **32**, 9839-9847.
74. S. P. Nunes and A. Car, *Industrial & Engineering Chemistry Research*, 2013, **52**, 993-1003.
75. P. Tyagi, I. E. Raschip, A. Deratani and D. Quemener, *Advanced materials (Deerfield Beach, Fla.)*, 2013, **25**, 3739–3744.
76. H. W. Huang, F. Liu, S. N. Chen, Q. Zhao, B. Liao, Y. F. Long, Y. L. Zeng and X. D. Xia, *Biosens. Bioelectron.*, 2013, **42**, 539-544.
77. L. W. E. Starmans, D. Burdinski, N. P. M. Haex, R. P. M. Moonen, G. J. Strijkers, K. Nicolay and H. Grull, *Plos One*, 2013, **8**, 2, 1-9.
78. S. Mahajan, V. Koul, V. Choudhary, G. Shishodia and A. C. Bharti, *Nanotechnology*, 2013, **24**,1-12.
79. S. Zeng and M. P. Xiong, *Biomaterials*, 2013, **34**, 6882-6892.
80. H. Wu, L. Zhu and V. P. Torchilin, *Biomaterials*, 2013, **34**, 1213-1222.
81. X. Guo, C. L. Shi, J. Wang, S. B. Di and S. B. Zhou, *Biomaterials*, 2013, **34**, 4544-4554.
82. K. Un, K. Sakai-Kato, Y. Oshima, T. Kawanishi and H. Okuda, *Biomaterials*, 2012, **33**, 8131-8141.
83. N. Mirahmadi, M. H. Babaei, A. M. Vali and S. Dadashzadeh, *Int J Pharm*, 2010, **383**, 7-13.
84. S. Y. Lin, W. Y. Zhao, H. C. Tsai, W. H. Hsu, C. L. Lo and G. H. Hsiue, *Biomacromolecules*, 2012, **13**, 664-675.
85. K. I. Joo, L. Xiao, S. L. Liu, Y. R. Liu, C. L. Lee, P. S. Conti, M. K. Wong, Z. B. Li and P. Wang, *Biomaterials*, 2013, **34**, 3098-3109.

86. C. Settembre, A. Fraldi, D. L. Medina and A. Ballabio, *Nature Reviews Molecular Cell Biology*, 2013, **14**, 283-296.
87. M. Galan, J. Sanchez Rodriguez, J. L. Jimenez, M. Relloso, M. Maly, F. J. de la Mata, M. A. Munoz-Fernandez and R. Gomez, *Organic & biomolecular chemistry*, 2014, **12**, 3222-3237.
88. Brechbiel, Martin W. Star, Robert A. Kobayashi, Hisataka, Methods for functional kidney imaging using small dendrimer contrast agents, US Patent 06852842, Feb 8 2005.
89. J. M. Oliveira, N. Kotobuki, A. P. Marques, R. P. Pirraco, J. Benesch, M. Hirose, S. A. Costa, J. F. Mano, H. Ohgushi and R. L. Reis, *Adv. Funct. Mater.*, 2008, **18**, 1840-1853.
90. T. McCarthy, P. Karellas, S. Henderson, M. Giannis, D. O'Keefe, G. Heery, J. Paull, B. Matthews and G. Holan, *Retrovirology*, 2005, **2**, 88.
91. L. M. Kaminskas, V. M. McLeod, G. M. Ryan, B. D. Kelly, J. M. Haynes, M. Williamson, N. Thienthong, D. J. Owen and C. J. H. Porter, *Journal of controlled release : official journal of the Controlled Release Society*, 2014, **183**. 18–26.
92. H. F. Zhang, D. Wang, R. Butler, N. L. Campbell, J. Long, B. E. Tan, D. J. Duncalf, A. J. Foster, A. Hopkinson, D. Taylor, D. Angus, A. I. Cooper and S. P. Rannard, *Nature Nanotechnology*, 2008, **3**, 506-511.
93. K. S. Soppimath, T. M. Aminabhavi, A. R. Kulkarni and W. E. Rudzinski, *J. Control. Release*, 2001, **70**, 1-20.
94. V. J. Pansare, M. J. Bruzek, D. H. Adamson, J. Anthony and R. K. Prud'homme, *Molecular Imaging and Biology*, 2014, **16**, 180-188.
95. A. Kowalczuk, R. Trzcinska, B. Trzebicka, A. H. E. Muller, A. Dworak and C. B. Tsvetanov, *Progress in Polymer Science*, 2014, **39**, 43-86.
96. R. Singh and J. W. Lillard, *Exp. Mol. Pathol.*, 2009, **86**, 215-223.
97. P. Bigini, S. Previdi, E. Casarin, D. Silvestri, M. B. Violatto, S. Facchin, L. Sitia, A. Rosato, G. Zuccolotto, N. Realdon, F. Fiordaliso, M. Salmona and M. Morpurgo, *Acs Nano*, 2014, **8**, 175-187.
98. B. E. Rolfe, I. Blakey, O. Squires, H. Peng, N. R. B. Boase, C. Alexander, P. G. Parsons, G. M. Boyle, A. K. Whittaker and K. J. Thurecht, *Journal of the American Chemical Society*, 2014, **136**, 2413-2419.
99. H. Yang, H. Mao, Z. Wan, A. Zhu, M. Guo, Y. Li, X. Li, J. Wan, X. Yang, X. Shuai and H. Chen, *Biomaterials*, 2013, **34**, 9124-9133.
100. A. Saraswathy, S. S. Nazeer, M. Jeevan, N. Nimi, S. Arumugam, V. S. Harikrishnan, P. R. H. Varma and R. S. Jayasree, *Colloids and surfaces. B, Biointerfaces*, 2014, **117**, 216-224.
101. A. L. B. de Barros, A.-M. Chacko, J. L. Mikitsh, A. Al Zaki, A. Salavati, B. Saboury, A. Tsourkas and A. Alavi, *Molecular imaging and biology : MIB : the official publication of the Academy of Molecular Imaging*, 2014, **16**, 330-339.
102. W. Du, A. M. Nystrom, L. Zhang, K. T. Powell, Y. Li, C. Cheng, S. A. Wickline and K. L. Wooley, *Biomacromolecules*, 2008, **9**, 2826-2833.

103. R. Bakalova, Z. Zhelev, D. Kokuryo, L. Spasov, I. Aoki and T. Saga, *International Journal of Nanomedicine*, 2011, **6**, 1719-1732.
104. C. E. Probst, P. Zrazhevskiy, V. Bagalkot and X. H. Gao, *Advanced Drug Delivery Reviews*, 2013, **65**, 703-718.
105. S. Inal, L. Chiappisi, J. D. Koelsch, M. Kraft, M.-S. Appavou, U. Scherf, M. Wagner, M. R. Hansen, M. Gradzielski, A. Laschewsky and D. Neher, *Journal of Physical Chemistry B*, 2013, **117**, 14576-14587.
106. X. Zhang, X. Zhang, S. Wang, M. Liu, L. Tao and Y. Wei, *Nanoscale*, 2013, **5**, 147-150.
107. X. Zhang, X. Zhang, B. Yang, M. Liu, W. Liu, Y. Chen and Y. Wei, *Polym. Chem.*, 2014, **5**, 356-360.
108. X. Zhang, X. Zhang, B. Yang, J. Hui, M. Liu, Z. Chi, S. Liu, J. Xu and Y. Wei, *Polym. Chem.*, 2014, **5**, 683-688.
109. Y. Wang, K. Zhou, G. Huang, C. Hensley, X. Huang, X. Ma, T. Zhao, B. D. Sumer, R. J. DeBerardinis and J. Gao, *Nature Materials*, 2014, **13**, 204-212.
110. C. Grazon, J. Rieger, R. Meallet-Renault, B. Charleux and G. Clavier, *Macromolecules*, 2013, **46**, 5167-5176.
111. J. R. Lakowicz, *Principles of Fluorescence Spectroscopy*, 3 edn., Springer Science+Business Media, LLC, University of Maryland School of Medicine, Baltimore, Maryland, USA, 2006.
112. J. B. Pawley, *Handbook of biological confocal microscopy*, 3rd ed. edn., Springer, New York, NY, 2006.
113. H. S. Choi, W. Liu, F. Liu, K. Nasr, P. Misra, M. G. Bawendi and J. V. Frangioni, *Nature Nanotechnology*, 2010, **5**, 42-47.
114. A. Y. G. a. A. R. Khokhlov, *Giant Molecules: Here, There, and Everywhere*, 2 edn., World Scientific Publishing Co. Pte. Ltd, Singapore, 1997.
115. V. R. Devadasu, V. Bhardwaj and M. Kumar, *Chemical Reviews*, 2013, **113**, 1686-1735.
116. J. C. Kraft, J. P. Freeling, Z. Y. Wang and R. J. Y. Ho, *J. Pharm. Sci.*, 2014, **103**, 29-52.
117. J. Gong, M. Chen, Y. Zheng, S. Wang and Y. Wang, *J. Control. Release*, 2012, **159**, 312-323.
118. J. W. Valle, A. Armstrong, C. Newman, V. Alakhov, G. Pietrzynski, J. Brewer, S. Campbell, P. Corrie, E. K. Rowinsky and M. Ranson, *Investigational New Drugs*, 2011, **29**, 1029-1037.
119. C. Deng, Y. J. Jiang, R. Cheng, F. H. Meng and Z. Y. Zhong, *Nano Today*, 2012, **7**, 467-480.
120. J. Ramos, J. Forcada and R. Hidalgo-Alvarez, *Chemical Reviews*, 2014, **114**, 367-428.
121. E. Soussan, S. Cassel, M. Blanzat and I. Rico-Lattes, *ANGEWANDTE CHEMIE-INTERNATIONAL EDITION*, 2009, **48**, 274-288.
122. Z. An, Q. Qiu and G. Liu, *Chem. Commun.*, 2011, **47**, 12424-12440.

123. N. B. Graham and A. Cameron, *Pure and Applied Chemistry*, 1998, **70**, 1271-1275.
124. J. Oh, R. Drumright, D. Siegwart and K. Matyjaszewski, *PROGRESS IN POLYMER SCIENCE*, 2008, **33**, 448-477.
125. G. Muralidharan and V. Runkana, *Industrial & Engineering Chemistry Research*, 2009, **48**, 8805-8811.
126. N. S. Rejinold, T. Baby, K. P. Chennazhi and R. Jayakumar, *Colloids and surfaces. B, Biointerfaces*, 2014, **114**, 209–217.
127. L. D. Wichterle O. , *Nature*, 1960, **185**, 117-118.
128. J. Kopecek, *Nature*, 2002, **417**, 388-391.
129. G. Deepa, A. K. T. Thulasidasan, R. J. Anto, J. J. Pillai and G. S. V. Kumar, *International journal of nanomedicine*, 2012, **7**, 4077-4088.
130. W. H. Blackburn and L. A. Lyon, *Colloid Polym. Sci.*, 2008, **286**, 563-569.
131. N. Singh and L. A. Lyon, *Colloid Polym. Sci.*, 2008, **286**, 1061-1069.
132. U. Katragadda, W. Fan, Y. Z. Wang, Q. Teng and C. Tan, *Plos One*, 2013, **8**, 3, 1-13.
133. K. McAllister, P. Sazani, M. Adam, M. J. Cho, M. Rubinstein, R. J. Samulski and J. M. DeSimone, *Journal of the American Chemical Society*, 2002, **124**, 15198-15207.
134. H. M. Shewan and J. R. Stokes, *Journal of Food Engineering*, 2013, **119**, 781-792.
135. Z. An, Q. Shi, W. Tang, C.-K. Tsung, C. J. Hawker and G. D. Stucky, *Journal of the American Chemical Society*, 2007, **129**, 14493-14499.
136. R. D. Swisher, *Surfactant Biodegradation*, 2 edn., Marcel Dekker, Inc., 270 Madison Avenue, New York, New York 10016, 1987.
137. D. Myers, *Surfaces, Interfaces and Colloids: Principles and applications*, John Wiley and Sons Inc., 1999.
138. S. B. Grassino, in *Polymer solutions*, The University of Southern Mississippi, 2005, vol. 2014.
139. S. Y. Kim and C. F. Zukoski, *Soft Matter*, 2012, **8**, 1801-1810.
140. J. S. Downey, R. S. Frank, W. H. Li and H. D. H. Stover, *Macromolecules*, 1999, **32**, 2838-2844.
141. T. Alfrey and C. C. Price, *Journal of Polymer Science Part a-Polymer Chemistry*, 1996, **34**, 157-162.
142. A. Servant, K. Haupt and M. Resmini, *Chemistry-a European Journal*, 2011, **17**, 11052-11059.
143. D. Carboni, K. Flavin, A. Servant, V. Gouverneur and M. Resmini, *Chemistry-a European Journal*, 2008, **14**, 7059-7065.
144. S. C. Maddock, P. Pasetto and M. Resmini, *Chem. Commun.*, 2004, 536-537.
145. D. Carboni, Queen Mary University of London, 2009.
146. P. Pasetto, S. C. Maddock and M. Resmini, *Analytica Chimica Acta*, 2005, **542**, 572-578.

147. J. Fried, *Polymer Science and Technology, Third Edition*, Prentice Hall, 2014.
148. A. M. L. I. Servant and M. Resmini, *Abstracts of Papers of the American Chemical Society*, 2009, **238**.
149. P. Bonomi, A. Servant and M. Resmini, *Journal of Molecular Recognition*, 2012, **25**, 352-360.
150. A. Einstein, *Annalen der Physik*, 1905, **17**, 549-560.
151. A. Elgart, I. Cherniakov, Y. Aldouby, A. J. Domb and A. Hoffman, *Chemistry and Physics of Lipids*, 2012, **165**, 438-453.
152. X. K. Shi, L. S. Teo, X. T. Pan, S. W. Chong, R. Kraut, V. Korzh and T. Wohland, *Dev. Dyn.*, 2009, **238**, 3156-3167.
153. S. De Tito, F. Morvan, A. Meyer, J. J. Vasseur, A. Cummaro, L. Petraccone, B. Pagano, E. Novellino, A. Randazzo, C. Giancola and D. Montesarchio, *Bioconjugate Chem.*, 2013, **24**, 1917-1927.
154. M. Arduini, F. Mancin, P. Tecilla and U. Tonellato, *Langmuir*, 2007, **23**, 8632-8636.
155. J. Yin, X. F. Guan, D. Wang and S. Y. Liu, *Langmuir*, 2009, **25**, 11367-11374.
156. D. A. Skoog, F. J. Holler and S. R. Crouch, *Principles of instrumental analysis*, 6th ed. / Douglas A. Skoog, F. James Holler, Stanley R. Crouch. edn., Thomson Brooks/Cole, Belmont, CA ; United Kingdom, 2007.
157. Y. Y. Li, H. Cheng, Z. G. Zhang, C. Wang, J. L. Zhu, Y. Liang, K. L. Zhang, S. X. Cheng, X. Z. Zhang and R. X. Zhuo, *Acs Nano*, 2008, **2**, 125-133.
158. H. S. Park, J. E. Lee, M. Y. Cho, J. H. Hong, S. H. Cho and Y. T. Lim, *Macromolecular Rapid Communications*, 2012, **33**, 1549-1555.
159. X. L. Jin, L. K. Hao, Y. L. Hu, M. Y. She, Y. N. Shi, M. Obst, J. L. Li and Z. Shi, *Sensors and Actuators B-Chemical*, 2013, **186**, 56-60.
160. R. I. Nooney, E. McCormack and C. McDonagh, *Analytical and Bioanalytical Chemistry*, 2012, **404**, 2807-2818.
161. J. Pill, B. Kraenzlin, J. Jander, T. Sattelkau, M. Sadick, M. H. Kloetzer, C. Deus, U. Kraemer and N. Gretz, *European Journal of Medicinal Chemistry*, 2005, **40**, 1056-1061.
162. E. J. Massey, P. de Souza, G. Findlay, M. Smithies, S. Shah, P. Spark, R. G. Newcombe, C. Phillips, C. A. J. Wardrop and G. T. Robinson, *Transfusion*, 2004, **44**, 151-157.
163. A. Janaszewska, B. Ziemba, K. Ciepluch, D. Appelhans, B. Voit, B. Klajnert and M. Bryszewska, *New Journal of Chemistry*, 2012, **36**, 350-353.
164. R. C. Ellis, IMVS Division of Pathology, South australia, vol. 2014.
165. J. H. Brannon and D. Magde, *Journal of Physical Chemistry*, 1978, **82**, 705-709.
166. R. Metivier, I. Leray and B. Valeur, *Photochemical & Photobiological Sciences*, 2004, **3**, 374-380.

167. G. Behl, M. Sikka, A. Chhikara and M. Chopra, *J. Colloid Interface Sci.*, 2014, **416**, 151-160.
168. P. J. Flory, *Principles of Polymer Chemistry*, Cornell University Press, United States of America, 1953.
169. M. Khoobi, S. Emami, G. Dehghan, A. Foroumadi, A. Ramazani and A. Shafiee, *Archiv Der Pharmazie*, 2011, **344**, 588-594.
170. V. D. Kancheva, P. V. Boranova, J. T. Nechev and Manolov, II, *Biochimie*, 2010, **92**, 1138-1146.
171. M. G. Neira-Velazquez, E. Hernandez-Hernandez, L. F. Ramos-deValle, C. A. Avila-Orta, Y. A. Perera-Mercado, S. G. Solis-Rosales, P. Gonzalez-Morones, A. Ponce-Pedraza, M. Avalos-Borja, R. I. Narro-Cespedes and P. Bartolo-Perez, *Plasma Processes and Polymers*, 2013, **10**, 627-633.
172. A. Krieg, C. Pietsch, A. Baumgaertel, M. D. Hager, C. R. Becer and U. S. Schubert, *Polym. Chem.*, 2010, **1**, 1669-1676.
173. A. Rashidzadeh, A. Olad, D. Salari and A. Reyhanitabar, *J. Polym. Res.*, 2014, **21**, 1-15.
174. W. Xiong, W. Wang, Y. Wang, Y. B. Zhao, H. B. Chen, H. B. Xu and X. L. Yang, *Colloid Surf. B-Biointerfaces*, 2011, **84**, 447-453.
175. G. E. Morris, B. Vincent and M. J. Snowden, *J. Colloid Interface Sci.*, 1997, **190**, 198-205.
176. Z. Y. Zeng, J. Patel, S. H. Lee, M. McCallum, A. Tyagi, M. D. Yan and K. J. Shea, *Journal of the American Chemical Society*, 2012, **134**, 2681-2690.
177. X. W. Zhuang, T. Ha, H. D. Kim, T. Centner, S. Labeit and S. Chu, *Proceedings of the National Academy of Sciences of the United States of America*, 2000, **97**, 14241-14244.
178. Malvern, *Zetasizer nano series user manual*, Malvern Instruments Ltd., Malvern, 2004.
179. M. P. R. Joseph P. Patterson, Christophe Chassenieux, Olivier Colombani and Rachel K. O'Reilly, *Chem Soc Rev*, 2014, **43**, 2412-2425.
180. J. C. Peter Buseck, *High-Resolution Transmission Electron Microscopy : and Associated Techniques*, Oxford University Press, New York, 1988.
181. D. L. Stirland, J. W. Nichols, S. Miura and Y. H. Bae, *Journal of controlled release : official journal of the Controlled Release Society*, 2013, **172**, 1045-1064.
182. O. Bar-Ilan, R. Albrecht, V. Fako and D. Furgeson, *SMALL*, 2009, **5**, 1897-1910.
183. V. Fako and D. Furgeson, *ADVANCED DRUG DELIVERY REVIEWS*, 2009, **61**, 478-486.
184. A. J. Thorley and T. D. Tetley, *Pharmacology & Therapeutics*, 2013, **140**, 176-185.
185. R. M. LoPachin and T. Gavin, *Environmental Health Perspectives*, 2012, **120**, 1650-1657.
186. C. Hodel and R. Bass, *Toxicology Letters*, 1992, **64-5**, 149-155.

187. Society of Toxicology, 07-08- 2014. https://www.toxicology.org/gp/fda.asp
188. B. Events, *Fish Modules 1-3*, Bioscientific Events, 2012.
189. S. Festing, in *2010/63/EU*, understanding Animal research, London, 2010.
190. W. M. S. R. a. R. L. Burch, *The Principles of Humane Experiemntal Technique*, Methuen, London, 1959.
191. X. Ke, D. J. Coady, C. Yang, A. C. Engler, J. L. Hedrick and Y. Y. Yang, *Polym. Chem.*, 2014, **5**, 2621-2628.
192. O. Issarachot, J. Suksiriworapong, M. Takano, R. Yumoto and V. B. Junyaprasert, *Journal of Nanoparticle Research*, 2014, **16**, 1-15.
193. N. Alam, V. Khare, R. Dubey, A. Saneja, M. Kushwaha, G. Singh, N. Sharma, B. Chandan and P. N. Gupta, *Materials science & engineering. C, Materials for biological applications*, 2014, **38**, 85–93.
194. G. Fotakis and J. A. Timbrell, *Toxicology Letters*, 2006, **160**, 171-177.
195. E. M. Larson, W. F. Obritsch and D. J. Doughman, *Investigative Ophthalmology & Visual Science*, 1996, **37**, 1097-1097.
196. C. Schmidtke, E. Poselt, J. Ostermann, A. Pietsch, H. Kloust, H. Tran, T. Schotten, N. G. Bastus, R. Eggers and H. Weller, *Nanoscale*, 2013, **5**, 7433-7444.
197. S. S. D. Kumar, S. Mahadevan, R. Vijayaraghavan, A. B. Mandal and D. R. MacFarlane, *European Journal of Pharmaceutical Sciences*, 2014, **51**, 34-44.
198. Z. Zhang, L. Xu, H. Chen and X. Li, *The Journal of pharmacy and pharmacology*, 2014, **66**, 557-563.
199. E. Almouazen, S. Bourgeois, L. P. Jordheim, H. Fessi and S. Briancon, *Pharmaceutical Research*, 2013, **30**, 1137-1146.
200. S. K. Li, F. H. Meng, Z. J. Wang, Y. N. Zhong, M. Zheng, H. Y. Liu and Z. Y. Zhong, *European Journal of Pharmaceutics and Biopharmaceutics*, 2012, **82**, 103-111.
201. Q. H. Gao, Q. Liang, F. Yu, J. Xu, Q. H. Zhao and B. W. Sun, *Colloid Surf. B-Biointerfaces*, 2011, **88**, 741-748.
202. D. Das, R. Das, J. Mandal, A. Ghosh and S. Pal, *Journal of Applied Polymer Science*, 2014, **131**, 1-12.
203. A. O. Burts, L. Liao, Y. Y. Lu, D. A. Tirrell and J. A. Johnson, *Photochemistry and photobiology*, 2014, **90**, 380–385.
204. S. Sebastian Payyappilly, S. Dhara and S. Chattopadhyay, *Soft matter*, 2014, **10**. 2150–2159.
205. Z. Teixeira, C. A. Dreiss, M. J. Lawrence, R. K. Heenan, D. Machado, G. Z. Justo, S. S. Guterres and N. Duran, *J. Colloid Interface Sci.*, 2012, **382**, 36-47.
206. M. A. Bedell, N. A. Jenkins and N. G. Copeland, *Genes & Development*, 1997, **11**, 1-10.

207. R. P. Bulcao, F. A. Freitas, C. G. Venturini, E. Dallegrave, J. Durgante, G. Goethel, C. T. S. Cerski, P. Zielinsky, A. R. Pohlmann, S. S. Guterres and S. C. Garcia, *Toxicological Sciences*, 2013, **132**, 162-176.
208. M. F. Liu, M. H. Li, S. L. Sun, B. X. Li, D. Du, J. L. Sun, F. Y. Cao, H. C. Li, F. Jia, T. F. Wang, N. D. Chang, H. Yu, Q. Wang and H. S. S. Peng, *Biomaterials*, 2014, **35**, 3697-3707.
209. K. D. Manandhar, T. P. Yadav, V. K. Prajapati, S. Kumar, M. Rai, A. Dube, O. N. Srivastava and S. Sundar, *Journal of Antimicrobial Chemotherapy*, 2008, **62**, 376-380.
210. C. S. Huang and M. L. Hu, *Food and Chemical Toxicology*, 2011, **49**, 1381-1386.
211. T. M. Huong, T. Ishida, H. Harashima and H. Kiwada, *Biological & Pharmaceutical Bulletin*, 2001, **24**, 439-441.
212. M. A. Bedell, D. A. Largaespada, N. A. Jenkins and N. G. Copeland, *Genes & Development*, 1997, **11**, 11-43.
213. H. F. Liu, C. M. Zhang, Y. L. Tan, J. G. Wang, K. Wang, Y. Y. Zhao, G. Jia, Y. J. Hou, S. X. Wang and J. C. Zhang, *Journal of Nanoparticle Research*, 2014, **16**, 1-11.
214. G. Prencipe, S. M. Tabakman, K. Welsher, Z. Liu, A. P. Goodwin, L. Zhang, J. Henry and H. J. Dai, *Journal of the American Chemical Society*, 2009, **131**, 4783-4787.
215. R. B. Athawale, D. S. Jain, K. K. Singh and R. P. Gude, *Biomedicine & Pharmacotherapy*, 2014, **68**, 231-240.
216. Y. Yamamoto, I. Hyodo, M. Takigahira, Y. Koga, M. Yasunaga, M. Harada, T. Hayashi, Y. Kato and Y. Matsumura, *International journal of cancer. Journal international du cancer*, 2014, **135**, 214–223.
217. R. I. El-Gogary, N. Rubio, J. T. W. Wang, W. T. Al-Jamal, M. Bourgognon, H. Kafa, M. Naeem, R. Klippstein, V. Abbate, F. Leroux, S. Bals, G. Van Tendeloo, A. O. Kamel, G. A. S. Awad, N. D. Mortada and K. T. Al-Jamal, *Acs Nano*, 2014, **8**, 1384-1401.
218. H. M. He, S. Chen, J. Z. Zhou, Y. Dou, L. Song, L. Che, X. Zhou, X. Chen, Y. Jia, J. X. Zhang, S. H. Li and X. H. Li, *Biomaterials*, 2013, **34**, 5344-5358.
219. Y. Liu, L. Feng, T. Liu, L. Zhang, Y. Yao, D. Yu, L. Wang and N. Zhang, *Nanoscale*, 2014, **6**, 3231–3242.
220. K. Y. Pu, A. J. Shuhendler, J. V. Jokerst, J. G. Mei, S. S. Gambhir, Z. N. Bao and J. H. Rao, *Nature Nanotechnology*, 2014, **9**, 233-239.
221. T. Suzuki, M. Ichihara, K. Hyodo, E. Yamamoto, T. Ishida, H. Kiwada, H. Ishihara and H. Kikuchi, *Int. J. Pharm.*, 2012, **436**, 636-643.
222. B. Tavares and S. Santos Lopes, *Acta Medica Portuguesa*, 2013, **26**, 583-592.
223. P. McGrath and C.-Q. Li, *Drug Discovery Today*, 2008, **13**, 394-401.
224. D. Bechet, P. Couleaud, C. Frochot, M. L. Viriot, F. Guillemin and M. Barberi-Heyob, *Trends in Biotechnology*, 2008, **26**, 612-621.

225. C. Nüsslein-Volhard and R. Dahm, *Zebrafish : a practical approach*, Oxford University Press, Oxford, 2002.
226. M. Westerfield, *The zebrafish book: A guide for the laboratory use of zebrafish*, 5th edn., University of Oregon Express, Institute of Neuroscience, University of Oregon, 1993.
227. P. Spohn, C. Hirsch, F. Hasler, A. Bruinink, H. F. Krug and P. Wick, *Environmental Pollution*, 2009, **157**, 1134-1139.
228. J. P. Cheng, C. M. Chan, L. M. Veca, W. L. Poon, P. K. Chan, L. W. Qu, Y. P. Sun and S. H. Cheng, *Toxicology and Applied Pharmacology*, 2009, **235**, 216-225.
229. N. Lubick, *Environmental Science & Technology*, 2007, **41**, 7958-7959.
230. R. J. Griffitt, R. Weil, K. A. Hyndman, N. D. Denslow, K. Powers, D. Taylor and D. S. Barber, *Environmental Science & Technology*, 2007, **41**, 8178-8186.
231. R. J. Griffitt, K. Hyndman, N. D. Denslow and D. S. Barber, *Toxicological Sciences*, 2009, **107**, 404-415.
232. X. S. Zhu, L. Zhu, Z. H. Duan, R. Q. Qi, Y. Li and Y. P. Lang, *Journal of Environmental Science and Health Part a-Toxic/Hazardous Substances & Environmental Engineering*, 2008, **43**, 278-284.
233. T. C. K. Heiden, E. Dengler, W. J. Kao, W. Heideman and R. E. Peterson, *Toxicology and Applied Pharmacology*, 2007, **225**, 70-79.
234. I. A. Jaiyesimi, A. U. Buzdar, D. A. Decker and G. N. Hortobagyi, *Journal of Clinical Oncology*, 1995, **13**, 513-529.
235. WebMD, RXList, New York, 2013, vol. 2014.
236. D. Rubert Nogueira, M. Mitjans, M. Rosa Infante and M. P. Vinardell, *Int. J. Pharm.*, 2011, **420**, 51-58.
237. R. Hamid, Y. Rotshteyn, L. Rabadi, R. Parikh and P. Bullock, *Toxicology in Vitro*, 2004, **18**, 703-710.
238. F. Denizot and R. Lang, *Journal of Immunological Methods*, 1986, **89**, 271-277.
239. S. Pavagadhi, M. Sathishkumar and R. Balasubramanian, *Water research*, 2014, **55,** 280-291.
240. J. A. McLeish, T. J. A. Chico, H. B. Taylor, C. Tucker, K. Donaldson and S. B. Brown, *Thrombosis and Haemostasis*, 2010, **103**, 797-807.
241. Z. Clemente, V. Castro, M. A. M. Moura, C. M. Jonsson and L. F. Fraceto, *Aquatic Toxicology*, 2014, **147**, 129-139.
242. O. f. E. C.-o. a. Development, ed. O. G. F. T. T. O. CHEMICALS, 2013.
243. M. A. Khan, C. A. Davis, G. L. Foley, M. A. Friedman and L. G. Hansen, *Toxicological Sciences*, 1999, **47**, 151-157.
244. N. N. He, X. Li, D. F. Feng, M. Wu, R. Chen, T. H. Chen, D. Y. Chen and X. Z. Feng, *Chemical Research in Toxicology*, 2013, **26**, 89-95.
245. S. Sun, Y. H. Gui, Y. X. Wang, L. X. Qian, X. F. Liu, Q. Jiang and H. Y. Song, *Acta Biochimica Et Biophysica Sinica*, 2009, **41**, 86-96.

246. Y. Lei, Q. Xiao, S. Huang, W. S. Xu, Z. Zhang, Z. K. He, Y. Liu and F. J. Deng, *Journal of Nanoparticle Research*, 2011, **13**, 6895-6906.
247. F. Rocha, J. Dias, S. Engrola, P. Gavaia, I. Geurden, M. T. Dinis and S. Panserat, *The Journal of experimental biology*, 2014, **217**, 1139-1149.
248. J. J. Zhu, Y. Q. Xu, J. H. He, H. P. Yu, C. J. Huang, J. M. Gao, Q. X. Dong, Y. X. Xuan and C. Q. Li, *Journal of Applied Toxicology*, 2014, **34**, 139-148.
249. W. J. Veneman, O. W. Stockhammer, L. de Boer, S. A. J. Zaat, A. H. Meijer and H. P. Spaink, *Bmc Genomics*, 2013, **14**, 1-15.
250. P. L. Lam and R. Gambari, *J. Control. Release*, 2014, **178**, 25-45.
251. T. A. Yap and P. Workman, *Annual Review of Pharmacology and Toxicology, Vol 52*, 2012, **52**, 549-573.
252. A. K. Patri, J. F. Kukowska-Latallo and J. R. Baker, *Advanced Drug Delivery Reviews*, 2005, **57**, 2203-2214.
253. L. Kozlovskaya and D. Stepensky, *J. Control. Release*, 2013, **171**, 17-23.
254. M. Morishita, A. M. Lowman, K. Takayama, T. Nagai and N. A. Peppas, *J. Control. Release*, 2002, **81**, 25-32.
255. P. Valot, M. Baba, J. M. Nedelec and N. Sintes-Zydowicz, *Int. J. Pharm.*, 2009, **369**, 53-63.
256. M. S. Moorthy, J. H. Bae, M. J. Kim, S. H. Kim and C. S. Ha, *Particle & Particle Systems Characterization*, 2013, **30**, 1044-1055.
257. L. Li, Q. Yang, Z. Zhou, J. Zhong and Y. Huang, *Biomaterials*, 2014, **35**, 5171-5187.
258. M. V. Polyakov, *Zhur. Fiz. Khim.*, 1931, **2**, 799–805.
259. B. Sellergren and C. J. Allender, *Advanced Drug Delivery Reviews*, 2005, **57**, 1733-1741.
260. F. H. Dickey, *Proceedings of the National Academy of Sciences of the United States of America*, 1949, **35**, 227-229.
261. G. Wulff and A. Sarhan, *Angewandte Chemie-International Edition*, 1972, **11**, 341-342.
262. B. Claude, P. Morin, S. Bayoudh and J. de Ceaurriz, *Journal of Chromatography A*, 2008, **1196**, 81-88.
263. C. Alexander, H. S. Andersson, L. I. Andersson, R. J. Ansell, N. Kirsch, I. A. Nicholls, J. O'Mahony and M. J. Whitcombe, *Journal of Molecular Recognition*, 2006, **19**, 106-180.
264. G. Wulff, W. Vesper, R. Grobeeinsler and A. Sarhan, *Makromolekulare Chemie-Macromolecular Chemistry and Physics*, 1977, **178**, 2799-2816.
265. A. G. Mayes and M. J. Whitcombe, *Advanced Drug Delivery Reviews*, 2005, **57**, 1742-1778.
266. T. J. Berg JM, Stryer L, in *Biochemistry* W H Freeman, New York, 5th edition edn., 2002.
267. M. J. Whitcombe, N. Kirsch and I. A. Nicholls, *Journal of molecular recognition : JMR*, 2014, **27**, 297-401.
268. P. S. Sharma, M. Dabrowski, F. D'Souza and W. Kutner, *Trac-Trends in Analytical Chemistry*, 2013, **51**, 146-157.

269. A. A. Volkert and A. J. Haes, *Analyst*, 2014, **139**, 21-31.
270. W. J. Cheong, S. H. Yang and F. Ali, *Journal of Separation Science*, 2013, **36**, 609-628.
271. E. Amut, Q. Fu, Q. Fang, R. Liu, A. P. Xiao, A. G. Zeng and C. Chang, *J. Polym. Res.*, 2010, **17**, 401-409.
272. M. Resmini, K. Flavin and D. Carboni, *Topics in current chemistry*, 2012, **325**.
273. A. Hui, H. Sheardown and L. Jones, *Materials*, 2012, **5**, 85-107.
274. M. Esfandyari-Manesh, M. Javanbakht, R. Dinarvand and F. Atyabi, *J. Mater. Sci.-Mater. Med.*, 2012, **23**, 963-972.
275. C. Alvarez-Lorenzo and A. Concheiro, *Journal of Chromatography B-Analytical Technologies in the Biomedical and Life Sciences*, 2004, **804**, 231-245.
276. G. Cirillo, O. I. Parisi, M. Curcio, F. Puoci, F. Iemma, U. G. Spizzirri and N. Picci, *Journal of Pharmacy and Pharmacology*, 2010, **62**, 577-582.
277. A. D. Vaughan, J. B. Zhang and M. E. Byrne, *Aiche Journal*, 2010, **56**, 268-279.
278. V. D. Salian and M. E. Byrne, *Macromolecular Chemistry and Physics*, 2013, **214**, 2355-2366.
279. M. Javanbakht, S. Mohammadi, M. Esfandyari-Manesh and M. Abdouss, *Journal of Applied Polymer Science*, 2011, **119**, 1586-1593.
280. S. Nie, Y. Xing, G. J. Kim and J. W. Simons, in *Annual Review of Biomedical Engineering*, 2007, vol. 9, pp. 257-288.
281. T. Piacham, C. Nantasenamat, C. Isarankura-Na-Ayudhya and V. Prachayasittikul, *Excli Journal*, 2013, **12**, 701-718.
282. J. Swarbrick, *Encyclopedia of pharmaceutical technology*, 3rd ed. / edited by James Swarbrick. edn., Informa Healthcare, New York ; London, 2007.
283. X. Ni, M. Castanares, A. Mukherjee and S. E. Lupold, *Current Medicinal Chemistry*, 2011, **18**, 4206-4214.
284. S. Parveen, R. Misra and S. K. Sahoo, *Nanomedicine-Nanotechnology Biology and Medicine*, 2012, **8**, 147-166.
285. H.-Z. Jia, J.-Y. Zhu, X.-L. Wang, H. Cheng, G. Chen, Y.-F. Zhao, X. Zeng, J. Feng, X.-Z. Zhang and R.-X. Zhuo, *Biomaterials*, 2014, **35**, 5240-5249.
286. Y. Matsumura, *Advanced Drug Delivery Reviews*, 2011, **63**, 184-192.
287. Y. Matsumura and H. Maeda, *Cancer Research*, 1986, **46**, 6387-6392.
288. S. Herrlich, S. Spieth, S. Messner and R. Zengerle, *Advanced Drug Delivery Reviews*, 2012, **64**, 1617-1627.
289. A. M. Young and S. M. Ho, *J. Control. Release*, 2008, **127**, 162-172.
290. P. E. Thorpe, *Clinical Cancer Research*, 2004, **10**, 415-427.
291. S. Ran, B. N. Gao, S. Duffy, L. Watkins, N. Rote and P. E. Thorpe, *Cancer Research*, 1998, **58**, 4646-4653.
292. E. S. Lee, K. Na and Y. H. Bae, *J. Control. Release*, 2003, **91**, 103-113.
293. B. H. Tan and K. C. Tam, *Polymer*, 2007, **48**, 6589-6597.

294. C.-K. Chen, Q. Wang, C. H. Jones, Y. Yu, H. Zhang, W.-C. Law, C. K. Lai, Q. Zeng, P. N. Prasad, B. A. Pfeifer and C. Cheng, *Langmuir : the ACS journal of surfaces and colloids*, 2014, **30**, 4111–4119.
295. K. H. Min, J.-H. Kim, S. M. Bae, H. Shin, M. S. Kim, S. Park, H. Lee, R.-W. Park, I.-S. Kim, K. Kim, I. C. Kwon, S. Y. Jeong and D. S. Lee, *J. Control. Release*, 2010, **144**, 259-266.
296. J. I. MacGregor and V. C. Jordan, *Pharmacological Reviews*, 1998, **50**, 151-196.
297. B. S. Katzenellenbogen, K. L. Kendra, M. J. Norman and Y. Berthois, *Cancer Research*, 1987, **47**, 4355-4360.
298. J. S. Chawla and M. M. Amiji, *Int. J. Pharm.*, 2002, **249**, 127-138.
299. W. Z. Lu, G. K. Poon, P. L. Carmichael and R. B. Cole, *Analytical Chemistry*, 1996, **68**, 668-674.
300. A. S. Tatavarti, K. A. Mehta, L. L. Augsburger and S. W. Hoag, *J. Pharm. Sci.*, 2004, **93**, 2319-2331.
301. T. Loftsson, H. H. Sigurdsson, M. Masson and N. Schipper, *Pharmazie*, 2004, **59**, 25-29.
302. M. K. Chun, C. S. Cho and H. K. Choi, *J. Control. Release*, 2002, **81**, 327-334.
303. N. G. Peter Wothers, Stuart Waren, Jonathon Clayden, *Organic Chemistry*, Oxford University Press, Oxford, 2001.
304. A. Servant, Queen Mary, University of London, 2010.
305. J. Y. Kim, J. H. Jung, D. E. Lee and J. Joo, *Synthetic Metals*, 2002, **126**, 311-316.
306. S.-Y. Park, M. Ebihara, Y. Kubota, K. Funabiki and M. Matsui, *Dyes and Pigments*, 2009, **82**, 258-267.
307. Q.-L. Tang, Y.-J. Zhu, J. Wu, F. Chen and S.-W. Cao, *Nanomedicine-Nanotechnology Biology and Medicine*, 2011, **7**, 428-434.
308. G. P. Yan, R. F. Zong, L. A. Li, T. Fu, F. Liu and X. H. Yu, *Pharmaceutical Research*, 2010, **27**, 2743-2752.
309. S. T. Hsu and Y. L. Yao, *Journal of Applied Polymer Science*, 2013, **130**, 4147-4156.
310. P. H. Moghaddam, V. Ramezani, E. Esfandi, A. Vatanara, M. Nabi-Meibodi, M. Darabi, K. Gilani and A. R. Najafabadi, *Powder Technology*, 2013, **239**, 478-483.
311. Y. C. Kuo and H. F. Ko, *Biomaterials*, 2013, **34**, 4818-4830.
312. F. Tavassolian, G. Kamalinia, H. Rouhani, M. Amini, S. N. Ostad, M. R. Khoshayand, F. Atyabi, M. R. Tehrani and R. Dinarvand, *Int. J. Pharm.*, 2014, **467**, 123–138.
313. W. T. Sun, Y. Zou, Y. P. Guo, L. Wang, X. Xiao, R. Sun and K. Zhao, *Journal of Nanoparticle Research*, 2014, **16**, 1-9.
314. M. Yigitoglu, G. Aydin and N. Isiklan, *Polymer Bulletin*, 2014, **71**, 385-414.

315. R. Cheng, F. Meng, C. Deng, H.-A. Klok and Z. Zhong, *Biomaterials*, 2013, **34**, 3647-3657.
316. Z. S. Ge and S. Y. Liu, *Chemical Society Reviews*, 2013, **42**, 7289-7325.
317. M. Schindler, S. Grabski, E. Hoff and S. M. Simon, *Biochemistry*, 1996, **35**, 2811-2817.
318. B. H. Yang, Y. P. Li, X. R. Sun, X. L. Meng, P. Chen and N. A. Liu, *Journal of Chemical Technology and Biotechnology*, 2013, **88**, 2169-2175.
319. C. Fang, F. M. Kievit, O. Veiseh, Z. R. Stephen, T. Z. Wang, D. H. Lee, R. G. Ellenbogen and M. Q. Zhang, *J. Control. Release*, 2012, **162**, 233-241.
320. X. H. Dai, C. Y. Hong and C. Y. Pan, *Macromolecular Chemistry and Physics*, 2012, **213**, 2192-2200.
321. A. Martinez, R. Olmo, I. Iglesias, J. M. Teijon and M. D. Blanco, *Pharmaceutical Research*, 2014, **31**, 182-193.
322. S. Barbieri, F. Sonvico, C. Como, G. Colombo, F. Zani, F. Buttini, R. Bettini, A. Rossi and P. Colombo, *J. Control. Release*, 2013, **167**, 276-283.
323. R. Vivek, V. N. Babu, R. Thangam, K. S. Subramanian and S. Kannan, *Colloid Surf. B-Biointerfaces*, 2013, **111**, 117-123.
324. T. J. Wilson and I. Kola, *Methods in molecular biology (Clifton, N.J.)*, 2001, **158**, 83-94.
325. K. Abremski and R. Hoess, *Journal of Biological Chemistry*, 1984, **259**, 1509-1514.
326. C. Mosimann, C. K. Kaufman, P. Li, E. K. Pugach, O. J. Tamplin and L. I. Zon, *Development*, 2011, **138**, 169-177.
327. F. Schwenk, U. Baron and K. Rajewsky, *Nucleic Acids Research*, 1995, **23**, 5080-5081.
328. S. Hans, J. Kaslin, D. Freudenreich and M. Brand, *Plos One*, 2009, **4**, 1-7.
329. Y. Y. Liu, Y. Chang, C. Yang, Z. T. Sang, T. Yang, W. Ang, W. W. Ye, Y. Q. Wei, C. Y. Gong and Y. F. Luo, *Nanoscale*, 2014, **6**, 4325-4337.
330. A. Molich and N. Heisler, *Journal of Experimental Biology*, 2005, **208**, 4137-4149.